



HADRON STRUCTURE
AND THE FEYNMAN-HELLMANN THEOREM
IN LATTICE QUANTUM CHROMODYNAMICS

Alexander John Chambers

Supervised by

Assoc. Prof. Ross Young and Assoc. Prof. James Zanotti

Department of Physics
School of Physical Sciences
The University of Adelaide

February 2018

Contents

Abstract	iii
Declaration	v
Acknowledgements	vii
1 Introduction	1
2 Quantum Chromodynamics	5
2.1 Mathematical Formulation	6
2.2 Features and Dynamics	8
3 Lattice QCD	11
3.1 Mathematical Formulation	12
3.2 Systematics	18
4 Hadronic Observables in Lattice QCD	21
4.1 Two-Point Functions and Spectroscopy	22
4.2 Three-Point Functions and Matrix Elements	29
5 The Feynman-Hellmann Theorem	37
5.1 Hamiltonian Quantum Mechanics	38
5.2 Hamiltonian Lattice QCD	41
5.3 Path-Integral Approach	47
6 The Spin Structure of Hadrons	55
6.1 Connected Contributions	57
6.2 Disconnected Contributions	63
6.3 Conclusions and Outlook	70
7 The Electromagnetic Structure of Hadrons: Form Factors	73
7.1 The Pion Form Factor	78
7.2 The Nucleon Form Factors	83
7.3 Conclusions and Outlook	87
8 The Electromagnetic Structure of Hadrons: Structure Functions	95
8.1 Unpolarised Nucleon Structure Functions	97
8.2 Conclusions and Outlook	101

9	Conclusions and Outlook	105
A	Notational Conventions	107
B	Minkowski and Euclidean Metrics	109
C	Clifford Algebra and the Dirac Matrices	111
D	Levi-Civita Symbol	113
E	Special Unitary Groups	115
F	Spin-Half Particles and the Dirac Equation	117
G	Dirac Projectors, Traces and Vertex Functions	121
H	Feynman-Hellmann Energy Shifts	127
I	Ensembles	131
J	Publications by the Author	133
	References	135

Abstract

The vast majority of visible matter in the universe is made up of protons and neutrons, the fundamental building blocks of atomic nuclei. Protons and neutrons are examples of hadrons, composite states formed from point-like quarks and gluons. Understanding the dynamics of quarks and gluons inside hadrons has far-reaching implications, from the properties of heavy nuclei to the dynamics of neutron stars.

Quantum Chromodynamics (QCD) is the gauge field theory (GFT) describing the interactions of colour-charged quarks and gluons. At the low energy scales relevant to hadron structure calculations, QCD is non-perturbative, and the techniques applied to other GFTs cannot be used. At the forefront of the non-perturbative methods is Lattice QCD, a first-principles approach in which physical observables are calculated numerically through a discretisation of the Feynman path integral.

Hadron structure calculations in lattice QCD have made significant advances in recent years, however many challenges still remain. Most notably amongst these are precise calculations of ‘disconnected’ contributions to hadronic quantities, the control of excited-state contamination, and the calculation of matrix elements at large boosts.

In this thesis we develop and show how a method based on the Feynman-Hellmann (FH) theorem deals with many of these issues. The method allows matrix elements to be determined indirectly, through the introduction of artificial couplings to the QCD Lagrangian, and the calculation of the resulting shifts in the hadron spectrum. We have calculated disconnected contributions to the axial charge of the nucleon, and see excellent agreement with existing stochastic results, as well as good excited-state control. Our results for the electromagnetic form factors of the proton are the first in lattice to show agreement with the linear decrease of $G_{E,p}/G_{M,p}$ observed in experiment. Additionally, exploratory simulations have shown that an extension of the FH theorem to second order allows direct access to the structure functions of the nucleon, another first in lattice QCD.

These calculations demonstrate an expanded scope for lattice studies of hadronic observables, particular for processes involving high momentum transfer. Extensions of this work will have important implications for future experimental investigations at the upgraded Continuous Electron Beam Accelerator Facility at .

Declaration

I certify that this work contains no material which has been accepted for the award of any other degree or diploma in my name, in any university or other tertiary institution and, to the best of my knowledge and belief, contains no material previously published or written by another person, except where due reference has been made in the text. In addition, I certify that no part of this work will, in the future, be used in a submission in my name, for any other degree or diploma in any university or other tertiary institution without the prior approval of the University of Adelaide and where applicable, any partner institution responsible for the joint-award of this degree.

I give permission for the digital version of my thesis to be made available on the web, via the University's digital research repository, the Library Search and also through web search engines, unless permission has been granted by the University to restrict access for a period of time.

I acknowledge the support I have received for my research through the provision of an Australian Government Research Training Program Scholarship.

Acknowledgements

Four years, over 150 pages, and a newly-developed coffee-dependence later, the PhD has finally come to an end. The entire experience has been something I will forever treasure, and this is due entirely to the people I have had the pleasure of sharing it with. Words can only express a fraction of the gratitude I have towards these people.

First of all I would like to thank Ross Young and James Zanotti, who as supervisors have gone above and beyond what could reasonably be expected of them. They have been incredibly patient, always helpful, and have had a huge impact on me personally. Ross has been an incredible partner in theory discussions, and an invaluable late-night reader of drafts. James has been a limitless source of information and advice, and has always kept me on track and well-prepared. Both James and Ross have been great friends, and I will miss the time spent with them.

James and Ross have shared the load somewhat with my long-distance pseudo-supervisors and collaborators. Roger Horsley, who was such a wonderful host during my stay in Edinburgh. Paul Rakow, whose discussions during my stay in Liverpool helped so much with the theory aspects of this project. Gerrit Schierholz, who has been a wonderful source of inspiration for the directions my project has taken, and Holger Perlt, who has been an extraordinarily warm and friendly part of my physics upbringing. I would also like to thank David Richards, who very kindly hosted me at Jefferson Lab, an extremely exciting part of my PhD experience. Also Will Detmold, who along with Phiala Shanahan was a very warm host during my visit to MIT, and provided some very thoughtful and fun discussions.

The early years of my physics education were strongly influenced by two of my tutors. First of all Lewis Tunstall, who has an incredible gift for teaching, and who made up my mind to continue on in physics and pursue a PhD. Secondly Phiala Shanahan, who has helped me not only in the classroom, but also professionally and in my future beyond physics. In my own tutoring at the university I have tried my hardest to demonstrate the same enthusiasm and passion that Lewis and Phiala demonstrated to me.

I would like to thank Sharon Johnson and Silvana Santucci for all the administrative work they've done to support me over the last few years, especially in organising my trip to the UK and the US in 2016. Also Jeanette Roulston, who has been a huge help and Ramona Adorjan, who been an invaluable support on the technical side.

My day-to-day PhD life has been spent in the company of some amazing physicists and friends, who have kept me sane throughout the last four years. In particular I'd like to mention Sophie Hollitt, who has been an incredible help in matters both scientific and professional, and Finn Stokes, who has been an enthusiastic partner in physics discussion in the office. Additionally Kim Somfleth, who as the other

student champion of the Feynman-Hellmann technique has been a massive help over the years.

I would love to thank my parents, who it goes without saying have always been a huge support, and have always encouraged me to strive further and set the bar higher in my education. It goes without saying that I would not be where I am now without them, and I will forever be infinitely grateful for that. My sister as well, who has been alongside me on her own academic journey, and her boyfriend Michael, who from the very early day of this thesis immediately offered his time for proofreading, and to whom I am so grateful. I would also like to thank Caroline's parents, and the rest of her family, who have also been incredibly supportive.

Finally, I want to thank my partner Caroline, who is the only person to have suffered possibly more than myself in the production of this thesis. She has very generously sacrificed me to late nights and weekend writing and editing, and has always had a smile to offer in the most difficult times of the last few years.

Computing Resources

The generation of the gauge ensembles used in this thesis has been performed using the Berlin Quantum Chromodynamics (BQCD) lattice QCD program [1], on the IBM BlueGeneQ using DIRAC 2 resources (EPCC, Edinburgh, UK), the BlueGene P and Q at NIC (Jülich, Germany) and the Cray XC30 at HLRN (Berlin-Hannover, Germany). Some of the simulations were undertaken using resources awarded at the NCI National Facility in Canberra, Australia, and the iVEC facilities at the Pawsey Supercomputing Centre. These resources are provided through the National Computational Merit Allocation Scheme and the University of Adelaide Partner Share supported by the Australian Government. This work was supported in part through supercomputing resources provided by the Phoenix HPC service at the University of Adelaide. The BlueGene codes are optimised using Bagel [2]. Matrix inversion and the calculation of correlation functions has been performed using the Chroma software library [3].

Chapter 1

Introduction

“Our imagination is stretched to the utmost, not, as in fiction, to imagine things which are not really there, but just to comprehend those things which ‘are’ there.”

—Richard Feynman, lecture at Cornell University (1964)

The fundamental aim of all scientific endeavour is to gain a deeper understanding of the natural world and the laws that drive its evolution. By this measure then, the development of the Standard Model (SM) of particle physics during the second half of the 20th century should rank as one of the greatest scientific achievements in human history. The SM has allowed physicists to describe the interactions of the most minuscule elements of our universe with unprecedented precision. From the tiniest nuclear interactions, to cosmic-scale events like the Big Bang, there is little in modern physics that is not directly or indirectly influenced by these developments.

The smallest indivisible elements of matter are point-like quarks and leptons, the former coming together to form protons, neutrons and other hadrons. Quarks were first proposed independently by Gell-Mann and Zweig in 1964 [4, 5] to tame the ‘zoo’ of particle discoveries made at particle accelerators in the ’50s and ’60s. They were confirmed experimentally in 1968 in deep inelastic scattering (DIS) experiments at the Stanford Linear Accelerator Center (SLAC) [6, 7], and are now an integral component of the SM.

The interactions of quarks are described by Quantum Chromodynamics (QCD), the sector of the SM that governs the strong nuclear force. In the SM, particles exert and experience forces through the exchange of gauge bosons. In QCD this role is played by gluons, massless particles which mediate the interactions of ‘colour charged’ particles. The dynamics of quarks and gluons in QCD are discussed in Chapter 2. Exactly how these dynamics generate the observed properties of hadrons is the question addressed by the field of hadron structure.

An important feature of QCD is that gluons are self-interacting, and the theory is non-perturbative at the low-energy scales relevant to hadron structure calculations. An approach at the forefront of the non-perturbative techniques is lattice QCD, a first-principles approach in which physical observables are determined through numerical estimation of the Feynman path integral. This is technically challenging,

due the high dimensionality of the integrals involved. Lattice QCD is described in detail in Chapter 3.

Lattice has made significant progress in recent years, notably in calculations of nuclear observables, scattering amplitudes and resonances. However, there remain many outstanding challenges in the calculation of general hadronic matrix elements, described in Chapter 4. One of these is the calculation of so-called ‘disconnected’ contributions to hadronic matrix elements, associated with the contribution of sea quarks and gluons. These contributions are impossible to evaluate explicitly, and must be determined through stochastic estimation. Various stochastic approaches have matured significantly in recent years, however these analyses are complicated and suffer from a great deal of noise. Another problem is excited-state contamination in lattice three-point functions, an issue that has only recently begun to be rigorously controlled. Finally, calculations of observables for highly boosted hadrons continue to suffer from poor signal-to-noise ratios, due to the way finite boosts are implemented in lattice.

In this thesis we demonstrate a new approach to calculating hadronic observables in lattice QCD, through an application of the Feynman-Hellmann (FH) theorem. Described in Chapter 5, the FH theorem relates shifts in the energy eigenstates of a theory with matrix elements of derivatives of the Hamiltonian operator. In the FH approach to lattice, hadronic matrix elements are determined by introducing artificial couplings to the QCD Lagrangian, and calculating the resulting shifts in the hadron spectrum. This turns the problem of matrix element extraction into one of hadron spectroscopy, in which excited-state control is greatly simplified. The approach allows disconnected contributions to be included simply, by the generation of gauge ensembles including the new coupling.

In Chapter 6 we perform calculations of connected and disconnected contributions to the axial charges of hadrons, interpreted as the contributions of quark spin to the spin of the hadron. This calculation demonstrates how disconnected contributions may be straightforwardly included through the FH technique. Our results for the disconnected contributions compare extremely well with the stochastically estimated results, and are shown to be at least computationally competitive. A comparison with a variationally improved calculation also shows we have good excited-state control, which is simplified through the analysis of two-point functions.

In Chapter 7 we use an extension of the FH theorem to non-forward matrix elements to calculate the electromagnetic form factors of the pion and nucleon. We are able to extract signals at boosts far larger than have previously been possible in lattice, and find a linear drop-off in the ratio of the electric and magnetic form factors of the nucleon which matches extremely well with experiment. This is a first for lattice QCD, and further work incorporating recently developed momentum-smeared interpolating operators is expected to improve these results further.

Finally, in Chapter 8, we employ a second-order extension of the FH theorem to access structure functions of the nucleon. Lattice calculations have previously been limited to the lowest moments of the parton distribution functions (PDFs), and extractions of the full structure functions have never-before been possible. This proof-of-principle simulation has given us confidence that precise lattice determinations of the structure functions including all twists will soon be possible.

The FH technique has a huge variety of applications in lattice, and we have only begun to scratch the surface in terms of the calculations using the method. Future work in this area will continue to provide insight into the physical processes at play

in current and developing experimental efforts around the world.

Chapter 2

Quantum Chromodynamics

“It is fun to speculate about the way quarks would behave if they were physical particles of finite mass (instead of purely mathematical entities as they would be in the limit of infinite mass). A search for stable quarks . . . at the highest energy accelerators would help to reassure us of the non-existence of real quarks.”

—M. Gell-Mann, Phys. Lett. 8 (1964) [4]

The SM of particle physics is one of the greatest achievements of modern physics, providing a complete description of electromagnetism and the strong and weak nuclear forces, three of the four fundamental forces of nature. It predicted the existence of the W^\pm and Z^0 bosons and the top and charm quarks, long before they were discovered experimentally, as well as several properties of weak neutral currents. It has survived many experimental challenges, and with experimental confirmation of the Higgs boson [8, 9], all elementary particles postulated by the SM have been observed. While many current theoretical and experimental efforts are now focussed on uncovering physics beyond the SM, there remain many challenges within the existing framework to tackle.

The SM postulates the existence of 12 elementary spin-half particles, consisting of six flavours of quarks, and three flavours each of leptons and neutrinos. Forces in the standard model are mediated by the exchange of spin-one gauge bosons, which arise as a consequence of imposing the local gauge symmetry of $SU(3)_{\text{colour}} \times SU(2)_{\text{weak isospin}} \times U(1)_{\text{weak hypercharge}}$. The photon is the mediator of the electromagnetic force, the charged and neutral weak bosons (W^\pm and Z^0) mediate the weak nuclear force, and the gluon mediates the strong nuclear force. Quarks, leptons and the weak bosons gain their mass through a coupling to the Higgs field, excitations of which provide the final SM boson, the spin-zero Higgs. In the original formulation of the SM, neutrinos were massless. However, experimental confirmation of neutrino flavour oscillations [10] (for which Kajita and McDonald were award the Nobel Prize in Physics 2015 [11]) showed this was not the case, and massive neutrinos can be included in the standard model through various mechanisms (see e.g. [12] for a recent review). The particles of the SM are summarised in Fig. 2.1.

In this thesis we are concerned primarily with the strong sector of the SM, governed by QCD. QCD describes the interactions of particles carrying ‘colour

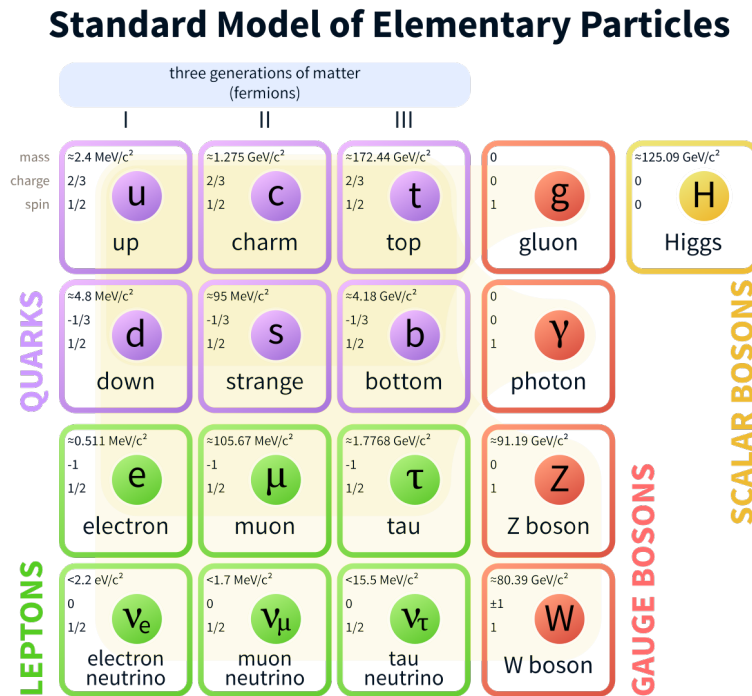


Figure 2.1: Elementary particles of the SM, including their mass, charge (in units of the magnitude of the electron charge), and spin. Image obtained from [13].

charge' through the exchange of gluons. In the SM, the elementary particles carrying colour charge are the six flavours of quark, and the gluons themselves. QCD has many interesting features that distinguish it from other gauge field theories (GFTs) in the SM, most notably asymptotic freedom and colour confinement, which will be discussed in further detail in Section 2.2. As the interaction responsible for binding quarks inside hadrons and forming composite particles like the proton and neutron, understanding the dynamics of QCD is vital for our knowledge of the fundamental structure of matter. Predictions of the theory are important inputs to phenomenological models, nuclear physics and high-energy astrophysical phenomena.

In this chapter we will begin in Section 2.1 by describing the mathematical formulation of QCD. In Section 2.2 we will discuss some of the qualitative dynamics that arise from its Lagrangian.

2.1 Mathematical Formulation

QCD is the Yang-Mills GFT [14] of the non-Abelian $SU(3)$ Lie Group. It introduces six flavours of spin-half quark transforming in the fundamental representation of $SU(3)$, and a spin-one gluon field transforming in the adjoint representation of $SU(3)$. The special unitary group is summarised in Appendix E. The fundamental and adjoint representations of $SU(3)$ have dimension 3 and $3^2 - 1 = 8$ respectively, and hence there are three quark 'colours', and eight colour varieties of gluon. The quark fields for each flavour, $[\psi_f(x)]_\alpha^a$, are four-component spinor fields for each colour. The gluon fields $[A_\mu(x)]^u$ are Lorentz vector fields for each colour in the adjoint representation. Conventions for indexing various quantities in this thesis are

summarised in Appendix A.

The QCD Lagrangian density is fully constrained by renormalisability, and invariance under the local SU(3) gauge transformations

$$[\psi_f(x)]_\alpha^a \xrightarrow{\Omega} \Omega^{ab}(x)[\psi_f(x)]_\alpha^b, \quad (2.1)$$

$$[t^u]^{ab}[A_\mu(x)]^u \xrightarrow{\Omega} [\Omega(x)]^{ac}[t^u]^{cd}[A_\mu(x)]^u [\Omega^{-1}(x)]^{db} + \frac{i}{g}[\partial_\mu \Omega(x)]^{ac}[\Omega^{-1}(x)]^{cb}. \quad (2.2)$$

Here $\Omega(x)$ defines an independent SU(3) transformation at each point in spacetime, and t^u are the generators of SU(3) transformations, described in Appendix E. We assume the Einstein convention for sums over repeated indices. With these conditions, the QCD Lagrangian density is given by

$$\mathcal{L}(x) \equiv \sum_f [\bar{\psi}_f(x)]_\alpha^a [D_f(x)]_{\alpha\beta}^{ab} [\psi_f(x)]_\beta^b - \frac{1}{4} [F_{\mu\nu}(x)]^u [F^{\mu\nu}(x)]^u. \quad (2.3)$$

The Dirac operator D is defined as

$$[D_f(x)]_{\alpha\beta}^{ab} \equiv i[\gamma^\mu]_{\alpha\beta} [D_\mu(x)]^{ab} - m_f \delta_{\alpha\beta} \delta^{ab} \quad (2.4)$$

where m_f are the bare quark masses, γ^μ are the Dirac matrices of the Clifford algebra, and D_μ is the covariant derivative defined below. Conventions and explicit forms for the γ matrices are given in Appendix C. The covariant derivative is given by

$$[D_\mu(x)]^{ab} \equiv \delta^{ab} \partial_\mu - ig[t^u]^{ab}[A_\mu(x)]^u, \quad (2.5)$$

where g is the bare quark-gluon coupling. The field strength tensor $F_{\mu\nu}(x)$ is defined to be

$$[F_{\mu\nu}(x)]^u \equiv [\partial_\mu A_\nu(x)]^u - [\partial_\nu A_\mu(x)]^u + gf^{uvw}[A_\mu(x)]^v[A_\nu(x)]^w, \quad (2.6)$$

where f^{uvw} are the structure constants of SU(3), described in Appendix E. Assuming local terms and matrix-vector notation for sums over colour, adjoint-colour, flavour and Dirac spaces, Eq. (2.3) may be written in the compact form

$$\mathcal{L} = \bar{\psi} D \psi - \frac{1}{4} F_{\mu\nu} F^{\mu\nu}. \quad (2.7)$$

Respectively, the two terms in Eq. (2.7) give the fermion and pure-gauge contributions to the Lagrangian. The gluons are massless, as it is impossible to include a gluon mass term in the Lagrangian in a gauge-invariant way. The QCD Lagrangian is invariant under charge conjugation, parity transformations and time reversal separately. A CP-violating term is not forbidden, and the absence of CP-violation in experiment is the subject of the Strong CP Problem [15, 16].

With the Lagrangian density as given in Eq. (2.7), the fundamental Feynman diagrams and their corresponding Feynman rules can be derived. The fundamental quark-gluon and gluon-gluon interaction vertices are depicted in Fig. 2.2. Not included are diagrams involving Faddeev-Popov ghosts, which arise in the path-integral formulation as a consequence of gauge symmetry, but are otherwise unphysical. We will not describe the Feynman rules for QCD, since as we will discuss below, the application of perturbative methods is of limited use in hadronic studies.

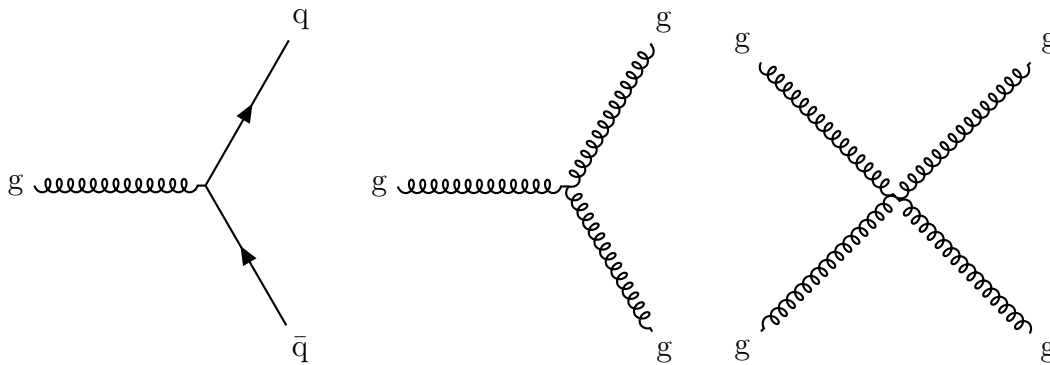


Figure 2.2: The fundamental interaction vertices of QCD. Time here is shown from left to right, with quarks represented by solid lines and gluons represented by springs.

2.2 Features and Dynamics

QCD exhibits two important distinguishing properties. The first of these is asymptotic freedom [17, 18], for which Politzer, Gross and Wilczek were awarded the 2004 Nobel Prize [19]. This is a feature only non-Abelian GFTs can possess. In Quantum Electrodynamics (QED), isolated electric charges polarise the vacuum, creating virtual electron-positron pairs in the surrounding space. Analogously to the polarisation of a dielectric in classical electromagnetism, these electron-positron pairs serve to ‘screen’ electric charge, and reduce the effective electromagnetic coupling. In a similar fashion, isolated colour charges (quarks) ‘colour-polarise’ the QCD vacuum, surrounding themselves with virtual coloured quark-antiquark pairs, which decrease the effective strong coupling at short distances. In QCD, however, the gluons also carry colour charge, and so an isolated colour charge also surrounds itself with virtual gluons which ‘anti-screen’ the colour charge, increasing the effective strong coupling. As long as the β function of QCD (here at leading order),

$$\beta(g) = -\beta_0 \frac{g^3}{16\pi^2}, \quad (2.8)$$

is negative, the anti-screening of the gluons dominates, and the effective strong coupling reduces asymptotically to zero at short distances (or equivalently, high-energy scales). This is satisfied so long as the number of active quark flavours

$$\beta_0 \equiv 11 - \frac{2}{3}N_f, \quad (2.9)$$

is greater than zero. That is, the number of quark flavours $N_f < 17$.

The second unique property of QCD is colour confinement. In nature, colour-charged states are never observed, only colour-singlets such as mesons (quark-antiquark states) and baryons (three quark or three antiquark states). As a result, no individual quark and gluon states have ever been observed. No proof of this colour confinement property exists, and proving its existence in QCD is an extension of the ‘Yang-Mills and Mass Gap’ Millennium Problem [20]. Qualitatively, as quarks are separated, it becomes energetically favourable to form quark-antiquark pairs in the vacuum, resulting in two colour-singlet states.

In quantum field theories (QFTs), experimentally measured cross-sections and decay rates are related to scattering amplitudes, which can be calculated as sums

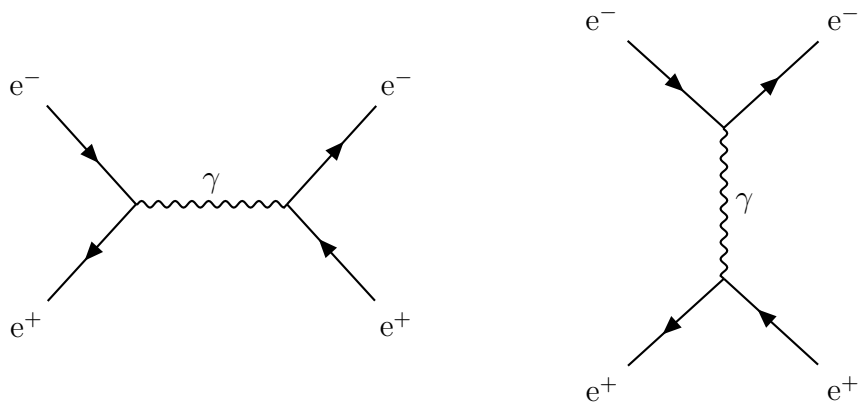


Figure 2.3: Lowest-order Feynman diagrams for electron-positron (Bhabha) scattering in QED.

of terms represented by Feynman diagrams. These represent particle interactions through the exchange of virtual particles, with Feynman rules defining the numerical contributions of different diagrams. Each node in a diagram contributes a factor of the effective coupling, and so provided the effective coupling of a theory is sufficiently small, the calculation of scattering amplitudes is perturbative, with diagrams up to a certain order included for the desired precision. For example, in Fig. 2.3 we show the lowest-order diagrams for electron-positron (Bhabha) scattering in QED. As each contains two nodes, they contribute proportionally to the effective electromagnetic coupling (fine-structure constant) squared, $\alpha_{\text{EM}}^2 \approx 5 \times 10^{-5}$. The next-order diagrams have four nodes, and contribute proportionally to $\alpha_{\text{EM}}^4 \approx 3 \times 10^{-9}$ and so on. As a result, the series-expansion in α_{EM} converges rapidly, and calculations in QED need only be performed to a few orders before the results become incredibly precise [21].

At leading order, the renormalised strong coupling

$$\alpha_{\text{S}}(Q^2) = \frac{4\pi}{\beta_0 \ln Q^2/\Lambda_{\text{QCD}}^2}, \quad (2.10)$$

where β_0 is the number of active quark flavours defined in Eq. (2.9), and $\Lambda_{\text{QCD}} \approx 0.2 \text{ GeV}$ is the natural scale of QCD. The running of the effective coupling as determined experimentally is shown in Fig. 2.4. At high-energy scales (short distances), asymptotic freedom ensures that the renormalised coupling runs to become small. As a result, QCD is perturbative at these scales, and the standard perturbative approach to field theory is appropriate. At the low-energy scales ($Q^2 \approx 1 \text{ GeV}^2$) relevant to hadronic studies however, the coupling $\alpha_{\text{S}} \approx 1$. In this regime, the perturbative expansion is no longer valid, as higher-order diagrams contribute similar or larger amounts to scattering amplitudes. For this reason, understanding the internal structure of composite particles requires a vastly different perspective, and non-perturbative approaches. One of these is lattice QCD, which we will discuss in the next chapter.

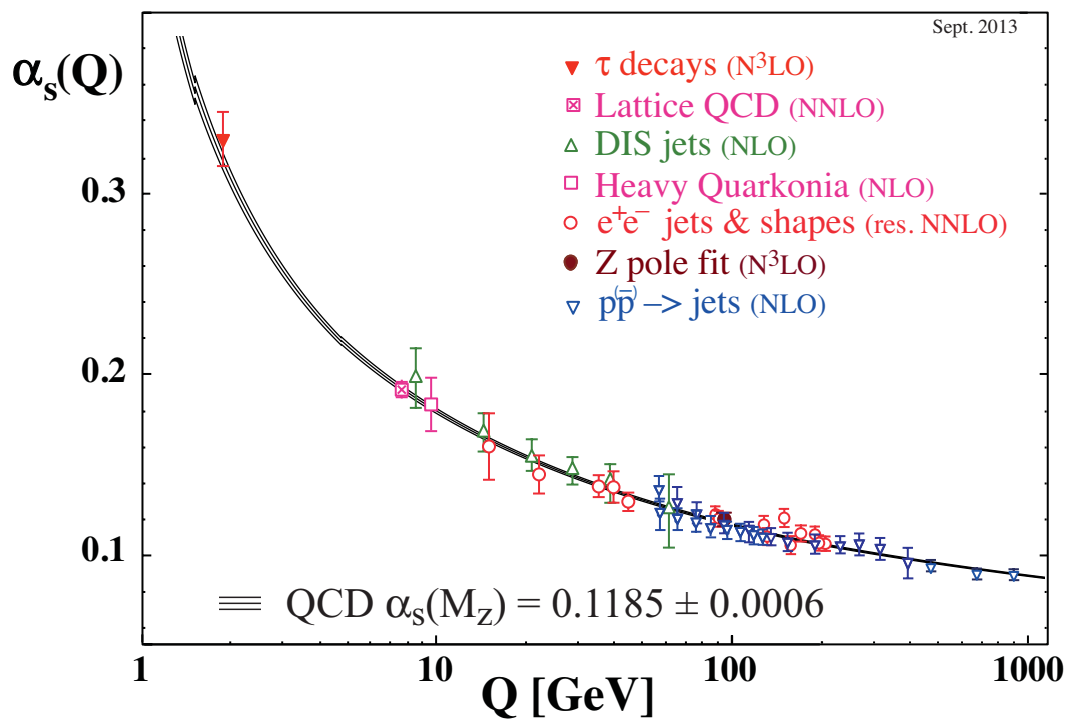


Figure 2.4: Running of the effective strong coupling α_s as a function of the energy scale Q from experimental results. Image obtained from [22].

Chapter 3

Lattice QCD

“[In this paper,] it is shown how to quantize a gauge field theory on a discrete lattice in Euclidean space-time, preserving exact gauge invariance and treating the gauge fields as angular variables.”

—K. G. Wilson, Phys. Rev. D10 (1974) [23]

First proposed in 1974 [23], lattice QCD is a systematically improvable, non-perturbative, computational approach to solving the equations of QCD. As the only direct probe of QCD at low energy scales, lattice calculations provide essential tests of the theory, and are important inputs to a variety of experimental and phenomenological efforts. Lattice has seen great success in studies of the hadron spectrum [24, 25], the QCD phase diagram [26], vacuum structure [27–30], and hadron structure [31–33].

Lattice QCD is based on the path-integral formulation of QCD [34], in which the expectation values of time-ordered products of operators are expressed as action-weighted integrals over the configuration space of fermion and gauge fields. Through the introduction of a grid of discretised spacetime points, these integrals can be evaluated using high-performance computing resources. The finite volume and non-zero spacing naturally introduce infrared and ultraviolet cutoffs respectively, and appropriate connections can be made with experimental results in the continuum limit.

In this chapter we begin in Section 3.1 by describing the theoretical formulation of lattice QCD. In Section 3.2 we briefly discuss the various lattice systematics, and the general procedures for making connections between lattice and experimental results.

3.1 Mathematical Formulation

3.1.1 Euclideanisation

In lattice QCD, our aim is to numerically evaluate the path-integral expression for the expectation value of an operator \mathcal{O} as given in Minkowski space,

$$\langle \mathcal{O} \rangle \equiv \frac{\int \mathcal{D}\bar{\psi} \mathcal{D}\psi \mathcal{D}A \mathcal{O}[\bar{\psi}, \psi, A] e^{iS[\bar{\psi}, \psi, A]}}{\int \mathcal{D}\bar{\psi} \mathcal{D}\psi \mathcal{D}A e^{iS[\bar{\psi}, \psi, A]}} , \quad (3.1)$$

where the integral is over the space of all possible quark and gluon field configurations, and the action S is defined in terms of the Lagrangian density in the usual way,

$$S \equiv \int d^4x \mathcal{L}(x). \quad (3.2)$$

In order to evaluate Eq. (3.1), we must first address the highly oscillatory Boltzmann factor e^{iS} in the numerator and denominator. This leads to the infamous numerical sign-problem, where complex contributions from the integrand cancel out almost exactly, and must be known to high-precision for the integral to be evaluated. To eliminate this factor, we perform a Wick rotation of the time coordinate, transforming the problem to Euclidean spacetime. The convention for the Wick rotation is here chosen to be

$$x_M^\mu \equiv (x_M^0, \mathbf{x}_M) \xrightarrow{\text{Wick}} x_\mu \equiv (\mathbf{x}, x_4) = (\mathbf{x}, ix_M^0), \quad (3.3)$$

where a subscript M is used to differentiate quantities in Minkowski space from their Euclidean counterparts. Lorentz indices for Euclidean quantities are all written down, as Lorentz-contravariant and covariant quantities are not distinguished. With the $(+, -, -, -)$ Minkowski metric, we can show the Wick rotation gives us the Euclidean metric up to a relative minus sign,

$$(x \cdot y)_M \equiv x_M^\mu g_{\mu\nu} y_M^\nu \xrightarrow{\text{Wick}} x \cdot y \equiv x_\mu \delta_{\mu\nu} x_\nu = -(x \cdot y)_M. \quad (3.4)$$

The γ matrices are transformed analogously to Eq. (3.3), with

$$\gamma_M^\mu \equiv (\gamma_M^0, \gamma_M^i) \xrightarrow{\text{Wick}} \gamma_\mu \equiv (\gamma_i, \gamma_4) = (-i\gamma_M^i, \gamma_M^0). \quad (3.5)$$

The resulting transformation properties of derivatives, slashed Lorentz vectors and slashed derivatives, as well as the properties of the transformed γ matrices are summarised in Appendices B and C.

Under the Wick rotation, the QCD Lagrangian density transforms as

$$\mathcal{L}_M \xrightarrow{\text{Wick}} \mathcal{L} = -\mathcal{L}_M, \quad (3.6)$$

where the Lagrangian density in Euclidean spacetime is given by,

$$\mathcal{L}(x) \equiv \sum_f \left[\bar{\psi}_f(x) \right]_\alpha^a [D_f(x)]_{\alpha\beta}^{ab} [\psi_f(x)]_\beta^b + \frac{1}{4} [F_{\mu\nu}(x)]^u [F_{\mu\nu}(x)]^u, \quad (3.7)$$

and the Dirac operator, covariant derivative and field strength tensor are

$$[D_f(x)]_{\alpha\beta}^{ab} \equiv [\gamma_\mu]_{\alpha\beta} [D_\mu(x)]^{ab} + m_f \delta_{\alpha\beta} \delta^{ab}, \quad (3.8)$$

$$[D_\mu(x)]^{ab} \equiv \delta^{ab} \partial_\mu + ig [t^u]^{ab} [A_\mu(x)]^u, \quad (3.9)$$

$$[F_{\mu\nu}(x)]^u \equiv [\partial_\nu A_\mu(x)]^u - [\partial_\mu A_\nu(x)]^u + ig f^{uvw} [A_\mu(x)]^v [A_\nu(x)]^w. \quad (3.10)$$

Noting that infinitesimal spacetime elements in Minkowski and Euclidean spacetime are related by a factor of i ,

$$d^4x_M \xrightarrow{\text{Wick}} d^4x = i d^4x_M, \quad (3.11)$$

we deduce that the effect of the Wick rotation on the QCD action is to introduce a factor of $-i$,

$$S_M \equiv \int d^4x_M \mathcal{L}_M \xrightarrow{\text{Wick}} S \equiv \int d^4x \mathcal{L} = -iS_M, \quad (3.12)$$

and that the Euclidean path-integral expression for the expectation value of an operator \mathcal{O} may then be written as

$$\langle \mathcal{O} \rangle = \frac{\int D\bar{\psi} D\psi DA \mathcal{O}[\bar{\psi}, \psi, A] e^{-S[\bar{\psi}, \psi, A]}}{\int D\bar{\psi} D\psi DA e^{-S[\bar{\psi}, \psi, A]}}. \quad (3.13)$$

As intended, the transformation to Euclidean spacetime has removed the offending Boltzmann factor.

3.1.2 Discretisation

In order to discretise the integral of Eq. (3.13), we first define a hypercubic $N_L^3 \times N_T$ grid of spacetime points, with isotropic separation a . While we will not consider them here, other lattice topologies have been explored [35, 36], and anisotropic lattices [37, 38] have important applications in finite-temperature QCD [39]. The fermion and adjoint fermion fields are defined on the grid without modification. The gauge fields are discretised in terms of link variables,

$$U_\mu(x) \equiv \mathcal{P} \exp \left[ig \int_0^a t A_\mu(x + a' \hat{\mu}) da' \right], \quad (3.14)$$

where \mathcal{P} here indicates path ordering of the A_μ , and we have omitted explicit colour and adjoint-colour indices for clarity. The link variables connect adjacent lattice sites, with the property that Hermitian conjugation ‘reverses’ the link,

$$U_\mu^\dagger(x) = U_{-\mu}(x + a\hat{\mu}). \quad (3.15)$$

Under the SU(3) transformation of Eq. (2.2), the link variables transform as

$$U_\mu(x) \xrightarrow{\Omega} \Omega(x) U_\mu(x) \Omega^{-1}(x + a\hat{\mu}), \quad (3.16)$$

and hence one can readily show that the trace of a product of link variables around a closed loop is gauge-invariant. These ‘Wilson loops’ will later allow us to construct gauge-invariant discretisations of the gluon action on the lattice. The discretisation of the fermion and gauge fields is represented pictorially in Fig. 3.1.

Gauge Action

In order to construct the gluon action on the lattice, we first consider the simplest Wilson loop, the plaquette,

$$\begin{aligned} P_{\mu\nu}(x) &\equiv U_\mu(x) U_\nu(x + a\hat{\mu}) U_{-\mu}(x + a\hat{\mu} + a\hat{\nu}) U_{-\nu}(x + a\hat{\nu}), \\ &= U_\mu(x) U_\nu(x + a\hat{\mu}) U_\mu^\dagger(x + a\hat{\nu}) U_\nu^\dagger(x). \end{aligned} \quad (3.17)$$

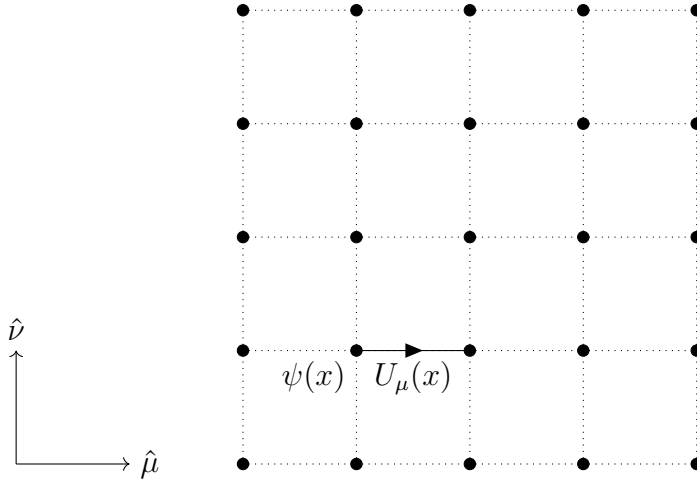


Figure 3.1: Graphical representation of the lattice, showing fermion fields defined at the lattice sites, and the gauge fields defined through link variables.

The plaquette is illustrated in Fig. 3.2. As previously discussed, it is straightforward to show using Eq. (3.16) that the traces of such closed loops of link variables are gauge invariant. The Wilson action for gluons is constructed from the plaquette as

$$[S_G]_{\text{W}}^{\text{latt}} \equiv \frac{\beta}{3} \sum_x \sum_{\mu < \nu} \text{Re Tr} [1 - P_{\mu\nu}(x)], \quad (3.18)$$

where we have here introduced the inverse bare coupling,

$$\beta \equiv \frac{6}{g^2}. \quad (3.19)$$

By Taylor-expanding the link variables in powers of the lattice spacing,

$$U_\mu(x) \approx 1 + igatA_\mu(x) + \mathcal{O}(a^2), \quad (3.20)$$

one may readily show that we recover the correct form of the gauge action from Eq. (3.18), up to $\mathcal{O}(a^2, a^2g^2)$ errors. Hence, in the limit that $a \rightarrow 0$, we recover the continuum gauge action. Reducing discretisation errors is the aim of the Symanzik improvement program [40], and involves the addition of higher-dimension operators with tunable parameters. In our simulations we use a tree-level Symanzik-improved gluon action, which includes higher dimension operators to cancel discretisation errors up to $\mathcal{O}(a^4)$.

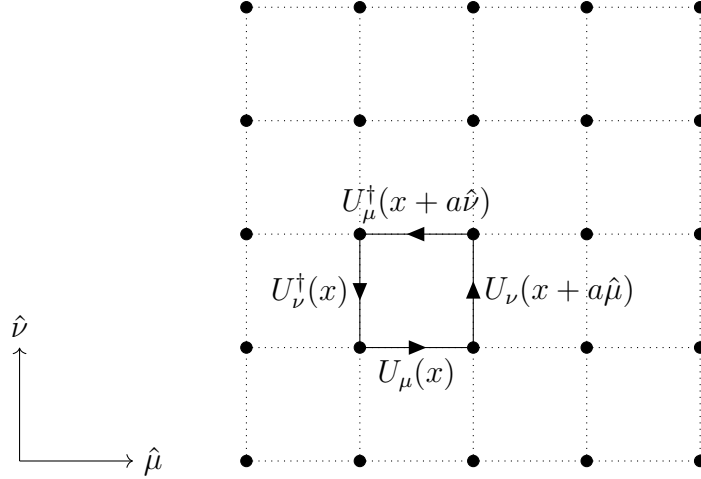
Fermion Action

The simplest discretisation of the fermion part of the QCD action is given by

$$[S_F]_{\text{naive}}^{\text{latt}} \equiv a^4 \sum_{f,x,y} \bar{\psi}_f(x) [D_f(x,y)]_{\text{naive}}^{\text{latt}} \psi_f(y), \quad (3.21)$$

where the naively discretised version of the Dirac operator in Eq. (3.8) for a single flavour is given by

$$[D_f(x,y)]_{\text{naive}}^{\text{latt}} \equiv \gamma_\mu \left[\frac{U_\mu(x)\delta_{x+a\hat{\mu},y} - U_{-\mu}(x)\delta_{x-a\hat{\mu},y}}{2a} \right] + m_f \delta_{x,y}. \quad (3.22)$$

Figure 3.2: The plaquette $P_{\mu\nu}(x)$ on the lattice.

The delta function here is the unit-normalised Kronecker delta in terms of discrete lattice sites, related to the Dirac delta by a factor of the lattice four-volume,

$$a^4 \delta^4(x - y) = \delta_{x,y} \equiv \begin{cases} 1 & x = y, \\ 0 & x \neq y. \end{cases} \quad (3.23)$$

The derivative in Eq. (3.8) has been replaced by a simple finite difference, and the transformation properties of Eqs. (2.1) and (3.16) may be used to show that, with the additional gauge links, this expression is gauge-invariant. Again, we may Taylor-expand the link variables as in Eq. (3.20), and show that Eq. (3.22) gives the correct form for the fermion action, up to $\mathcal{O}(a^2)$ errors.

The naive fermion action of Eq. (3.21) introduces the problem of ‘fermion doublers’, additional unphysical quark flavours. This may be demonstrated by considering the quark propagator, obtained on the lattice through the inversion of the Dirac matrix,

$$\sum_z [D_f(x, z)]_{\alpha\gamma}^{ac} [S_f(z, y)]_{\gamma\beta}^{cb} = \delta_{\alpha\beta} \delta_{x,y} \delta^{ab}. \quad (3.24)$$

In the limit the quark mass goes to zero, and the link variables are set to one (turning off interactions), we can determine the inverse of S_f and its Fourier transform explicitly, obtaining

$$[S(p)]_{\text{naive}}^{\text{latt}} = \frac{-ia^{-1} \sum_{\mu} \gamma_{\mu} \sin(p_{\mu}a)}{a^{-2} \sum_{\mu} \sin^2(p_{\mu}a)}. \quad (3.25)$$

For a non-zero lattice spacing, this propagator has additional unphysical poles in addition to the physical pole at $p = (0, 0, 0, 0)$, the so-called ‘doublers’.

Wilson’s solution was to include an extra term to push the doublers to higher energies, such that in the limit $a \rightarrow 0$, the doublers are infinitely heavy and decouple from the theory. The Wilson Dirac operator for a single flavour is given by

$$\frac{[D_f(x, y)]_{\text{W}}^{\text{latt}}}{C_f} \equiv \delta_{x,y} - \kappa_f [(r - \gamma_{\mu}) U_{\mu}(x) \delta_{x+a\hat{\mu},y} + (r + \gamma_{\mu}) U_{-\mu}(x) \delta_{x-a\hat{\mu},y}], \quad (3.26)$$

where the constant C_f and hopping parameter κ_f

$$C_f \equiv m_f + \frac{4r}{a} = \frac{1}{2a\kappa_f}, \quad (3.27)$$

$$\kappa_f \equiv \frac{1}{2m_f a + 8r}. \quad (3.28)$$

Noting the constant C_f is irrelevant and can be absorbed into the definition of the quark fields,

$$\psi_f \longrightarrow \frac{1}{\sqrt{2a\kappa_f}}\psi_f, \quad (3.29)$$

one may Taylor expand the link variables in Eq. (3.26) and check that one obtains the correct form for the fermion action in the continuum limit. In the limit $r \rightarrow 0$, one recovers the naive fermion operator of Eq. (3.22) from the Wilson operator. It is standard to set the value $r = 1$, in which case the quark masses are given in terms of the hopping parameters by

$$m_f = \frac{1}{2} \left(\frac{1}{\kappa_f} - \frac{1}{\kappa_c} \right). \quad (3.30)$$

The quark masses vanish for $\kappa_f = \kappa_c$, the critical value of the hopping parameter. In the free theory $\kappa_c = 1/8r$, however in the interacting theory, κ_c has multiplicative and additive renormalisations, as the Wilson term explicitly breaks chiral symmetry.

The inclusion of an extra term to address the fermion doublers has the unfortunate side-effect that one only recovers the correct fermion action from Eq. (3.26) up to $\mathcal{O}(a)$ errors. The inclusion of higher-dimension operators as part of the Symanzik improvement scheme to reduce these errors is therefore extremely important. In our simulations, we use the Sheikholeslami-Wohlert fermion action [41],

$$[S_G]_{\text{SW}}^{\text{latt}} \equiv [S_G]_{\text{W}}^{\text{latt}} - \frac{ac_{\text{SW}}r}{4} \sum_x \bar{\psi}(x) \sigma_{\mu\nu} T_{\mu\nu}(x) \psi(x), \quad (3.31)$$

with stout link smearing [42]. This action includes the ‘clover’ term, a sum of plaquettes,

$$T_{\mu\nu}(x) \equiv P_{\mu,\nu}(x) + P_{\nu,-\mu}(x) + P_{-\mu,-\nu}(x) + P_{-\nu,\mu}(x), \quad (3.32)$$

tunable by the parameter c_{SW} . This allows $\mathcal{O}(a)$ artefacts to be removed. The clover term is illustrated in Fig. 3.3.

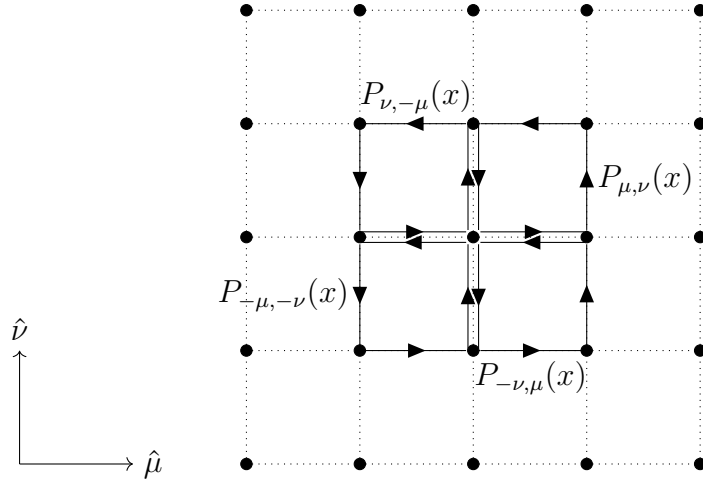
It is straightforward to show that the Wilson actions for the pure-gauge and fermion terms are invariant under parity transformations, charge conjugation and time reversal, as required by the discrete symmetries of QCD. The Dirac operator is also γ_5 -Hermitian, satisfying

$$\left(\gamma_5 [D]_{\text{W}}^{\text{latt}} \right)^\dagger = \gamma_5 [D]_{\text{W}}^{\text{latt}}, \quad (3.33)$$

where the conjugate transpose here acts on Dirac, colour and spatial indices. γ_5 -Hermiticity is essential for the Dirac operator, as it ensures the determinant of the matrix is real,

$$\det[D]^* = \det[D^\dagger] = \det[\gamma_5 D \gamma_5] = \det[D]. \quad (3.34)$$

This will become important in Section 3.1.3, as we will interpret a factor including this determinant as a probabilistic weighting.

Figure 3.3: The clover term $T_{\mu\nu}(x)$ on the lattice.

3.1.3 Monte-Carlo Importance Sampling

With the discretisation of the QCD fields and action complete, we can further simplify the expression for the path-integral in Eq. (3.13). The fermion part of this expression can be evaluated in closed form using the rules of Grassmanian integration for the anti-commuting quark fields to obtain

$$\langle \mathcal{O} \rangle = \frac{\int \mathcal{D}U \mathcal{W}\{\mathcal{O}\}[U] \prod_f \det[D_f(U)] e^{-S_G[U]}}{\int \mathcal{D}U \prod_f \det[D_f(U)] e^{-S_G[U]}}. \quad (3.35)$$

Here $\mathcal{W}\{\mathcal{O}\}$ represents the sum of all possible fully Wick contracted combinations of the fermion fields in \mathcal{O} , with relative signs determined by the parity of the particular permutation of the fields.

The high dimensionality of Eq. (3.35) suggests Monte Carlo methods are appropriate for its evaluation. The exponential factor ensures that only a small part of the infinite configuration space contributes significantly to the integral, and hence importance sampling should be used. Gauge fields are generated according to the distribution

$$\rho(U) \equiv \prod_f \det[D_f(U)] e^{-S_G[U]}, \quad (3.36)$$

through some Markov process, generally some variation of the Hybrid Monte-Carlo (HMC) algorithm [43]. The determinant of the Dirac operator is required to be real, and hence any discretisation of the fermion action must be γ_5 -Hermitian, as shown in Eq. (3.34), or otherwise have some other appropriate symmetry. The expectation value of the operator \mathcal{O} is then simply the unweighted average of the operator evaluated on each configuration,

$$\langle \mathcal{O} \rangle \approx \frac{1}{N} \sum_{i=1}^N \mathcal{W}\{\mathcal{O}\}[U_i] \equiv \langle \mathcal{W}\{\mathcal{O}\} \rangle_{\text{latt}}. \quad (3.37)$$

where the quark propagators in the fully Wick-contracted operator are calculated through the inversion of the Dirac matrix as in Eq. (3.24). It is for all intents-and-purposes impossible to evaluate the full inverse of the Dirac matrix, rather ‘columns’

of the propagator are determined by solving the system of linear equations

$$\sum_z [D_f(x, z)]_{\alpha\gamma}^{ac} [S_f(z, y_0)]_{\gamma\beta_0}^{cb_0} = \delta_{\alpha\beta_0} \delta_{x, y_0} \delta^{ab_0}, \quad (3.38)$$

for fixed spin, colour and spatial indices β_0 , b_0 and y_0 , through some iterative Krylov-space solver with various preconditioning (see e.g. [44–46]). This is repeated for each spin-colour combination, resulting in a total of twelve inversions for the calculation of the quark propagator from the single spacetime location y_0 to all other locations.

The generation of gauge fields is generally the most computationally intensive aspect of lattice calculations. Early lattice simulations made use of the quenched approximation $\det[D] = 1$ to speed up computation [47], ignoring the effects of quarks in the sea. The inclusion of dynamical fermions in gauge field generation is now standard, although far more computationally expensive, and significant effort is still being expended in devising more efficient algorithms (see e.g. [48–52]).

A significant factor in the cost of generating gauge fields and calculating quark propagators is the quark mass. Both processes require solving the system of equations in Eq. (3.38). With small quark masses, the Dirac operator has a high condition number, and iterative inversion algorithms converge more slowly and are unstable. Conversely, in the limit of infinite quark masses, the operator is diagonal and the inverse is trivial. For this reason, lattice simulations have traditionally been carried out at larger-than-physical quark masses, although calculations at the physical point are becoming more commonplace [53–59]. The quark mass is usually specified in terms of the pion mass, which is directly proportional to the light quark masses, and is an experimentally observable quantity which does not require renormalisation. Quantities calculated away from the physical point must then be extrapolated, which is discussed in Section 3.2.1

In calculations of hadronic observables for light mesons and baryons, and hyperons, contributions from heavier c , b and t quarks are not likely to be significant, and so the cost and complexity of simulations can be greatly reduced by simulating a reduced number of quark flavours. Additionally, since the QCD Lagrangian is approximately isospin-symmetric, simulating mass-degenerate u and d quarks also decreases the cost.

The generation of the gauge ensembles used in this thesis has been performed using the Berlin Quantum Chromodynamics (BQCD) lattice QCD program [1]. Matrix inversion and the calculation of correlation functions is performed using the Chroma software library [3]. The lattice volumes, hopping parameters and spacings of the ensembles used and generated in this thesis are summarised in Appendix I.

3.2 Systematics

In the formulation of the lattice regularisation in Section 3.1, the parameters introduced are the lattice spacing and volume, and the number of quark flavours and the quark masses. In order to make comparisons with experimental results, these systematics must be quantified, and in the cases of larger-than-physical quark masses, appropriate extrapolations must be made.

3.2.1 Quark Mass

As discussed in Section 3.1.3, lattice simulations have most commonly been performed with larger-than-physical quark masses, to speed-up the inversion of the Dirac operator. The results from these calculations must be extrapolated to the physical point through an application of chiral perturbation theory (ChPT) (see e.g. [60]). This involves expansions of quantities about the chiral limit $m_f \rightarrow 0$ in terms of the pion mass, where coefficients in the expansions can be related to low energy constants in the chiral limit.

There is some freedom in the path taken to the physical point, a common choice being to simulate physical heavy quarks, and vary the masses of the light u and d quarks. In our simulations, we simulate $2 + 1$ flavours of quarks, corresponding to mass-degenerate u and d quarks, and a separate heavier s quark. On the path to the physical quark mass, we begin from an $SU(3)_{\text{flavour}}$ -symmetric point, where all three quark flavours have the same mass, and keep the flavour-singlet quark mass fixed,

$$\bar{m} \equiv \frac{1}{3}(2m_s + m_l) = \text{constant} . \quad (3.39)$$

This has several advantages [61]. Firstly, starting with $SU(3)_{\text{flavour}}$ -symmetry and moving away from that point allows flavour-symmetry breaking effects to be easily investigated. Secondly, keeping the singlet mass fixed constrains expansions in flavour-symmetry breaking expansions, and flavour-singlet quantities are constant at leading order.

3.2.2 Finite Spacing and Scale Setting

In lattice calculations, all quantities are calculated in terms of the spacing a . This parameter is not specified directly, rather the bare coupling β and quark masses (through the hopping parameter in the case of Wilson fermions) are set, with the scale determined through matching to physical values. For a review of scale-setting methods, see e.g. [62] In our simulations, the scale is set by extrapolating, for fixed β and varying κ , a number of $SU(3)_{\text{flavour}}$ -singlet quantities to their physical values [61, 63–65]. As discussed in Section 3.2.1, the ensembles used in this thesis are generated with a fixed flavour-singlet quark mass, and flavour-singlet quantities are constant to leading order in $SU(3)_{\text{flavour}}$ -breaking expansions. Once determined, the lattice spacing is the same for all configurations with fixed β .

The effect of a discrete lattice spacing on the fermion and gauge actions have already been discussed, and there are various methods used to reduce these discretisation errors. In general however, a continuum extrapolation requires simulations at multiple values of a (multiple values of β , in our scale-setting scheme). Decreasing the lattice spacing has the knock-on effect of decreasing the volume, and so the number of lattice sites must be increased in order not to incur greater finite-volume artefacts. In this thesis, all ensembles have been generated with the same inverse coupling, and hence the same lattice spacing.

3.2.3 Finite Volume

Restricting the lattice to a finite volume with (anti)symmetric boundary conditions may be understood qualitatively to introduce errors from ‘wrap-around’ effects [66,

67]. Ideally, lattice calculations are performed on a number of different volumes, so it can be determined whether that such effects are significant. Generally, the requirement that $m_\pi L > 4$ has been a rule of thumb for various hadronic studies, although more rigorous constraints have been suggested [68]. The results of this thesis have been calculated on a single volume, with $m_\pi L \approx 5.6$. Future extensions of these calculations should quantify any finite volume effects.

3.2.4 Renormalisation

In the lattice regularisation of QCD, the discrete lattice spacing naturally serves as an ultraviolet regulator. In order to match lattice results with experimental results renormalised in some other scheme (i.e. modified minimal-subtraction ($\overline{\text{MS}}$)), it is necessary to connect the regulators of the two schemes. This must be achieved in a non-perturbative way at low-energy scales. In this work we use the approach of the regularisation-independent' momentum (RI'-MOM) subtraction scheme [69, 70] to determine the renormalisation of various lattice operators.

Chapter 4

Hadronic Observables in Lattice QCD

“In conclusion, we believe we have found a tractable method for extracting a variety of physical predictions from realistic lattice gauge theories including fermions. A convincing test of QCD for low energy phenomena is perhaps not too far in the future.”

—Weingarten, D., Phys. Lett. 109B (1982) [71]

In Chapter 3 we described how observable quantities may in-principle be calculated within the framework of lattice QCD. It was several years after the initial proposal, however, before algorithms had developed sufficiently to allow real numerical computations to be performed. Some of the earliest calculations in lattice were of the static-quark potential [72] and hadron masses and decay constants [71, 73].

In lattice hadron spectroscopy, the energies of hadron states are determined *ab initio* through the analysis of lattice two-point functions. The techniques applied to extract excited-state spectra are well-established, with calculations of charmed spectra [74] and resonances [75], as well as investigations including QED effects and isospin-symmetry breaking corrections [76], and multi-particle interpolators [77]. The calculation of hadronic matrix elements is a natural extension of these techniques, involving the analysis of lattice three-point functions. These methods have allowed calculation of quantities such as charges and decay rates [78], transition form factors [79, 80], and strangeness form factors [81].

In this chapter we will start in Section 4.1 by laying out the traditional two-point function approach to the calculation of hadronic energies. We will then proceed to discuss the three-point function techniques used to access hadronic matrix elements in Section 4.2. In the latter section we will emphasise some of the issues that arise in hadronic calculations, particularly excited-state contamination and disconnected contributions.

4.1 Two-Point Functions and Spectroscopy

In order to determine the energy of a hadronic state, we first define the Euclidean two-point correlation function as the expectation value

$$C_{\chi\tilde{\chi}}(x', x) \equiv \langle \chi(x') \tilde{\chi}(x) \rangle . \quad (4.1)$$

Here $\tilde{\chi}$ and χ are creation and annihilation operators chosen to couple to QCD eigenstates with particular quantum numbers. These interpolating operators create and annihilate an infinite tower of states from and to the vacuum. In the finite volume, the normally continuous spectrum of scattering states in QCD is discrete, although it is possible to access some information regarding the scattering states [82]. We label the QCD energy eigenstates $|X(\mathbf{p})\rangle$, with energy eigenvalues and normalisation,

$$H |X(\mathbf{p})\rangle = E_X(\mathbf{p}) |X(\mathbf{p})\rangle , \quad (4.2)$$

$$\langle X(\mathbf{p}) | Y(\mathbf{q}) \rangle = 2E_X(\mathbf{p}) (2\pi)^3 \delta_{XY} \delta^3(\mathbf{p} - \mathbf{q}) , \quad (4.3)$$

where H is the QCD Hamiltonian in the finite volume. The Dirac delta function is well-defined and finite in the discretised finite volume, with

$$\frac{(2\pi)^3}{V} \delta^3(\mathbf{p} - \mathbf{q}) = \delta_{\mathbf{p}, \mathbf{q}} \equiv \begin{cases} 1 & \mathbf{p} = \mathbf{q} , \\ 0 & \mathbf{p} \neq \mathbf{q} . \end{cases} \quad (4.4)$$

Since the QCD eigenstates form a complete set, we have the completeness relation

$$1 = \sum_{\mathbf{X}, \mathbf{k}} \frac{\Delta^3 k}{(2\pi)^3} \frac{1}{2E_X(\mathbf{k})} |X(\mathbf{k})\rangle \langle X(\mathbf{k})| , \quad (4.5)$$

where we use the notation $\Delta^3 k$ to refer to the discrete finite elements of momentum space,

$$\Delta^3 k = \frac{(2\pi)^3}{V} , \quad (4.6)$$

given finite size due to the restriction of Fourier modes allowed by the finite volume V . The four-momentum operator P generates spacetime translations, and so for a general translationally invariant operator \mathcal{O} in Euclidean spacetime we have that

$$\mathcal{O}(x) = e^{-i\mathbf{P}\cdot\mathbf{x}} e^{Ht} \mathcal{O}(0) e^{-Ht} e^{i\mathbf{P}\cdot\mathbf{x}} . \quad (4.7)$$

Using this to translate the creation and annihilation operators to the spacetime origin, inserting the completeness relation of Eq. (4.5), and noting that the vacuum has zero energy and momentum, Eq. (4.1) becomes

$$C_{\chi\tilde{\chi}}(x', x) = \sum_{\mathbf{X}, \mathbf{k}} \frac{\Delta^3 k}{(2\pi)^3} \frac{e^{-E_X(\mathbf{k})(t'-t)}}{2E_X(\mathbf{k})} e^{i\mathbf{k}\cdot(\mathbf{x}'-\mathbf{x})} \langle \Omega | \chi(0) | X(\mathbf{k}) \rangle \langle X(\mathbf{k}) | \tilde{\chi}(0) | \Omega \rangle . \quad (4.8)$$

Now consider the Fourier projection of the two-point function, defined as

$$G_{\chi\tilde{\chi}}(\mathbf{p}; t', t) \equiv \sum_{\mathbf{x}'} \Delta^3 x' e^{-i\mathbf{p}\cdot(\mathbf{x}'-\mathbf{x})} C_{\chi\tilde{\chi}}(x', x) , \quad (4.9)$$

where the sum can equivalently be taken over the source location \mathbf{x} . Inserting the decomposition of the two-point function in Eq. (4.8), and using the relation

$$\sum_{\mathbf{x}} \Delta^3 x e^{i\mathbf{p}\cdot\mathbf{x}} = (2\pi)^3 \delta^3(\mathbf{p}), \quad (4.10)$$

we obtain for the Fourier-projected two-point function,

$$G_{\chi\tilde{\chi}}(\mathbf{p}; \Delta t) = \sum_{\mathbf{X}} \frac{e^{-E_{\mathbf{X}}(\mathbf{p})\Delta t}}{2E_{\mathbf{X}}(\mathbf{p})} \langle \Omega | \chi(0) | \mathbf{X}(\mathbf{p}) \rangle \langle \mathbf{X}(\mathbf{p}) | \tilde{\chi}(0) | \Omega \rangle, \quad (4.11)$$

where we have written the time-dependence in terms of $\Delta t = t' - t$. This expression forms the basis for hadron spectroscopy calculations on the lattice. The Fourier-projected correlation function of Eq. (4.9) may be calculated using the techniques described in Chapter 3, and by extracting the time dependence of Eq. (4.11), one may in principle determine the entire spectrum of excited states coupling to the chosen operators.

In practice, there are many approaches to extracting excited states from the time-dependence of Eq. (4.11). A multi-exponential fit may be used to extract multiple low-lying energy states, with the higher-energy states being more difficult to constrain due to the rapid decay of their exponential terms. In this case, a rigorous estimation of the uncertainties and fit-dependence is very important (see e.g. [83]). Alternatively, one may consider calculating the two-point function for a basis of operators with different couplings to the tower of states. An analysis of this correlation matrix is the basis for the variational approach to hadron spectroscopy (see e.g. [77, 84–89]).

In our analyses we will only be concerned with the isolation of ground state energies, and hence we will make use of the most basic plateau identification method. Consider the limit of Eq. (4.11) as the time separation Δt becomes large. The dominant term in the sum of exponentials will be that of the lowest-energy state coupling to the interpolating operators,

$$G_{\chi\tilde{\chi}}(\mathbf{p}; \Delta t) \xrightarrow{\text{large } \Delta t} \frac{e^{-E_{X_0}(\mathbf{p})\Delta t}}{2E_{X_0}(\mathbf{p})} \sum_r \langle \Omega | \chi(0) | X_0(\mathbf{p}, r) \rangle \langle X_0(\mathbf{p}, r) | \tilde{\chi}(0) | \Omega \rangle. \quad (4.12)$$

Here the lowest-energy coupling state is denoted X_0 , and r labels the (possibly) degenerate eigenstates. In order to isolate this region where X_0 dominates, we introduce the effective energy,

$$E_{\chi\tilde{\chi},\text{eff}}(\mathbf{p}; \Delta t + a/2) \equiv \frac{1}{a} \ln \left| \frac{G_{\chi\tilde{\chi}}(\mathbf{p}; \Delta t)}{G_{\chi\tilde{\chi}}(\mathbf{p}; \Delta t + a)} \right|, \quad (4.13)$$

which plateaus to the energy of the lowest-energy coupling state for sufficiently large source-sink separations,

$$E_{\chi\tilde{\chi},\text{eff}}(\mathbf{p}; \Delta t + a/2) \xrightarrow{\text{large } \Delta t} E_{X_0}(\mathbf{p}). \quad (4.14)$$

Excited states manifest in the effective energy as non-constant behaviour prior to the plateau.

Through the plateau-identification procedure, the control of excited-state contamination is relatively straightforward, provided sufficient time is allowed for the

lowest-energy state to be saturated. The primary drawback is that the correlator suffers from increasingly poor signal-to-noise ratios at large times, and contamination from the so-called ‘backward-propagating state’. This is an artefact introduced by the periodic (up to a phase) boundary conditions of the lattice temporal dimension. Hadron interpolators couple to the backwards-propagating, time-reversed hadron state, which will ‘wrap-around’ the lattice time extent with a relative phase.

In order to improve overlap of lattice interpolators with the ground state, we make use of source and sink ‘smearing’ to construct extended operators. Hadron states are non-local, and ground state wavefunctions in particular are likely to be somewhat Gaussian-shaped. Smeared sources η are constructed through a smearing function which connects nearby lattice sites, and replace the identity in Eq. (3.38),

$$\sum_z [D_f(x, z)]_{\alpha\gamma}^{ac} [S_f(z, y_0)]_{\gamma\beta_0}^{cb_0} = \eta_{\alpha\beta_0}^{ab_0}(x, y_0). \quad (4.15)$$

Sink smearing can then also be applied to the resulting propagator. Different levels of smearing can be used to construct operator bases for the variational method, to better overlap with hadron excitations (see e.g. [86, 90]). In our simulations, we use gauge-invariant Jacobi smearing [91], tuned to optimise coupling with the ground-state nucleon.

4.1.1 Example: Pion Spectroscopy

The simplest interpolating operators for meson states take the form

$$\chi(x) = [\bar{\psi}_f(x)]_{\alpha}^a \Gamma_{\alpha\beta} [\psi_g(x)]_{\beta}^a, \quad (4.16)$$

$$\tilde{\chi}(x) = \chi^{\dagger} = \pm [\bar{\psi}_g(x)]_{\alpha}^a \Gamma_{\alpha\beta} [\psi_f(x)]_{\beta}^a, \quad (4.17)$$

where the relative sign depends on the γ_4 -Hermiticity of Γ . This factor comes into the amplitude of the correlation function, and hence is irrelevant for the extraction of energies. Note that the dagger operator here operates on the Dirac indices, and that both interpolators are colour-singlets. We define the overlap factors

$$Z_{\chi, X}(\mathbf{p}) \equiv \langle \Omega | \chi(0) | X(\mathbf{p}) \rangle, \quad (4.18)$$

$$\tilde{Z}_{X, \chi^{\dagger}}(\mathbf{p}) \equiv \langle X(\mathbf{p}) | \chi^{\dagger}(0) | \Omega \rangle = [Z_{\chi, X}(\mathbf{p})]^*, \quad (4.19)$$

where the final equality comes from Eq. (4.17). With these definitions, the expression for the momentum projected two-point function at large Δt in Eq. (4.12), including the backwards-propagating state, becomes

$$G_{\chi\tilde{\chi}}(\mathbf{p}; \Delta t) \xrightarrow{\text{large } \Delta t, T-\Delta t} \frac{|Z_{\chi, X_0}(\mathbf{p})|^2}{2E_{X_0}(\mathbf{p})} e^{-E_{X_0}(\mathbf{p})\frac{T}{2}} \begin{cases} \cosh [E_{X_0}(\mathbf{p})(\Delta t - T/2)], \\ -\sinh [E_{X_0}(\mathbf{p})(\Delta t - T/2)], \end{cases} \quad (4.20)$$

for states anti-symmetric or symmetric under time-reversal respectively. The amplitude of the correlation function at large times is real for interpolating operators that are Hermitian conjugates of each other as in Eqs. (4.16) and (4.17). For finite statistics, gauge noise will manifest as a small random phase, which is usually ignored by taking the real part of Eq. (4.20).

In order to calculate the mass of the pion, we first note that in the isospin-symmetric limit, the masses of all members of the isospin-triplet (π^+ , π^0 , π^-) are the same. Hence, we can use interpolators for any member of the triplet to calculate the pion mass. To begin with, we'll consider using the π^+ interpolators,

$$\chi_{\pi^+}(x) \equiv \bar{d}(x)\gamma_5 u(x), \quad (4.21)$$

$$\tilde{\chi}_{\pi^+}(x) \equiv \bar{u}(x)\gamma_5 d(x). \quad (4.22)$$

Under the parity transformations

$$\psi(\mathbf{x}, t) \xrightarrow{\text{P}} \gamma_4 \psi(-\mathbf{x}, t), \quad (4.23)$$

$$\bar{\psi}(\mathbf{x}, t) \xrightarrow{\text{P}} \bar{\psi}(-\mathbf{x}, t)\gamma_4, \quad (4.24)$$

the π^+ interpolators transform as

$$\chi_{\pi^+}(\mathbf{x}, t) \xrightarrow{\text{P}} -\chi_{\pi^+}(-\mathbf{x}, t), \quad (4.25)$$

$$\tilde{\chi}_{\pi^+}(\mathbf{x}, t) \xrightarrow{\text{P}} -\tilde{\chi}_{\pi^+}(-\mathbf{x}, t). \quad (4.26)$$

Since we are projecting to zero-momentum, the relative minus sign on the spatial dependence after a parity transformation is irrelevant, and so the operators have parity, as required for the pseudoscalar pion state. For the spectroscopy of boosted states, care needs to be taken to avoid parity-mixing [92], primarily in the analysis of excited states.

The π^+ two-point function is given by

$$C_{\pi^+}(x', x) \equiv \langle \chi_{\pi^+}(x') \tilde{\chi}_{\pi^+}(x) \rangle. \quad (4.27)$$

The estimate of this quantity on the lattice is given by Eq. (3.37) as the expectation value of the sum of all fully Wick-contracted combinations of the interpolators,

$$\begin{aligned} C_{\pi^+}(x', x) &\approx \left\langle \overline{\bar{d}(x')\gamma_5 u(x')\bar{u}(x)\gamma_5 d(x)} \right\rangle_{\text{latt}} \\ &= -\langle \text{Tr}[\gamma_5 S_d(x, x')\gamma_5 S_u(x', x)] \rangle_{\text{latt}}. \end{aligned} \quad (4.28)$$

In the isospin-symmetric limit, the u and d quark propagators are the same, and so the linear system of Eq. (3.38) need only be solved for a single flavour. Eq. (4.28) contains quark propagators from both $x \rightarrow x'$ and $x' \rightarrow x$, however we can use the γ_5 -Hermiticity of the Dirac operator (see Eq. (3.33)), which is inherited by the quark propagator, to show that

$$\left[S_f^*(x, x') \right]_{\alpha\alpha'}^{aa'} = [\gamma_5]_{\alpha\beta'} [S_f(x', x)]_{\beta'\beta}^{a'a} [\gamma_5]_{\beta\alpha'}. \quad (4.29)$$

Hence we only need to calculate the propagator from x to all possible sink locations x' to construct Eq. (4.28). We can then take the Fourier transform over \mathbf{x}' as in Eq. (4.9), at zero spatial momentum to construct the Fourier-projected π^+ two-point function,

$$G_{\pi^+}(\mathbf{p} = \mathbf{0}; \Delta t) = \sum_{\mathbf{x}'} \Delta^3 x' C_{\pi^+}(x', x), \quad (4.30)$$

which at sufficient source-sink separation times saturates the pion ground state,

$$G_{\pi^+}(\mathbf{p} = \mathbf{0}; \Delta t) \xrightarrow{\text{large } \Delta t, T - \Delta t} \frac{|Z_{\chi, \pi^+}(\mathbf{p} = \mathbf{0})|^2}{2m_\pi} e^{-m_\pi \frac{T}{2}} \cosh \left[m_\pi \left(\Delta t - \frac{T}{2} \right) \right]. \quad (4.31)$$

Fig. 4.1 shows the π correlator as calculated on an $N = 342$ subset of Ensemble 1, with $m_\pi = 470$ MeV (as calculated on the larger, full ensemble). The π^+ operators are anti-symmetric under time-reversal, and so we have included a cosh fit of the form given in Eq. (4.20). The linear behaviour on the logarithmic scale indicates the expected exponential decays of the forwards and backwards-propagating states. Fig. 4.2 shows the corresponding effective mass, where the non-constant behaviour at times prior to $\Delta t/a = 10$ and after $\Delta t/a = 54$ indicates the presence of excited-state contamination.

Avoiding the excited-state contamination, we fit to the region $10 \leq \Delta t/a \leq 54$. From this fit, the mass of the pion state is determined to be, in lattice units,

$$am_\pi = 0.1759(8). \quad (4.32)$$

Using the value of the lattice spacing determined through the scale setting procedure discussed in Section 3.2.2 (listed in Appendix I), and inserting appropriate factors of \hbar and c , we have

$$m_\pi = 469(13) \text{ MeV}. \quad (4.33)$$

This value is consistent with the value given in Appendix I, although not exactly the same, as this calculation has been carried out on a subset of Ensemble 1.

Suppose we had instead tried to calculate the pion mass using π^0 interpolators,

$$\chi_{\pi^0}(x) = \tilde{\chi}_{\pi^0}^\dagger(x) \equiv \frac{1}{\sqrt{2}} \left[\bar{u}(x) \gamma_5 u(x) - \bar{d}(x) \gamma_5 d(x) \right], \quad (4.34)$$

where the π^0 two-point function is given by

$$C_{\pi^0}(x', x) \equiv \langle \chi_{\pi^0}(x') \tilde{\chi}_{\pi^0}(x) \rangle. \quad (4.35)$$

There are far more Wick contractions to consider in this case, and the lattice estimate of the two-point function is given by the unwieldy expression

$$\begin{aligned} C_{\pi^0}(x', x) &\approx -\frac{1}{2} \langle \text{Tr}[\gamma_5 S_u(x, x') \gamma_5 S_u(x', x)] \rangle_{\text{latt}} \\ &\quad + \frac{1}{2} \langle \text{Tr}[\gamma_5 S_u(x', x')] \text{Tr}[\gamma_5 S_u(x, x)] \rangle_{\text{latt}} \\ &\quad - \frac{1}{2} \langle \text{Tr}[\gamma_5 S_u(x', x') \gamma_5 S_d(x, x)] \rangle_{\text{latt}} \\ &\quad + u \leftrightarrow d. \end{aligned} \quad (4.36)$$

Here we require not only propagators from x to x' (point-to-all), but propagators from x' to x' (all-to-all), with the Fourier transform taken over \mathbf{x}' . The two classes of contractions giving rise to these propagators are displayed diagrammatically in Fig. 4.3. Although they appear similar, these are not Feynman diagrams. To calculate all-to-all propagators explicitly, we require the full inverse of the Dirac operator as in Eq. (3.24), instead of a single spatial column from Eq. (3.38) for the point-to-all propagators. This is not possible in practice, and rather stochastic techniques must be used to estimate these propagators. This is a problem that will reoccur in our discussion of three-point functions in Section 4.2

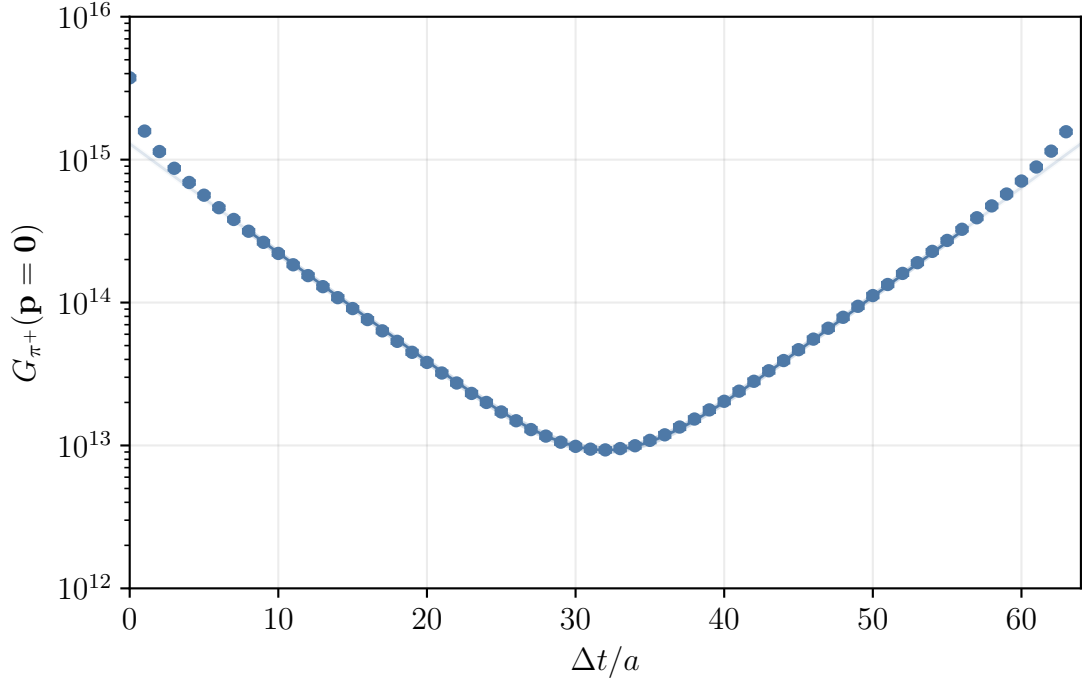


Figure 4.1: π^+ correlator with a cosh fit of the form given in Eq. (4.20). Calculated on an $N = 342$ subset of Ensemble 1, with $m_\pi = 470$ MeV (on the full ensemble).

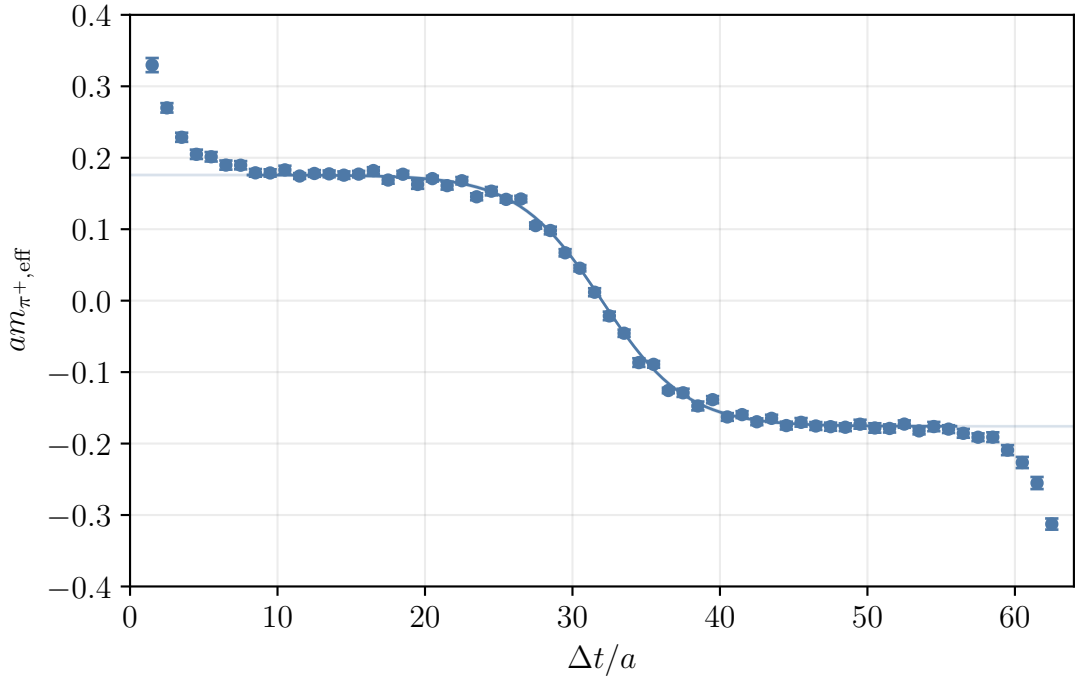


Figure 4.2: π^+ effective mass, with the effective mass transformation applied to the cosh fit of the form given in Fig. 4.1. Calculated on an $N = 342$ subset of Ensemble 1, with $m_\pi = 470$ MeV (on the full ensemble).



Figure 4.3: Two classes of contractions of u or d fields in the π^0 two-point function, Eq. (4.36).

4.1.2 Example: Nucleon Spectroscopy

For particles with an additional spin degree-of-freedom, the interpolating operators are generally of the form

$$\chi_\alpha(x) = \epsilon^{abc} [\psi_f(x)]_\alpha^a \left([\psi_g(x)]_\beta^b \Gamma_{\beta\gamma} [\psi_h(x)]_\gamma^c \right) + \text{similar terms}, \quad (4.37)$$

$$\tilde{\chi}_\alpha(x) = \bar{\chi}_\alpha(x) = \epsilon^{abc} \left([\bar{\psi}_g(x)]_\beta^a \Gamma_{\beta\gamma} [\bar{\psi}_h(x)]_\gamma^b \right) [\bar{\psi}_f(x)]_\alpha^c + \text{similar terms}. \quad (4.38)$$

The antisymmetric tensor here ensures the colour antisymmetry of the interpolators, and that there remains a free Dirac index. This is generally contracted with some projection matrix to determine spin and parity projection, so the two-point function is given by

$$C_{\chi\bar{\chi}}(\Gamma_{\text{proj}}; x', x) \equiv [\Gamma_{\text{proj}}]_{\alpha\beta} \langle \chi_\alpha(x') \bar{\chi}_\beta(x) \rangle. \quad (4.39)$$

In this case, one defines overlap factors

$$Z_{\chi,X}(\mathbf{p}) u_\alpha(p, \sigma) \equiv \langle \Omega | \chi_\alpha(0) | X(\mathbf{p}, \sigma) \rangle, \quad (4.40)$$

$$\tilde{Z}_{\bar{\chi},\bar{X}}(\mathbf{p}) \bar{u}_\alpha(p, \sigma) \equiv \langle X(\mathbf{p}, \sigma) | \bar{\chi}_\alpha(0) | \Omega \rangle = Z_{\chi,X}^*(\mathbf{p}) \bar{u}_\alpha(p, \sigma), \quad (4.41)$$

and the final result may be expressed as

$$C_{\chi\bar{\chi}}(\Gamma_{\text{proj}}; \mathbf{p}; \Delta t) \xrightarrow{\text{large } \Delta t} 4 |Z_{\chi,X_0}(\mathbf{p})|^2 F_2(\Gamma_{\text{proj}}; \mathbf{p}, m_{X_0}) \frac{e^{-E_{X_0}(\mathbf{p})\Delta t}}{2E_{X_0}(\mathbf{p})}. \quad (4.42)$$

Here F_2 is defined as

$$F_2(\Gamma_{\text{proj}}; \mathbf{p}, m) \equiv \frac{1}{4} \sum_{\sigma} [\Gamma_{\text{proj}}]_{\alpha\beta} u_\alpha(p, \sigma) \bar{u}_\beta(p, \sigma), \quad (4.43)$$

where $u(p, \sigma)$ is the spinor component of the positive-energy plane-wave solution to the free Dirac equation, described in Appendix F. Values of F_2 for common choices of Γ_{proj} can be found in Appendix G. As in Eq. (4.20), the amplitude of this correlation function is real for adjoint-conjugate operators as in Eqs. (4.37) and (4.38), up to gauge noise.

In order to extract the nucleon mass, we may consider proton or nucleon interpolators, as they are mass-degenerate in the isospin-symmetric limit. For the proton, appropriate interpolators are given by

$$[\chi_{\text{P}}(x)]_\alpha = \epsilon^{abc} [u(x)]_\alpha^a \left([u(x)]_\beta^b [C\gamma_5]_{\beta\gamma} [d(x)]_\gamma^c \right), \quad (4.44)$$

$$[\tilde{\chi}_{\text{P}}(x)]_\alpha = \epsilon^{abc} \left([\bar{u}(x)]_\beta^a [C\gamma_5]_{\beta\gamma} [\bar{d}(x)]_\gamma^b \right) [\bar{u}(x)]_\alpha^c, \quad (4.45)$$

where C is the charge-conjugation matrix, defined by the relation

$$C\gamma_\mu C^{-1} = -\gamma_\mu^T. \quad (4.46)$$

These are contracted with the Dirac projector

$$\Gamma_{\text{unpol}} \equiv \frac{1}{2}(\mathbb{I} + \gamma_4), \quad (4.47)$$

which projects definite positive parity. One may show using the transformation properties of the fermion fields in Eqs. (4.23) and (4.24) that this projector achieves the correct parity transformation for the interpolators of Eq. (4.44). Unlike in the meson case, the forwards and backwards-propagating state of a baryon correlation function are not in general symmetric or anti-symmetric. After projection to definite parity, the forwards and backwards-propagating states are parity partners, and hence it is standard to merely fit to the plateau region of the forwards propagating state, and ignore the other half of the correlator.

The two-point function of the proton is given by

$$C_p(\Gamma_{\text{unpol}}; x', x) \equiv [\Gamma_{\text{unpol}}]_{\alpha\beta} \langle [\chi_p(x')]_\alpha [\tilde{\chi}_p(x)]_\beta \rangle, \quad (4.48)$$

which after considering all possible fully Wick contracted combinations becomes

$$C_p(\Gamma_{\text{unpol}}; x', x) \approx \epsilon^{a'b'c'} \epsilon^{abc} [C\gamma_5]_{\alpha'\beta'} [C\gamma_5]_{\alpha\beta} [\Gamma_{\text{unpol}}]_{\gamma\gamma'} \left[\langle [S_d(x', x)]_{\beta'\beta}^{b'b} [S_u(x', x)]_{\alpha'\alpha}^{a'a} [S_u(x', x)]_{\gamma'\gamma}^{c'c} \rangle_{\text{latt}} - \langle [S_d(x', x)]_{\beta'\beta}^{b'b} [S_u(x', x)]_{\alpha'\gamma}^{a'c} [S_u(x', x)]_{\gamma'\alpha}^{c'a} \rangle_{\text{latt}} \right], \quad (4.49)$$

where no all-to-all propagators are involved. This is a general property for baryon two-point functions, where the creation and annihilation operators are always constructed from adjoint fermion and fermion fields respectively. We can construct the Fourier-projected two-point function,

$$G_p(\mathbf{p} = \mathbf{0}; \Delta t) = \sum_{\mathbf{x}'} \Delta^3 x' C_p(x', x) \stackrel{\text{large } \Delta t}{\propto} e^{-m_N \Delta t}, \quad (4.50)$$

which is shown in Fig. 4.4, as calculated on an $N = 342$ subset of Ensemble 1, with $m_\pi = 470$ MeV. In this case we only show early times where we observe the forwards-propagating state, and see the expected exponential decay of Eq. (4.50). Fig. 4.5 shows the corresponding effective mass. We see the expected exponential decay of the correlator, and the plateau in the effective mass at large times.

From an exponential fit to the plateau region, we extract the nucleon mass

$$am_N = 0.4540(66) \implies m_N = 1211(38) \text{ MeV}. \quad (4.51)$$

This is consistent with the value calculated on the full ensemble, $m_N = 1246(36)$ MeV.

4.2 Three-Point Functions and Matrix Elements

Aside from hadron energies, hadronic matrix elements are some of the most commonly calculated quantities in lattice QCD. These are accessed through the Euclidean three-point function, defined as

$$C_{\tilde{\chi}\mathcal{O}\chi}(x', y, x) \equiv \langle \chi(x') \mathcal{O}(y) \tilde{\chi}(x) \rangle. \quad (4.52)$$

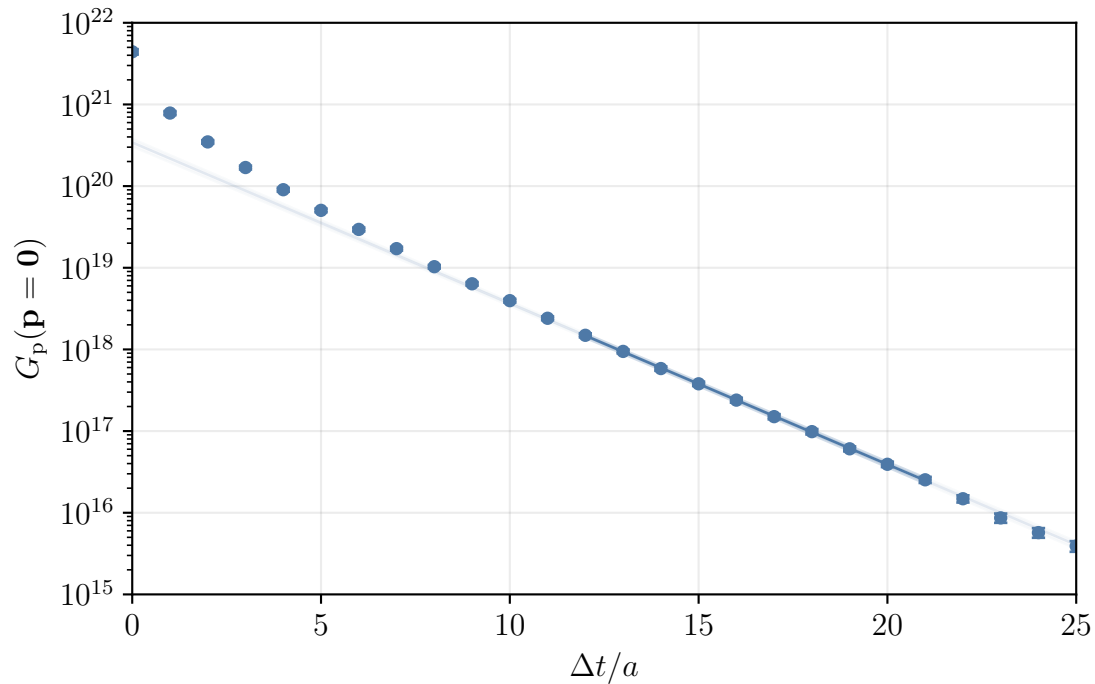


Figure 4.4: Proton correlator with an exponential fit of the form given in Eq. (4.50). Calculated on an $N = 342$ subset of Ensemble 1, with $m_\pi = 470$ MeV.

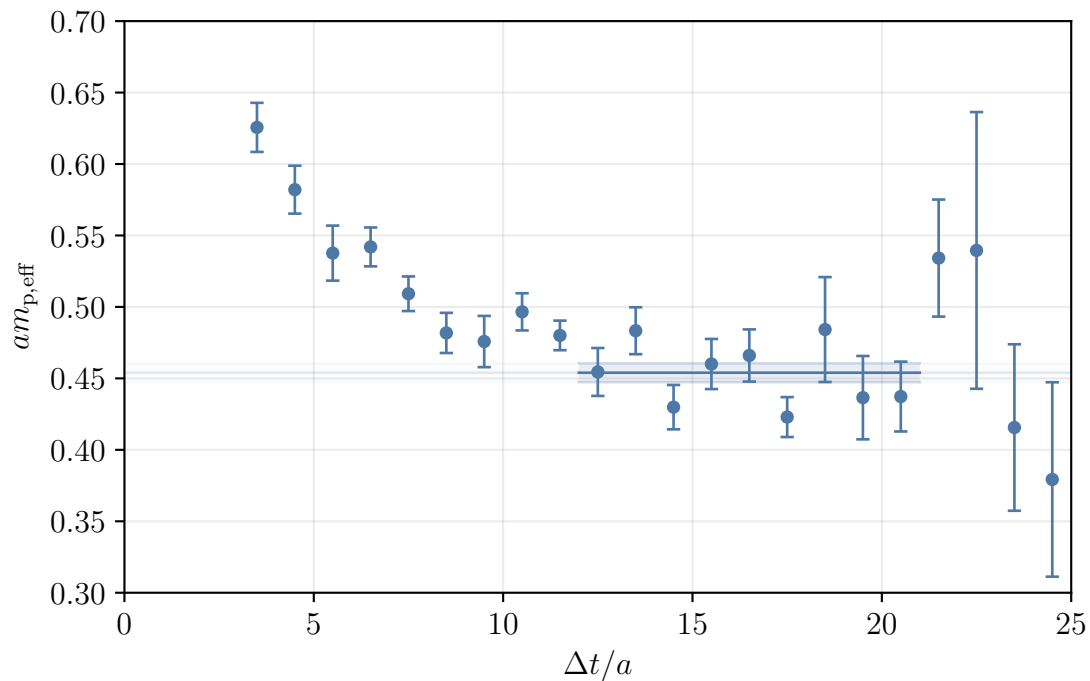


Figure 4.5: Proton effective mass with the transformed exponential fit of Fig. 4.4. Calculated on an $N = 342$ subset of Ensemble 1, with $m_\pi = 470$ MeV.

Here $\tilde{\chi}$ and χ are again interpolators coupling to QCD eigenstates, and \mathcal{O} is some local current operator, e.g. a quark bilinear such as $\bar{\psi}\gamma_\mu\gamma_5\psi$. Inserting two complete sets of states between the operators, and translating the operators to the spacetime origin through Section 5.2, we have

$$C_{\chi\mathcal{O}\tilde{\chi}}(x', y, x) = \sum_{\substack{X, \mathbf{k} \\ Y, \mathbf{l}}} \int \frac{\Delta^3 k}{(2\pi)^3} \frac{\Delta^3 l}{(2\pi)^3} \frac{e^{-E_X(\mathbf{k})(t'-\tau)} e^{-E_Y(\mathbf{l})(\tau-t)}}{2E_X(\mathbf{k}) 2E_Y(\mathbf{l})} e^{i\mathbf{k}\cdot(\mathbf{x}'-\mathbf{y})} e^{i\mathbf{l}\cdot(\mathbf{y}-\mathbf{x})} \langle \Omega | \chi(0) | X(\mathbf{k}) \rangle \langle X(\mathbf{k}) | \mathcal{O}(0) | Y(\mathbf{l}) \rangle \langle Y(\mathbf{l}) | \tilde{\chi}(0) | \Omega \rangle. \quad (4.53)$$

We define the Fourier-projected three-point function as

$$G_{\chi\mathcal{O}\tilde{\chi}}(\mathbf{p}', \mathbf{p}; t', \tau, t) \equiv \sum_{\mathbf{x}', \mathbf{y}} \Delta^3 x' \Delta^3 y e^{-i\mathbf{p}'\cdot(\mathbf{x}'-\mathbf{y})} e^{-i\mathbf{p}\cdot(\mathbf{y}-\mathbf{x})} C_{\chi\mathcal{O}\tilde{\chi}}(x', y, x), \quad (4.54)$$

where the sum can be taken over any two of the spatial variables. This expression projects momentum \mathbf{p}' and \mathbf{p} at the sink and source respectively, or equivalently, momentum \mathbf{p} at the source and an insertion of momentum $\mathbf{q} = \mathbf{p}' - \mathbf{p}$ through the current. Using the decomposition of the three-point function in Eq. (4.53), we have

$$G_{\chi\mathcal{O}\tilde{\chi}}(\mathbf{p}', \mathbf{p}; t', \tau, t) = \sum_{X, Y} \frac{e^{-E_X(\mathbf{p}')(t'-\tau)} e^{-E_Y(\mathbf{p})(\tau-t)}}{2E_X(\mathbf{p}') 2E_Y(\mathbf{p})} \langle \Omega | \chi(0) | X(\mathbf{p}') \rangle \langle X(\mathbf{p}') | \mathcal{O}(0) | Y(\mathbf{p}) \rangle \langle Y(\mathbf{p}) | \tilde{\chi}(0) | \Omega \rangle. \quad (4.55)$$

This expression forms the basis of hadronic matrix element calculations in lattice QCD. It includes the matrix elements of the operator \mathcal{O} for all states coupling to the interpolators, and hence includes transitions as well as forward matrix elements.

Analogously to the plateau-isolation method of Section 4.1, we may consider a simple analysis of the three-point function in the limit of large $(t' - \tau)$ and $(\tau - t)$ (i.e. sufficiently far from the source and sink times). In this regime, it is the lowest coupling state in the sum of exponentials that dominates, and hence we have

$$G_{\chi\mathcal{O}\tilde{\chi}}(\mathbf{p}', \mathbf{p}; t', \tau, t) \xrightarrow{\text{large } t'-\tau, \tau-t} \frac{e^{-E_{X_0}(\mathbf{p}')(t'-\tau)} e^{-E_{X_0}(\mathbf{p})(\tau-t)}}{2E_{X_0}(\mathbf{p}') 2E_{X_0}(\mathbf{p})} \sum_{r', r} \langle \Omega | \chi(0) | X_0(\mathbf{p}', r') \rangle \langle X_0(\mathbf{p}', r') | \mathcal{O}(0) | X_0(\mathbf{p}, r) \rangle \langle X_0(\mathbf{p}, r) | \tilde{\chi}(0) | \Omega \rangle. \quad (4.56)$$

Here r' and r again label the possibly degenerate eigenstates. One can then take the ratio of this quantity with two-point functions formed from $\tilde{\chi}$ and χ to eliminate the exponential time-dependence and overlap factors, and form a quantity

$$R_{\chi\mathcal{O}\tilde{\chi}}(\mathbf{p}', \mathbf{p}; t', \tau, t) \xrightarrow{\text{large } t'-\tau, \tau-t} \frac{1}{\Omega} \sum_{r', r} \langle \Omega | \chi(0) | X_0(\mathbf{p}', r') \rangle \langle X_0(\mathbf{p}', r') | \mathcal{O}(0) | X_0(\mathbf{p}, r) \rangle \langle X_0(\mathbf{p}, r) | \tilde{\chi}(0) | \Omega \rangle. \quad (4.57)$$

While plateau identification in the two-point function calculation is relatively unambiguous, it is possible to observe false plateaux in ratios of two and three-point functions, in cases where the source-current and current-sink separation are insufficiently large. This can lead to significant systematic shifts in the values determined for observables [93]. There are several alternative approaches to three-point function

analysis that attempt to address the excited-state issue, one of the most robust being the variational method already mentioned (see e.g. [94–101]). One of the advantages of the FH method we will discuss in the next chapter is that matrix elements are extracted from two-point functions, and excited-state control is much more straightforward.

4.2.1 Example: Vector Matrix Elements of the Pion

In the case of interpolators chosen to couple to spin-zero states with no additional degrees of freedom, the ratio of Eq. (4.57) becomes simply

$$R_{\chi\mathcal{O}\tilde{\chi}}(\mathbf{p}', \mathbf{p}; t', \tau, t) \stackrel{\text{large } t', \tau, t}{\propto} \langle X_0(\mathbf{p}') | \mathcal{O}(0) | X_0(\mathbf{p}) \rangle . \quad (4.58)$$

Suppose then, we wish to calculate the u contributions to form factor of the π^+ , which can be obtained from the vector matrix element

$$\langle \pi^+(\mathbf{p}') | \mathcal{V}_4^u(0) | \pi^+(\mathbf{p}) \rangle = [E_{\pi^+}(\mathbf{p}') + E_{\pi^+}(\mathbf{p})] F_{\pi^+}^u(Q^2) . \quad (4.59)$$

Here the vector current density is defined as

$$\mathcal{V}_\mu^f(x) \equiv \bar{\psi}_f(x) \gamma_\mu \psi_f(x) , \quad (4.60)$$

and the form factor $F_{\pi^+}(Q^2)$ is a function of the invariant momentum

$$Q^2 \equiv q^2 = (p' - p)^2 . \quad (4.61)$$

We will discuss the physical significance of the pion form factor further in Chapter 7. As we already have interpolators for the π^+ in Eqs. (4.21) and (4.22), we can construct the relevant three-point function,

$$\begin{aligned} C_{\pi^+, \mathcal{V}_4^u}(x', y, x) &\equiv \langle \chi_{\pi^+}(x') \mathcal{V}_4^u(y) \chi_{\pi^+}(x) \rangle \\ &= \langle \bar{d}(x') \gamma_5 u(x') \bar{u}(y) \gamma_4 u(y) \bar{u}(x) \gamma_5 d(x) \rangle . \end{aligned} \quad (4.62)$$

There are two possible fully Wick-contracted combinations of this expression. The first combination involves contractions between the current and the interpolators, and is referred to as the connected contribution,

$$\left[C_{\pi^+, \mathcal{V}_4^u}(x', y, x) \right]_{\text{conn}} = \left\langle \overbrace{\bar{d}(x') \gamma_5 \overbrace{u(x') \bar{u}(y) \gamma_4 \overbrace{u(y) \bar{u}(x)} \gamma_5 d(x)}^{\text{latt}}} \right\rangle . \quad (4.63)$$

This is represented diagrammatically in Fig. 4.6. The second combination involves no contractions between the current and the interpolators, and is referred to as the disconnected contribution,

$$\left[C_{\pi^+, \mathcal{V}_4^u}(x', y, x) \right]_{\text{disc}} = \left\langle \overbrace{\bar{d}(x') \gamma_5 \overbrace{u(x') \bar{u}(y) \gamma_4 \overbrace{u(y) \bar{u}(x)} \gamma_5 d(x)}^{\text{latt}}} \right\rangle , \quad (4.64)$$

This is illustrated in Fig. 4.7. It is important to note that the disconnected loop still couples to the three-point function through the background gauge field (gluon lines that are not shown).

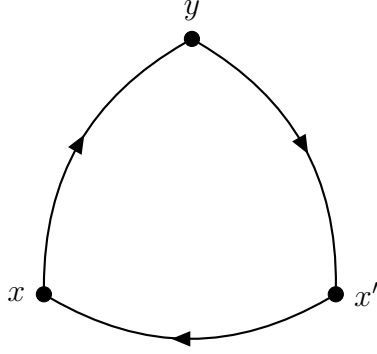


Figure 4.6: Diagram representing the connected contraction of Eq. (4.63)

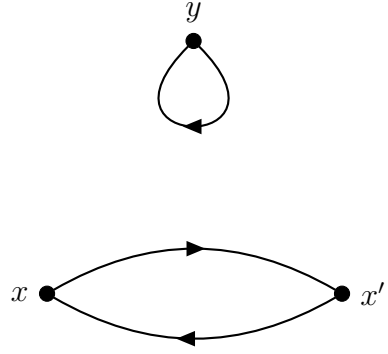


Figure 4.7: Diagram representing the disconnected contraction of Eq. (4.64).

The full three-point function is given by the sum of connected and disconnected contributions,

$$C_{\pi^+, \mathcal{V}_4^u}(x', y, x) = [C_{\pi^+, \mathcal{V}_4^u}(x', y, x)]_{\text{conn}} + [C_{\pi^+, \mathcal{V}_4^u}(x', y, x)]_{\text{disc}}, \quad (4.65)$$

and as in the case of spectroscopy with the π^0 operator in Section 4.1.1, the evaluation of the second contribution requires the calculation of all-to-all propagators. This is an infeasible task for any reasonably sized lattice and Dirac operator. Stochastic methods take the approach of sampling the full space of all-to-all propagators to estimate these contributions, and have made significant progress in recent years (see e.g. [81, 102–105] amongst many others). However these techniques are noisy and require complex analyses. This is the primary motivation for the FH method described in Chapter 5, which provides an alternative approach to accessing disconnected contributions.

Fortunately, in this case, the disconnected contributions to the π^+ form factor from the u and d quarks cancel in the isospin-symmetric limit (this is not true in general). In isolating only the u contribution, we are restricted to calculating the connected contribution, by first constructing the Fourier-projected three-point function,

$$G_{\pi^+, \mathcal{V}_4^u}(\mathbf{p}', \mathbf{p}; t', \tau, t) \equiv \sum_{\mathbf{x}', \mathbf{y}} \Delta^3 x' \Delta^3 y e^{-i\mathbf{p}' \cdot (\mathbf{x}' - \mathbf{y})} e^{-i\mathbf{p} \cdot (\mathbf{y} - \mathbf{x})} C_{\pi^+, \mathcal{V}_4^u}(x', y, x), \quad (4.66)$$

which at large times isolates the vector matrix element,

$$G_{\pi^+, \mathcal{V}_4^u}(\mathbf{p}', \mathbf{p}; t', \tau, t) \xrightarrow{\text{large } t' - \tau, \tau - t} Z_{\chi, \pi^+}(\mathbf{p}') \tilde{Z}_{\chi, \pi^+}(\mathbf{p}) \frac{e^{-E_{\pi^+}(\mathbf{p}')(t' - \tau)}}{2E_{\pi^+}(\mathbf{p}')} \frac{e^{-E_{\pi^+}(\mathbf{p})(\tau - t)}}{2E_{\pi^+}(\mathbf{p})} \langle \pi^+(\mathbf{p}') | \mathcal{V}_4^u(0) | \pi^+(\mathbf{p}) \rangle. \quad (4.67)$$

Taking a ratio of this quantity with two-point functions constructed according to Section 4.1.1, we can eliminate the exponential time-dependence and obtain

$$R_{\pi^+, \mathcal{V}_4^u}(\mathbf{p}', \mathbf{p}; t', \tau, t) \xrightarrow{\text{large } t' - \tau, \tau - t} \frac{\langle \pi(\mathbf{p}') | \mathcal{V}_4^u(0) | \pi(\mathbf{p}) \rangle}{\langle \pi(\mathbf{p}') | \pi(\mathbf{p}) \rangle} = [E_{\pi}(\mathbf{p}') + E_{\pi}(\mathbf{p})] F_{\pi^+}^u(Q^2). \quad (4.68)$$

So in the large-time separation limit, we extract the appropriate contribution to the form factor, up to some known kinematic factors.

4.2.2 Example: Axial Charge of the Proton

In the case of interpolators coupling to spin-half baryon states, the ratio of Eq. (4.57) becomes

$$R_{\chi\mathcal{O}\tilde{\chi}}(\Gamma_{\text{proj}}; \mathbf{p}', \mathbf{p}; t', \tau, t) \stackrel{\text{large } t'-\tau, \tau-t}{\propto} F_3(\Gamma_{\text{proj}}, \Gamma_{\mathcal{O}, X_0}; \mathbf{p}', \mathbf{p}, m_{X_0}), \quad (4.69)$$

where Γ_{proj} is the Dirac projector contracted with the interpolators as in Section 4.1.2. Here $\Gamma_{\mathcal{O}, X_0}$ is the vertex function defined by the relation

$$\langle X(\mathbf{p}', \sigma') | \mathcal{O}(0) | X(\mathbf{p}, \sigma) \rangle = \bar{u}(p', \sigma') \Gamma_{\mathcal{O}, X} u(p, \sigma), \quad (4.70)$$

and the function F_3 is defined as

$$F_3(\Gamma_{\text{proj}}, \Gamma_{\mathcal{O}, X}; \mathbf{p}', \mathbf{p}, m_X) \equiv \frac{1}{4} \sum_{\sigma' \sigma} [\Gamma_{\text{proj}}]_{\alpha\beta} u_\alpha(p', \sigma') \bar{u}(p', \sigma') \Gamma_{\mathcal{O}, X} u(p, \sigma) \bar{u}_\beta(p, \sigma). \quad (4.71)$$

Explicit values for F_3 for different Dirac projectors and vertex functions are given in Appendix G.

Suppose we want to calculate the axial charge of the u quark in the proton, Δu_p , which can be obtained through the forward axial matrix element

$$\langle p(\mathbf{p}, \sigma) | \mathcal{A}_3^u(0) | p(\mathbf{p}, \sigma) \rangle = 2im_p s_3(p, \sigma) \Delta u_p. \quad (4.72)$$

Here the axial current density is defined as

$$\mathcal{A}_\mu^f(x) \equiv \bar{\psi}_f(x) \gamma_\mu \gamma_5 \psi_f(x), \quad (4.73)$$

m_p is the proton mass, and s_μ is the four-spin vector (described in Appendix F). We will discuss the physical relevance of the axial charge in more depth in Chapter 6. In this case, the spin-dependence of the matrix element indicates we need to consider polarised proton states, and so we make use of the polarised projector

$$\Gamma_{\text{pol}\pm} \equiv \Gamma_{P_\pm} \Gamma_{S_\pm} = \frac{1}{2} (\mathbb{I} + \gamma_4) \frac{1}{2} (\mathbb{I} \mp i \hat{\mathbf{e}} \cdot \boldsymbol{\gamma} \gamma_5). \quad (4.74)$$

This projects definite positive parity and definite up/down spin along $\hat{\mathbf{e}}$. Using the proton interpolators of Eq. (4.44) the relevant three-point function is

$$C_{p, \mathcal{A}_3^u}(\Gamma_{\text{pol}\pm}; x', y, x) \equiv [\Gamma_{\text{pol}\pm}]_{\alpha\beta} \langle [\chi_p(x')]_\alpha \mathcal{A}_3^u(y) [\tilde{\chi}_p(x)]_\beta \rangle, \quad (4.75)$$

given in full by

$$C_{p, \mathcal{A}_3^u}(\Gamma_{\text{pol}\pm}; x', y, x) = [\Gamma_{\text{pol}\pm}]_{\alpha\beta} \epsilon^{a'b'c'} \epsilon^{abc} \left\langle u_\alpha^a(x') \left([u^T(x')] \right)^{b'} C \gamma_5 [d(x')]^c \right\rangle \bar{u}(y) \gamma_\mu \gamma_5 u(y) \left([\bar{u}(x)]^a C \gamma_5 [\bar{d}(x)]^b \right) \bar{u}_\beta^c(x), \quad (4.76)$$

where we have omitted some Dirac indices, implied by matrix-vector notation. The two classes of contractions for the u quark are presented diagrammatically in Fig. 4.8. As in Section 4.2.1, contractions of the three-point function result in the same disconnected contributions as we have previously encountered.

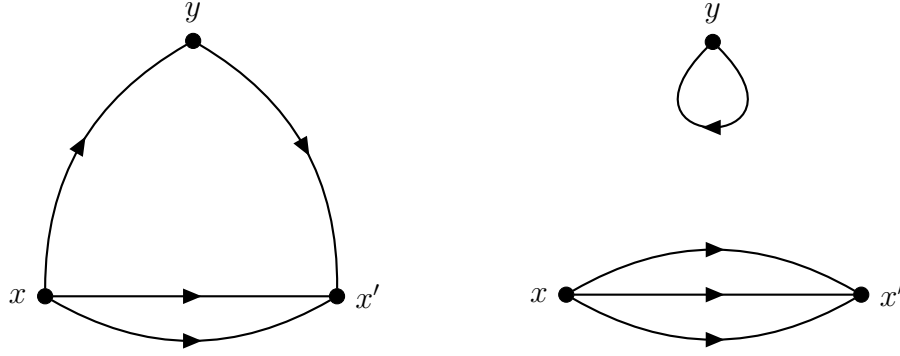


Figure 4.8: Diagrams representing the connected and disconnected contractions of Eq. (4.75).

The vertex function for the axial current is given by

$$\Gamma_{\mathcal{A}_{\mu,p}^f} = \gamma_{\mu}\gamma_5 g_{A,p}^f(Q^2) - i\gamma_5 \frac{q_{\mu}}{2m_p} g_{AP,p}^f(Q^2), \quad (4.77)$$

and so we can calculate the relevant F_3 function,

$$F_3(\Gamma_{\text{pol}\pm}, \Gamma_{\mathcal{A}_3^y,p}; \mathbf{p}' = \mathbf{0}, \mathbf{p} = \mathbf{0}, m_p) = \pm 2im_p^2 \Delta u_p. \quad (4.78)$$

Hence at large time separations, the ratio of three and two-point functions goes as

$$R_{p,\mathcal{A}_3^y}(\Gamma_{\text{pol}\pm}; \mathbf{p}' = \mathbf{0}, -\mathbf{p}; t', \tau, t) \stackrel{\text{large}}{\propto} t'^{-\tau, \tau-t} \pm 2im_p^2 \Delta u_p. \quad (4.79)$$

That is, the constructed ratio plateaus to Δu_p , up to known kinematic factors.

4.2.3 Example: Vector Matrix Elements of the Proton

As a final example, suppose we wish to calculate the d contribution to the Sachs magnetic form factor of the proton, which can be accessed through a spatial vector matrix element in the Breit frame,

$$\langle p(\mathbf{q}/2, \sigma') | \mathcal{V}_2^d(0) | p(-\mathbf{q}/2, \sigma) \rangle = [\mathbf{s} \times \mathbf{q}]_2 G_{M,p}^d(Q^2) \delta_{\sigma'\sigma}. \quad (4.80)$$

Here the vector current density is as defined in Eq. (4.60), and the invariant Q^2 is as defined in Eq. (4.61). We will discuss the electromagnetic form factors of the proton in more depth in Chapter 7. Using the proton interpolators of Eq. (4.44) and the polarised, positive-parity projector, the relevant three-point function is

$$C_{p,\mathcal{V}_2^d}(\Gamma_{\text{pol}\pm}; x', y, x) = [\Gamma_{\text{pol}\pm}]_{\alpha\beta} \langle [\chi_P(x')]_{\alpha} \mathcal{V}_2^d(y) [\tilde{\chi}_P(x)]_{\beta} \rangle, \quad (4.81)$$

given in full by

$$C_{p,\mathcal{V}_2^d}(\Gamma_{\text{pol}\pm}; x', y, x) = \epsilon^{a'b'c'} \epsilon^{abc} [\Gamma_{\text{pol}\pm}]_{\alpha\beta} \langle [u(x')]_{\alpha}^{a'} \left([u^T(x')] \right)^{b'} C\gamma_5 [d(x')]^{c'} \bar{d}(y) \gamma_2 d(y) (\bar{u}_a(x) C\gamma_5 \bar{d}_b^T(x)) [\bar{u}(x)]_{\beta}^c \rangle. \quad (4.82)$$

Again, considering all possible contractions of this three-point function, we obtain both connected and disconnected contributions to this quantity. Unlike in the

calculation of the π^+ form factor however, the u and d contributions to the full form factor of the proton do not cancel in the isospin-symmetric limit. Ignoring the issue of disconnected contributions for the moment, one can show that the vertex function for the vector current,

$$\Gamma_{\mathcal{V}_\mu^f, \text{p}} = \gamma_\mu F_{1,\text{p}}^f(Q^2) + \sigma_{\mu\nu} \frac{q_\nu}{2m_{\text{p}}} F_{2,\text{p}}^f(Q^2), \quad (4.83)$$

where $F_{1,\text{p}}^f$ and $F_{2,\text{p}}^f$ are individual flavour contributions to the Pauli and Dirac form factors of the proton. Since the function F_3 is linear in its Dirac matrices, we can calculate

$$F_3(\Gamma_{\text{pol}\pm}, \Gamma_{\mathcal{V}_2^d, \text{p}}; \mathbf{q}/2, -\mathbf{q}/2, m_{\text{p}}) = \frac{1}{4} [E_{\text{p}}(\mathbf{q}/2) + m_{\text{p}}] [\mathbf{s} \times \mathbf{q}]_2 G_{\text{M},\text{p}}^d(Q^2), \quad (4.84)$$

where we have used the definition of the Sachs magnetic form factor,

$$G_{\text{M},\text{p}}^f(Q^2) \equiv F_{1,\text{p}}^f(Q^2) + F_{2,\text{p}}^f(Q^2). \quad (4.85)$$

Hence, at sufficiently large source-current-sink separation, the ratio of three and two-point functions gives

$$R_{\text{p}, \mathcal{V}_2^d}(\Gamma_{\text{pol}\pm}; \mathbf{q}/2, -\mathbf{q}/2; t', \tau, t) \stackrel{\text{large } t'-\tau, \tau-t}{\propto} \frac{1}{4} [E_{\text{p}}(\mathbf{q}/2) + m_{\text{p}}] [\mathbf{s} \times \mathbf{q}]_2 G_{\text{M},\text{p}}^d(Q^2). \quad (4.86)$$

That is, we can extract the connected contribution to $G_{\text{M},\text{p}}^d$ up to known kinematics factors.

Chapter 5

The Feynman-Hellmann Theorem

“Formulas have been developed to calculate the forces in a molecular system directly, rather than indirectly through the agency of energy. This permits an independent calculation of the slope of the curves of energy vs. position of the nuclei, and may thus increase the accuracy, or decrease the labour involved in the calculation of these curves.”

—R. P. Feynman, Phys. Rev. 56 (1939) [106]

The Feynman-Hellmann (FH) theorem is a well-known result of quantum mechanics, relating derivatives of the Hamiltonian to derivatives of energy eigenvalues. Proven by various authors in the 1930s [106–109], the result has important applications in materials physics, molecular chemistry and molecular biology [110–113]. Extensions of the theorem to QFT [114] have for many years been used in lattice QCD to calculate sigma terms [115–118]. The use of varying electromagnetic fields to calculate magnetic moments and electric polarisabilities [119–123] is another related application.

As originally derived in quantum mechanics, the FH theorem states that for a Hamiltonian depending on some continuous parameter λ , the derivative of the energy of an eigenstate $|\psi\rangle$ is given by

$$\frac{dE_\psi}{d\lambda} = \langle\psi|\frac{d\hat{H}}{d\lambda}|\psi\rangle. \quad (5.1)$$

In the original context, one identifies the derivative of the energy as being proportional to a force exerted on the particle described by $|\psi\rangle$,

$$F_\psi = -\frac{dE_\psi}{d\lambda}. \quad (5.2)$$

Therefore, once the configuration (and hence Hamiltonian) of a system is known, the forces can be obtained through Eq. (5.1), and resulting motion of the system can be determined through classical mechanics. In [106] for example, this is applied to a system of nuclei and electrons.

The FH relation allows sigma terms to be calculated in lattice QCD through the shifts in hadron masses resulting from changes in the quark masses. Specifically, shifts in hadron masses are related to the scalar matrix elements,

$$\frac{\partial m_X}{\partial m_f} \propto \langle X(\mathbf{p})|\bar{\psi}_f(0)\psi_f(0)|X(\mathbf{p})\rangle = \frac{\sigma_f}{m_f}. \quad (5.3)$$

This application makes use of a parameter already present in the QCD Lagrangian. The idea of the method implemented in this thesis is to calculate matrix elements of an extended set of operators by introducing new terms to the Lagrangian. This is based on the proposal of [124] amongst others, and several variants of the approach are being pursued [125, 126].

In this chapter we begin in Section 5.1 by deriving the FH relation in quantum mechanics. We then make a simple extension to lattice QCD through a substitution argument in Section 5.2, and introduce the FH method. We finish by deriving the same results through a path integral approach in Section 5.3.

5.1 Hamiltonian Quantum Mechanics

5.1.1 Non-Degenerate Eigenstates

Consider a Hermitian, λ -dependent Hamiltonian operator \hat{H} with a set of orthogonal eigenstates $|\psi_n\rangle$, such that at some point λ_0 ,

$$\hat{H}(\lambda_0) |\psi_n(\lambda_0)\rangle = E_n(\lambda_0) |\psi_n(\lambda_0)\rangle, \quad (5.4)$$

$$\langle \psi_n(\lambda_0) | \psi_m(\lambda_0) \rangle = \delta_{nm} \langle \psi_n(\lambda_0) | \psi_n(\lambda_0) \rangle. \quad (5.5)$$

Here we imply by the labelling of the energies and eigenstates in terms of λ that these quantities are continuous with respect to λ about λ_0 . Taking the derivative of Eq. (5.4) with respect to λ , we have

$$\left(\hat{H} - E_n \right) \frac{d|\psi_n\rangle}{d\lambda} + \left(\frac{d\hat{H}}{d\lambda} - \frac{dE_n}{d\lambda} \right) |\psi_n\rangle = 0, \quad (5.6)$$

where we have omitted explicit λ -dependence for clarity, assuming all quantities are to be evaluated at λ_0 . Taking the inner product of $\langle \psi_n |$ with Eq. (5.6), and using the Hermiticity of the Hamiltonian at λ_0 , we obtain

$$\frac{dE_n}{d\lambda} = \frac{\langle \psi_n | \frac{d\hat{H}}{d\lambda} | \psi_n \rangle}{\langle \psi_n | \psi_n \rangle}. \quad (5.7)$$

This is the familiar form of the FH theorem, and is true about any point λ_0 where the Hamiltonian is Hermitian, and the derivative of the wave function in Eq. (5.6) is well-defined. That is, the wavefunctions are differentiable at λ_0 . The denominator is often omitted by virtue of unit-normalised eigenstates, however we will retain it for when we later consider the extension to lattice QCD, and the normalisation of states is relativistic.

Next, let's consider the derivative of the wavefunction as it appears in Eq. (5.6). Since the unperturbed eigenstates form a complete set, we can write at λ_0 ,

$$\frac{d|\psi_n\rangle}{d\lambda} = \sum_{\substack{l \\ l \neq n}} c_{nl} |\psi_l\rangle. \quad (5.8)$$

We are free to omit the $m = n$ term, since if $\frac{d|\psi_n\rangle}{d\lambda}$ satisfies Eq. (5.6), then so does $\frac{d|\psi_n\rangle}{d\lambda} + \alpha |\psi_n\rangle$ for any α , and we can choose to subtract this term from the expansion. The perturbed wavefunction will not in general be normalised, however. Substituting

Eq. (5.8) into Eq. (5.6), taking the inner product with $\langle\psi_m|$ for some $m \neq n$, we obtain

$$c_{nm} = \frac{1}{(E_n - E_m)} \frac{\langle\psi_m|\frac{d\hat{H}}{d\lambda}|\psi_n\rangle}{\langle\psi_m|\psi_m\rangle}. \quad (5.9)$$

Substituting these into Eq. (5.8) we obtain an expression for the derivative of the wavefunction,

$$\frac{d|\psi_n\rangle}{d\lambda} = \sum_{\substack{m \\ m \neq n}} \frac{1}{(E_n - E_m)} \frac{\langle\psi_m|\frac{d\hat{H}}{d\lambda}|\psi_n\rangle}{\langle\psi_m|\psi_m\rangle} |\psi_m\rangle. \quad (5.10)$$

In the case where the original eigenstates are non-degenerate, this expression is well-defined. However, if $E_n = E_m$ for any $n \neq m$, then the energy denominator goes to zero, and the derivative is undefined. In this case, Eq. (5.6) is ill-defined, and our result for the first-order energy shift in Eq. (5.7) is untrustworthy. Eq. (5.10) may be well-defined if $\langle\psi_m|\frac{d\hat{H}}{d\lambda}|\psi_n\rangle$ is also zero, which suggests that in order to derive an expression for the energy shifts of degenerate spectra, we need to find new eigenstates which diagonalise the first derivative of the Hamiltonian.

5.1.2 Degenerate Eigenstates

Suppose we have a λ -dependent Hamiltonian \hat{H} and a set of orthogonal (but possibly energy-degenerate) eigenstates $|\psi_n^r\rangle$, with degeneracy labelled by a superscript r or s , such that at some point λ_0 we have

$$\hat{H}(\lambda_0) |\psi_n^r(\lambda_0)\rangle = E_n(\lambda_0) |\psi_n^r(\lambda_0)\rangle, \quad (5.11)$$

$$\langle\psi_n^r(\lambda_0)|\psi_m^s(\lambda_0)\rangle = \delta_{nm}\delta^{rs} \langle\psi_n^r(\lambda_0)|\psi_n^r(\lambda_0)\rangle. \quad (5.12)$$

In the previous section, the derivatives of eigenstates were ill-defined for a degenerate spectrum. However, Eq. (5.10) suggested that if we can find eigenstates that diagonalise the derivative of the Hamiltonian, we may be able to obtain well-defined derivatives. Hence our strategy is to attempt to form ‘good’ linear combinations of the original eigenstates,

$$|\phi_n^r(\lambda_0)\rangle = \sum_t v_n^{rt} |\psi_n^t(\lambda_0)\rangle, \quad (5.13)$$

and consider the eigenvalue problem in terms of these new eigenstates,

$$\hat{H}(\lambda_0) |\phi_n^r(\lambda_0)\rangle = E_n^r(\lambda_0) |\phi_n^r(\lambda_0)\rangle. \quad (5.14)$$

Here we label the energy eigenvalues with an additional degeneracy index to track the possible degeneracy-breaking that occurs. When there is no perturbation of λ ,

$$E_n^r(\lambda_0) = E_n(\lambda_0). \quad (5.15)$$

Taking the derivative of Eq. (5.14) with respect to λ about λ_0 , we obtain

$$\left(\hat{H} - E_n^r\right) \frac{d|\phi_n^r\rangle}{d\lambda} + \left(\frac{d\hat{H}}{d\lambda} - \frac{dE_n^r}{d\lambda}\right) |\phi_n^r\rangle = 0, \quad (5.16)$$

where again, we have omitted explicit λ -dependence, and assumed all quantities are to be evaluated at λ_0 . Taking the inner product of $\langle \psi_n^s |$ with Eq. (5.16), and substituting in the decomposition of Eq. (5.13), we obtain

$$\sum_t \frac{\langle \psi_n^s | \frac{d\hat{H}}{d\lambda} | \psi_n^t \rangle}{\langle \psi_n^s | \psi_n^s \rangle} v_n^{rt} = \frac{dE_n^r}{d\lambda} v_n^{rs}. \quad (5.17)$$

This is an eigenvalue equation for the matrix

$$W_n^{rs} \equiv \frac{\langle \psi_n^r | \frac{d\hat{H}}{d\lambda} | \psi_n^s \rangle}{\langle \psi_n^r | \psi_n^r \rangle}, \quad (5.18)$$

where the eigenvectors $(v_n^r)^s$ determine the new ‘good’ eigenstates through Eq. (5.13), and the eigenvalues are the first derivatives of the corresponding energies. The matrix formed from the eigenvectors diagonalises W_n , and so the derivative of the Hamiltonian is diagonal in the new eigenstates. This matches our expectation from examining Eq. (5.10).

We can check that the derivatives of the new wavefunctions are indeed well-defined. The new eigenstates form a complete set, and so analogously to Eq. (5.8), we may write the first derivatives of the new eigenstates as

$$\frac{d|\phi_n^r\rangle}{d\lambda} = \sum_{\substack{l,t \\ l \neq n}} c_{nl}^{rt} |\phi_l^t\rangle, \quad (5.19)$$

where the $m = n$ terms are omitted by analogous arguments to those made in the non-degenerate case. Taking the inner product of $\langle \phi_m^s |$ with Eq. (5.16) for $m \neq n$ and $s \neq r$, and substituting the decomposition of the derivative, we obtain

$$c_{nm}^{rs} = \frac{1}{E_n - E_m} \frac{\langle \phi_m^s | \frac{d\hat{H}}{d\lambda} | \phi_n^r \rangle}{\langle \phi_m^s | \phi_m^s \rangle}, \quad (5.20)$$

and so the first derivatives of the new eigenstates are given by

$$\frac{d|\phi_n^r\rangle}{d\lambda} = \sum_{\substack{m,s \\ m \neq n}} \frac{1}{E_n - E_m} \frac{\langle \phi_m^s | \frac{d\hat{H}}{d\lambda} | \phi_n^r \rangle}{\langle \phi_m^s | \phi_m^s \rangle} |\phi_m^s\rangle. \quad (5.21)$$

The energy denominator never goes to zero, as the energy eigenvalues are distinct for $m \neq n$. Hence the derivatives of the new eigenstates are well-defined. Taking the overlap of $\langle \phi_n^r |$ with Eq. (5.16), we obtain

$$\frac{dE_n^r}{d\lambda} = \frac{\langle \phi_n^r | \frac{d\hat{H}}{d\lambda} | \phi_n^r \rangle}{\langle \phi_n^r | \phi_n^r \rangle}. \quad (5.22)$$

Hence we see that Eq. (5.7) applies to the newly formed eigenstates, as expected.

5.1.3 Summary: The Feynman-Hellmann Theorem

Suppose λ -dependent Hamiltonian \hat{H} Hermitian at some point λ_0 , with possibly degenerate eigenstates $|\psi_n^r\rangle$ and eigenvalues E_n . For each energy level n , if the matrix

$$W_n^{rs} \equiv \frac{\langle \psi_n^r | \frac{d\hat{H}}{d\lambda} | \psi_n^s \rangle}{\langle \psi_n^r | \psi_n^r \rangle}. \quad (5.23)$$

is diagonal, then the first derivatives of the energy about λ_0 are given by

$$\frac{dE_n^r}{d\lambda} = W_n^{rr} = \frac{\langle \psi_n^r | \frac{d\hat{H}}{d\lambda} | \psi_n^r \rangle}{\langle \psi_n^r | \psi_n^r \rangle}, \quad r \text{ not summed.} \quad (5.24)$$

Otherwise, the derivatives of the eigenstates are not well-defined about λ_0 , and instead the eigenvectors v_n^r of W_n determine new linear combinations of the original eigenstates,

$$|\phi_n^r\rangle = \sum_s (v_n^r)^s |\psi_n^s\rangle, \quad (5.25)$$

which do have well-defined derivatives. The corresponding eigenvalues give the first derivatives of the energies of the new eigenstates with respect to λ . The derivatives of the energies also be found through Eq. (5.24) in terms of the new eigenstates.

There are a few important things to note about these results. Firstly, the Hamiltonian is only required to be Hermitian at λ_0 , and hence the result applies to Hamiltonians such as

$$\hat{H}(\lambda) = \hat{H} + \lambda \hat{V}, \quad (5.26)$$

where the potential \hat{V} is non-Hermitian. The energy shifts will in general be complex, however. This will be important in our calculation of disconnected contributions to quark axial charges in Chapter 6, where we include a non-Hermitian potential in the QCD Lagrangian to avoid introducing a sign-problem in gauge-field generation.

Secondly, a sufficient condition for W_n to be diagonal is that the degenerate eigenstates are distinct eigenstates of an operator \hat{O} commuting with the derivative of the Hamiltonian at λ_0 . That is, if the degenerate eigenstates can be distinguished by their distinct eigenvalues with an expanded set of operators commuting with $\frac{d\hat{H}}{d\lambda}$, then these eigenstates are already ‘good’ eigenstates. This means that for derivatives of the Hamiltonian commuting with the spin operator, for example, we do not need to consider the effect of spin-degeneracy on the energy shifts.

5.2 Hamiltonian Lattice QCD

We can now translate the results of Section 5.1 to a lattice setting. The Hamiltonian operator becomes an integrated Hamiltonian density,

$$\hat{H} \longrightarrow \sum_{\mathbf{x}} \Delta^3 x \mathcal{H}(x), \quad (5.27)$$

and the natural particle eigenstates include definite momentum quantum numbers,

$$|\psi_n^r\rangle \longrightarrow |X(\mathbf{p}, r)\rangle, \quad (5.28)$$

$$E_n \longrightarrow E_X(\mathbf{p}). \quad (5.29)$$

Here we are explicitly labelling degenerate states, which we generally ignored in Chapter 4. These states have relativistic normalisation

$$\langle X(\mathbf{p}, r) | Y(\mathbf{q}, s) \rangle = 2E_X(\mathbf{p}) (2\pi)^3 \delta_{XY} \delta_{rs} \delta^3(\mathbf{p} - \mathbf{q}). \quad (5.30)$$

For each set of degenerate eigenstates, the matrix of Eq. (5.23) becomes

$$W_X(\mathbf{p}', r'; \mathbf{p}, r) = \frac{1}{2E_X(\mathbf{p})} \frac{1}{V} \sum_{\mathbf{x}} \Delta^3 x \langle X(\mathbf{p}', r') | \frac{d\mathcal{H}(x)}{d\lambda} | X(\mathbf{p}, r) \rangle, \quad (5.31)$$

where we have used the properties of the Dirac delta in the finite volume given in Eq. (4.4). If the matrix of Eq. (5.31) is diagonal, then the first derivative of the energy of the r th degenerate state is given by

$$\frac{dE_X(\mathbf{p}, r)}{d\lambda} = \frac{1}{2E_X(\mathbf{p})} \frac{1}{V} \sum_{\mathbf{x}} \Delta^3 x \langle X(\mathbf{p}, r) | \frac{d\mathcal{H}(x)}{d\lambda} | X(\mathbf{p}, r) \rangle. \quad (5.32)$$

If W_X is not diagonal, we first construct new eigenstates from its eigenvectors, and apply Eq. (5.32) to these new eigenstates (correctly normalised).

There are two specific cases of Hamiltonian derivatives that are useful for us to consider, the first being a derivative that is a translationally invariant. Rotational symmetry leads to degeneracy of states with momentum in different directions, however if the derivative of the Hamiltonian density can be translated to the origin through Section 5.2, or equivalently, the momentum operator commutes with the derivative of the Hamiltonian, then the matrix in Eq. (5.31) is diagonal in momentum,

$$W_X(\mathbf{p}', r'; \mathbf{p}, r) = \frac{1}{2E_X(\mathbf{p})} \langle X(\mathbf{p}', r') | \frac{d\mathcal{H}(0)}{d\lambda} | X(\mathbf{p}, r) \rangle \delta_{\mathbf{p}', \mathbf{p}}. \quad (5.33)$$

Hence, we need only need to consider degeneracies with respect to the other quantum numbers,

$$W_X(\mathbf{p}; r'; r) = \frac{1}{2E_X(\mathbf{p})} \langle X(\mathbf{p}, r') | \frac{d\mathcal{H}(0)}{d\lambda} | X(\mathbf{p}, r) \rangle. \quad (5.34)$$

If W_X is diagonal in r' and r as well, then the energy derivatives are given by

$$\frac{dE_X(\mathbf{p}, r)}{d\lambda} = \frac{1}{2E_X(\mathbf{p})} \langle X(\mathbf{p}, r) | \frac{d\mathcal{H}(0)}{d\lambda} | X(\mathbf{p}, r) \rangle. \quad (5.35)$$

Eqs. (5.34) and (5.35) will be most useful when we attempt to calculate the forward matrix elements of hadrons.

The second case we consider is when the derivative of the Hamiltonian density takes the form

$$\frac{d\mathcal{H}(x)}{d\lambda} = (e^{i\mathbf{q}\cdot\mathbf{x}} + e^{-i\mathbf{q}\cdot\mathbf{x}}) \mathcal{O}(x), \quad (5.36)$$

where \mathbf{q} is some three-momentum, and the operator \mathcal{O} can be translated to the origin through . In this case, the matrix of Eq. (5.31) is given by

$$W_X(\mathbf{p}', r'; \mathbf{p}, r) = \frac{1}{2E_X(\mathbf{p})} \langle X(\mathbf{p}', r') | \mathcal{O}(0) | X(\mathbf{p}, r) \rangle \delta_{\mathbf{p}', \mathbf{p} \pm \mathbf{q}}. \quad (5.37)$$

That is, terms in the matrix which do not satisfy $\mathbf{p} \pm \mathbf{q} = \mathbf{p}'$ are zero. Eq. (5.37) will be useful when we consider the calculation of the non-forward matrix elements of hadrons.

5.2.1 The Feynman-Hellmann Method

We are now ready to describe the FH approach to calculating hadron observables in lattice QCD. Suppose we wish to determine matrix elements of the form

$$\langle X(\mathbf{p}', r') | \mathcal{O}(0) | X(\mathbf{p}, r) \rangle, \quad (5.38)$$

for some translationally invariant operator \mathcal{O} . We begin by adding a new term to the QCD Hamiltonian density

$$\mathcal{H}(x) \longrightarrow \mathcal{H}'(x, \lambda) = \mathcal{H}(x) + \lambda \left(e^{i\mathbf{q}\cdot\mathbf{x}} + e^{-i\mathbf{q}\cdot\mathbf{x}} \right) \mathcal{O}(x), \quad (5.39)$$

so that the derivative of the Hamiltonian is given by

$$\left. \frac{d\mathcal{H}'(x, \lambda)}{d\lambda} \right|_{\lambda=0} = \left(e^{i\mathbf{q}\cdot\mathbf{x}} + e^{-i\mathbf{q}\cdot\mathbf{x}} \right) \mathcal{O}(x). \quad (5.40)$$

We then form the matrix of Eq. (5.37),

$$W_X(\mathbf{p}', r'; \mathbf{p}, r) = \frac{1}{2E_X(\mathbf{p}')} \langle X(\mathbf{p}', r') | \mathcal{O}(0) | X(\mathbf{p}, r) \rangle \delta_{\mathbf{p}', \mathbf{p} \pm \mathbf{q}}. \quad (5.41)$$

If $\mathbf{q} = \mathbf{0}$, and W_X is diagonal in all other degeneracies, then we have

$$\left. \frac{dE_X(\mathbf{p}, r)}{d\lambda} \right|_{\lambda=0} = \frac{1}{2E_X(\mathbf{p})} \langle X(\mathbf{p}, r) | \mathcal{O}(0) | X(\mathbf{p}, r) \rangle, \quad (5.42)$$

where the matrix element is evaluated at $\lambda = 0$ (at the physical point). Otherwise if $\mathbf{q} \neq \mathbf{0}$ or W_X is not diagonal in some degeneracies, we find the eigenvectors and eigenvalues of W_X , which give new QCD eigenstates and the corresponding first derivatives of their energies. In either case, we obtain a relationship between derivatives of the energies of QCD eigenstates, and the matrix elements of interest. The energies can be calculated using the methods of Section 4.1 for various values of λ , and the derivative calculated to determine the matrix elements.

For sets of degenerate eigenstates not satisfying $\mathbf{p}' = \mathbf{p} \pm \mathbf{q}$, W_X will have all zero elements, and there will be no corresponding first-order energy shifts. For this reason, we can only calculate non-forward matrix elements for Breit frame kinematics.

In order to implement the modification of Eq. (5.39) in lattice QCD, we need to add additional terms to the fermion action of Section 3.1.2. This modification can in general be made at two stages in a lattice calculation. The first is during the generation of gauge fields through the HMC algorithm, where the probabilistic weighting of Eq. (3.36) includes the determinant of the fermion operator. The second is during the inversion of the fermion operator to calculate quark propagators according to Eq. (3.38). Respectively, these modifications allow access to the disconnected or connected pieces of matrix elements.

We will see in Chapters 6 to 8 that the FH approach has many advantages over the standard three-point function techniques discussed in Section 4.2. Since matrix elements are calculated through energy shifts, we need only analyse lattice two-point functions, and so the control of excited states is much simpler. Disconnected contributions are straightforward to include, requiring only the generation of new gauge fields. While this may seem unnecessarily costly, we will show in Chapter 6 that in comparison to stochastic estimations of disconnected contributions, the FH approach is at least competitive in terms of signal-to-cost. Finally, the way in which non-forward matrix elements are calculated gives significant improvements in signal-to-noise ratios, as we will show in Chapter 7.

Below, we will discuss three specific examples of the FH method.

5.2.2 Example: Axial Charge of the Proton

Suppose we want to calculate the axial charge of the u quark in the proton Δu_p , as in Section 4.2.2, but through the FH method. Recall that this can be defined through the forward axial matrix element

$$\langle p(\mathbf{p}, \sigma) | \mathcal{A}_3^u(0) | p(\mathbf{p}, \sigma) \rangle = 2im_p s_3(p, \sigma) \Delta u_p, \quad (4.72)$$

where s_μ is the four-spin vector (described in Appendix F), and the axial current density

$$\mathcal{A}_\mu^f(x) \equiv \bar{\psi}_f(x) \gamma_\mu \gamma_5 \psi_f(x). \quad (4.73)$$

We will discuss the physical relevance of axial charges in more detail in Chapter 6. We begin by adding an axial coupling to the QCD Hamiltonian density,

$$\mathcal{H} \longrightarrow \mathcal{H}'(\lambda) = \mathcal{H} - i\lambda \mathcal{A}_3^u, \quad (5.43)$$

so that the derivative of the Hamiltonian density is given by

$$\left. \frac{d\mathcal{H}'(\lambda)}{d\lambda} \right|_{\lambda=0} = -i\mathcal{A}_3^u. \quad (5.44)$$

The proton has momentum and spin degeneracies we must take into account, and so we form the matrix

$$W_p(\mathbf{p}', \sigma'; \mathbf{p}, \sigma) = -\frac{i}{2E_p(\mathbf{p}')} \langle p(\mathbf{p}', \sigma') | \mathcal{A}_3^u(0) | p(\mathbf{p}, \sigma) \rangle \delta_{\mathbf{p}', \mathbf{p} \pm \mathbf{q}}. \quad (5.45)$$

Since we have set $\mathbf{q} = \mathbf{0}$ in our modification to the Hamiltonian, and the axial operator is translationally invariant, W_p is diagonal in momentum. Also, since the axial operator commutes with the spin operator, W_p will be diagonal in the spin. Therefore, W_p is fully diagonal, and the first derivatives of the energies of the degenerate proton states are given by Eq. (5.42),

$$\left. \frac{dE_p(\mathbf{p}, \sigma)}{d\lambda} \right|_{\lambda=0} = -\frac{i}{2E_p(\mathbf{p})} \langle p(\mathbf{p}, \sigma) | \mathcal{A}_3^u(0) | p(\mathbf{p}, \sigma) \rangle = \frac{m_p}{E_p(\mathbf{p})} s_3(p, \sigma) \Delta u_p. \quad (5.46)$$

Specifically, for a proton at rest, we have

$$\left. \frac{dE_p(\mathbf{p} = \mathbf{0}, \sigma)}{d\lambda} \right|_{\lambda=0} = \sigma \Delta u_p, \quad (5.47)$$

where $\sigma = \pm 1$ for the spin-up/down proton state. That is, the derivative of the energy is exactly the axial charge of the u quark in the proton we wish to extract.

On the lattice, the proton and neutron are degenerate in the isospin-symmetric limit, and so we should consider isospin-degeneracy in determining the energy shifts. In this case however, the third component of the isospin operator commutes with the axial current, and so the matrix W is diagonal in isospin.

5.2.3 Example: Vector Matrix Elements of the Pion

Now let's consider the calculation of the u quark contribution to the form factor of the π^+ as in Section 4.2.1. These can be defined through the non-forward matrix element

$$\langle \pi^+(\mathbf{p}') | \mathcal{V}_4^u(0) | \pi^+(\mathbf{p}) \rangle = [E_{\pi^+}(\mathbf{p}') + E_{\pi^+}(\mathbf{p})] F_{\pi^+}^u(Q^2), \quad (4.59)$$

where the vector current density is

$$\mathcal{V}_\mu^f(x) \equiv \bar{\psi}_f(x) \gamma_\mu \psi_f(x). \quad (4.60)$$

We will discuss the electromagnetic form factors in more detail in Chapter 7. To perform the calculation here, we begin by adding a vector coupling to the QCD Hamiltonian,

$$\mathcal{H}(x) \longrightarrow \mathcal{H}'(x, \lambda) = \mathcal{H}(x) + \lambda (e^{i\mathbf{q}\cdot\mathbf{x}} + e^{-i\mathbf{q}\cdot\mathbf{x}}) \mathcal{V}_4^u(x), \quad (5.48)$$

where we choose as an example, $(L/2\pi)\mathbf{q} = (2, 0, 0)$. In this case, the derivative of the Hamiltonian is given by

$$\left. \frac{d\mathcal{H}'(x)}{d\lambda} \right|_{\lambda=0} = (e^{i\mathbf{q}\cdot\mathbf{x}} + e^{-i\mathbf{q}\cdot\mathbf{x}}) \mathcal{V}_4^u(x). \quad (5.49)$$

Unlike the proton, the π^+ has no spin degeneracies, however it does have momentum degeneracies, and isospin degeneracy in the isospin-symmetric limit. The isospin operator commutes with the vector current, and so the matrix W is diagonal in isospin. Hence, we need only consider momentum degeneracy, and can form the matrix

$$W_{\pi^+}(\mathbf{p}'; \mathbf{p}) = \frac{1}{2E_{\pi^+}(\mathbf{p}')} \langle \pi^+(\mathbf{p}') | \mathcal{V}_4^u(0) | \pi^+(\mathbf{p}) \rangle \delta_{\mathbf{p}', \mathbf{p} \pm \mathbf{q}}, \quad (5.50)$$

for each set of degenerate momentum. Since these states are energy degenerate, we must have that $\mathbf{p}'^2 = \mathbf{p}^2$, and hence we can show that the Breit frame condition is equivalent to

$$\mathbf{p}' \cdot \mathbf{q} = -\mathbf{p} \cdot \mathbf{q} = \pm \frac{1}{2} \mathbf{q}^2. \quad (5.51)$$

For our choice of \mathbf{q} therefore, the only matrices with non-zero elements are those with momenta satisfying (in lattice momentum units of $L/2\pi$),

$$\mathbf{p}' - \mathbf{p} = \mathbf{q} = (2, 0, 0) \implies p'_y = p_y, \quad p'_z = p_z, \quad (5.52)$$

$$\mathbf{p}' \cdot \mathbf{q} = 2p'_x = -\mathbf{p} \cdot \mathbf{q} = -2p_x = \frac{1}{2} \mathbf{q}^2 = 2 \implies p'_x = -p_x = \pm 1. \quad (5.53)$$

Choosing $p_y = p_z = 0$ for now, we have a matrix with non-zero elements where

$$\mathbf{p} = (\pm 1, 0, 0), \quad (5.54)$$

$$\mathbf{p}' = (\mp 1, 0, 0) = -\mathbf{p}. \quad (5.55)$$

The corresponding matrix is given by,

$$\begin{aligned} W_{\pi^+} &= \frac{\delta_{+\mathbf{p},-\mathbf{p}}}{2E_{\pi^+}(\mathbf{p})} \begin{bmatrix} \langle \pi^+(+\mathbf{p}) | \mathcal{V}_4^u(0) | \pi^+(+\mathbf{p}) \rangle & \langle \pi^+(+\mathbf{p}) | \mathcal{V}_4^u(0) | \pi^+(-\mathbf{p}) \rangle \\ \langle \pi^+(-\mathbf{p}) | \mathcal{V}_4^u(0) | \pi^+(+\mathbf{p}) \rangle & \langle \pi^+(-\mathbf{p}) | \mathcal{V}_4^u(0) | \pi^+(-\mathbf{p}) \rangle \end{bmatrix} \\ &= \begin{bmatrix} 0 & 1 \\ 1 & 0 \end{bmatrix} F_{\pi^+}^u(Q^2) \end{aligned} \quad (5.56)$$

This matrix has normalised eigenvectors and eigenvalues

$$v_1 = \begin{bmatrix} +\frac{1}{\sqrt{2}} \\ +\frac{1}{\sqrt{2}} \end{bmatrix}, \quad e_1 = +F_{\pi^+}^u(Q^2), \quad (5.57)$$

$$v_2 = \begin{bmatrix} +\frac{1}{\sqrt{2}} \\ -\frac{1}{\sqrt{2}} \end{bmatrix}, \quad e_2 = -F_{\pi^+}^u(Q^2). \quad (5.58)$$

Hence our new eigenstates and their energy derivatives are

$$|\pi_1^+\rangle = \frac{1}{\sqrt{2}} [|\pi^+(+\mathbf{p})\rangle + |\pi^+(-\mathbf{p})\rangle], \quad \left. \frac{dE_{\pi_1^+}}{d\lambda} \right|_{\lambda=0} = +F_{\pi^+}^u(Q^2), \quad (5.59)$$

$$|\pi_2^+\rangle = \frac{1}{\sqrt{2}} [|\pi^+(+\mathbf{p})\rangle - |\pi^+(-\mathbf{p})\rangle], \quad \left. \frac{dE_{\pi_2^+}}{d\lambda} \right|_{\lambda=0} = -F_{\pi^+}^u(Q^2). \quad (5.60)$$

We will discuss how these states are accessed on the lattice in more detail in Section 5.3.4

5.2.4 Example: Vector Matrix Elements of the Proton

Finally, let's consider the calculation of the d quark contributions to the Sachs magnetic form factor of the proton, as in Section 4.2.3. Recall this can be defined through the matrix element

$$\langle \mathbf{p}(\mathbf{q}/2, \sigma') | \mathcal{V}_2^d(0) | \mathbf{p}(-\mathbf{q}/2, \sigma) \rangle = [\mathbf{s} \times \mathbf{q}]_2 G_{M,p}^d(Q^2) \delta_{\sigma'\sigma}. \quad (4.80)$$

In order to access this matrix element, we make a similar modification to the Hamiltonian as in Eq. (5.48),

$$\mathcal{H}(x) \longrightarrow \mathcal{H}'(x, \lambda) = \mathcal{H}(x) + \lambda (e^{i\mathbf{q}\cdot\mathbf{x}} + e^{-i\mathbf{q}\cdot\mathbf{x}}) \mathcal{V}_2^d(x), \quad (5.61)$$

where we again choose $(L/2\pi)\mathbf{q} = (2, 0, 0)$. As the spin operator commutes with the vector current, we do not need to consider the effects of spin-degeneracy. The only degeneracy therefore is the momentum degeneracy. As in Section 5.2.3, the only relevant matrices with non-zero elements are those with momenta satisfying the conditions of Eq. (5.51). Choosing the momenta of Eq. (5.54) again, we have the matrix

$$\begin{aligned} W_p &= \frac{\delta_{+\mathbf{p},-\mathbf{p}}}{2E_p(\mathbf{p})} \begin{bmatrix} \langle \mathbf{p}(+\mathbf{p}, \sigma) | \mathcal{V}_2^u(0) | \mathbf{p}(+\mathbf{p}, \sigma) \rangle & \langle \mathbf{p}(+\mathbf{p}, \sigma) | \mathcal{V}_2^u(0) | \mathbf{p}(-\mathbf{p}, \sigma) \rangle \\ \langle \mathbf{p}(-\mathbf{p}, \sigma) | \mathcal{V}_2^u(0) | \mathbf{p}(+\mathbf{p}, \sigma) \rangle & \langle \mathbf{p}(-\mathbf{p}, \sigma) | \mathcal{V}_2^u(0) | \mathbf{p}(-\mathbf{p}, \sigma) \rangle \end{bmatrix}, \\ &= \begin{bmatrix} 0 & 1 \\ -1 & 0 \end{bmatrix} [\mathbf{s} \times \mathbf{q}]_2 G_{M,p}^d(Q^2) \end{aligned} \quad (5.62)$$

This matrix has normalised eigenvectors and eigenvalues

$$v_1 = \begin{bmatrix} +\frac{1}{\sqrt{2}} \\ +\frac{i}{\sqrt{2}} \end{bmatrix}, \quad e_1 = +i[\mathbf{s} \times \mathbf{q}]_2 G_{M,p}^d(Q^2), \quad (5.63)$$

$$v_2 = \begin{bmatrix} +\frac{1}{\sqrt{2}} \\ -\frac{i}{\sqrt{2}} \end{bmatrix}, \quad e_2 = -i[\mathbf{s} \times \mathbf{q}]_2 G_{M,p}^d(Q^2). \quad (5.64)$$

Hence our new eigenstates and their energy derivatives are

$$|p_1(\sigma)\rangle = \frac{1}{\sqrt{2}}[|p(+\mathbf{p}, \sigma)\rangle + |p(-\mathbf{p}, \sigma)\rangle], \quad \left. \frac{dE_{p_1}(\sigma)}{d\lambda} \right|_{\lambda=0} = +i[\mathbf{s} \times \mathbf{q}]_2 G_{M,p}^d(Q^2), \quad (5.65)$$

$$|p_2(\sigma)\rangle = \frac{1}{\sqrt{2}}[|p(+\mathbf{p}, \sigma)\rangle - |p(-\mathbf{p}, \sigma)\rangle], \quad \left. \frac{dE_{p_2}(\sigma)}{d\lambda} \right|_{\lambda=0} = -i[\mathbf{s} \times \mathbf{q}]_2 G_{M,p}^d(Q^2). \quad (5.66)$$

We will discuss this calculation in more detail in Chapter 7.

5.2.5 Extension to Second Order

One aspect of the FH method we haven't yet mentioned is its extension to second-order derivatives. Taking the derivative of Eq. (5.6), substituting the expression of the derivative of the wavefunction in Eq. (5.10), and taking the inner product with $\langle\psi_n|$ we obtain, at least in the case of a non-degenerate spectrum,

$$\frac{d^2 E_n}{d\lambda^2} = \frac{\langle\psi_n|\frac{d^2\hat{H}}{d\lambda^2}|\psi_n\rangle}{\langle\psi_n|\psi_n\rangle} + 2 \sum_{\substack{m \\ m \neq n}} \frac{1}{E_n - E_m} \frac{\langle\psi_n|\frac{d\hat{H}}{d\lambda}|\psi_m\rangle}{\langle\psi_n|\psi_n\rangle} \frac{\langle\psi_m|\frac{d\hat{H}}{d\lambda}|\psi_n\rangle}{\langle\psi_m|\psi_m\rangle}, \quad (5.67)$$

where the second term includes transitions between different energy levels. For a modified Hamiltonian of the form

$$\hat{H} \longrightarrow \hat{H}'(\lambda) = \hat{H} + \lambda\hat{O}, \quad (5.68)$$

the second-order energy derivatives are given by

$$\frac{d^2 E_n}{d\lambda^2} = 2 \sum_{\substack{m \\ m \neq n}} \frac{1}{E_n - E_m} \frac{\langle\psi_n|\hat{O}|\psi_m\rangle}{\langle\psi_n|\psi_n\rangle} \frac{\langle\psi_m|\hat{O}|\psi_n\rangle}{\langle\psi_m|\psi_m\rangle}. \quad (5.69)$$

Here we can see then, at least in principle, how transition matrix elements could be calculated through second-order energy shifts. Once momentum-degeneracy is taken into account, or the insertion of momentum through the operator \hat{O} in a lattice context, deriving analogous expressions is possible, but becomes much more complicated. This will be the subject of an upcoming publication [127]. We perform a calculation of this type in Chapter 8.

5.3 Path-Integral Approach

The derivation of the FH theorem beginning with the path-integral expression of QCD is slightly more involved than the quantum mechanical discussion of Section 5.2.

Suppose the QCD Lagrangian depends on some parameter λ , and we have a λ -independent operator \mathcal{O} . Suppose also that the physical value of the parameter (which may be zero) corresponds to λ_0 . The expectation value of \mathcal{O} in the Feynman path-integral formalism at the physical point is given by

$$\langle \mathcal{O} \rangle_{\lambda_0} = \frac{\int \mathcal{D}U \mathcal{O} e^{-S(\lambda_0)}}{\int \mathcal{D}U e^{-S(\lambda_0)}}, \quad (5.70)$$

where U here is a shorthand for all the different fermion and gauge fields, and the subscript λ_0 represents evaluation of the expectation value at $\lambda = \lambda_0$. Taking the derivative with respect to λ at λ_0 , we obtain

$$\frac{d\langle \mathcal{O} \rangle}{d\lambda} = \langle \mathcal{O} \rangle \left\langle \frac{dS}{d\lambda} \right\rangle - \left\langle \mathcal{T} \left\{ \mathcal{O} \frac{dS}{d\lambda} \right\} \right\rangle, \quad (5.71)$$

where we have dropped explicit λ -dependence, and all quantities are implicitly evaluated at λ_0 . $\mathcal{T}\{\dots\}$ here indicates time ordering. Here we have assumed that the expectation value of \mathcal{O} is differentiable with respect to λ .

5.3.1 Forward Matrix Elements

We would like to use the result of Eq. (5.71) to derive a useful expression for determining forward matrix elements in lattice QCD. Suppose we may write the first derivative of the action with respect to λ at λ_0 in the form

$$\frac{dS}{d\lambda} = \int d\tau \sum_{\mathbf{y}} d^3y \mathcal{O}(\mathbf{y}, \tau), \quad (5.72)$$

where \mathcal{O} is a translationally invariant operator. For simplicity we will here consider a continuous, infinite temporal extent, rather than the finite, discrete time-dimension of the lattice. This allows us to ignore finite volume artefacts in the time extent, and a finite temporal extent is not required for a discrete QCD spectrum. Consider the lattice two-point function defined in Eq. (4.9). From the result of Eq. (5.71), we have that

$$\begin{aligned} \frac{d}{d\lambda} G_{\chi\tilde{\chi}}(\mathbf{p}; t', t) &= G_{\chi\tilde{\chi}}(\mathbf{p}; t', t) \left\langle \frac{dS}{d\lambda} \right\rangle - \int_{-\infty}^t d\tau G_{\chi\tilde{\chi}\mathcal{O}}(\mathbf{p}, \mathbf{0}; t', t, \tau) \\ &\quad - \int_t^{t'} d\tau G_{\chi\mathcal{O}\tilde{\chi}}(\mathbf{p}, \mathbf{p}; t', \tau, t) \\ &\quad - \int_{t'}^{\infty} d\tau G_{\mathcal{O}\chi\tilde{\chi}}(\mathbf{0}, \mathbf{p}; \tau, t', t), \end{aligned} \quad (5.73)$$

where the Fourier-projected three-point function is defined in Eq. (4.54). Since the operator \mathcal{O} is translationally invariant, we can use the decomposition of the Fourier-projected two-point function in Eq. (4.11) to calculate the derivative

$$\begin{aligned} \frac{d}{d\lambda} G_{\chi\tilde{\chi}}(\mathbf{p}; t', t) &= - \sum_{\mathbf{X}, r} \frac{e^{-E_{\mathbf{X}}(\mathbf{p})(t'-t)}}{2E_{\mathbf{X}}(\mathbf{p})} \left[\left(t' - t + \frac{1}{E_{\mathbf{X}}(\mathbf{p})} \right) \frac{dE_{\mathbf{X}}(\mathbf{p}, r)}{d\lambda} - \frac{d}{d\lambda} \right] \\ &\quad \langle \Omega | \chi(0) | \mathbf{X}(\mathbf{p}, r) \rangle \langle \mathbf{X}(\mathbf{p}, r) | \tilde{\chi}(0) | \Omega \rangle. \end{aligned} \quad (5.74)$$

We have assumed here that the eigenstate basis $|X(\mathbf{p}, r)\rangle$ is a ‘good’ basis that perturbs smoothly as λ is changed. The integrals where the current falls outside the interpolating operators are easily calculated using the decomposition of Eq. (4.55),

$$\int_{-\infty}^t d\tau G_{\chi\tilde{\chi}\mathcal{O}}(\mathbf{p}, \mathbf{0}; t', t, \tau) = \sum_{\substack{X,r \\ Y,s}} \frac{e^{-E_X(\mathbf{p})(t'-t)}}{4E_X(\mathbf{p})E_Y^2(\mathbf{0})} \\ \langle\Omega|\chi(0)|X(\mathbf{p}, r)\rangle \langle X(\mathbf{p}, r)|\tilde{\chi}(0)|Y(\mathbf{0}, s)\rangle \langle Y(\mathbf{0}, s)|\mathcal{O}(0)|\Omega\rangle, \quad (5.75)$$

$$\int_{t'}^{\infty} d\tau G_{\mathcal{O}\chi\tilde{\chi}}(\mathbf{0}, \mathbf{p}; \tau, t', t) = \sum_{\substack{X,r \\ Y,s}} \frac{e^{-E_X(\mathbf{p})(t'-t)}}{4E_X(\mathbf{p})E_Y^2(\mathbf{0})} \\ \langle\Omega|\mathcal{O}(0)|Y(\mathbf{0}, s)\rangle \langle Y(\mathbf{0}, s)|\chi(0)|X(\mathbf{p}, r)\rangle \langle X(\mathbf{p}, r)|\tilde{\chi}(0)|\Omega\rangle. \quad (5.76)$$

In the case of baryon interpolators and a quark-bilinear operator \mathcal{O} , the states coupling to both the interpolators and the \mathcal{O} may be baryon/anti-baryon states, for example. The integral where the current falls between the interpolators is slightly more complicated. We split the sum into terms involving degenerate and non-degenerate states,

$$\int_t^{t'} d\tau G_{\chi\mathcal{O}\tilde{\chi}}(\mathbf{p}, \mathbf{p}; t', \tau, t) = I_{\text{nondegen}} + I_{\text{degen}}, \quad (5.77)$$

given respectively by

$$I_{\text{nondegen}} = \sum_{\substack{X,r \\ Y,s \\ X \neq Y}} \frac{e^{-E_X(\mathbf{p})(t'-t)} - e^{-E_Y(\mathbf{p})(t'-t)}}{4E_Y(\mathbf{p})E_X(\mathbf{p})(E_Y(\mathbf{p}) - E_X(\mathbf{p}))} \\ \langle\Omega|\chi(0)|Y(\mathbf{p}, s)\rangle \langle Y(\mathbf{p}, s)|\mathcal{O}(0)|X(\mathbf{p}, r)\rangle \langle X(\mathbf{p}, r)|\tilde{\chi}(0)|\Omega\rangle, \quad (5.78)$$

$$I_{\text{degen}} = (t' - t) \sum_{X,r,s} \frac{e^{-E_X(\mathbf{p})(t'-t)}}{4E_X^2(\mathbf{p})} \langle\Omega|\chi(0)|X(\mathbf{p}, r)\rangle \langle X(\mathbf{p}, r)|\mathcal{O}(0)|X(\mathbf{p}, s)\rangle \\ \langle X(\mathbf{p}, s)|\tilde{\chi}(0)|\Omega\rangle. \quad (5.79)$$

The energy denominator in the first term is never zero, and so this expression is always well-defined. Since the results above are true for all times t' and t , we are free to substitute Eqs. (5.74) to (5.77) into Eq. (5.73) and match up terms with identical $(t' - t)$ -dependence. For the $(t' - t)$ -enhanced terms we have

$$\sum_{X,r} \frac{e^{-E_X(\mathbf{p})(t'-t)}}{2E_X(\mathbf{p})} \frac{dE_X(\mathbf{p}, r)}{d\lambda} \langle\Omega|\chi(0)|X(\mathbf{p}, r)\rangle \langle X(\mathbf{p}, r)|\tilde{\chi}(0)|\Omega\rangle = \\ \sum_{X,r,s} \frac{e^{-E_X(\mathbf{p})(t'-t)}}{4E_X^2(\mathbf{p})} \langle\Omega|\chi(0)|X(\mathbf{p}, r)\rangle \langle X(\mathbf{p}, r)|\mathcal{O}(0)|X(\mathbf{p}, s)\rangle \langle X(\mathbf{p}, s)|\tilde{\chi}(0)|\Omega\rangle. \quad (5.80)$$

In the limit of large $(t' - t)$, the lowest-energy state coupling to the interpolating operators dominates the sum of exponentials, and so we obtain

$$\sum_r \frac{dE_{X_0}(\mathbf{p}, r)}{d\lambda} \langle\Omega|\chi(0)|X_0(\mathbf{p}, r)\rangle \langle X_0(\mathbf{p}, r)|\tilde{\chi}(0)|\Omega\rangle = \\ \frac{1}{2E_{X_0}(\mathbf{p})} \sum_{r,s} \langle\Omega|\chi(0)|X_0(\mathbf{p}, r)\rangle \langle X_0(\mathbf{p}, r)|\mathcal{O}(0)|X_0(\mathbf{p}, s)\rangle \langle X_0(\mathbf{p}, s)|\tilde{\chi}(0)|\Omega\rangle. \quad (5.81)$$

By forming idealised ‘perfect’ operators which couple only to certain excited states, we can extend this result to any hadronic state,

$$\sum_r \frac{dE_X(\mathbf{p}, r)}{d\lambda} \langle \Omega | \chi(0) | X(\mathbf{p}, r) \rangle \langle X(\mathbf{p}, r) | \tilde{\chi}(0) | \Omega \rangle = \frac{1}{2E_X(\mathbf{p})} \sum_{r,s} \langle \Omega | \chi(0) | X(\mathbf{p}, r) \rangle \langle X(\mathbf{p}, r) | \mathcal{O}(0) | X(\mathbf{p}, s) \rangle \langle X(\mathbf{p}, s) | \tilde{\chi}(0) | \Omega \rangle . \quad (5.82)$$

We now have a result involving the energy derivatives of the hadron spectrum, and matrix elements of the operator \mathcal{O} . At this stage, we have not derived an expression for the shift in the amplitude of the correlation function, however, one would expect that this expression is contingent on this derivative being well-defined, and that a diagonalisation procedure as discussed in Section 5.1 would be required if that were not the case.

5.3.2 Example: Axial Charge of the Proton

In the case of interpolators coupling to spin-zero mesons, Eq. (5.82) becomes simply

$$\frac{dE_X(\mathbf{p})}{d\lambda} = \frac{1}{2E_X(\mathbf{p})} \langle X(\mathbf{p}) | \mathcal{O}(0) | X(\mathbf{p}) \rangle . \quad (5.83)$$

In the case of interpolators coupling to spin-half baryons, however, the expression is more complicated,

$$F_{2,\text{FH}}(\Gamma_{\text{proj}}; \mathbf{p}, m_X) = \frac{F_3(\Gamma_{\text{proj}}, \Gamma_{\mathcal{O},X}; \mathbf{p}, \mathbf{p}, m_X)}{2E_X(\mathbf{p})} , \quad (5.84)$$

where the function $F_{2,\text{FH}}$ is defined as

$$F_{2,\text{FH}}(\Gamma_{\text{proj}}; \mathbf{p}, m_X) = \frac{1}{4} \sum_{\sigma} [\Gamma_{\text{proj}}]_{\alpha\beta} u_{\alpha}(p, \sigma) \bar{u}_{\beta}(p, \sigma) \frac{dE_X(\mathbf{p}, \sigma)}{d\lambda} , \quad (5.85)$$

and F_3 is as defined in Eq. (4.71). Values of $F_{2,\text{FH}}$ calculated for the basis of Dirac matrices and common projectors can be found in Appendix H.

Suppose then we wish to calculate the axial charge of the u quark in the proton through the FH method as in Section 5.2.2. In this case, we begin by adding an axial coupling to the QCD Lagrangian density,

$$\mathcal{L} \longrightarrow \mathcal{L}'(\lambda) = \mathcal{L} - i\lambda \mathcal{A}_3^u , \quad (5.86)$$

We have already established in Section 5.2.2 that the standard spin and momentum-dependent proton eigenstates have well-defined derivatives about $\lambda = 0$. That is, the standard basis of proton states perturbs smoothly with the introduced coupling to the axial field. Hence, the energy shifts are simply given by Eq. (5.88). For a projector chosen to project positive parity and definite spin, $\Gamma_{\text{proj}} = \Gamma_{\text{pol}\pm}$, $F_{2,\text{FH}}$ is given by

$$F_{2,\text{FH}}(\Gamma_{\text{pol}\pm}; \mathbf{p}, m_X) = \frac{1}{4} [E_X(\mathbf{p}) + m_X] \frac{dE_X(\mathbf{p}, \pm)}{d\lambda} , \quad (5.87)$$

and hence for a positive-parity, spin-polarised state, the energy shifts are given by

$$\left. \frac{dE_X(\mathbf{p}, \pm)}{d\lambda} \right|_{\lambda=0} = \frac{2F_3(\Gamma_{\text{pol}\pm}, \Gamma_{\mathcal{O},X}; \mathbf{p}, \mathbf{p}, m_X)}{E_X(\mathbf{p})[E_X(\mathbf{p}) + m_X]}. \quad (5.88)$$

The vertex function for the axial current is given in Eq. (4.77), and we can therefore evaluate

$$F_3(\Gamma_{\text{pol}\pm}, \Gamma_{-iA_3^u, \mathbf{p}}; \mathbf{p}' = \mathbf{0}, \mathbf{p} = \mathbf{0}, m_p) = \pm m_p^2 \Delta u_p. \quad (5.89)$$

Hence, the energy shifts in the proton state at rest are given by

$$\left. \frac{dE_p(\mathbf{p} = \mathbf{0}, \sigma)}{d\lambda} \right|_{\lambda=0} = \sigma \Delta u_p, \quad (5.90)$$

which is consistent with our result of Section 5.2.2.

5.3.3 Non-Forward Matrix Elements

Now let's consider derivatives of the QCD action of the form

$$\frac{dS}{d\lambda} = \int d\tau \sum_{\mathbf{y}} \Delta^3 y \left[e^{i\mathbf{q}\cdot(\mathbf{y}-\mathbf{x})} + e^{-i\mathbf{q}\cdot(\mathbf{y}-\mathbf{x})} \right] \mathcal{O}(\mathbf{y}, \tau), \quad (5.91)$$

for some translationally invariant operator \mathcal{O} . Consider the two-point function formed from interpolators χ and $\tilde{\chi}$ projected to definite momentum \mathbf{p}' , relative to the spatial position \mathbf{x} , similarly to the previous section. We have

$$\begin{aligned} \frac{d}{d\lambda} G_{\chi\tilde{\chi}}(\mathbf{p}'; t', t) &= G_{\chi\tilde{\chi}}(\mathbf{p}'; t', t) \left\langle \frac{dS}{d\lambda} \right\rangle - \int_{-\infty}^t d\tau G_{\chi\tilde{\chi}\mathcal{O}}(\mathbf{p}', \mathbf{q}; t', t, \tau) \\ &\quad - \int_t^{t'} d\tau G_{\chi\mathcal{O}\tilde{\chi}}(\mathbf{p}', \mathbf{p}; t', \tau, t) \\ &\quad - \int_{t'}^{\infty} d\tau G_{\mathcal{O}\chi\tilde{\chi}}(-\mathbf{q}, \mathbf{p}; \tau, t', t) \\ &\quad + (\mathbf{q} \rightarrow -\mathbf{q}), \end{aligned} \quad (5.92)$$

where momenta are related by $\mathbf{p} + \mathbf{q} = \mathbf{p}'$. As before, we may evaluate the integrals where the current falls outside of the interpolators quite straightforwardly,

$$\begin{aligned} \int_{-\infty}^t d\tau G_{\chi\tilde{\chi}\mathcal{O}}(\mathbf{p}', \mathbf{q}; t', t, \tau) &= \sum_{\substack{X,r \\ Y,s}} \frac{e^{-E_X(\mathbf{p}')(t'-t)}}{4E_X(\mathbf{p}')E_Y^2(\mathbf{q})} \\ &\langle \Omega | \chi(0) | X(\mathbf{p}', r) \rangle \langle X(\mathbf{p}', r) | \tilde{\chi}(0) | Y(\mathbf{q}, s) \rangle \langle Y(\mathbf{q}, s) | \mathcal{O}(0) | \Omega \rangle, \end{aligned} \quad (5.93)$$

$$\begin{aligned} \int_{t'}^{\infty} d\tau G_{\mathcal{O}\chi\tilde{\chi}}(-\mathbf{q}, \mathbf{p}; \tau, t', t) &= \sum_{\substack{X,r \\ Y,s}} \frac{e^{-E_X(\mathbf{p})(t'-t)}}{4E_X(\mathbf{p})E_Y^2(\mathbf{q})} \\ &\langle \Omega | \mathcal{O}(0) | Y(-\mathbf{q}, s) \rangle \langle Y(-\mathbf{q}, s) | \chi(0) | X(\mathbf{p}, r) \rangle \langle X(\mathbf{p}, r) | \tilde{\chi}(0) | \Omega \rangle. \end{aligned} \quad (5.94)$$

To evaluate the term where the current falls between the interpolators, we again split the sum into terms involving degenerate or non-degenerate states,

$$\int_t^{t'} d\tau G_{\chi\mathcal{O}\tilde{\chi}}(\mathbf{p}', \mathbf{p}; t', \tau, t) = I_{\text{degen}} + I_{\text{nondegen}}, \quad (5.95)$$

where the two contributions are given by

$$I_{\text{nondegen}} = \sum_{\substack{X,r \\ Y,s \\ X \neq Y}} \frac{e^{-E_n(\mathbf{p})(t'-t)} - e^{-E_m(\mathbf{p}')(t'-t)}}{4E_Y(\mathbf{p}')E_X(\mathbf{p})[E_Y(\mathbf{p}') - E_X(\mathbf{p})]} \\ \langle \Omega | \chi(0) | Y(\mathbf{p}', s) \rangle \langle Y(\mathbf{p}', s) | \mathcal{O}(0) | X(\mathbf{p}, r) \rangle \langle X(\mathbf{p}, r) | \tilde{\chi}(0) | \Omega \rangle, \quad (5.96)$$

$$I_{\text{degen}} = (t' - t) \delta_{|\mathbf{p}'|, |\mathbf{p}|} \sum_{X,r,s} \frac{e^{-E_X(\mathbf{p}')(t'-t)}}{4E_X^2(\mathbf{p}')} \\ \langle \Omega | \chi(0) | X(\mathbf{p}', r') \rangle \langle X(\mathbf{p}', r') | \mathcal{O}(0) | X(\mathbf{p}, r) \rangle \langle X(\mathbf{p}, r) | \tilde{\chi}(0) | \Omega \rangle. \quad (5.97)$$

The $(t' - t)$ -enhanced term only exists if $|\mathbf{p}'| = |\mathbf{p}|$. This matches our expectation of Section 5.2 that we can only determine energy shifts for Breit-frame matrix elements.

To evaluate the derivative of the two-point function in Eq. (5.92), we need to be slightly more careful. We know from Sections 5.2.3 and 5.2.4 that the normal momentum eigenstates do not perturb smoothly, and so we cannot simply take the derivative of Eq. (4.5) as it presently stands. Rather for each pair of momenta $\mathbf{p}, \mathbf{p} + \mathbf{q}$ satisfying $|\mathbf{p}| = |\mathbf{p} + \mathbf{q}|$, we form new eigenstates

$$|X(\mathbf{p})\rangle, |X(\mathbf{p} + \mathbf{q})\rangle \longrightarrow |X_+(\mathbf{p})\rangle, |X_-(\mathbf{p})\rangle, \quad (5.98)$$

given by

$$|X_+(\mathbf{p})\rangle = \frac{1}{\sqrt{2}} [|X(\mathbf{p} + \mathbf{q})\rangle + \alpha |X(\mathbf{p})\rangle], \quad (5.99)$$

$$|X_-(\mathbf{p})\rangle = \frac{1}{\sqrt{2}} [|X(\mathbf{p} + \mathbf{q})\rangle - \alpha |X(\mathbf{p})\rangle], \quad (5.100)$$

where the coefficient α satisfies

$$|\alpha|^2 = 1. \quad (5.101)$$

We can then rewrite the completeness relation of Eq. (4.5) in terms of the new basis,

$$1 = \sum_{\substack{X,\mathbf{k},r \\ |\mathbf{k} \pm \mathbf{q}| \neq |\mathbf{k}|}} \frac{\Delta^3 k}{(2\pi)^3} \frac{1}{2E_X(\mathbf{k})} |X(\mathbf{k}, r)\rangle \langle X(\mathbf{k}, r)| \\ + \sum_{\substack{X,\mathbf{k},r \\ |\mathbf{k} + \mathbf{q}| = |\mathbf{k}|}} \frac{\Delta^3 k}{(2\pi)^3} \frac{1}{2E_X(\mathbf{k})} [|X_+(\mathbf{k}, r)\rangle \langle X_+(\mathbf{k}, r)| + |X_-(\mathbf{k}, r)\rangle \langle X_-(\mathbf{k}, r)|]. \quad (5.102)$$

Substituting this completeness relation into the expression for the two-point function of Eq. (4.9), and performing the necessary algebra, we can obtain an expression for

the derivative. Matching up $(t' - t)$ dependence in Eqs. (5.93) to (5.95), we then obtain

$$\begin{aligned} & \sum_{X,r} \frac{e^{-E_X(\mathbf{p}')(t'-t)}}{2E_X(\mathbf{p}')} \langle \Omega | \chi(0) | X(\mathbf{p}', r) \rangle \langle X(\mathbf{p}', r) | \tilde{\chi}(0) | \Omega \rangle \frac{dE_X(\mathbf{p}', r)}{d\lambda} = \\ & \sum_{X,r,s} \frac{e^{-E_X(\mathbf{p}')(t'-t)}}{4E_X^2(\mathbf{p}')} \langle \Omega | \chi(0) | X(\mathbf{p}', r') \rangle \langle X(\mathbf{p}', r') | \mathcal{O}(0) | X(\mathbf{p}, r) \rangle \langle X(\mathbf{p}, r) | \tilde{\chi}(0) | \Omega \rangle . \end{aligned} \quad (5.103)$$

In the large $(t' - t)$ limit, the lowest-energy coupling state will dominate the sum of exponentials on both sides of Eq. (5.103). Hence, we have

$$\begin{aligned} & \sum_{X_0,r} \frac{e^{-E_{X_0}(\mathbf{p}')(t'-t)}}{2E_{X_0}(\mathbf{p}')} \langle \Omega | \chi(0) | X_0(\mathbf{p}', r) \rangle \langle X_0(\mathbf{p}', r) | \tilde{\chi}(0) | \Omega \rangle \frac{dE_{X_0}(\mathbf{p}', r)}{d\lambda} = \\ & \sum_{X_0,r,s} \frac{e^{-E_{X_0}(\mathbf{p}')(t'-t)}}{4E_{X_0}^2(\mathbf{p}')} \langle \Omega | \chi(0) | X_0(\mathbf{p}', r') \rangle \langle X_0(\mathbf{p}', r') | \mathcal{O}(0) | X_0(\mathbf{p}, r) \rangle \langle X_0(\mathbf{p}, r) | \tilde{\chi}(0) | \Omega \rangle . \end{aligned} \quad (5.104)$$

By considering idealised ‘perfect’ operators coupling only to excited states, we can state the result more generally as

$$\begin{aligned} & \sum_r \frac{e^{-E_X(\mathbf{p}')(t'-t)}}{2E_X(\mathbf{p}')} \langle \Omega | \chi(0) | X(\mathbf{p}', r) \rangle \langle X(\mathbf{p}', r) | \tilde{\chi}(0) | \Omega \rangle \frac{dE_X(\mathbf{p}', r)}{d\lambda} = \\ & \sum_{r,s} \frac{e^{-E_X(\mathbf{p}')(t'-t)}}{4E_X^2(\mathbf{p}')} \langle \Omega | \chi(0) | X(\mathbf{p}', r') \rangle \langle X(\mathbf{p}', r') | \mathcal{O}(0) | X(\mathbf{p}, r) \rangle \langle X(\mathbf{p}, r) | \tilde{\chi}(0) | \Omega \rangle . \end{aligned} \quad (5.105)$$

5.3.4 Example: Pion Form Factor

For a spin-zero meson, the non-forward FH relation becomes

$$\left. \frac{dE_X(\mathbf{p}')}{d\lambda} \right|_{\lambda=0} = \frac{1}{2E_X(\mathbf{p}')} \langle X(\mathbf{p}') | \mathcal{O}(0) | X(\mathbf{p}) \rangle . \quad (5.106)$$

Suppose then, we wish to again calculate the u contribution to the π^+ form factor, defined through Eq. (4.59). We make a modification to the Lagrangian of the form

$$\mathcal{L}(y) \longrightarrow \mathcal{L}'(y, \lambda) = \mathcal{L}(y) + \lambda \left(e^{i\mathbf{q}\cdot(\mathbf{y}-\mathbf{x})} + e^{-i\mathbf{q}\cdot(\mathbf{y}-\mathbf{x})} \right) \mathcal{V}_4^u(y) , \quad (5.107)$$

such that the derivative of the energy of the pion state projected to momentum \mathbf{p}' (with Fourier-phases relative to the correlator source x) on the lattice is given by

$$\left. \frac{dE_{\pi^+}(\mathbf{p}')}{d\lambda} \right|_{\lambda=0} = \frac{1}{2E_{\pi^+}(\mathbf{p}')} \langle \pi^+(\mathbf{p}') | \mathcal{V}_4^u(0) | \pi^+(\mathbf{p}) \rangle = F_{\pi^+}^u(Q^2) , \quad (5.108)$$

provided $|\mathbf{p}'| = |\mathbf{p}|$. This matches our expectation of Section 5.2.3.

5.3.5 Example: Vector Matrix Elements of the Proton

For spin-half baryons, the non-forward FH relation becomes

$$F_{2,\text{FH}}(\Gamma_{\text{proj}}; \mathbf{p}', m_X) = \frac{1}{2E_X(\mathbf{p}')} F_3(\Gamma_{\text{proj}}, \Gamma_{\mathcal{O},X}; \mathbf{p}', \mathbf{p}, m_X), \quad (5.109)$$

where the function $F_{2,\text{FH}}$ is defined in Eq. (5.85). As in Section 5.3.2, we have the result that for definite positive-parity and spin projection,

$$\frac{dE_X(\mathbf{p}', \pm)}{d\lambda} = \frac{2F_3(\Gamma_{\text{pol}\pm}, \Gamma_{\mathcal{O},X}; \mathbf{p}', \mathbf{p}, m_X)}{E_X(\mathbf{p}') [E_X(\mathbf{p}') + m_X]}. \quad (5.110)$$

FH energy shifts resulting from the inclusion of quark-bilinear operators for the entire Dirac basis, and for common Dirac projectors of spin-half states, are given in Appendix H.

To calculate the d contribution to the Sachs magnetic form factor of the proton as in Section 5.2.4, we include a vector coupling in the Lagrangian,

$$\mathcal{L}(y) \longrightarrow \mathcal{L}'(y, \lambda) = \mathcal{L}(y) + \lambda \left(e^{i\mathbf{q}\cdot(\mathbf{y}-\mathbf{x})} + e^{-i\mathbf{q}\cdot(\mathbf{y}-\mathbf{x})} \right) \mathcal{V}_2^d(y). \quad (5.111)$$

The vertex function of the vector current is given by

$$\Gamma_{\mathcal{V}_{\mu,p}^f} = \gamma_{\mu} F_{1,p}^f(Q^2) + \sigma_{\mu\nu} \frac{q_{\nu}}{2m_p} F_{2,p}^f(Q^2), \quad (4.83)$$

and hence we can calculate for a momentum projection \mathbf{p}' chosen such that $\mathbf{p} = \mathbf{p}' - \mathbf{q} = -\mathbf{p}'$,

$$F_3(\Gamma_{\text{pol}\pm}, \Gamma_{\mathcal{V}_{2,p}^d}; \mathbf{p}', -\mathbf{p}', m_p) = \frac{1}{4} [E_p(\mathbf{p}') + m_p] [\mathbf{s} \times \mathbf{q}]_2 G_{M,p}^d(Q^2), \quad (5.112)$$

and hence the energy shifts extracted from spin-polarised proton correlators projected to momentum \mathbf{p}' relative to some lattice source location \mathbf{x} are

$$\left. \frac{dE_p(\mathbf{p}', \sigma)}{d\lambda} \right|_{\lambda=0} = \frac{[\mathbf{s} \times \mathbf{q}]_2}{2E_p(\mathbf{p}')} G_{M,p}^d. \quad (5.113)$$

Chapter 6

The Spin Structure of Hadrons

“In conclusion, measurements have been presented of the spin asymmetries in deep inelastic scattering of polarised muons on polarised protons. . . the result[s] impl[y] that, in the scaling limit, a rather small fraction of the spin of the proton is carried by the spin of the quarks.”

—J. Ashman et al., Phys. Lett. B206 (1988) [128]

The fundamental aim of hadron structure calculations in lattice QCD is to determine how QCD generates the observed properties of hadrons. For some observables, such as electric charge, this deduction is straightforward. The origin of hadronic spin however, is a question with a vexed history, and has been the subject of an enormous amount of computational effort in lattice QCD.

To begin with, we consider the spin-half proton. From a quark model perspective, the proton is a bound state of spin-half quarks. The quarks arrange themselves such that one of them is always oppositely polarised to the other two. This naive picture is illustrated in Fig. 6.1. In full QCD however, we know that the proton is an extremely complex object, and a snapshot of its internal dynamics would look far more like Fig. 6.2. Here, valence quarks in the proton interact via the exchange of spin-one gluons, sea quark-pairs are created and annihilated in the vacuum, and all these components move with non-zero orbital angular momentum (OAM). In general, one should expect contributions from all these forms of angular momentum to the overall proton spin.

The various spin fractions in the proton are summarised in the Ji sum-rule [129], which includes contributions from quark spin, quark OAM, and gluon angular momentum (AM),

$$\frac{1}{2} = \frac{1}{2} \underbrace{\Delta\Sigma_p}_{\text{quark spin}} + \underbrace{L_q}_{\text{quark OAM}} + \underbrace{J_g}_{\text{gluon AM}} . \quad (6.1)$$

Analogous spin sum rules may be written down for other hadrons. One may alternatively consider the Jaffe-Manohar decomposition [130],

$$\frac{1}{2} = \frac{1}{2} \underbrace{\Delta\Sigma}_{\text{quark spin}} + \underbrace{\mathcal{L}_q}_{\text{quark OAM}} + \underbrace{\Delta G}_{\text{gluon spin}} + \underbrace{\mathcal{L}_g}_{\text{gluon OAM}} , \quad (6.2)$$

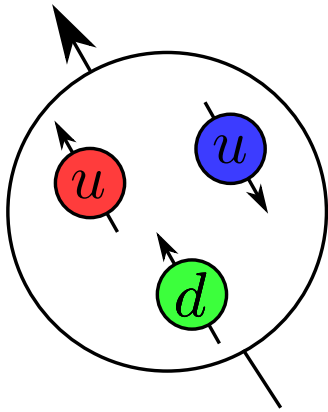


Figure 6.1: A quark-model view of the spin-structure of the proton.

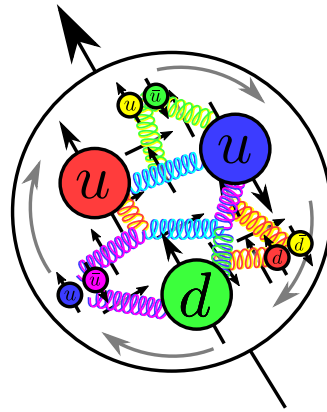


Figure 6.2: A more complicated but complete QCD picture of spin in the proton.

which splits the gluon term into gauge-invariant spin and OAM contributions. $\Delta\Sigma$ is equivalent in both decompositions, but \mathcal{L}_q and L_q are only the same in the infinite momentum frame [131]. The Ji decomposition of Eq. (6.1) is preferred in a lattice context, as each term can be expressed in terms of the expectation value of a gauge-invariant local operator.

In this thesis, $\Delta\Sigma$ will be of particular interest to us, interpreted as the fraction of the spin of a hadron carried by the spin of its quarks. In the naive quark model, the quark spin fraction of the proton $\Delta\Sigma_p = 1$, and all the other contributions vanish. More sophisticated models of angular momentum in the proton suggest that even taking gluon degrees of freedom into account, the quark spin contribution should still be dominant, with $\Delta\Sigma_p \approx 60 - 70\%$ [132]. In 1987, measurements of the spin-dependent structure functions of the proton indicated that the contribution of quark spin to the total proton spin was much smaller than expected, with $\Delta\Sigma_p = (1 \pm 12 \pm 24)\%$ [128]. At the time, this prompted a ‘Proton Spin Crisis’, as theorists struggled to explain why the contribution from quark spin was so small, and conversely, why contributions from other degrees of freedom were so large (see [133–136] for comprehensive reviews). Later measurements put the contribution from quark spin at around 30% [137–142], but nevertheless this is a far stretch from the 60–70% typically predicted by phenomenological models. Recent experimental results suggest that the contribution from gluon spin, ΔG in the Jaffe-Manohar sum rule of Eq. (6.2), may be much larger than expected, of the order 30% [143, 144]. Together with orbital angular momentum, this may go some way to solving the spin picture [135, 145–148].

$\Delta\Sigma_X$ for a particular hadron may be separated into individual flavour contributions,

$$\Delta\Sigma_X = \sum_f \Delta f_X, \quad (6.3)$$

which are defined through the forward limit of the axial matrix elements,

$$\langle X(\mathbf{p}, \sigma) | \mathcal{A}_\mu^f(0) | X(\mathbf{p}, \sigma) \rangle = 2im_X s_\mu(p, \sigma) \Delta f_X. \quad (6.4)$$

Here the axial current density is given by

$$\mathcal{A}_\mu^f(x) \equiv \bar{\psi}_f(x) \gamma_\mu \gamma_5 \psi_f(x), \quad (6.5)$$

and m_X and s_μ are the mass and spin-vector of the hadron respectively (conventions for the spin-vector are summarised in Appendix F). We discussed the calculation of the matrix element of Eq. (6.4) in lattice QCD in Section 4.2.2, where we noted the contribution of disconnected contractions to the three-point function. In the isospin-symmetric limit, the disconnected contributions to the u and d matrix elements of the proton are equal, and hence the isovector axial charge,

$$g_{A,p}^{u-d} \equiv \Delta u_p - \Delta d_p, \quad (6.6)$$

has no disconnected contributions. This quantity has been the focus of the majority of lattice studies of proton spin, as one avoids the costly stochastic estimation of quark loops in the vacuum.

Historically, a generally flat trend in $g_{A,p}^{u-d}$ was seen at higher pion masses, leading lattice results to underestimate the experimental result by around 10%. Finite-volume and chiral effects were considered to be significant contributions to this discrepancy [149–151]. With larger lattice volumes, more sophisticated considerations of the chiral dependence, and calculations at lighter and near-to-physical pion masses, these problems have largely been dealt with (see [152–155] for a selection of recent calculations, and also the review [156]).

Despite these significant improvements however, there remain many outstanding challenges. Firstly, calculating $\Delta\Sigma$ and the full decomposition into individual flavour contributions as in Eq. (6.3) requires evaluation of the disconnected quantities. Significant progress has been made in this area (see e.g. [105, 157]), however it has proven to be notoriously difficult to extract a non-zero signal. Additionally, there has been a great deal of debate surrounding the difficulty in controlling excited-state contamination in three-point functions [97, 158–162]. This has significantly contributed to underestimations of $g_{A,p}^{u-d}$, and is likely to be an important factor in calculations of $\Delta\Sigma_p$.

In this chapter, we demonstrate how the techniques developed in Chapter 5 may be applied to calculate both connected and disconnected contributions to quark axial charges in hadrons. We begin in Section 6.1 by calculating the connected contributions to validate the methods, by comparing the results obtained with calculations performed using the three-point methods of Section 4.2. We then proceed in Section 6.2 to calculate the disconnected contributions through the generation of new gauge ensembles with an appropriately modified QCD Lagrangian. The work discussed in this chapter has been published in [163, 164].

6.1 Connected Contributions

To determine the axial matrix elements through the FH method, we need to consider Lagrangians which include a coupling to the axial current. We have discussed examples of such Lagrangians in Sections 5.2.2 and 5.3.2. For our calculation we choose a modification to the QCD Lagrangian of the form

$$\mathcal{L} \longrightarrow \mathcal{L}'(\lambda) = \mathcal{L} - i\lambda_f \mathcal{A}_3^f, \quad (6.7)$$

where λ_f are freely varying real parameters for each simulated flavour, and \mathcal{A}_3^f is the third spatial component of the axial current density defined in Eq. (6.5).

Ensemble	N_{meas}	$a\lambda_f$
1	342	-0.0125, -0.025, -0.0375, -0.05
2	307	-0.0125, -0.025
3	450	-0.01, -0.02

Table 6.1: Summary of statistics for the calculation of the connected contributions to quark axial charges. λ is non-zero for only a single flavour at any one time. The referenced ensembles are summarised in Appendix I.

By application of the results developed in Sections 5.2.2 and 5.3.2, the first-order λ -dependence of the energy of a spin-polarised hadron at rest is given by

$$\left. \frac{\partial E_X(\mathbf{p} = \mathbf{0}, \sigma)}{\partial \lambda_f} \right|_{\lambda=0} = \sigma \Delta f_X, \quad (6.8)$$

where we have chosen the spin-polarisation axis to be the z axis. With the factor of i included, we ensure the extra term in the Lagrangian is Hermitian, and that resulting perturbations to the hadron spectrum are real.

6.1.1 Simulation Details

To extract the connected contributions to the axial charges, we perform simulations with the modified Lagrangian in Eq. (6.7) for several non-zero values of λ , where only a single flavour component is non-zero at a time. This is implemented as a modification to the Wilson Dirac operator, which is inverted through Eq. (3.38) to generate quark propagators which experience the additional axial coupling. The underlying gauge fields are unmodified, so this simulation is partially quenched, and disconnected contributions are not included. Correlation functions for the various hadrons are constructed according to the methods of Section 4.1, and the energy shifts as functions of λ are extracted to determine the axial charges through Eq. (6.8). This analysis is discussed in Section 6.1.2. The unmodified ensembles used are described in Appendix I, and Table 6.1 summarises the statistics of the calculation and the values of λ simulated on each ensemble.

Each additional value of λ requires an additional inversion of a newly modified Dirac matrix, however we will show in Chapter 7 that by simulating at extremely small values of λ , the $\lambda = 0$ propagator may be used as an initial guess in the inversion algorithm. This significantly reduces the cost of simulating additional values of λ , and we will show in our results that the signals extracted from small values of λ are desirable, as they avoid higher-order contamination.

6.1.2 Analysis

At times sufficiently later than the source time, the correlation function of a particle decays exponentially as in Eq. (4.12). This still holds with a modified Lagrangian, but the amplitude and energy of the correlation function become λ -dependent,

$$G(\lambda) \xrightarrow{\text{large } t} A(\lambda)e^{-E(\lambda)t}. \quad (6.9)$$

Here A is the amplitude of the correlation function, including overlap and energy factors. For notational simplicity we are assuming a source time of $t = 0$, so $t = \Delta t$. To isolate a precise signal for the energy shifts, we take ratios of different spin and parity projections of correlators, which allows us to take advantage of the correlation between the different signals. Taking the ratio of $\lambda \neq 0$ and $\lambda = 0$ correlators allows us to isolate the pure energy shifts,

$$\frac{G(\lambda, t)}{G(\lambda = 0, t)} \xrightarrow{\text{large } t} \frac{A(\lambda)}{A(\lambda = 0)} e^{-\Delta E(\lambda)t}, \quad (6.10)$$

where ΔE is defined as

$$\Delta E(\lambda) \equiv E(\lambda) - E(\lambda = 0). \quad (6.11)$$

Flipping the spin-projection of the hadron state is equivalent to flipping the sign of the axial coupling in the Lagrangian of Eq. (6.7). Hence, we form ratios of spin-up and down projections (labelled by up and down arrows) to isolate the energy shifts of the spin-up state at odd order in λ ,

$$\frac{G_{\uparrow}(\lambda, t)}{G_{\downarrow}(\lambda, t)} \xrightarrow{\text{large } t} \frac{A_{\uparrow}(\lambda)}{A_{\downarrow}(\lambda)} e^{-2E_{\uparrow, \text{odd}}(\lambda)t}, \quad (6.12)$$

where the shifts at odd order are defined as

$$E_{\text{odd}} \equiv \frac{1}{2}[E(\lambda) - E(-\lambda)]. \quad (6.13)$$

Finally, we recall from Section 4.1.2 that the backwards-propagating state of the negative-parity-projected proton operator is the positive-parity proton state. Under parity and time reversal, the axial operator changes sign, and hence this is again equivalent to flipping the sign of λ . Analogously to the ratio of spin-up and down projections, a ratio of these differently projected states allows us to isolate energies at odd order in λ . Combining all of these projections, we form the ratio

$$R(\lambda, t) \equiv \left| \frac{G_{\uparrow}^{+}(\lambda, t) G_{\downarrow}^{-}(\lambda, -t) G_{\downarrow}^{+}(0, t) G_{\uparrow}^{-}(0, -t)}{G_{\uparrow}^{+}(0, t) G_{\downarrow}^{-}(0, -t) G_{\downarrow}^{+}(\lambda, t) G_{\uparrow}^{-}(\lambda, -t)} \right|^{\frac{1}{4}} \quad (6.14)$$

where superscript \pm here refers to positive and negative-parity projection. At sufficiently large source-sink time separations, this ratio isolates the odd-order energy shifts,

$$R(\lambda, t) \xrightarrow{\text{large } t} B(\lambda) e^{-\Delta E_{\text{odd}}(\lambda)t}, \quad (6.15)$$

where B is some λ -dependent amplitude we can ignore, as we are only concerned with energy shifts extracted through the time-dependence of the ratio.

Removing energy shifts at even order in λ has the advantage that contamination to the linear term comes in only at $\mathcal{O}(\lambda^3)$,

$$\Delta E_{\text{odd}} = \lambda \left[\frac{dE}{d\lambda} \right]_{\lambda=0} + \mathcal{O}(\lambda^3), \quad (6.16)$$

and should be heavily suppressed for sufficiently small λ . To find the saturation region of the ratio in Eq. (6.14), we define the effective energy shift analogously to the effective energy of Eq. (4.13),

$$\Delta E_{\text{eff}}(t + a/2) \equiv \frac{1}{a} \ln \left| \frac{R(\lambda, t)}{R(\lambda, t + a)} \right|, \quad (6.17)$$

which at large times plateaus to the odd-order energy shift.

$$\Delta E_{\text{eff}}(t + a/2) \xrightarrow{\text{large } t} \Delta E_{\text{odd}}(\lambda). \quad (6.18)$$

Since we expect the energy shifts to be directly proportional to the quark axial charges from Eq. (6.8), we define the effective axial charge as a scaling of the effective energy shift,

$$\Delta f_{\text{eff}}(\lambda, t) \equiv \frac{\Delta E_{\text{eff}}(\mathbf{p} = \mathbf{0}; t)}{\lambda_f}. \quad (6.19)$$

At sufficiently large times, this quantity should plateau to the axial charge up to $\mathcal{O}(\lambda^2)$ contamination,

$$\Delta f_{\text{eff}}(\lambda, t) \xrightarrow{\text{large } t} \Delta f + \mathcal{O}(\lambda_f^2). \quad (6.20)$$

Results renormalised in the $\overline{\text{MS}}$ scheme at scale of 2 GeV are obtained by use of the non-singlet renormalisation of the axial current, determined through the FH method in [165],

$$[\Delta f]_{\text{conn}}^{\overline{\text{MS}}(2 \text{ GeV})} = Z_{A, \text{NS}}^{\overline{\text{MS}}(2 \text{ GeV})} [\Delta f]_{\text{conn}}^{\text{latt}}. \quad (6.21)$$

6.1.3 Results

Fig. 6.3 shows the effective axial charge of the u quark in the proton as a function of time, as calculated on an $N = 342$ subset of Ensemble 1, with $m_\pi = 470$ MeV. As λ is increased, some slight deviation of the results can be observed, indicating contamination from higher-order λ terms. If no higher-order contamination were present, the signal plateaux should not shift systematically as λ is changed. The signal-to-noise ratio begins to worsen as λ is increased, which suggests that when forming correlated ratios of the form of Eq. (6.14), it is advantageous to simulate at very small values of λ .

Fig. 6.4 shows the energy shifts extracted from the correlation functions as a function of λ , for axial couplings to the u or d quarks. Also included is a fit to linear and cubic terms in λ . The λ^3 contamination here is far more subtle, and we appear to mostly constrain the linear behaviour with the smallest λ point. Table 6.2 shows the fit parameters for a variety of polynomial fits to the u -quark data of Fig. 6.4. Including a cubic term does shift the linear term slightly, however higher-order terms are unnecessary to determine the linear term with confidence. This matches our expectation from Fig. 6.3 that cubic contamination is minor.

The linear parameter from the linear and cubic fit (the linear slope observed about $\lambda = 0$) determines the unrenormalised value for the quark axial charge through

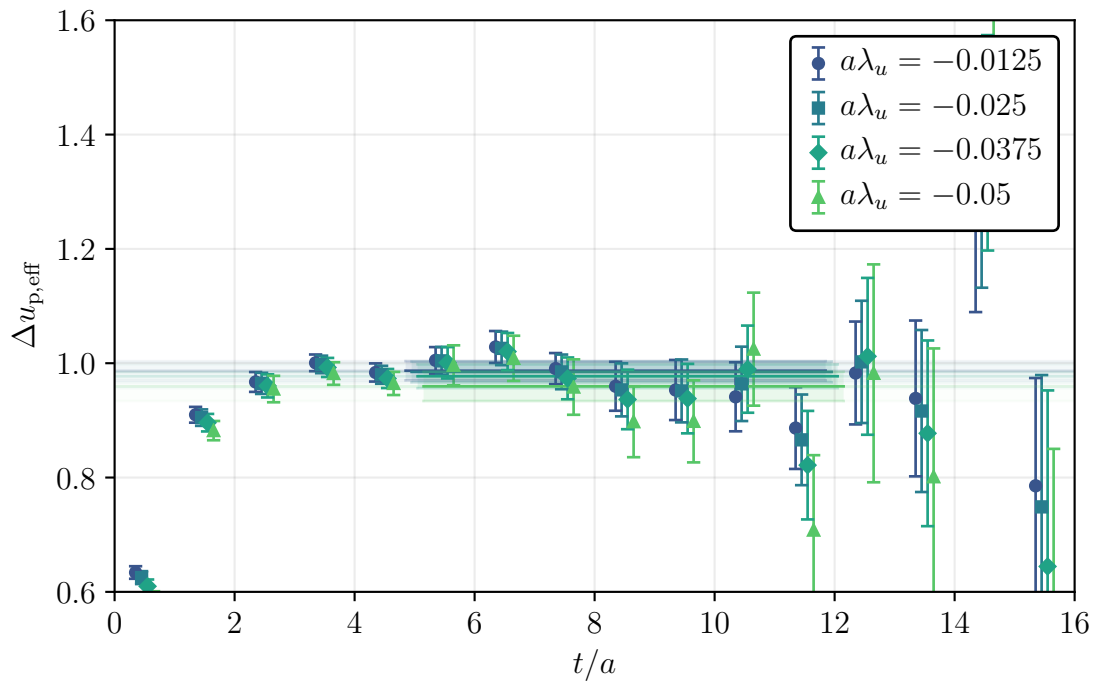


Figure 6.3: Effective axial charge of the u quark in the proton for different values of λ_u . The data sets have been shifted horizontally by a small amount for clarity. Calculated on an $N = 342$ subset of Ensemble 1, with $m_\pi = 470$ MeV.

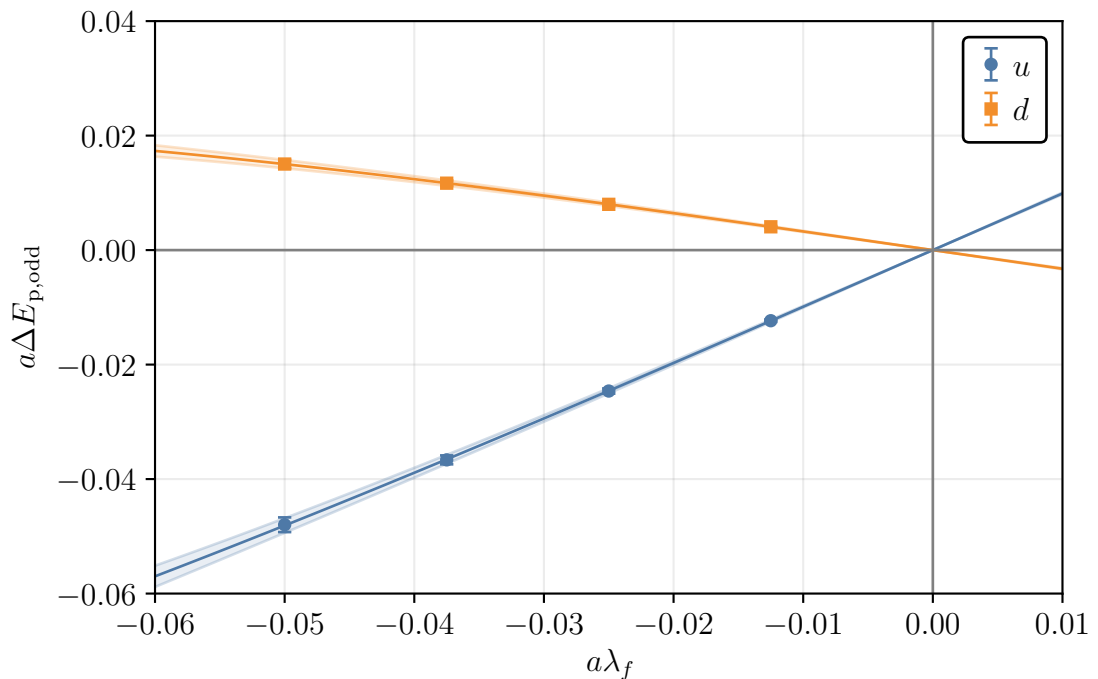


Figure 6.4: Proton energy shifts for an axial current coupling to the u or d quark as a function of $\lambda_{u/d}$. Also included is a fit to linear and cubic λ terms. Calculated on an $N = 342$ subset of Ensemble 1, with $m_\pi = 470$ MeV.

$a\lambda_u$	$a\lambda_u^3$	$a\lambda_u^5$
0.980(19)		
0.990(16)	-11.3(5.8)	
0.987(17)	-2.0(6.7)	-3700(1200)

Table 6.2: Fit parameters for a variety of polynomial fits to proton energy shifts resulting from an axial coupling to the u quark. Calculated on an $N = 342$ subset of Ensemble 1, with $m_\pi = 470$ MeV.

Eq. (6.8). Through our analysis, we determine for the isovector axial charge in the proton, at $m_\pi = 470$ MeV,

$$\left[g_{A,p}^{u-d} \right]_{\text{conn}}^{\overline{\text{MS}}(2 \text{ GeV})} = 1.112(18). \quad (6.22)$$

We compare this with the results of a variationally improved analysis in [93] performed on the same ensembles, with approximately four times the number of measurements,

$$\left[g_{A,p}^{u-d} \right]_{\text{conn}}^{\overline{\text{MS}}(2 \text{ GeV})} = 1.118(16). \quad (6.23)$$

As previously discussed, excited-state control has been a significant issue in calculations of $g_{A,p}^{u-d}$, and the variational method has been extremely successful in this regard. The consistency of our result indicates then that we too are able to achieve excellent levels of excited-state control in the FH approach.

A single small value of λ is sufficient to constrain the linear energy shift, with an additional value required to verify linearity. Along with the unperturbed propagator, three inversions of the Dirac operator are required to determine an axial charge on a single ensemble. In the three-point extraction of [93], three inversions are also required, and so we note that we are able to extract a consistent value, with similar precision, and an approximately four-fold decrease in computational cost. We will show in Chapter 3 that by simulating extremely small value of λ , we can significantly reduce the cost of additional simulations, and improve this situation further.

An advantage of the FH approach is that the calculated perturbed quark propagators may be used to construct a variety of hadrons. For a spin- s hadron we may define the more general sum-rule,

$$s = \frac{1}{2} \Delta\Sigma + L_q + J_g. \quad (6.24)$$

Hence, to compare the relative contributions of quark spin to hadronic spin, we determine the normalised quark spin contribution,

$$\widehat{\Delta\Sigma}^s \equiv \frac{\Delta\Sigma}{2s}, \quad (6.25)$$

which can be interpreted as the relative contribution of quark spin to the total hadron spin.

Fig. 6.5 shows the renormalised connected contributions to $\widehat{\Delta\Sigma}$ for a variety of hadrons, calculated through the statistics summarised in Table 6.1. Interestingly we find that at the $\text{SU}(3)_{\text{flavour}}$ -symmetric point of our simulations the connected

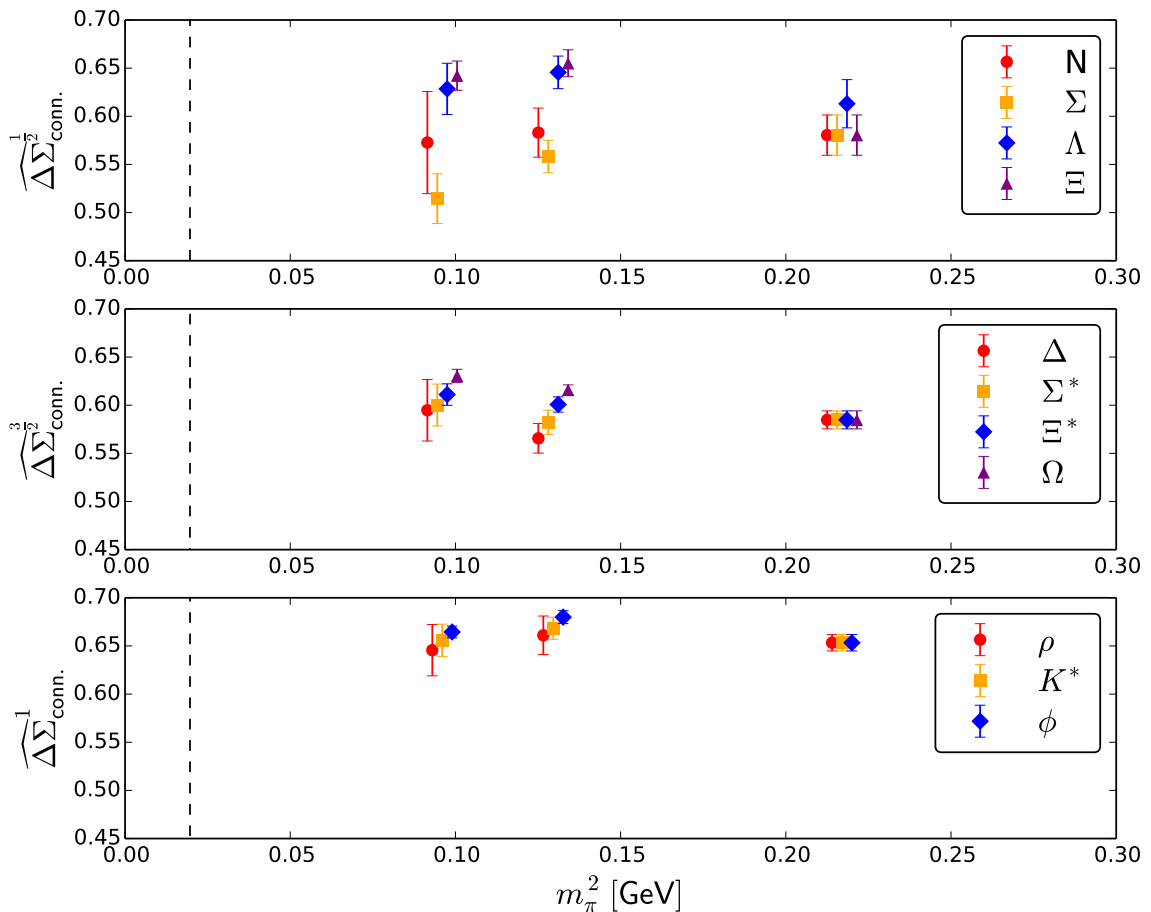


Figure 6.5: Total fractional connected quark spin contributions to various hadrons as a function of quark mass. The dotted line indicates the physical quark mass. Calculated on Ensembles 1 to 3.

quark spin fraction is around 55 – 70%, irrespective of the hadron in question. This is in line with the general expectation of relativistic corrections to quark-model wave functions [166–168]. Away from the flavour-symmetric point, we find flavour-symmetry breaking effects that could lead to significant breakdown of this universality in the light-quark domain [169].

6.2 Disconnected Contributions

We are now prepared to tackle the calculation of disconnected contributions to the axial charges. While no more theoretically challenging than the calculation of Section 6.1, the disconnected calculation has a small subtlety that must be addressed. As discussed in Section 3.1.3, gauge fields are generated according to the probability distribution

$$\rho(U) \equiv \prod_f \det[D_f(U)] e^{-S_G[U]}, \quad (6.26)$$

which includes the determinant of the Dirac operator. To interpret this expression as a probability density, we require that the determinant be real, and hence, as

discussed in Section 3.1.2, the Dirac operator D must satisfy γ_5 -Hermiticity,

$$(\gamma_5 D)^\dagger = \gamma_5 D. \quad (6.27)$$

However, the operator included in the modified Lagrangian in Eq. (6.7) does not satisfy this condition, and any attempt to employ the Hybrid Monte-Carlo algorithm with this Lagrangian will rapidly break down. To avoid this issue, we make a modification to the Lagrangian of the form

$$\mathcal{L} \rightarrow \mathcal{L}'(\lambda) = \mathcal{L} + \lambda_f \mathcal{A}_3^f. \quad (6.28)$$

While the included operator now satisfies γ_5 -Hermiticity, it is no longer Hermitian, and hence perturbations to the hadron spectrum are no longer real in general. In Chapter 5 we determined that we may still employ the FH results, but must consider phase shifts in the hadron correlation function, rather than energy shifts. In Sections 4.1.1 and 4.1.2 we noted that the correlation functions of mesons and baryons are real, up to gauge noise, for symmetric creation and annihilation operators. Hence, we expect the FH signal to manifest as a non-zero phase in the correlation function,

$$G(\lambda, t) = A(\lambda) e^{-[E(\lambda) + i\phi(\lambda)]t}. \quad (6.29)$$

For a spin-polarised hadron at rest, shifts in the phase are given by the FH relation,

$$\left. \frac{\partial \phi_X(\mathbf{p} = \mathbf{0}, \sigma)}{\partial \lambda_f} \right|_{\lambda=0} = \sigma \Delta f_X. \quad (6.30)$$

In order to verify this interpretation of the phase shifts, we first attempt to reproduce our results for the connected contributions from Section 6.1. This relatively small computational investment allows us to validate the phase analysis techniques before the more costly generation of gauge fields is performed.

6.2.1 Simulation Details: Validation

To calculate connected contributions to the quark axial charges through correlator phase shifts, we make the modification to the QCD Lagrangian of Eq. (6.28) to the Dirac operator, and calculate perturbed propagators on unmodified gauge fields. We perform this for $a\lambda = 0.0015, 0.015, 0.05, 0.1$, with only a single quark flavour modified at once, on an $N = 351$ subset of Ensemble 1, with $m_\pi = 470$ MeV.

6.2.2 Analysis

Extracting phase shifts from the hadron correlator is only slightly more complicated than the calculating energy shifts. The symmetries of the axial operator remain unchanged, and so we isolate phase shifts at odd order in λ by forming the ratio

$$R(\lambda, t) = \arg \left[\frac{G_\uparrow^+(\lambda, t) G_\downarrow^-(\lambda, -t) G_\downarrow^+(0, t) G_\uparrow^-(0, -t)}{G_\uparrow^+(0, t) G_\downarrow^-(0, -t) G_\downarrow^+(\lambda, t) G_\uparrow^-(\lambda, -t)} \right]^{\frac{1}{4}} = \delta - \phi_{\text{odd}} t, \quad (6.31)$$

where δ is a phase arising from the complex amplitude, and ϕ_{odd} is defined analogously to the odd-order energy shift of Eq. (6.13),

$$\phi_{\text{odd}} \equiv \frac{1}{2} [\phi(\lambda) - \phi(-\lambda)]. \quad (6.32)$$

Since phase shifts can only be determined unambiguously on the interval $(-\pi, \pi)$, we must be careful to ensure that λ is not so large as to cause excessive phase shifts. Analogously to the effective energy shift of Eq. (6.17), we define the effective phase of the ratio of Eq. (6.31) as

$$\phi_{\text{eff}}(t + a/2) \equiv \frac{1}{a}[R(\lambda, t) - R(\lambda, t + a)], \quad (6.33)$$

which at large times should plateau to the phase shift,

$$\phi_{\text{eff}}(t + a/2) \xrightarrow{\text{large } t} \phi_{\text{odd}}. \quad (6.34)$$

We then define the effective axial charge determined through the phase shift as

$$\Delta f_{\text{eff}} \equiv \frac{\phi_{\text{eff}}}{\lambda_f}, \quad (6.35)$$

which at large times should plateau to the axial charge, up to higher-order contamination in λ ,

$$\Delta f_{\text{eff}} \xrightarrow{\text{large } t} \Delta f + \mathcal{O}(\lambda_f^2). \quad (6.36)$$

6.2.3 Results: Validation

Fig. 6.6 shows the connected contribution to the effective axial charge of the u quark in the proton. Included for comparison is the value determined through the analysis of Section 6.1. The signal extracted at small values of λ appears to be consistent with the previous calculation, however at $a\lambda_u = 0.05$ we see a small shift in the effective charge, indicating that we have left the linear regime. This is also apparent in Fig. 6.7, where we show the extracted proton phase shifts for couplings to the u and d quarks, as a function of λ . Again, for comparison we have included the fits to the energy shifts from Fig. 6.4. While the cubic contamination at large values of λ is more significant, the linear term appears to be consistent. We obtain for the renormalised connected contributions to the u and d axial charges in the proton,

$$[\Delta u_p]_{\text{conn}}^{\text{latt}} = 0.990(16), \quad (6.37)$$

$$[\Delta d_p]_{\text{conn}}^{\text{latt}} = 0.327(11). \quad (6.38)$$

These can be compared with the extraction of the same quantities in Section 6.1,

$$[\Delta u_p]_{\text{conn}}^{\text{latt}} = 0.990(13), \quad (6.39)$$

$$[\Delta d_p]_{\text{conn}}^{\text{latt}} = 0.321(07). \quad (6.40)$$

The quantities are consistent within error. Hence, we are confident that we can extract accurate and precise values for hadronic quantities from correlator phase shifts, and can now proceed to the full disconnected calculation.

6.2.4 Simulation Details: Disconnected Calculation

To perform the disconnected calculation, we generate new gauge ensembles with the modified Lagrangian of Eq. (6.28), with the axial coupling applied to the u ,

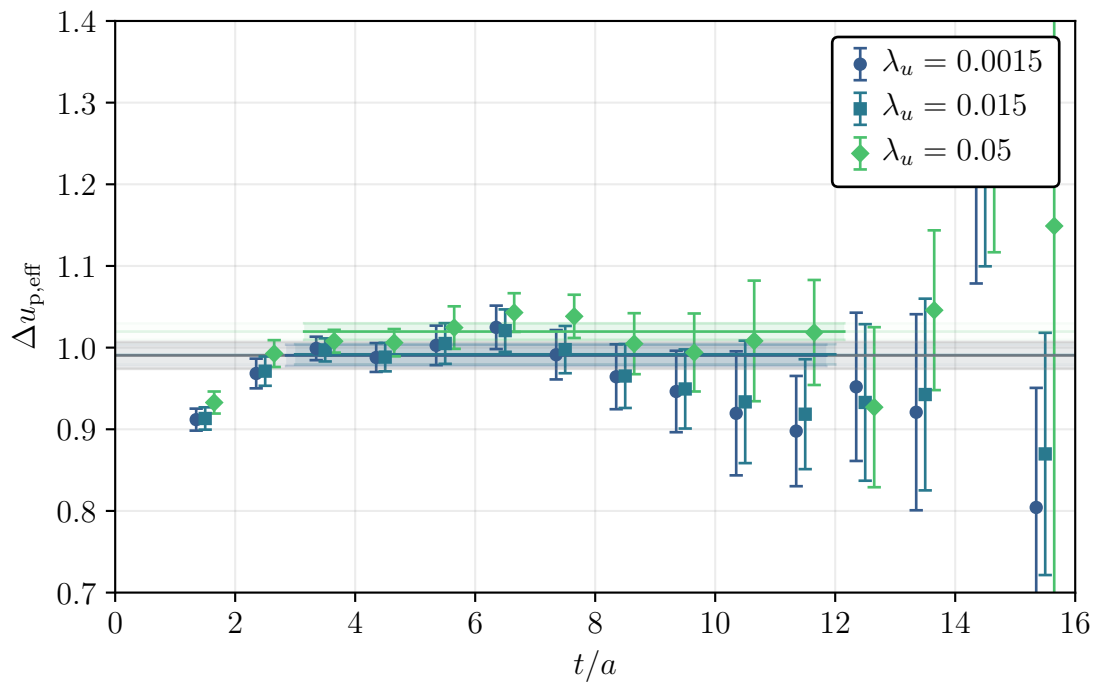


Figure 6.6: Connected effective axial charge of the u quark in the proton, along with the axial charge determined in Section 6.1 (in grey). Calculated on an $N = 342$ subset of Ensemble 1, with $m_\pi = 470$ MeV.

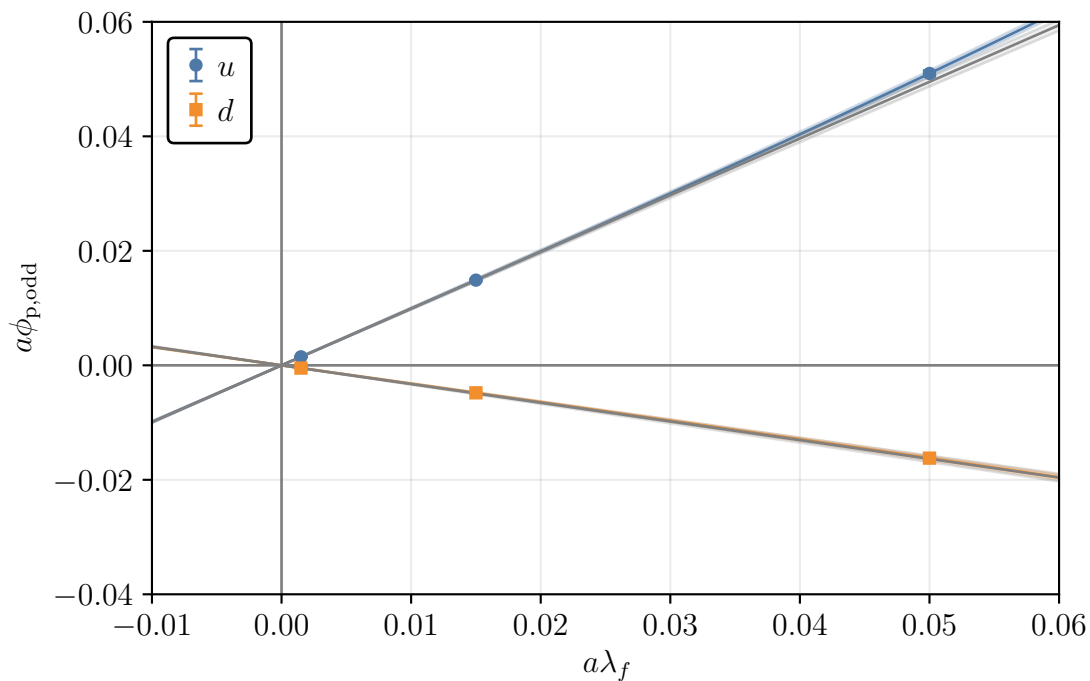


Figure 6.7: Connected phase shifts in the proton extracted for modifications to the u and d quarks, with a fit including linear and cubic terms. Also shown in grey is the linear slope expected from the data of Section 6.1. Calculated on an $N = 342$ subset of Ensemble 1, with $m_\pi = 470$ MeV.

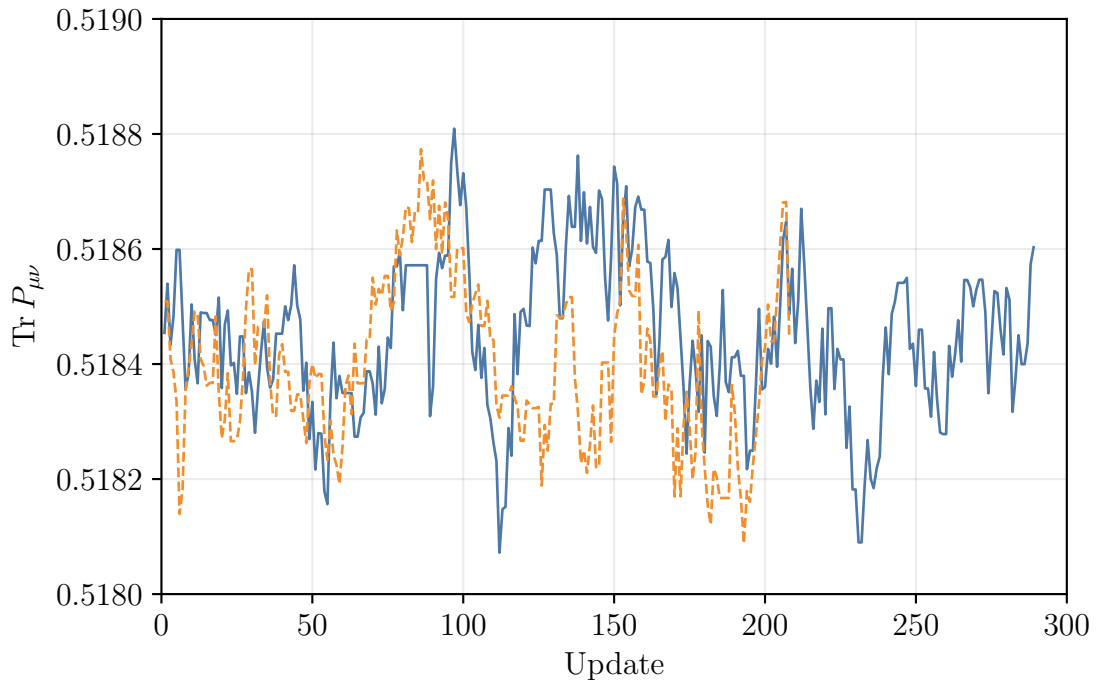


Figure 6.8: Value of the trace of the plaquette on Ensemble A1, for two different Monte Carlo chains.

d and s quark simultaneously. Since there is no correlation between the different ensembles generated, we cannot take advantage of ratios involving $\lambda \neq 0$ and $\lambda = 0$ correlators, which will affect the qualities of the signals extracted. For this reason, by simulating with axial coupling to multiple quark flavours simultaneously, we increase the magnitude of the extracted signal, hopefully boosting signal-to-noise ratios. The statistics of the newly generated ensembles are summarised in Appendix I. In future simulations we are considering the use of reweighting [170, 171] or parallel tempering [172, 173] to generate correlated gauge ensembles with different axial couplings, to improve extracted signals.

Fig. 6.8 shows the average value of the traced plaquette as defined in Eq. (3.17) on Ensemble A1 for two HMC trajectories, after thermalisation has occurred. The value of the plaquette oscillates between reasonable values, and does not appear to diverge over the time frame. We have confidence, therefore, that the introduction of the axial coupling of Eq. (6.28) has not severely affected the configurations.

Table 6.3 summarises the statistics of this calculation. We have calculated quark propagators from both an unmodified Dirac operator, and a modified Dirac operator including the axial coupling. That is, the modification to the QCD Lagrangian can be written as

$$\mathcal{L} \rightarrow \mathcal{L}'(\lambda) = \mathcal{L} + (\lambda_{f,\text{conn}} + \lambda_{f,\text{disc}})\mathcal{A}_3^f, \quad (6.41)$$

Ensemble	N_{meas}	$a\lambda_{\text{conn}}$
1	351	0.0, 0.0015, 0.015, 0.05, 0.1
A1	490	-0.0125, -0.00625, 0.0, 0.00625, 0.0125, 0.03
A2	374	-0.0125, -0.00625, 0.0, 0.00625, 0.0125, 0.03
A3	522	-0.03, 0.0, 0.00625, 0.0125
A4	593	-0.025, 0.0, 0.0125, 0.05
A5	864	-0.025, 0.0, 0.0125, 0.05

Table 6.3: Statistics of the calculation of disconnected contribution to axial charges. Full details of each ensemble can be found in Appendix I. $a\lambda_{\text{conn}}$ here refers to the values of λ used for the calculation of modified quark propagators, allowing access to the connected contributions.

and the phase shifts

$$\left. \frac{\partial \phi_X(\mathbf{p} = \mathbf{0}, \sigma)}{\partial \lambda_{f,\text{conn}}} \right|_{\lambda=0} = \sigma \Delta f_{X,\text{conn}}, \quad (6.42)$$

$$\left. \frac{\partial \phi_X(\mathbf{p} = \mathbf{0}, \sigma)}{\partial \lambda_{f,\text{conn}}} \right|_{\lambda=0} = \sigma \Delta f_{X,\text{disc}}. \quad (6.43)$$

Hence we can determine not only the disconnected contributions to the axial charges, but the full quantities including both contributions. Relative to the cost of generating new gauge ensembles, these additional propagators are extremely cheap.

Using the propagators calculated, we construct hadron two-point functions as before, and determine the phase shifts through the analysis of Section 6.2.2, where disconnected phase are determined through the ratio of Eq. (6.31) without the $\lambda_{\text{disc}} = 0$ contributions, as these are not correlated, as already discussed.

6.2.5 Results: Disconnected Calculation

Fig. 6.9 shows the effective proton phase shifts observed with λ_{disc} applied equally to the three simulated quark flavours in the sea, as calculated at the heaviest pion mass $m_\pi = 470$ MeV. These shifts do not include any connected contribution. The signal is much less clean here as in the validation calculation, particularly for the smallest value of λ_{disc} , as we are not able to take advantage of the correlations of a $\lambda_{\text{disc}} = 0$ result. Despite this, we are able to extract a statistically significant non-zero signals for the larger values of λ_{disc} . Fig. 6.10 shows the extracted proton phase shifts as a functions of λ . Here it is clear that the smallest value of λ is not useful in constraining the fit, and in future simulations we will have a better idea of the range of λ it is most useful to simulate.

To make use of the full statistics available to us, and the relatively low cost of simulating additional connected λ , we perform a global fit to the phase shifts including perturbations due to both disconnected and connected axial couplings,

$$\phi = \lambda_{f,\text{conn}} \left. \frac{\partial \phi}{\partial \lambda_{f,\text{conn}}} \right|_{\lambda=0} + \lambda_{f,\text{disc}} \left. \frac{\partial \phi}{\partial \lambda_{f,\text{disc}}} \right|_{\lambda=0}. \quad (6.44)$$

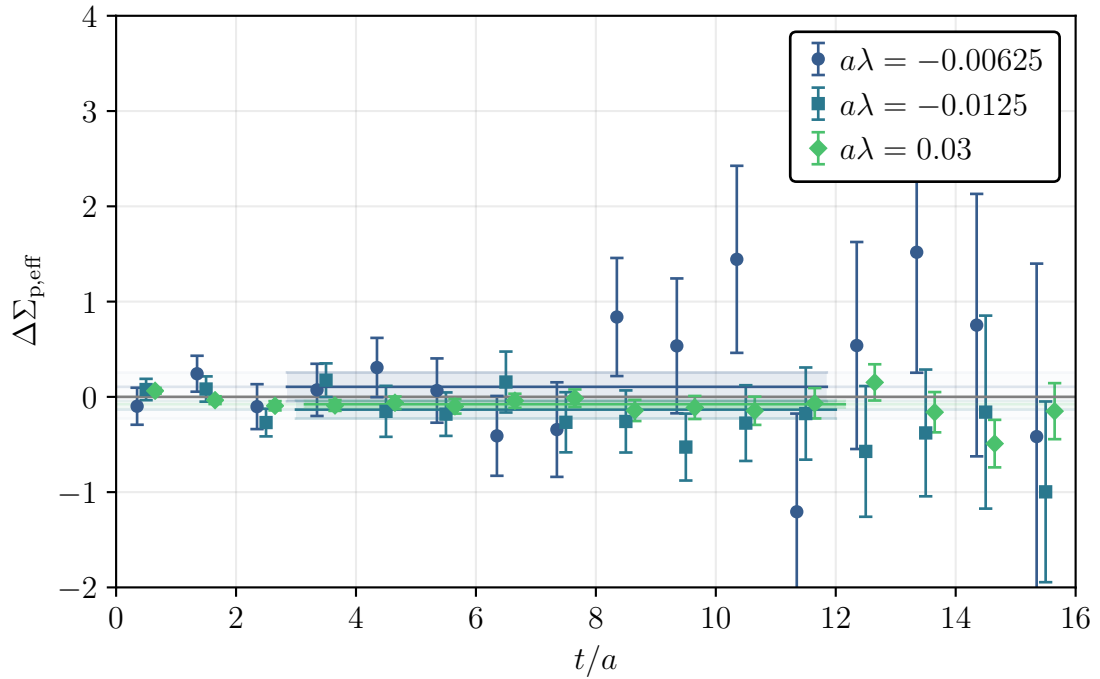


Figure 6.9: Total disconnected effective axial charge of the proton, calculated on Ensembles A1 to A3, with $m_\pi = 470$ MeV.

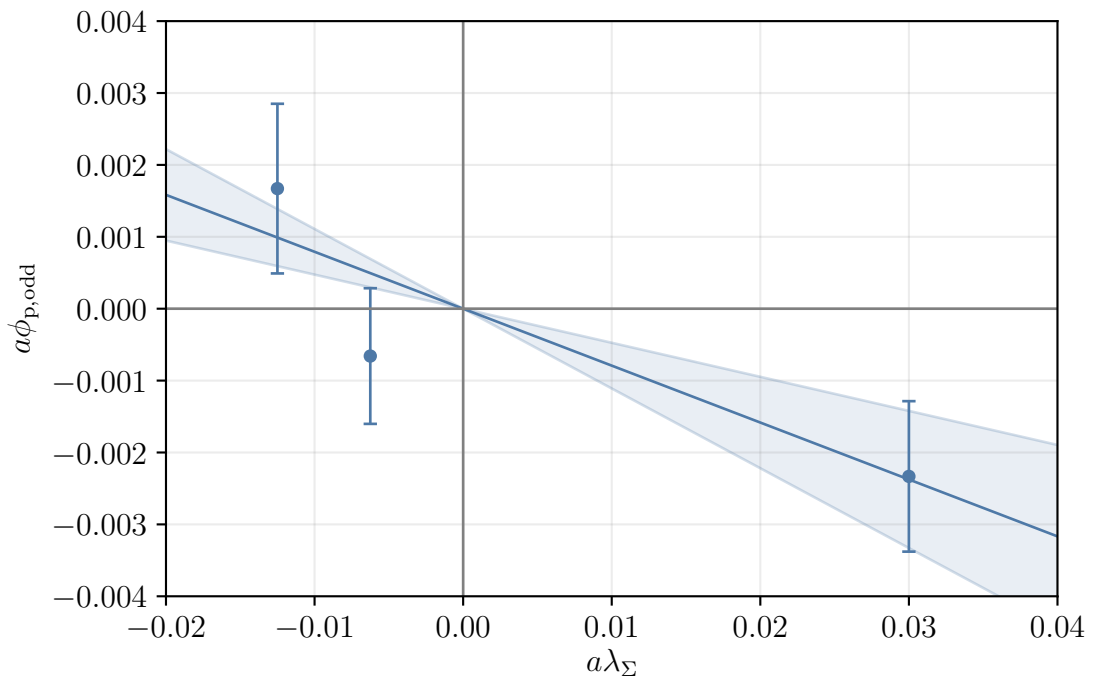


Figure 6.10: Disconnected proton phase shifts calculated for different axial coupling strengths, calculated on Ensembles A1 to A3, with $m_\pi = 470$ MeV.

To renormalise the disconnected contributions, we must include mixing between the connected and disconnected contributions,

$$[\Delta\Sigma]_{\text{disc}}^{\overline{\text{MS}}} = Z_{A,S}^{\overline{\text{MS}}} \Delta\Sigma_{\text{disc}} + \left(Z_{A,S}^{\overline{\text{MS}}} - Z_{A,\text{NS}}^{\overline{\text{MS}}} \right) \Delta\Sigma_{\text{conn}}, \quad (6.45)$$

where subscript S and NS here refer to singlet and non-singlet renormalisation.

At the $\text{SU}(3)_{\text{flavour}}$ -symmetric point, the contributions from the u , d and s are equal, and we determine the disconnected strange quark spin contribution

$$[\Delta s_{\text{p}}]_{\text{disc}}^{\overline{\text{MS}}(2 \text{ GeV})} = \frac{1}{3} [\Delta\Sigma_{\text{p}}]_{\text{disc}}^{\overline{\text{MS}}(2 \text{ GeV})} = -0.018(9). \quad (6.46)$$

As the proton has no valence strange content, the strange axial charge is a purely disconnected quantity. As a point of comparison, we quote the renormalised result for Δs_{p} stochastically estimated in [105], at a pion mass of $m_{\pi} \approx 285 \text{ MeV}$,

$$[\Delta s_{\text{p}}]_{\text{disc}}^{\overline{\text{MS}}(2 \text{ GeV})} = -0.023(10). \quad (6.47)$$

There is good agreement between these results, and the flavour-symmetry-breaking effects do not appear to be severe over this range of pion masses. The precision is comparable as well.

Away from the symmetric point, we can only estimate the strange contribution assuming $\text{SU}(3)_{\text{flavour}}$ -symmetry breaking effects are minor. The strange quark spin contributions determined for the proton are shown in Fig. 6.11, in comparison with a selection of other cutting-edge results [105, 174, 175]. In terms of accuracy and precision, our results compare excellently with the results of other collaborations, although this is only qualitative, as we have not determined the strange quark contribution specifically at the lighter mass point.

Quantifying the computational cost of the FH approach relative to existing techniques is difficult, due to the wide variety of lattice and algorithmic schemes used. The calculation of $\Delta\Sigma_{\text{disc}}$ presented here at $m_{\pi} \approx 470 \text{ MeV}$ we estimate to be roughly equivalent to a total of 3×10^4 inversions of the Dirac operator. This is based on the number of conjugate-gradient (CG) iterations performed during gauge field generation and the calculation of quark propagators. We estimate the results of [105], at a lighter pion mass of $m_{\pi} \approx 285 \text{ MeV}$, required of the order of 1×10^5 measurements, based on the stated number of CG iterations, and an estimate of the number of inversions required for the calculation of a quark propagator at the simulated mass. Similarly the calculations in [175] are stated to have required approximately 1.5×10^5 measurements, at a pion mass of 370 MeV . All three techniques produce uncertainties which are broadly comparable, and hence we conclude that for this particular calculation, the FH method is at least competitive.

6.3 Conclusions and Outlook

In this chapter we have calculated both connected and disconnected contributions to the quark axial charges of hadrons through the FH method. We have shown quark-spin suppression in the light hadrons and hyperons is universal, with connected contributions of the order 60–70%, and have begun to investigate the effects of $\text{SU}(3)_{\text{flavour}}$ -symmetry breaking on individual flavour contributions. Results for Δs are consistent with previous investigations, showing a contribution of around -2% at

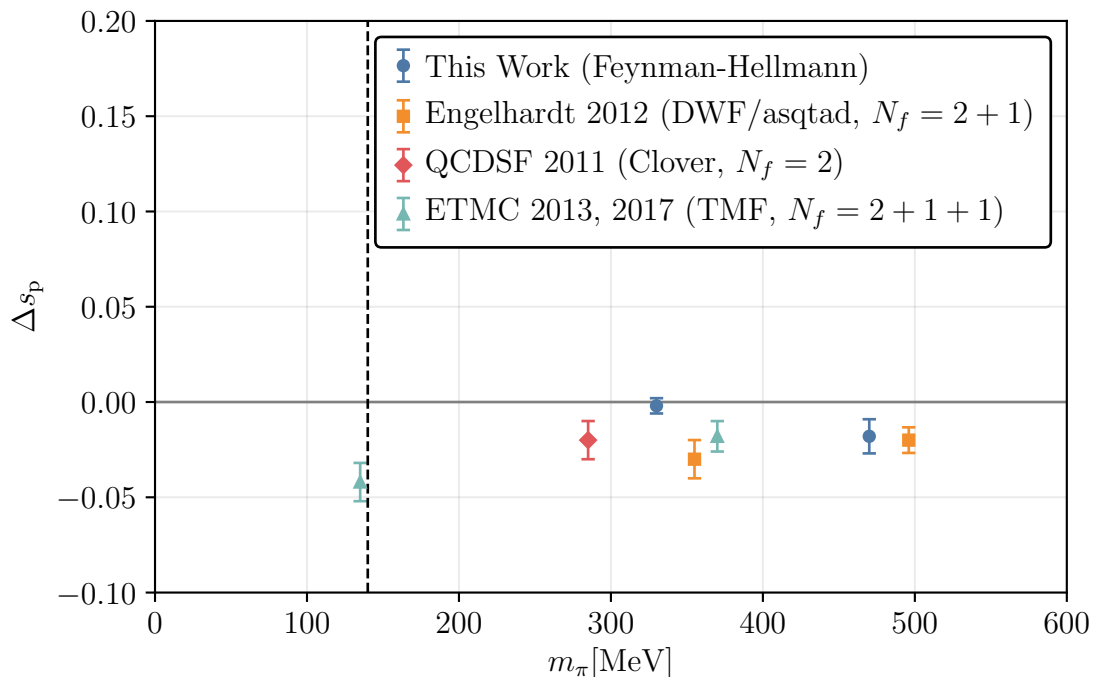


Figure 6.11: Strange quark spin contribution to the proton as a function of m_π , in comparison with results of [105, 174, 175].

heavier pion masses. Our calculation of the disconnected contributions to $\Delta\Sigma$ show minimal evidence of flavour-symmetry breaking effects within the current precision.

From the results obtained, there are some clear advantages to the FH approach. As evidenced by the comparison with the standard three-point function approach, the method is highly cost-effective for studies of a single operator, and there is excellent control of excited states through the analysis of two-point functions. The method appears to be at least competitive with existing stochastic techniques for calculating disconnected contributions, and future investigations will focus on improving signal-to-noise in this case, Reweighting and parallel-tempering are both attractive options for generating correlated gauge ensembles, to better isolate phase shifts in hadron correlators.

Although the results were not discussed here, the disconnected contributions to quark spin fractions of other hadrons can be constructed from the results of the existing calculation, and such results may be important inputs to spin structure investigations of a greater range of particles. The disconnected technique in general can be applied to a far wider range of hadronic observables, for instance, tensor charges and strangeness form factors.

Chapter 7

The Electromagnetic Structure of Hadrons: Form Factors

“This reduction at large angles below the curve for point charge represents the effect of a ‘structure factor’ or a ‘form factor’ for the proton and hence indicates the finite size of the proton. . . . the experiment indicates the proton is not a point.”

—R. W. McCallister and R. Hofstadter, Phys. Rev. D102 (1956) [176]

Investigations of the electromagnetic structure of matter have a history extending back to the 1950s, with the first high-energy studies of the charge and magnetisation densities of atomic nuclei [177]. Probes of the charge density of the proton soon followed [176, 178], and there now exists an extended experimental program aimed at understanding how the electromagnetic structure of hadrons emerges from the dynamics of QCD. An important part of this endeavour is the determination of electromagnetic form factors, which are important inputs to the elastic components of electromagnetic interactions.

The spacelike electromagnetic form factors $F_{i,X}$ of a hadron can be defined through a decomposition of the electromagnetic matrix elements,

$$\langle X(\mathbf{p}') | \mathcal{J}_\mu(0) | X(\mathbf{p}) \rangle = \sum_i [c_{i,X}]_\mu F_{i,X}(Q^2), \quad (7.1)$$

where the known kinematic factors $[c_{i,X}]_\mu$ are determined through Lorentz-invariance and other symmetries. The electromagnetic current here is the usual charge-weighted sum of vector current densities,

$$\mathcal{J}_\mu(x) = \sum_f e_f \mathcal{V}_\mu^f(x), \quad (7.2)$$

$$\mathcal{V}_\mu^f(x) \equiv \bar{\psi}_f(x) \gamma_\mu \psi_f(x), \quad (7.3)$$

and the form factors $F_{i,X}(Q^2)$ are functions of the invariant momentum

$$Q^2 \equiv q^2 = (p' - p)^2. \quad (7.4)$$

In Minkowski space, $Q^2 \equiv -q^2 > 0$ for spacelike momentum transfers. With the Wick rotation to Euclidean space, the relative minus sign between Q^2 and

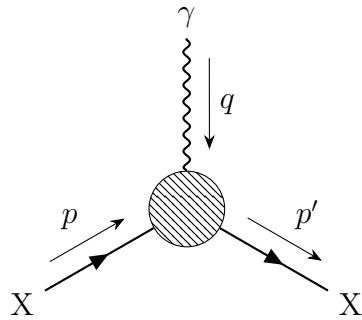


Figure 7.1: Hadron-photon vertex parameterised by the electromagnetic form factors.

q^2 vanishes. The form factors $F_{i,X}$ parameterise the electromagnetic interaction of Eq. (7.1), determining the corresponding amplitude for the effective vertex illustrated in Fig. 7.1. At low-energies, the QCD dynamics which determine the amplitude of this vertex are fundamentally non-perturbative, and the form factors must be determined empirically, or through a non-perturbative method such as lattice QCD.

Physically, form factors have traditionally been interpreted in the non-relativistic limit as three-dimensional Fourier transforms of charge and magnetisation distributions in hadrons. This is not strictly correct [179], and rather form factors should be identified as two-dimensional Fourier transforms of transverse charge and magnetisation densities, as defined in the transverse plane of a fast-moving hadron. For the case of a spin-zero meson with a single form factor F , the transverse charge density

$$\rho(\mathbf{b}) = \int \frac{d^2k}{(2\pi)^2} e^{-i\mathbf{k}\cdot\mathbf{b}} F(Q^2 = \mathbf{k}^2) = \int_0^\infty \frac{d|Q|}{2\pi} |Q| J_0(|Q||\mathbf{b}|) F(Q^2), \quad (7.5)$$

where \mathbf{b} is the impact parameter in the transverse plane, J_0 is a cylindrical Bessel function of the first kind, and the second equality is the result of evaluating the angular component of the integral. This relation between the form factor and transverse charge density allows the definition of a corresponding charge radius,

$$\langle r^2 \rangle \equiv -\frac{6}{F(0)} \left. \frac{dF(Q^2)}{dQ^2} \right|_{Q^2=0}. \quad (7.6)$$

For these reasons, it is clear that determining form factors over a wide range of energies is desirable, as they provide important information about the extended spatial structure of hadrons [180–183].

In this thesis we will focus on the electromagnetic structure of two particles, the first being the pion. The vector matrix element of the pion is parameterised by a single form factor,

$$\langle \pi(\mathbf{p}') | \mathcal{J}_\mu(0) | \pi(\mathbf{p}) \rangle = -i(p' + p)_\mu F_\pi(Q^2), \quad (7.7)$$

which can be related to the transverse charge density and charge radius of the pion through Eqs. (7.5) and (7.6). F_π is well-known at small momentum transfers from pion scattering off atomic electrons [184–190], shown diagrammatically in Fig. 7.2. At higher energies, scattered pions begin to probe the atomic nucleus, and so F_π is instead determined through pion electroproduction off nucleon targets [191–199], shown

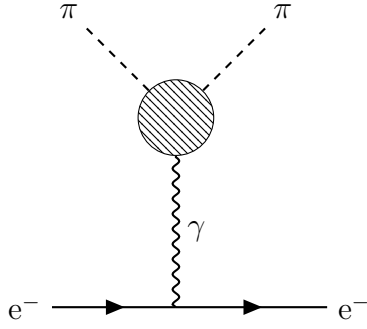


Figure 7.2: Diagram for pion-electron scattering, primary method for accessing F_π at low Q^2 .

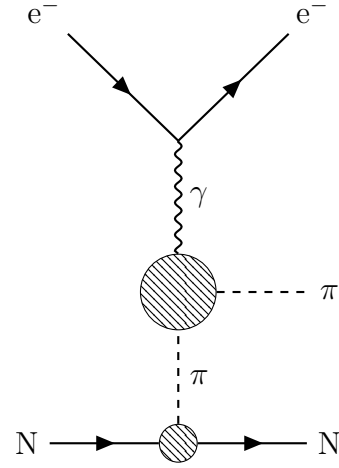


Figure 7.3: Diagram for pion electroproduction off the nucleon, primary method for accessing F_π at high Q^2 .

diagrammatically in Fig. 7.3. Extractions at high momentum transfers have proven challenging, due in part to the model dependence of the pion-nuclear interaction in Fig. 7.3. A selection of data for F_π from various experimental efforts [189, 193, 198–200] is shown in Fig. 7.4. Also included is the prediction of the vector meson dominance (VMD) model [201],

$$F_\pi(Q^2) \approx \frac{1}{1 + Q^2/m_\rho^2}, \quad (7.8)$$

where m_ρ is the mass of the ρ meson. In practice, VMD describes F_π well only in the low- Q^2 region. At very large Q^2 , perturbative QCD (pQCD) predicts an approximate $1/Q^2$ decay of F_π [202–205], with

$$F_\pi(Q^2) \xrightarrow{\text{large } Q^2} \frac{16\pi}{Q^2} \alpha_S(Q^2) f_\pi, \quad (7.9)$$

where f_π is the pion decay constant, and α_S is the renormalised strong coupling of Eq. (2.10). However, there is significant disagreement about the nature of the transition to the asymptotic regime [205, 206], and at present the experimental data is unable to discriminate between different models. The 12 GeV upgrade of the Continuous Electron Beam Accelerator Facility (CEBAF) at Jefferson Lab (JLab) will hopefully go some way to addressing the lack of precise experimental data in this intermediate Q^2 region.

The second particle of interest in this thesis is the proton. Due to its extra spin degree-of-freedom, the vector matrix elements of the proton are decomposed into two form factors,

$$\langle p(\mathbf{p}', \sigma') | \mathcal{J}_\mu(0) | p(\mathbf{p}, \sigma) \rangle = \bar{u}(p', \sigma') \left[\gamma_\mu F_{1,p}(Q^2) + \sigma_{\mu\nu} \frac{q_\nu}{2m_p} F_{2,p}(Q^2) \right] u(p, \sigma). \quad (7.10)$$

Here $F_{1,p}$ and $F_{2,p}$ are the Pauli and Dirac form factors of the proton, and u is the positive-energy spinor solution to the free Dirac equation (described in Appendix F).

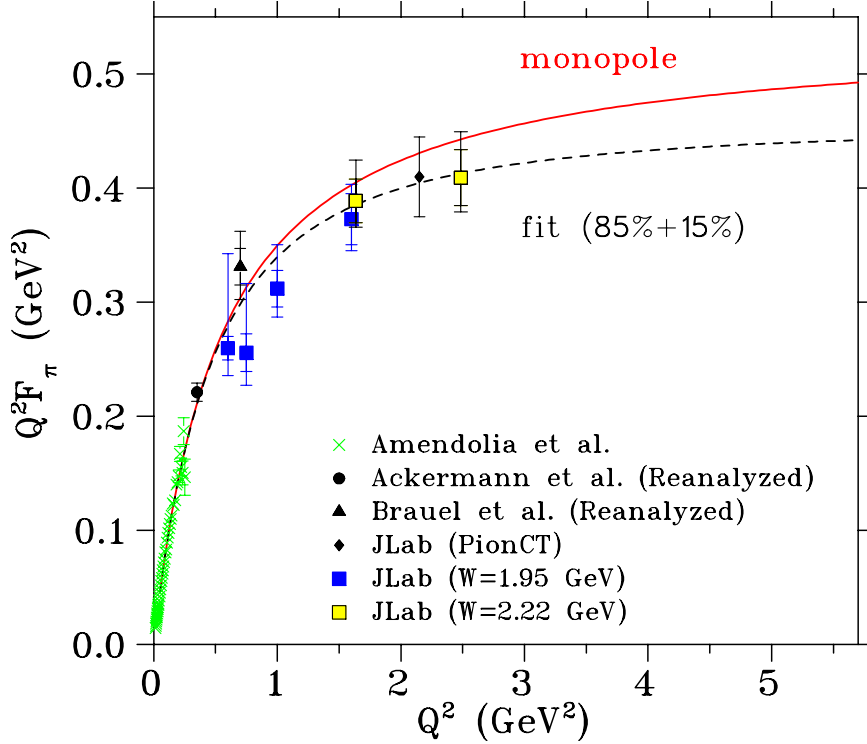


Figure 7.4: Form factor of the pion determined through experiment [189, 193, 198–200]. Included also is the monopole dependence expected at low Q^2 from VMD, and a fit including 85% of the VMD monopole, and 15% dipole correction. Image obtained from [199].

In the frame where $-\mathbf{p}' = \mathbf{p} = \mathbf{q}/2$, the matrix element can be written as

$$\langle p(-\mathbf{q}/2, \sigma') | \mathcal{J}_\mu(0) | p(\mathbf{q}/2, \sigma) \rangle = \begin{cases} 2m_p G_{E,p}(Q^2) \delta_{\sigma'\sigma} & \mu = 4, \\ [\mathbf{s} \times \mathbf{q}]_i G_{M,p}(Q^2) \delta_{\sigma'\sigma} & \mu = i, \end{cases} \quad (7.11)$$

where \mathbf{s} is the relativistic three-spin of the proton (defined in Appendix F), and the Sachs electromagnetic form factors $G_{E,p}$ and $G_{M,p}$ are defined as

$$G_{E,p}(Q^2) \equiv F_{1,p}(Q^2) - \frac{Q^2}{4m_p^2} F_{2,p}(Q^2), \quad (7.12)$$

$$G_{M,p}(Q^2) \equiv F_{1,p}(Q^2) + F_{2,p}(Q^2). \quad (7.13)$$

The Sachs form factors are the most straightforward to interpret physically, as they are (non-relativistically) three-dimensional Fourier transforms of charge and magnetisation distributions. More correctly, the Pauli and Dirac form factors are two-dimensional Fourier transforms of transverse charge and magnetisation densities, through analogous relations to Eq. (7.5),

$$\rho_{E,p}(\mathbf{b}) = \int_0^\infty \frac{d|Q|}{2\pi} |Q| J_0(|Q||\mathbf{b}|) F_{1,p}(Q^2), \quad (7.14)$$

$$\rho_{M,p}(\mathbf{b}) = |\mathbf{b}| \sin^2(\phi) \int_0^\infty \frac{d|Q|}{2\pi} Q^2 J_1(|Q||\mathbf{b}|) F_{2,p}(Q^2). \quad (7.15)$$

Here J_1 is a cylindrical Bessel function of the first kind, and ϕ is the angle between the impact parameter \mathbf{b} and the proton polarisation. The electric and magnetic radii

of the proton are given by

$$\langle r^2 \rangle_{\text{E,p}} = -\frac{6}{G_{\text{E,p}}(0)} \left. \frac{dG_{\text{E,p}}(Q^2)}{dQ^2} \right|_{Q^2=0}, \quad (7.16)$$

$$\langle r^2 \rangle_{\text{M,p}} = -\frac{6}{G_{\text{M,p}}(0)} \left. \frac{dG_{\text{M,p}}(Q^2)}{dQ^2} \right|_{Q^2=0}, \quad (7.17)$$

and in the forward limit,

$$G_{\text{E,p}}(0) = F_{1,\text{p}}(0) = 1, \quad (7.18)$$

$$G_{\text{M,p}}(0) = 1 + F_{2,\text{p}}(0) = \mu_{\text{p}}, \quad (7.19)$$

where the first relation is a consequence of charge conservation, and μ_{p} is the magnetic moment of the proton.

Early experimental results for the electromagnetic form factors of the proton were obtained using the Rosenbluth separation technique in electron-proton scattering [207–210]. Broadly, these results indicated that the electric and magnetic form factors scaled proportionally for $Q^2 \lesssim 6 \text{ GeV}^2$, with $\mu_{\text{p}} G_{\text{E,p}}/G_{\text{M,p}} \approx 1$. This was later found to be in disagreement with recoil polarisation experiments at JLab which showed $\mu_{\text{p}} G_{\text{E,p}}/G_{\text{M,p}}$ decreasing approximately linearly for $Q^2 \gtrsim 0.5 \text{ GeV}^2$ [211–215]. Results from both techniques are shown in Fig. 7.5. This discrepancy is now largely understood through studies of two-photon exchange effects in the Rosenbluth method [216, 217]. Additionally, models including the effects of quark orbital angular momentum favour the more recent results [218].

Despite experimental progress, it is still unknown whether the linear Q^2 trend continues and crosses zero, or if the fall-off with Q^2 slows down. This has important consequences for our understanding of nucleon structure [180, 219, 220]. Based on our previous discussion of transverse charge densities, a zero-crossing in G_{E} would correspond to a dominance of negative charge in the central region of the proton. Experimental results are as yet unable to obtain precise results at the relevant momentum scales, and so this remains an open question. Resolving the scaling of the form factors in the high- Q^2 domain is another of the key physics goals of the upgraded CEBAF at JLab.

Lattice calculations of hadronic form factors have typically focussed on the study of processes at low momentum transfer [223–228], and there have been only limited studies of the form factors at large $Q^2 \gtrsim 3 \text{ GeV}^2$ [100, 229]. As the form factors are decreasing functions of Q^2 , signal-to-noise ratios increase as one attempts to probe higher energy scales. This is compounded by a deterioration of the signal as the momentum of a hadron state is increased. In order to avoid this issue, three-point functions projected to zero sink momentum are commonly studied, and hence the possible momentum transfers are limited by the maximum momentum available at the source. With limited statistical signal, it has therefore been difficult to assess the degree of excited-state contamination, which can lead to significant systematic uncertainty [93, 97, 100, 101, 227].

A recently introduced technique which may go some way to improving this situation is the method of momentum-smearred interpolators [230]. Lattice interpolators generally have some level of smearing applied (as discussed in Section 4.1), either to improve the overlap of hadron operators with ground states, or to generate variational bases for the variational method (discussed in Section 4.2). After being

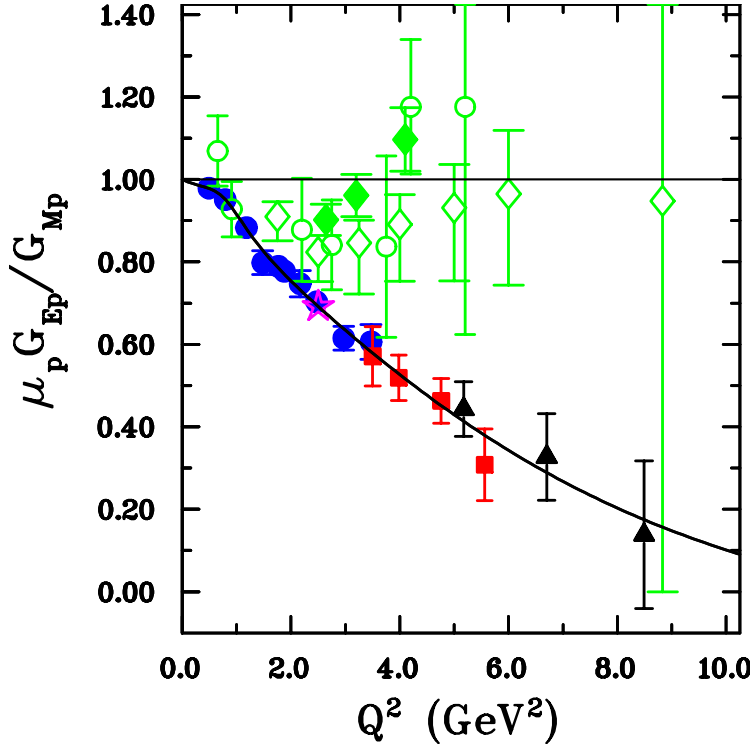


Figure 7.5: Ratio of the electric and magnetic form factors of the proton determined through various experiments [208–210, 213–215, 221], with a fit to the data from [212]. Image obtained from [222].

Fourier-transformed to momentum space, these smeared operators have good overlap with unboosted states, but poor overlap with boosted states. Momentum-smeared operators include an additional phase in the smearing function to improve overlap with specific momentum projections. This method has already seen great deal of success in calculations of parton distributions [231–233].

In this chapter we will demonstrate how one may access high-momentum transfer form factors on the lattice using an extension of the FH theorem to non-forward matrix elements. We will begin in Section 7.1 by calculating the electromagnetic form factor of the pion, before proceeding to extract form factors for both the proton and neutron in Section 7.2. This work of this chapter has been published in [234].

7.1 The Pion Form Factor

Individual flavour contributions to the electromagnetic form factor of the pion are defined through the matrix elements

$$\langle \pi(\mathbf{p}') | \mathcal{V}_\mu^f(0) | \pi(\mathbf{p}) \rangle = -i(p' + p)_\mu F_\pi^f(Q^2), \quad (7.20)$$

where the vector current density and invariant momentum Q^2 are as defined in Eqs. (7.3) and (7.4), and the full pion form factor

$$F_\pi(Q^2) = \sum_f e_f F_\pi^f(Q^2). \quad (7.21)$$

To determine the matrix elements of Eq. (7.20), we consider Lagrangians including a coupling with momentum transfer to the vector current, as in Sections 5.2.3 and 5.3.4. Here we modify the Lagrangian such that

$$\mathcal{L}(x) \longrightarrow \mathcal{L}'(x) = \mathcal{L}(x) + 2\lambda_f \cos(\mathbf{q} \cdot \mathbf{x}) \mathcal{V}_4^f(x), \quad (7.22)$$

and hence the linear shift in the energy of a pion projected to momentum \mathbf{p}' is given by

$$\left. \frac{dE_\pi(\mathbf{p}')}{d\lambda_f} \right|_{\lambda=0} = -i \frac{[p' + p]_4}{2E_\pi(\mathbf{p})} F_\pi^f(Q^2) = F_\pi^f(Q^2), \quad (7.23)$$

and similarly for $\mathbf{p}' \leftrightarrow \mathbf{p}$, where \mathbf{p}' and \mathbf{p} satisfy the generalised Breit frame condition $E_\pi(\mathbf{p}') = E_\pi(\mathbf{p})$. If instead we had chosen to couple to a spatial component of the vector current, then the first derivative of the energy would vanish for $\mathbf{p}' = -\mathbf{p}$,

$$\left. \frac{dE_\pi(\mathbf{p}')}{d\lambda_f} \right|_{\lambda=0} = -i \frac{[p' + p]_i}{2E_\pi(\mathbf{p})} F_\pi^f(Q^2) = 0. \quad (7.24)$$

Choosing momenta such that $\mathbf{p}' \neq -\mathbf{p}$ would allow extraction of the pion form factor through a spatial coupling, however it will later be advantageous for us to consider only $\mathbf{p}' = -\mathbf{p}$ kinematics in the calculation of the nucleon form factors, and we will then be able to reuse propagators generated during this calculation.

7.1.1 Simulation Details

In this simulation we include the coupling to the vector current in Eq. (7.22) in the Dirac operator, and only access connected contributions to F_π . In principle, one could generate gauge ensembles including the vector coupling, and calculate the disconnected contributions as well, however ensembles would need to be generated for each choice of \mathbf{q} . In any case, as already discussed in Section 4.2.1, the disconnected contributions vanish in the isospin-symmetric limit, and so such calculations would only be of interest for identifying individual flavour contributions. The perturbed propagators are calculated for a coupling to the u quark only, as in the isospin-symmetric limit, the connected u and \bar{d} contributions to the form factor of the π^+ state we simulate are equal, and hence

$$[F_{\pi^+}^u]_{\text{conn}} = -[F_{\pi^+}^d]_{\text{conn}}. \quad (7.25)$$

The disconnected contributions cancel, and hence the full pion form factor as defined in Eq. (7.21) is given by

$$F_\pi = F_{\pi^+} = \frac{2}{3}[F_{\pi^+}^u]_{\text{conn}} - \frac{1}{3}[F_{\pi^+}^d]_{\text{conn}} = [F_{\pi^+}^u]_{\text{conn}}. \quad (7.26)$$

We choose to simulate $a\lambda = 10^{-4}$ or -10^{-5} , on an $N = 1691$ subset of Ensemble 1, with $m_\pi = 470$ MeV. The values of λ simulated here are significantly smaller than those of the calculation in Chapter 6. This is motivated by our observation that when forming correlated ratios, there is no degradation in signal-to-noise for very small values of λ . Simulating such small values allows us to be confident we remain within the linear λ regime, and we can use the unperturbed $\lambda = 0$ propagator as

$(L/2\pi)\mathbf{q}$	$(L/2\pi)\mathbf{p}'$	$(L/2\pi)\mathbf{p}$	$(L/2\pi)^2Q^2$
(2, 0, 0)	$\pm(1, 0, 0)$	$\mp(1, 0, 0)$	4
(2, 2, 0)	$\pm(1, 1, 0)$	$\mp(1, 1, 0)$	8
(2, 2, 2)	$\pm(1, 1, 1)$	$\mp(1, 1, 1)$	12
(4, 0, 0)	$\pm(2, 0, 0)$	$\mp(2, 0, 0)$	16
(4, 2, 0)	$\pm(2, 1, 0)$	$\mp(2, 1, 0)$	20
(4, 2, 2)	$\pm(2, 1, 1)$	$\mp(2, 1, 1)$	24
(4, 4, 0)	$\pm(2, 2, 0)$	$\mp(2, 2, 0)$	32

Table 7.1: Kinematic choices simulated for the calculation of the pion form factor. There is no way to achieve $(L/2\pi)^2Q^2 = 28$ for integer choices of the momentum components on the lattice.

an initial guess for the $\lambda \neq 0$ inversion, which reduces the computational cost of additional values of λ by the order of 50%. The values of the momentum insertion \mathbf{q} chosen are summarised in Table 7.1, where we note all momenta are chosen such that Breit frame momentum projections satisfy $\mathbf{p}' = -\mathbf{p}$. These choices of \mathbf{p}' and \mathbf{p} minimise the magnitude of the momentum projection at the source and sink for each \mathbf{q} , and hence we achieve the best signal-to-noise ratio for any particular Q^2 .

7.1.2 Analysis

The form of the pion correlation function is given in Section 4.1.1. With the modification to the Lagrangian of Eq. (7.23), the amplitude and energy become λ -dependent,

$$G(\lambda, t) \xrightarrow{\text{large } t, T-t} A(\lambda) \cosh \left[E(\lambda) \left(t - \frac{T}{2} \right) \right]. \quad (7.27)$$

As in the analysis of axial charges in of Section 6.1.2, we take advantage of the symmetries of the vector operator to better isolate the energy shifts. Under time-reversal, the temporal component of the vector current changes sign, which results in opposite shifts of the energies of the forwards and backwards-propagating states. It is possible to show that the shift in the couplings is opposite also, and so to first order in λ , the pion correlator at large times is of the form

$$G(\lambda, t) \xrightarrow{\text{large } t, T-t} (A + \Delta A) e^{-(E+\Delta E)t} + (A - \Delta A) e^{-(E-\Delta E)(T-t)}, \quad (7.28)$$

where ΔA and ΔE are the first-order amplitude and energy shifts,

$$\Delta A = \Delta \lambda \frac{dA}{d\lambda}, \quad (7.29)$$

$$\Delta E = \Delta \lambda \frac{dE}{d\lambda}. \quad (7.30)$$

At small boosts where F_π is of order 1, it is necessary for us to fit to this form to correctly describe the behaviour. At large boosts, the signal in the region of forwards/backwards-propagating overlap around $T/2$ is poor, and the signals decay quickly enough that we consider the signal in the forwards or backwards-propagating region separately,

$$G(\lambda, t) \xrightarrow{\text{large } t} A(\lambda) e^{-E(\lambda)t}. \quad (7.31)$$

We average different momentum Breit-frame momentum projections of the correlator,

$$G(\lambda, \pm\mathbf{p}, t) \equiv \frac{1}{2}[G(\lambda, +\mathbf{p}, t) + G(\lambda, -\mathbf{p}, t)], \quad (7.32)$$

and form the ratio

$$R(\lambda, \pm\mathbf{p}, t) \equiv \left| \frac{G(\lambda, \pm\mathbf{p}, t) G(0, \pm\mathbf{p}, -t)}{G(0, \pm\mathbf{p}, t) G(\lambda, \pm\mathbf{p}, -t)} \right|^{\frac{1}{2}}. \quad (7.33)$$

At large times, R isolates the odd-order energy shifts as defined in Eq. (6.13),

$$R(\lambda, \pm\mathbf{p}, t) \xrightarrow{\text{large } t} B(\lambda, \mathbf{p}) e^{-\Delta E_{\text{odd}}(\lambda, \mathbf{p})t}. \quad (7.34)$$

Here B is some λ -dependent amplitude which we are not presently interested in. Isolating odd-order energy shifts ensures contamination to the linear term comes in only at $\mathcal{O}(\lambda^3)$. Analogously to the effective charge of Eq. (6.19), we define the effective form factor

$$F_{\pi, \text{eff}}^f(\lambda, \pm\mathbf{p}, t) \equiv \frac{\Delta E_{\pi, \text{eff}}(\lambda, \pm\mathbf{p}, t)}{\lambda_f} \quad (7.35)$$

where ΔE_{eff} is as defined in Eq. (6.17). At large times, this quantity plateaus to the pion form factor,

$$F_{\pi, \text{eff}}^f(\lambda, \pm\mathbf{p}, t) \xrightarrow{\text{large } t} F_{\pi}^f(Q^2) + \mathcal{O}(\lambda_f^2), \quad (7.36)$$

provided we remain within the regime of linear λ -dependence.

In the continuum, conservation of the local vector current means the vector vertex does not renormalise. On the lattice however, the local vector current is not conserved, and so to determine physical values for the form factors, we apply scaling to enforce charge conservation at $Q^2 = 0$,

$$F_{\pi}(Q^2 = 0) = 1. \quad (7.37)$$

Hence our final results are given by

$$F_{\pi}(Q^2) = \frac{[F_{\pi}(Q^2)]^{\text{latt}}}{[F_{\pi}(Q^2 = 0)]^{\text{latt}}}, \quad (7.38)$$

where there is no scale-dependence on the continuum quantity.

7.1.3 Results

Fig. 7.6 shows the effective pion form factor for different values of Q^2 and λ . The signals for the simulated vector couplings, $a\lambda = 10^{-4}$ and -10^{-5} , are numerically identical, despite a difference of an order of magnitude between the couplings. Hence we can be extremely confident that we are in the linear regime. This is emphasised in Fig. 7.7, which shows the energy shifts as a function of λ for the same Q^2 values. Fig. 7.8 shows the effective form factor for a momentum projection which doesn't satisfy the Breit frame condition, where we note no statistically significant non-zero signal can be extracted for this projection. This is consistent with the expectations

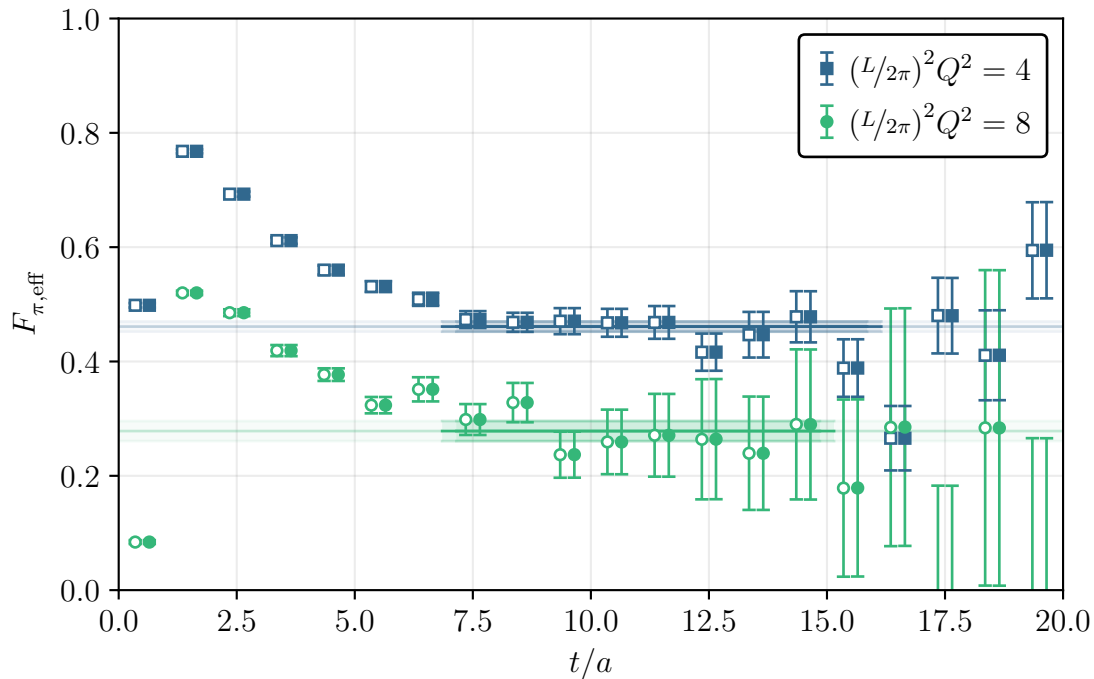


Figure 7.6: Effective pion form factor for different values of Q^2 , and $a\lambda = 10^{-4}, -10^{-5}$ (filled and unfilled markers). This was calculated on an $N = 1691$ subset of Ensemble 1, with $m_\pi = 470$ MeV.

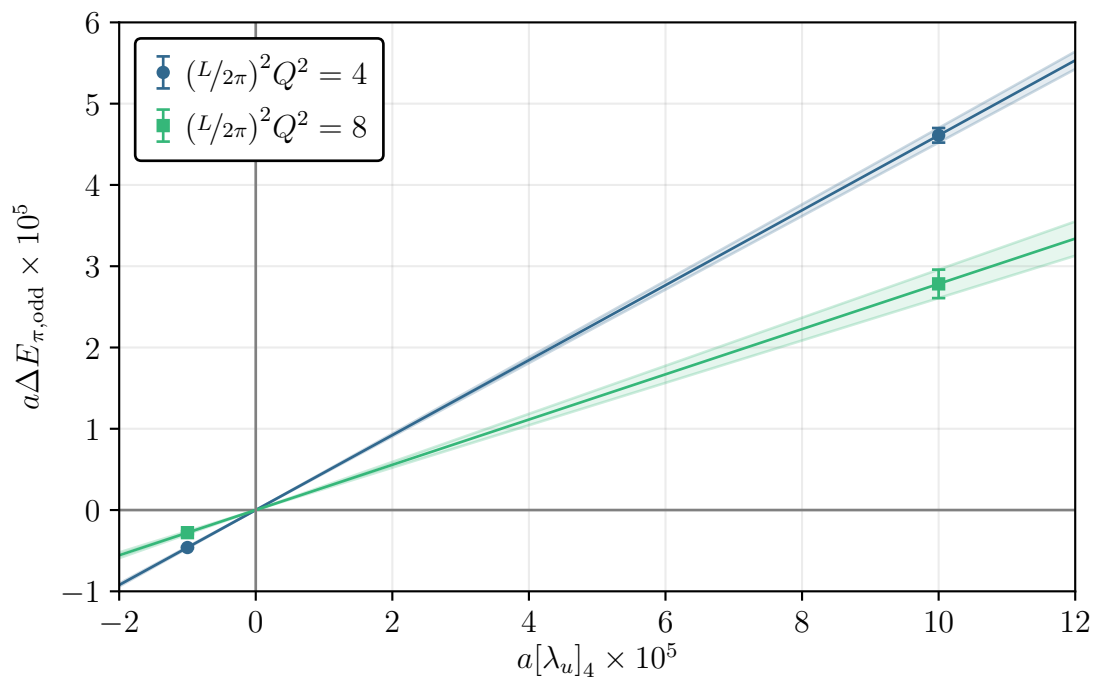


Figure 7.7: Pion energy shifts as a function of λ for different values of Q^2 . These were calculated on an $N = 1691$ subset of Ensemble 1, with $m_\pi = 470$ MeV.

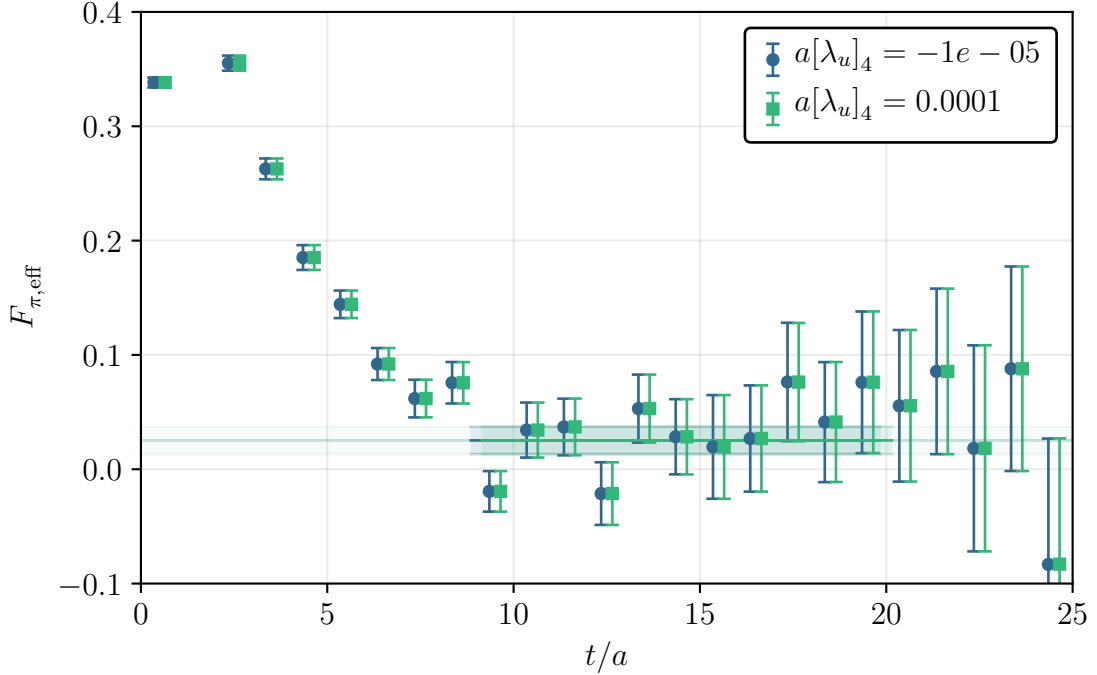


Figure 7.8: Effective pion form factor for $(L/2\pi)^2 Q^2 = 4$, where $(L/2\pi)\mathbf{q} = (2, 0, 0)$ and the momentum projection $(L/2\pi)\mathbf{p}' = (0, 1, 0)$ (a projection which doesn't satisfy the Breit frame condition). This was calculated on an $N = 1691$ subset of Ensemble 1, with $m_\pi = 470$ MeV.

of Section 5.3 that no energy shift will be observed at first order in λ for non-Breit kinematics.

Figs. 7.9 and 7.10 show the pion form factor as a function of Q^2 , with experimental results from JLab [198, 199]. Also included on these plots is the behaviour expected from Eq. (7.8), and on the lower plot the behaviour predicted by pQCD is also indicated. The ρ mass, pion decay constant and number of flavours input to these predictions are different at the physical point, and for the lattice results, and have been set appropriately. The large simulated pion mass ($m_\pi \approx 470$ MeV) has a significant effect on the pion form factor. Qualitatively, heavier quarks are likely to remain closer to the centre of the pion state and decrease the charge radius, decreasing the magnitude of the slope of the form factor near $Q^2 = 0$. While the results are not yet precise enough to begin to discriminate between various models, we have optimism that this will be possible with future extensions to this work, including the use of momentum-smearred interpolators [230].

7.2 The Nucleon Form Factors

Individual flavour contributions to the Pauli and Dirac form factors of the proton are defined through the vector matrix elements

$$\langle \mathbf{p}(\mathbf{p}', \sigma') | \mathcal{V}_\mu^f(0) | \mathbf{p}(\mathbf{p}, \sigma) \rangle = \bar{u}(p', \sigma') \left[\gamma_\mu F_{1,p}^f(Q^2) + \sigma_{\mu\nu} \frac{q_\nu}{2m_p} F_{2,p}^f(Q^2) \right] u(p, \sigma), \quad (7.39)$$

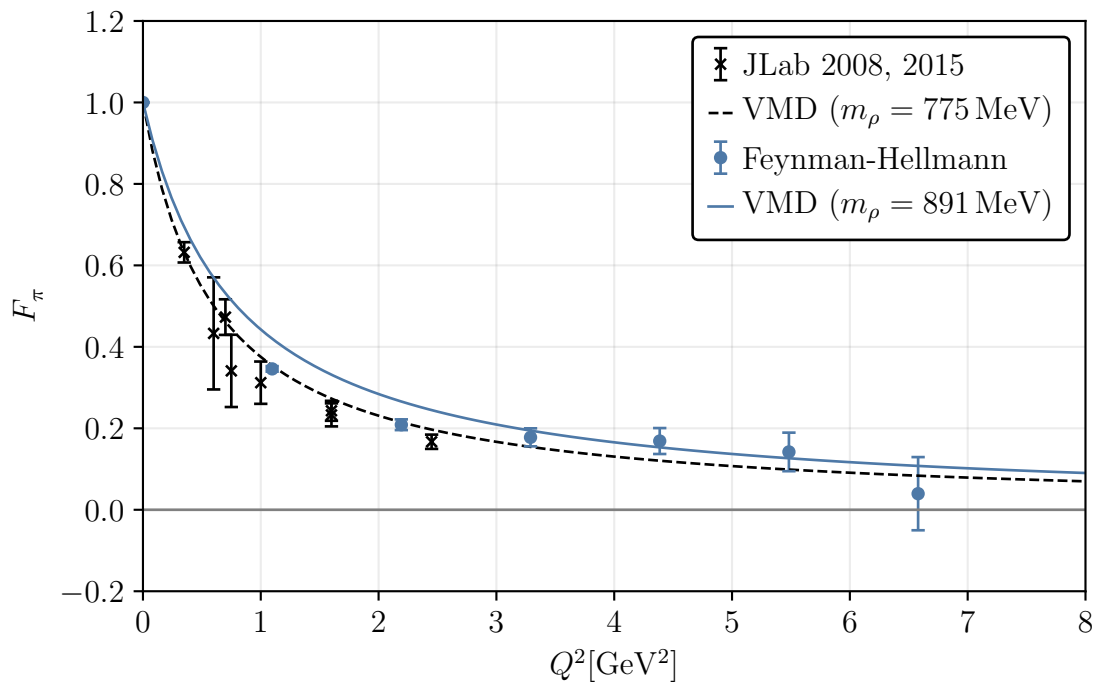


Figure 7.9: F_π calculated through the FH method, in comparison with results from JLab [198, 199]. The behaviour predicted by VMD is included merely to guide the eye. This was calculated on an $N = 1691$ subset of Ensemble 1, with $m_\pi = 470$ MeV.

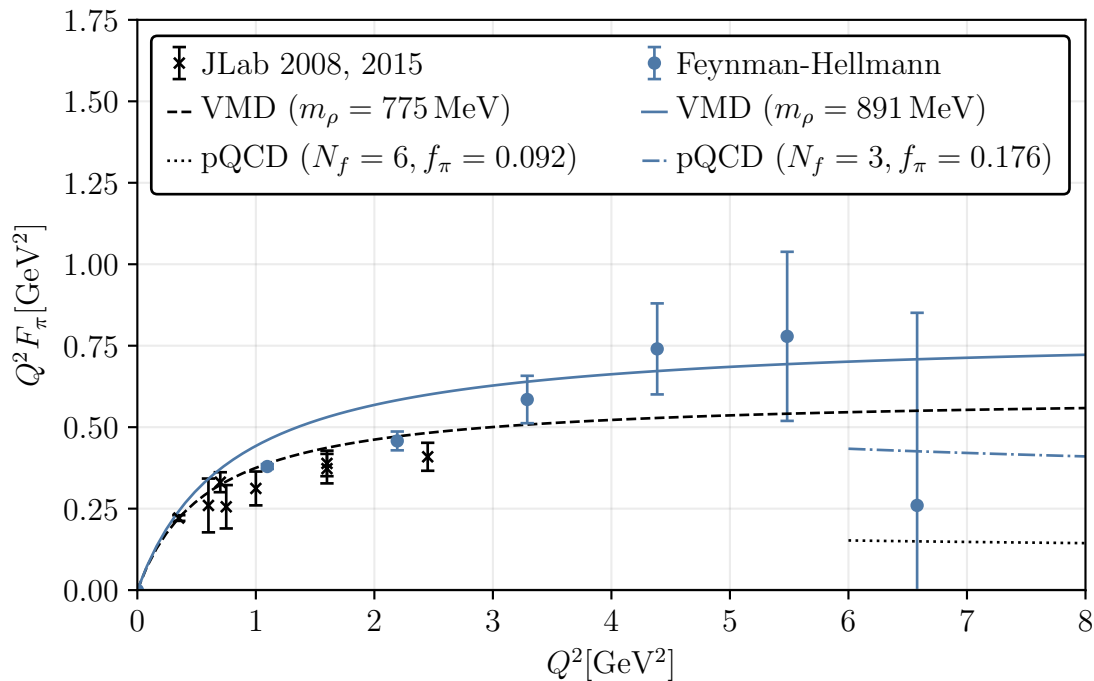


Figure 7.10: $Q^2 F_\pi$ calculated through the FH method, in comparison with results from JLab [198, 199]. The behaviour predicted by VMD is included, as well as the asymptotic behaviour predicted by pQCD. This was calculated on an $N = 1691$ subset of Ensemble 1, with $m_\pi = 470$ MeV.

where the full form factors are then given by

$$F_{1,\mathbf{p}} = \sum_f e_f F_{1,\mathbf{p}}^f, \quad (7.40)$$

$$F_{2,\mathbf{p}} = \sum_f e_f F_{2,\mathbf{p}}^f, \quad (7.41)$$

and similarly for the Sachs form factors. We have discussed modified Lagrangians to calculate the vector form factors of the nucleon in Sections 5.2.4 and 5.3.5. Here we make a modification to the Lagrangian

$$\mathcal{L}(x) \longrightarrow \mathcal{L}'(x) = \mathcal{L}(x) + 2[\lambda_f]_\mu \cos(\mathbf{q} \cdot \mathbf{x}) \mathcal{V}_\mu^f(x), \quad (7.42)$$

where $[\lambda_f]_\mu$ are freely varying real parameters. General energy shifts for a vector coupling of this form are given in Appendix H. For Breit frame kinematics where $\mathbf{p}' \neq -\mathbf{p}$, a spin-polarised nucleon state with a coupling to a spatial component of the vector current experiences both energy and phase shifts. Hence to simplify the analysis, we constrain ourselves to $\mathbf{p}' = -\mathbf{p}$ kinematics, where we have

$$\left. \frac{dE_{\mathbf{p}}(\mathbf{p})}{d[\lambda_f]_4} \right|_{\lambda=0} = \frac{m_{\mathbf{p}}}{E_{\mathbf{p}}(\mathbf{p})} G_{\mathbf{E},\mathbf{p}}^f(Q^2), \quad (7.43)$$

$$\left. \frac{dE_{\mathbf{p}}(\mathbf{p}, \sigma)}{d[\lambda_f]_i} \right|_{\lambda=0} = \frac{[\mathbf{s} \times \mathbf{q}]_i}{2E_{\mathbf{p}}(\mathbf{p})} G_{\mathbf{M},\mathbf{p}}^f(Q^2). \quad (7.44)$$

When $\mathbf{p}' = -\mathbf{p}$, one may show that $\mathbf{s} \times \mathbf{q} = \hat{\mathbf{e}} \times \mathbf{q}$. This choice of momentum projection allows us to isolate the electric and magnetic form factors directly, and so these are the kinematics we choose.

7.2.1 Simulation Details

For this calculation, we make the modification to the Lagrangian of Eq. (7.42) to the Dirac operator, accessing only connected contributions to the form factors. The vector coupling is included with $a\lambda_2$ and $a\lambda_4$ taking values of 10^{-4} or -10^{-5} separately, so we only couple to temporal or spatial components at once. The quark propagators calculated to construct the pion form factor in Section 7.1 are reused in this calculation, highlighting again an advantage of the FH method in the reuse of propagators for calculations involving different hadrons. The extra propagators are calculated on the same $N = 1691$ subset of Ensemble 1, with $m_\pi = 470$ MeV. The momenta simulated are given in Table 7.1

In the isospin-symmetric limit, individual flavour contributions to the form factors of the proton and neutron are related by

$$G_{\mathbf{E},\mathbf{p}}^u = G_{\mathbf{E},\mathbf{n}}^d, \quad (7.45)$$

$$G_{\mathbf{E},\mathbf{p}}^d = G_{\mathbf{E},\mathbf{n}}^u, \quad (7.46)$$

and similarly for the other form factors. Hence, we can construct the form factors of the neutron from the results obtained through our analysis of the proton form factors.

7.2.2 Analysis

The analysis of the correlation functions proceeds as in Section 7.1.2, with additional consideration of the spin projection. For the temporal component, the extracted signal is not spin-dependent, and so there is no effect from changing the spin-projection of the nucleon. Hence we form the ratio

$$R_E(\lambda, \pm \mathbf{p}, t) \equiv \left| \frac{G^+(\lambda, \pm \mathbf{p}, t) G^-(0, \pm \mathbf{p}, -t)}{G^+(0, \pm \mathbf{p}, t) G^-(\lambda, \pm \mathbf{p}, -t)} \right|^{\frac{1}{4}}, \quad (7.47)$$

where superscript \pm here refers to positive or negative-parity projection. Under time-reversal and parity flip, the spatial components of the vector current remain unchanged, and so we average these correlators,

$$G^\pm(\lambda, \mathbf{p}, \pm t) \equiv \frac{1}{2} [G^+(\lambda, \mathbf{p}, t) + G^-(\lambda, \mathbf{p}, -t)]. \quad (7.48)$$

Under a spin or momentum flip however, the sign changes, and so we form the ratio

$$R_M(\lambda, \pm \mathbf{p}, t) \equiv \left| \frac{G_\uparrow^\pm(\lambda, \mathbf{p}, \pm t) G_\downarrow^\pm(0, \mathbf{p}, \pm t) G_\uparrow^\pm(0, -\mathbf{p}, \pm t) G_\downarrow^\pm(\lambda, -\mathbf{p}, \pm t)}{G_\uparrow^\pm(0, \mathbf{p}, \pm t) G_\downarrow^\pm(\lambda, \mathbf{p}, \pm t) G_\uparrow^\pm(\lambda, -\mathbf{p}, \pm t) G_\downarrow^\pm(0, -\mathbf{p}, \pm t)} \right|^{\frac{1}{4}}. \quad (7.49)$$

At large times, these ratios isolate the odd-order energy shifts

$$R_E(\lambda, \pm \mathbf{p}, t) \xrightarrow{\text{large } t} B(\lambda) e^{-\Delta E_{\text{odd}}(\lambda)t}, \quad (7.50)$$

$$R_M(\lambda, \pm \mathbf{p}, t) \xrightarrow{\text{large } t} C(\lambda) e^{-\Delta E_{\text{odd}}(\lambda)t}. \quad (7.51)$$

As before, these ratios isolate energy shifts at odd order in λ , and based on the results of Section 7.1, we expect to see little evidence of cubic contamination. We define effective electric and magnetic form factors

$$G_{E,\text{eff}}^f = \frac{E(\mathbf{p}) \Delta E_{\text{eff}}}{m [\lambda_f]_4} \xrightarrow{\text{large } t} G_E^f + \mathcal{O}([\lambda_f]_4^2), \quad (7.52)$$

$$G_{M,\text{eff}}^f = \frac{2E(\mathbf{p}, \sigma) \Delta E_{\text{eff}}}{[\mathbf{s} \times \mathbf{q}]_i [\lambda_f]_i} \xrightarrow{\text{large } t} G_M^f + \mathcal{O}([\lambda_f]_2^2) \quad (i \text{ not summed}), \quad (7.53)$$

which at large times plateau to their respective form factors.

As in Section 7.1.2, renormalised results are determined by enforcing charge conservation, in this case the forward limit of the electric form factor of the proton,

$$G_{E,p}(0) = 1. \quad (7.54)$$

Our final results are therefore given by

$$G_{E,p}(Q^2) = \frac{[G_{E,p}]^{\text{latt}}}{[G_{E,p}(0)]^{\text{latt}}}, \quad (7.55)$$

$$G_{M,p}(Q^2) = \frac{[G_{M,p}]^{\text{latt}}}{[G_{E,p}(0)]^{\text{latt}}}, \quad (7.56)$$

where as discussed in Section 7.1.2, there is no scale-dependence.

7.2.3 Results

Fig. 7.11 shows the effective electric and magnetic form factors of the proton for different values of Q^2 and λ . We are able to identify very clean plateaus, and as in the pion case, there is no numerical difference between the effective form factors over an order of magnitude change in λ . Hence we are again extremely confident we are well-within the linear regime. Fig. 7.12 shows the extracted energy shifts as functions of λ , where this linearity is again emphasised.

Figs. 7.13 and 7.14 show the electric and magnetic form factors of the proton and neutron extracted in this calculation, along with results of a variationally improved three-point function extraction on the same ensemble [235], and a parameterisation of experimental data. The statistical signal for the new FH approach is seen to extend to much larger Q^2 than has been accessible in the past. A large factor in this is the Breit frame kinematics used, which allow momentum transfers to be accessed through minimal source and sink momenta. We note excellent agreement with the three-point function calculation in the region of overlap, indicating that we are able to control excited-state contamination well in this calculation.

Fig. 7.15 shows the ratio of electric and magnetic form factors for the proton, which matches the linear trend of the experimental data extremely well. This is somewhat surprising given the unphysical simulated pion mass of 470 MeV, and suggests that the quark mass dependence of this ratio warrants further study. Fig. 7.15 shows the same ratio for the neutron.

7.3 Conclusions and Outlook

In this chapter we have shown how an extension of the FH method to non-forward matrix elements allows the extraction of nucleon and pion form factors at much higher momentum transfers than previously possible. We have calculated the form factors of the pion, proton and neutron up to $Q^2 \approx 6.5 \text{ GeV}^2$. Results for the ratio $G_{E,p}/G_{M,p}$ show the linear decrease expected from experiment, the first lattice results to do so.

The high-momentum form factors extracted in this work demonstrate a significantly expanded scope for lattice QCD to address this phenomenologically interesting domain of hadron structure, and opens up a vista of possibilities for determining other hadronic and nuclear quantities at high momentum transfer. While only the beginning of a systematic program of form factor calculations using this technique, results obtained here have already generated a great deal of interest in the experimental community. Improved calculations will be extremely relevant to pending experiments investigating the high- Q^2 dependence of the form factors discussed. In the nucleon case, the Q^2 range we have been now able to access would allow for tighter constraints to be placed on the distribution of charge and magnetisation at small impact parameter.

The initial calculations presented here have been performed at a single heavy pion mass, lattice spacing and volume. Future work to investigate lattice systematics will therefore be extremely important. Additionally, we believe we can improve the signals obtained through the use of momentum-smearing operators as described in [230]. In principle this is a straightforward extension, however one must consider the construction of operators which overlap equally well with both $\pm\mathbf{p}$ states. If

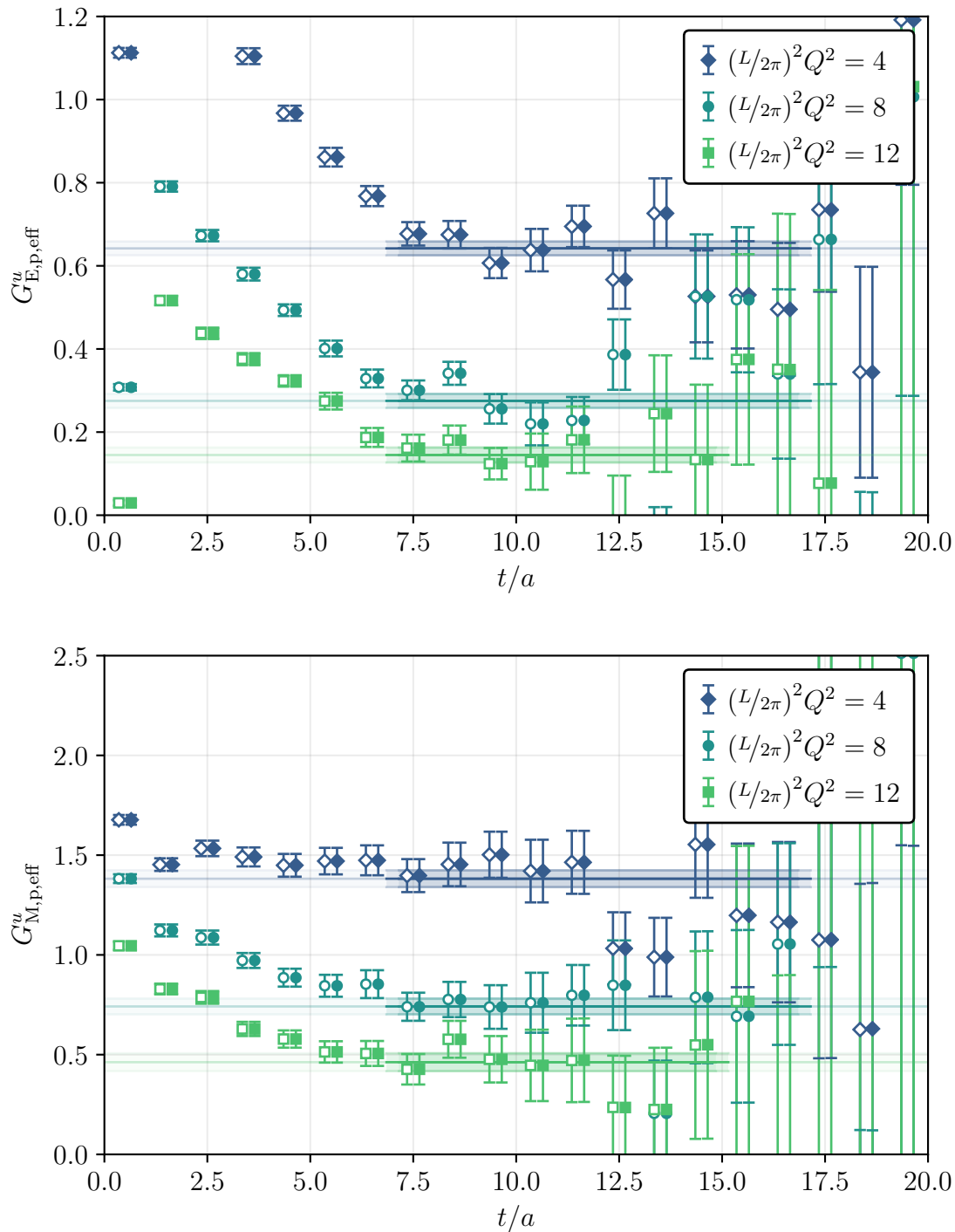


Figure 7.11: u quark contributions to the effective electric and magnetic form factors of the proton for different momentum transfers and $a\lambda = 10^{-4}, -10^{-5}$ (filled and unfilled markers). These were calculated on an $N = 1691$ subset of Ensemble 1, with $m_\pi = 470$ MeV.

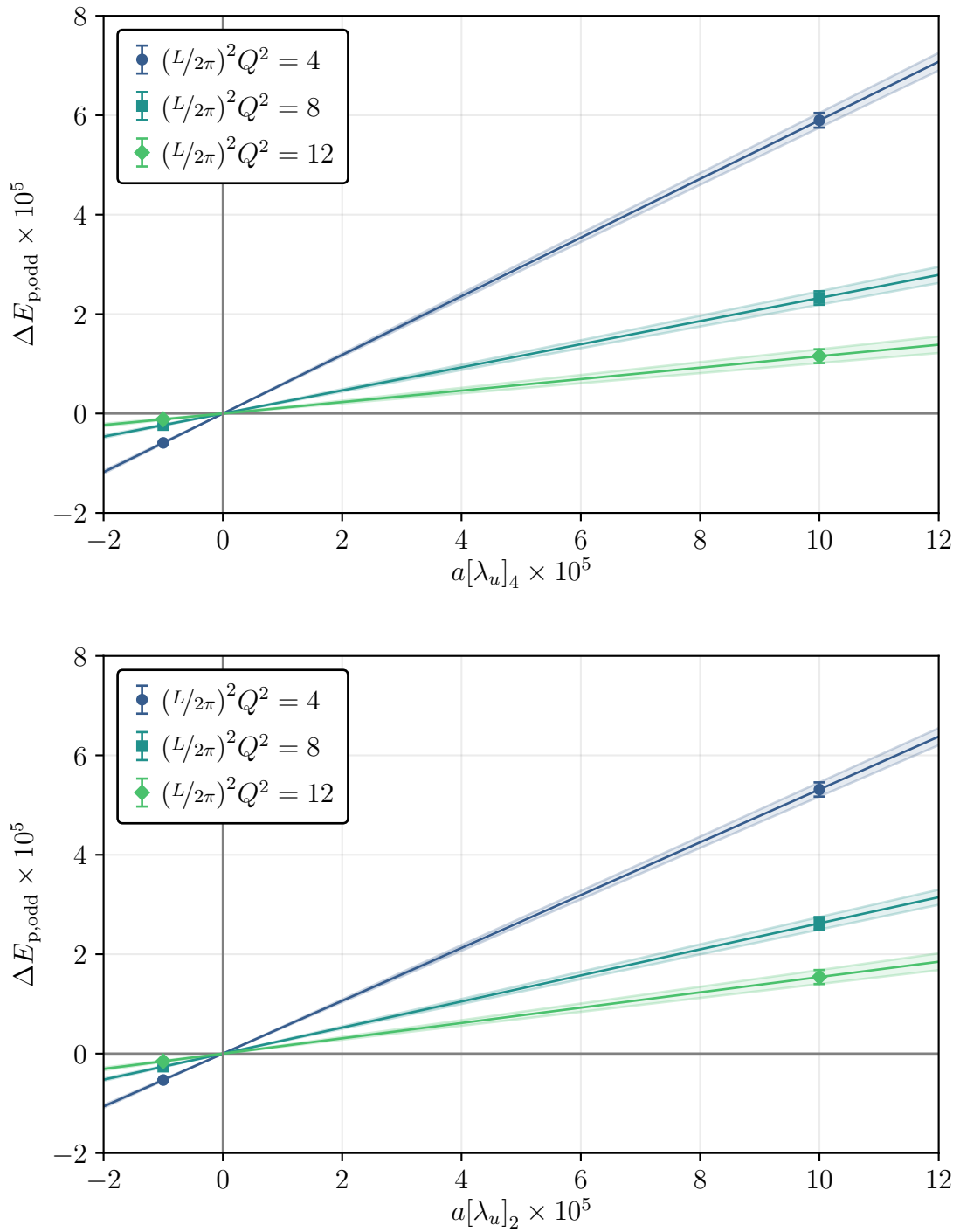


Figure 7.12: Energy shifts as functions of λ_2 and λ_4 for vector couplings to the u quark in the proton. These were calculated on an $N = 1691$ subset of Ensemble 1, with $m_\pi = 470$ MeV.

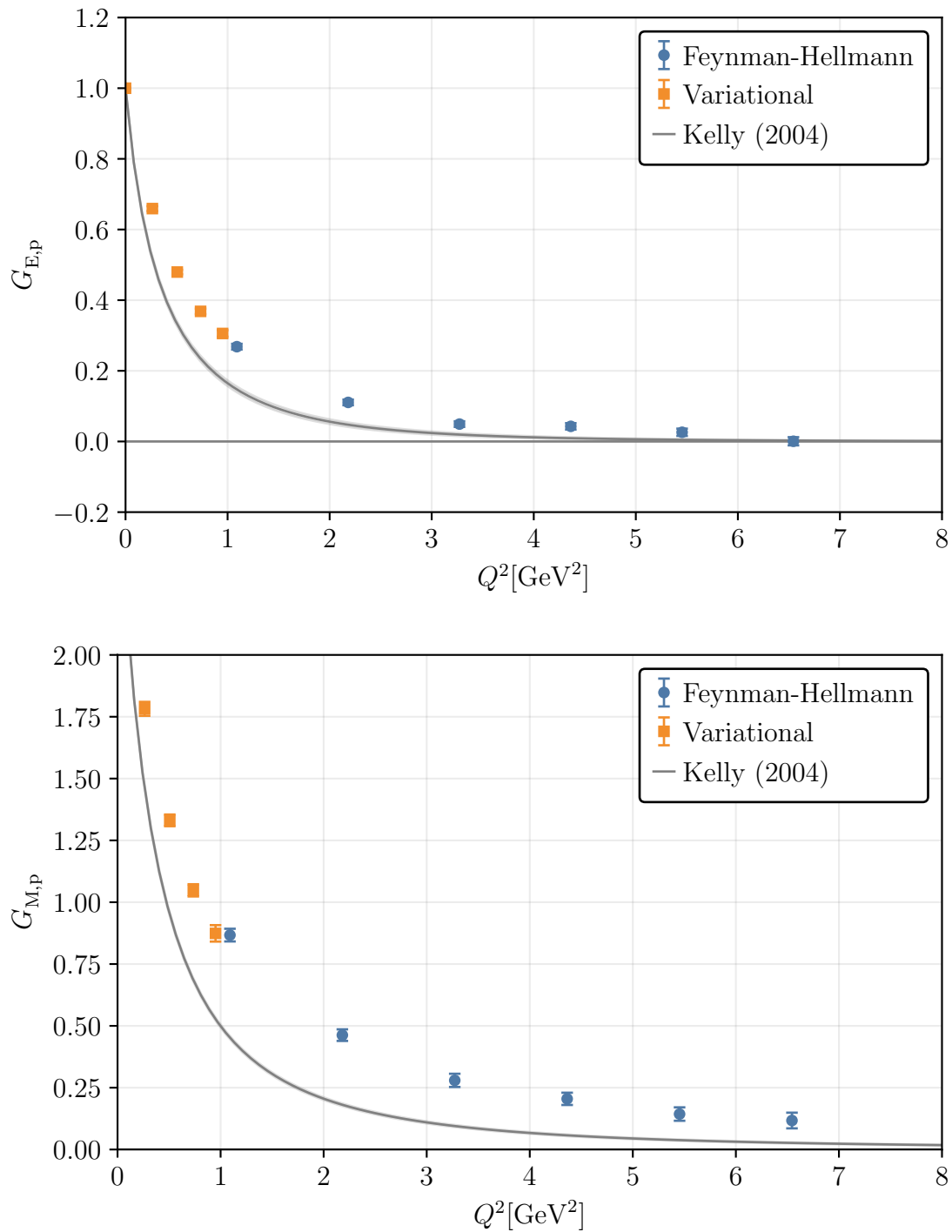


Figure 7.13: Electric and magnetic form factors of the proton and extracted through the FH technique, in comparison with variationally improved results of [235] and Kelly parameterisations of the experimental data [236]. These were calculated on an $N = 1691$ subset of Ensemble 1, with $m_\pi = 470$ MeV.

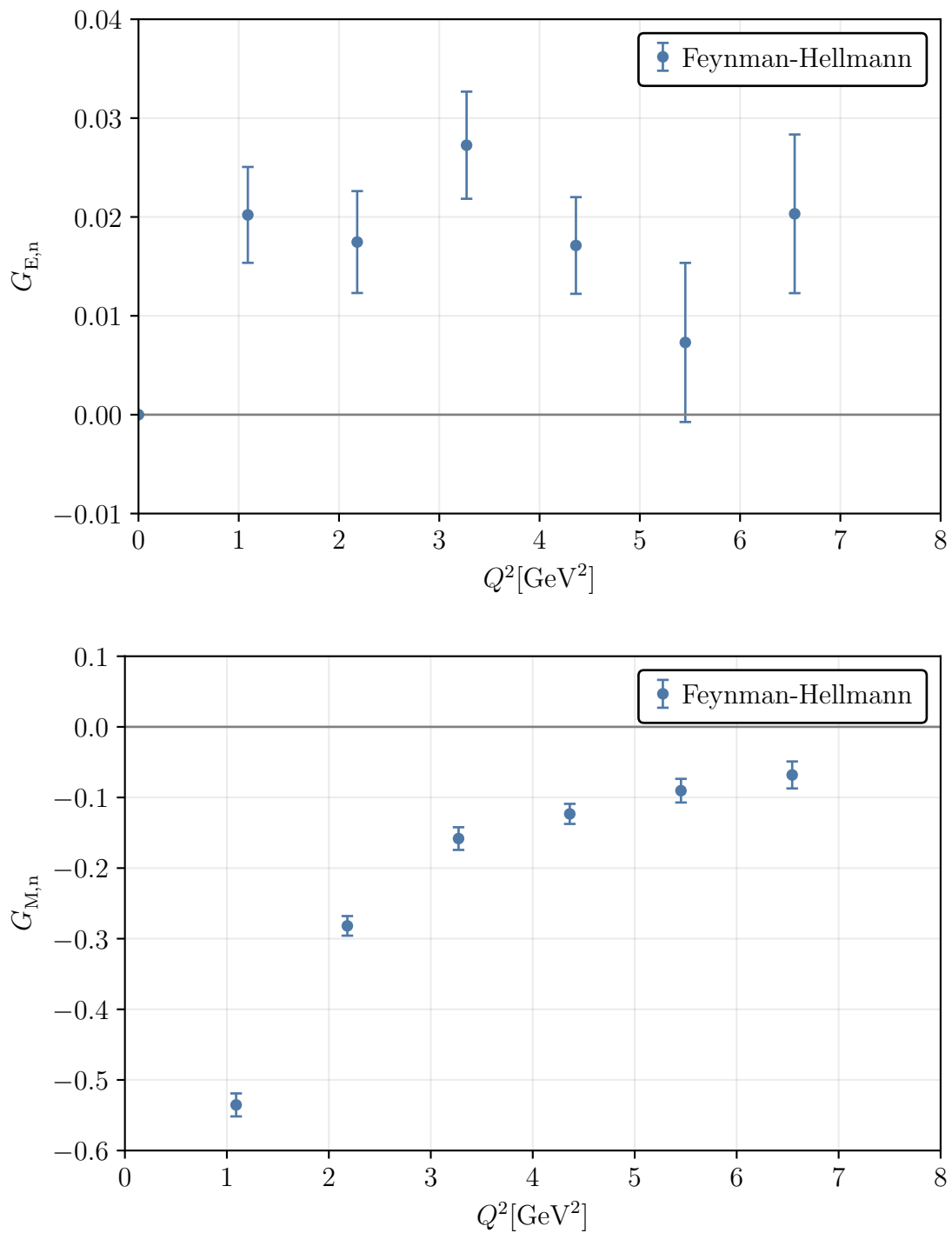


Figure 7.14: Electric and magnetic form factors of the neutron extracted through the FH technique. These were calculated on an $N = 1691$ subset of Ensemble 1, with $m_\pi = 470$ MeV.

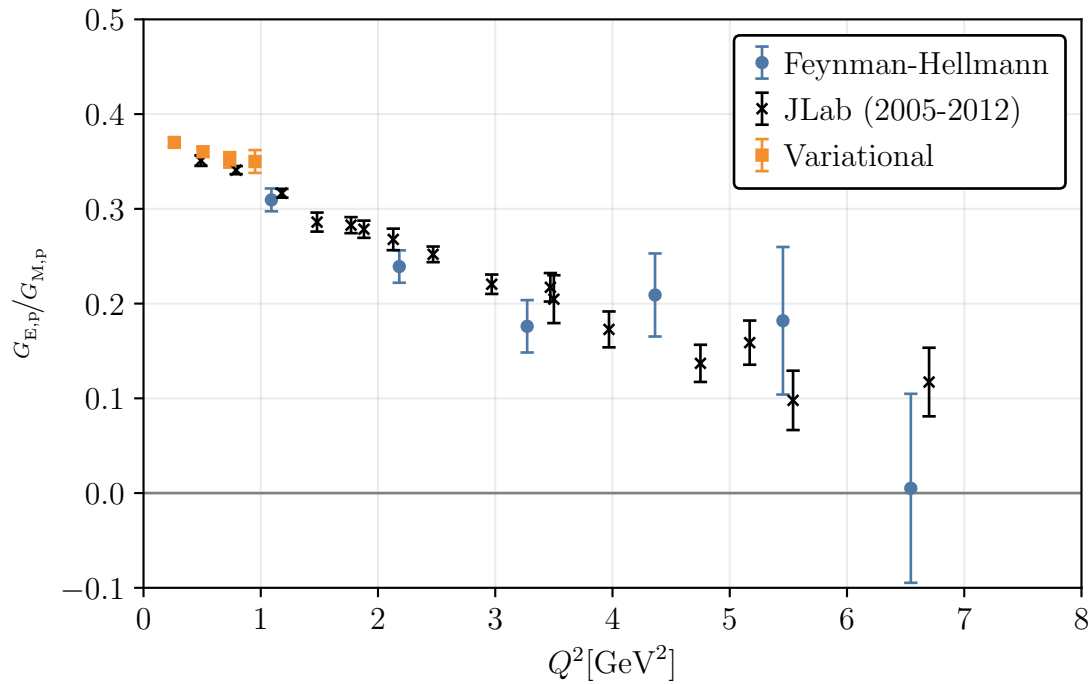


Figure 7.15: Ratio of electric and magnetic form factors for the proton, calculated on an $N = 1691$ subset of Ensemble 1, with $m_\pi = 470$ MeV. Included for comparison are experimental results for JLab, and the results of a variationally improved three-point function calculation on the same ensemble [235].

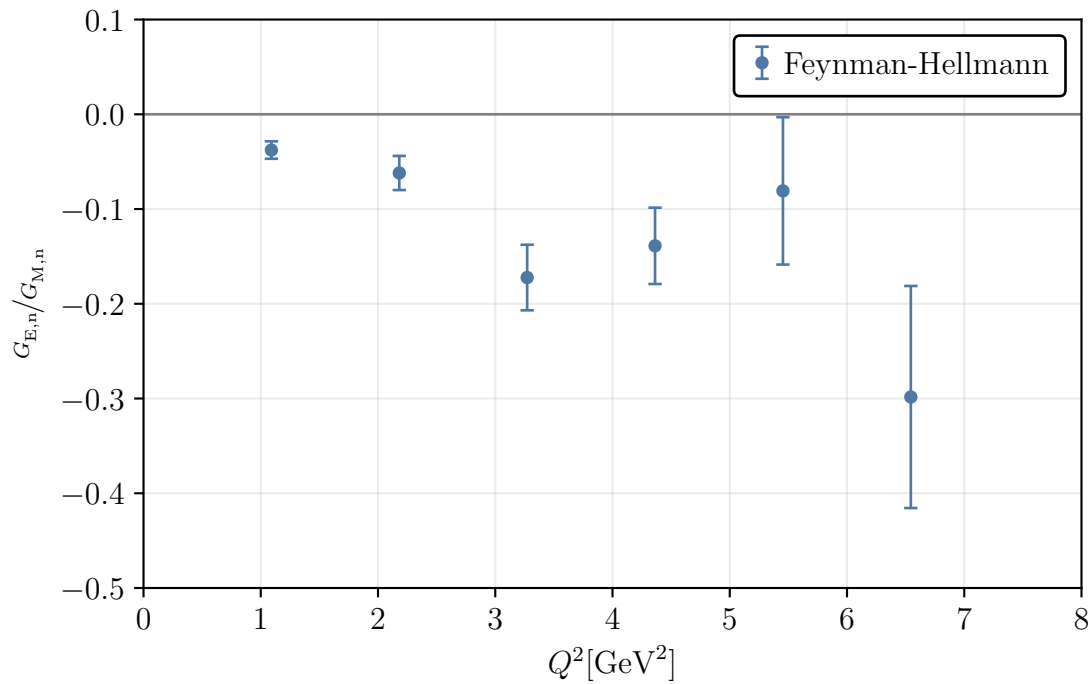


Figure 7.16: Ratio of electric and magnetic form factors for the neutron, calculated on an $N = 1691$ subset of Ensemble 1, with $m_\pi = 470$ MeV.

this smearing is applied at the quark level, then the hadron interpolators will couple to states with a variety of momenta, and we would not expect as dramatic an improvement as has been seen in other applications of this technique.

Chapter 8

The Electromagnetic Structure of Hadrons: Structure Functions

“A model for highly inelastic electron-nucleon scattering at high energies is studied and compared with existing data. This model envisages the proton to be composed of pointlike constituents (‘partons’) from which the electron scatters incoherently. . . we suggest that a good way to find out about the internal structure of the proton is to look at it.”

—J. D. Bjorken and E. A. Paschos, Phys. Rev. 185 (1969) [237]

Deep inelastic scattering (DIS) experiments have been an integral part of hadronic studies for many years [238–240], having provided the first experimental evidence for the existence of quarks [6, 7] in the late 1960s. DIS studies have been instrumental in investigations of hadron spin structure [128], PDFs [241, 242], generalised parton distributions (GPDs) [243–245], spin and transverse-spin asymmetries [246, 247], fragmentation functions [248], and much more. Electromagnetic structure functions are important quantities in the analysis of DIS processes, serving as the inelastic analogue of the form factors of Chapter 7.

The fundamental interaction of lepton-hadron DIS is shown in Fig. 8.1, where an incoming electron scatters from a hadron target, producing a different final hadronic state. The amplitude for this process includes the hadron tensor, defined conventionally in Minkowski spacetime as

$$\left[W_{\mu\nu}^X(p, q) \right]_{\epsilon'\epsilon} \equiv \frac{1}{4\pi} \int d^4y e^{iq\cdot y} \langle X(\mathbf{p}, \epsilon') | [\mathcal{J}_\mu(y), \mathcal{J}_\nu(0)] | X(\mathbf{p}, \epsilon) \rangle, \quad (8.1)$$

where ϵ and ϵ' are the polarisations of the initial and final hadron states, and the electromagnetic current density is as defined in Eq. (7.2). In the case of lepton-proton scattering, we can insert a complete set of states and apply translational invariance as in Section 5.2 to obtain

$$\begin{aligned} \left[W_{\mu\nu}^p(p, q) \right]_{\epsilon'\epsilon} &= \frac{1}{2} \sum_Y \int d^3k \\ &\left[\delta^4(q + p - k) \langle p(\mathbf{p}, \epsilon') | \mathcal{J}_\mu(0) | Y(\mathbf{k}) \rangle \langle Y(\mathbf{k}) | \mathcal{J}_\nu(0) | p(\mathbf{p}, \epsilon) \rangle \right. \\ &\quad \left. - \delta^4(q + k - p) \langle p(\mathbf{p}, \epsilon') | \mathcal{J}_\nu(0) | Y(\mathbf{k}) \rangle \langle Y(\mathbf{k}) | \mathcal{J}_\mu(0) | p(\mathbf{p}, \epsilon) \rangle \right]. \quad (8.2) \end{aligned}$$

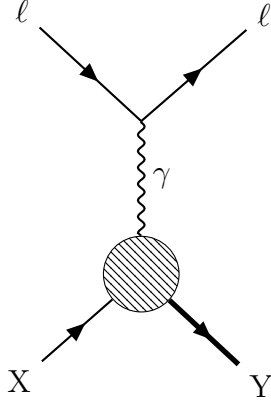


Figure 8.1: Fundamental lepton-hadron interaction relevant to DIS experiments.

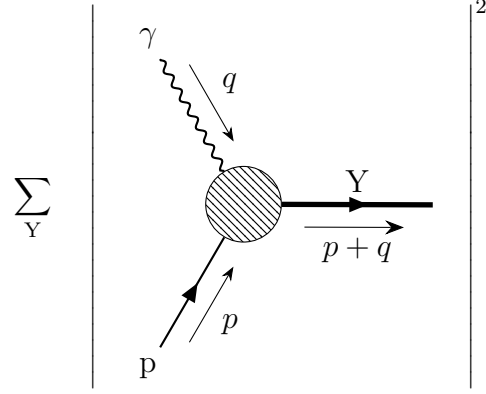


Figure 8.2: Inelastic electromagnetic vertex described by the hadron tensor of the proton.

Kinematically we require that $E_Y(\mathbf{k}) \geq E_p(\mathbf{p})$ since $m_Y^2 \geq m_p^2$ for all Y . Since the photon exchange is spacelike, $q^0 > 0$, and only the first delta function in Eq. (8.2) can be satisfied. Hence, at least for the proton, Eq. (8.1) is equivalent to

$$\left[W_{\mu\nu}^p(p, q) \right]_{\sigma'\sigma} = \frac{1}{4\pi} \int d^4y e^{iq \cdot y} \langle p(\mathbf{p}, \sigma') | \mathcal{J}_\mu(y) \mathcal{J}_\nu(0) | p(\mathbf{p}, \sigma) \rangle. \quad (8.3)$$

That is, the tensor can be defined without the commutator of the two currents, in which case the amplitude is represented diagrammatically by the diagram of Fig. 8.2. The commutator is included conventionally as it gives $W_{\mu\nu}$ a convenient analytic structure in the complex plane.

For the spin-half proton, the hadron tensor in terms of the spin-polarisation is given by

$$W_{\mu\nu}^p(p, q, s) \equiv \text{Tr} \left[\rho W_{\mu\nu}^p(p, q) \right], \quad (8.4)$$

where the spin-density matrix,

$$\rho \equiv \frac{1}{2} (\mathbb{I} + \boldsymbol{\sigma} \cdot \mathbf{s}). \quad (8.5)$$

Here $\boldsymbol{\sigma}$ are the Pauli matrices, and \mathbf{s} is the relativistic three-spin. Eq. (8.5) is defined analogously to the spin-projection operator of Appendix G. Through a tensor decomposition and enforcement of Lorentz, parity and time-reversal invariance, and photon crossing symmetry, Eq. (8.4) may be decomposed into a number of spin-independent and spin-dependent structure functions,

$$\begin{aligned} W_{\mu\nu}^p(p, q, \mathbf{s}) = & \left(-g_{\mu\nu} + \frac{q_\mu q_\nu}{q^2} \right) F_{1,p}(x, Q^2) + \frac{1}{p \cdot q} \left(p_\mu - \frac{p \cdot q}{q^2} q_\mu \right) \left(p_\nu - \frac{p \cdot q}{q^2} q_\nu \right) F_{2,p}(x, Q^2) \\ & - \epsilon_{\mu\nu\kappa\lambda} \frac{q^\kappa s^\lambda}{p \cdot q} g_{1,p}(x, Q^2) - \epsilon_{\mu\nu\kappa\lambda} \frac{q_\kappa (p \cdot q s_\lambda - s \cdot q p_\lambda)}{(p \cdot q)^2} g_{2,p}(x, Q^2). \end{aligned} \quad (8.6)$$

Just as the form factors of parameterised the amplitude of the elastic electromagnetic vertex, the structure functions parameterise the inelastic vertex of Fig. 8.2. The

structure functions are functions of the invariant Q^2 defined in Eq. (7.4), and Bjorken variable x ,

$$x = \frac{Q^2}{2p \cdot q}, \quad (8.7)$$

interpreted in the infinite-momentum frame as the fraction of the total hadron momentum carried by the parton struck by the incoming photon.

An important outcome of the DIS experiments was the confirmation of Bjorken scaling, a property originally predicted through current algebra methods [249]. In the high- Q^2 limit, the structure functions at fixed x are independent of the scale, Q^2 , at leading order. As a result, at high energies, hadronic systems should behave like practically independent collections of point-like constituents. This set the stage for the introduction of the parton model [237, 250, 251], the precursor to the identification of the point-like constituents as quarks and gluons, and asymptotic freedom. In modern times, precise determinations of the structure functions are important inputs to high-energy physics at the Tevatron and Large Hadron Collider (LHC). For an overview of experimental results for the structure functions, see e.g. [238].

Historically, lattice calculations have been limited to calculations of the lowest Mellin moments of the PDFs (see [252–255] for a selection of results), which can be expressed, up to higher-twist effects, in terms of local operators through the operator-product expansion (OPE) [256]. QCD factorisation rules [257] allow the structure functions to be expressed as convolutions of perturbative cross-sections and the PDFs [258]. As power-divergent mixing occurs between twist-two operators on the lattice, these calculations are in practice limited to the lowest three moments, and the PDFs, and hence structure functions, cannot be properly reconstructed [259].

In this chapter we show how the FH method applied to second-derivatives of the energy can be used to calculate the structure functions of the hadron tensor. In section Section 8.1 we will demonstrate the calculation of the Compton amplitude of the nucleon, which can be related to the structure functions of the hadron tensor through the optical theorem. This work discussed here has been published in [260].

8.1 Unpolarised Nucleon Structure Functions

In the calculation of the structure functions through the FH method, we are restricted to calculations of time-ordered products of operators. For this reason, we do not access the hadron tensor directly, but rather the Compton amplitude of the proton, defined here in Euclidean spacetime similarly to Eq. (8.1) but with a time-ordered current,

$$\left[T_{\mu\nu}^{\text{p}}(p, q) \right]_{\sigma'\sigma} \equiv \int d^4y e^{iq \cdot y} \langle \text{p}(\mathbf{p}, \sigma') | \text{T} \{ \mathcal{J}_\mu(y) \mathcal{J}_\nu(0) \} | \text{p}(\mathbf{p}, \sigma) \rangle. \quad (8.8)$$

The effective four-point vertex described by the Compton amplitude is presented diagrammatically in Fig. 8.3. Eq. (8.8) is contracted with the spin-density matrix of Eq. (8.5) to define the Compton amplitude in terms of the spin-polarisation vector,

$$T_{\mu\nu}^{\text{p}}(p, q, s) \equiv \text{Tr} \left[\rho T_{\mu\nu}^{\text{p}}(p, q) \right]. \quad (8.9)$$

Analogously to the hadron tensor, this amplitude may be decomposed in terms of unpolarised and polarised Compton structure functions,

$$\begin{aligned}
 T_{\mu\nu}^{\text{p}}(p, q, s) = & \\
 & \left(\delta_{\mu\nu} + \frac{q_\mu q_\nu}{q^2} \right) \mathcal{F}_{1,\text{p}}(\omega, Q^2) + \frac{1}{p \cdot q} \left(p_\mu - \frac{p \cdot q}{q^2} q_\mu \right) \left(p_\nu - \frac{p \cdot q}{q^2} q_\nu \right) \mathcal{F}_{2,\text{p}}(\omega, Q^2) \\
 & - \epsilon_{\mu\nu\kappa\lambda} \frac{q_\kappa s_\lambda}{p \cdot q} \mathcal{G}_{1,\text{p}}(\omega, Q^2) - \epsilon_{\mu\nu\kappa\lambda} \frac{q_\kappa [(p \cdot q) s_\lambda - (s \cdot q) p_\lambda]}{(p \cdot q)^2} \mathcal{G}_{2,\text{p}}(\omega, Q^2), \quad (8.10)
 \end{aligned}$$

which are functions of the invariant Q^2 , and the inverse Bjorken variable

$$\omega = \frac{1}{x}. \quad (8.11)$$

In the following discussions we will focus on the unpolarised structure functions, although the methods we will discuss can be extended simply to the polarised structure functions. Through the optical theorem and the analytic structure of the Compton structure functions in the complex plane, one may show that

$$\mathcal{F}_{1,\text{p}}(\omega, Q^2) = 4\omega^2 \int_0^1 dx x \frac{F_{1,\text{p}}(x, Q^2)}{1 - (\omega x)^2}, \quad (8.12)$$

$$\mathcal{F}_{2,\text{p}}(\omega, Q^2) = 4\omega \int_0^1 dx \frac{F_{2,\text{p}}(x, Q^2)}{1 - (\omega x)^2}. \quad (8.13)$$

Performing a Taylor expansion of the denominator then, the Compton structure functions can be written in terms of moments of the structure functions of the hadron tensor,

$$\mathcal{F}_{1,\text{p}}(\omega, Q^2) = \sum_{n=2,4,\dots} 4\omega^n \int_0^1 x^{n-1} F_{1,\text{p}}(x, Q^2), \quad (8.14)$$

$$\mathcal{F}_{2,\text{p}}(\omega, Q^2) = \sum_{n=1,3,\dots} 4\omega^n \int_0^1 x^{n-1} F_{1,\text{p}}(x, Q^2). \quad (8.15)$$

Our strategy therefore is to calculate the Compton structure functions, and through a polynomial fit extract moments of the structure functions of the hadron tensor through Eqs. (8.14) and (8.15). The structure functions can then be reconstructed through an inverse Mellin transform.

We have touched on the extension of the FH method to second order briefly in Section 5.2.5. One may show that, with a modification to the Lagrangian of the form,

$$\mathcal{L}(y) \longrightarrow \mathcal{L}'(y) = \mathcal{L}(y) + 2\lambda_f \cos(\mathbf{q} \cdot \mathbf{y}) \mathcal{V}_3^f(y), \quad (8.16)$$

that the second derivative of the energy of the polarised proton with respect to the vector coupling of a single flavour is given by

$$\left. \frac{\partial^2 E_{\text{p}}(\mathbf{p}, \sigma)}{\partial \lambda_f^2} \right|_{\lambda=0}^{\Gamma_{\text{unpol}}} = -\frac{1}{2E_{\text{p}}(\mathbf{p})} T_{33}^{\text{p},ff}(p, q, s = 0), \quad (8.17)$$

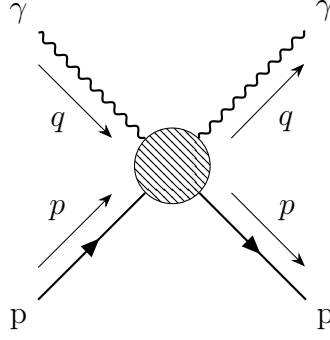


Figure 8.3: Diagram for the Compton amplitude of the proton defined in Eq. (8.8).

where $T_{\mu\nu}^{p,fg}$ are individual flavour contributions to the Compton amplitude of the proton, defined through

$$T_{\mu\nu}^{p,fg}(p, q) = \int d^4y e^{iq \cdot y} \langle p(\mathbf{p}, \sigma') | T \{ \mathcal{V}_\mu^f(y) \mathcal{V}_\nu^g(0) \} | p(\mathbf{p}, \sigma) \rangle, \quad (8.18)$$

and the full structure functions are given by

$$\mathcal{F}_{1,p}(\omega, Q^2) = \sum_{f,g} e_f e_g \mathcal{F}_{1,p}^{fg}(\omega, Q^2), \quad (8.19)$$

$$\mathcal{F}_{2,p}(\omega, Q^2) = \sum_{f,g} e_f e_g \mathcal{F}_{2,p}^{fg}(\omega, Q^2), \quad (8.20)$$

and similarly for the polarised structure functions. For the relation of Eq. (8.17), the momenta \mathbf{p} and \mathbf{q} are not required to satisfy the Breit frame condition $|\mathbf{p}| = |\mathbf{p} + \mathbf{q}|$. In fact, if they are chosen specifically to not satisfy this condition, then based on our discussions of Sections 5.3.4 and 5.3.5, the first derivative of the energy is zero, and we do not need to deal with linear contamination of the quadratic signal. More details of the derivation of this relation are discussed in [127].

8.1.1 Simulation Details

To implement the modification of the Lagrangian in Eq. (8.16), we calculate quark propagators through the inversion of a modified Dirac operator, accessing only connected contributions. We perform this for $a\lambda_f = 0.0375, -0.075$, where we note we use much larger values of λ than those chosen in Chapter 7. In our previous calculations, simulating small values of λ allowed us to access linear energy shifts without quadratic contamination. In this calculation, we wish to avoid swamping the quadratic signal by any remnant linear signal that exists due to discretisation effects on the lattice. The action for only a single quark flavour is modified at once, and hence we only access flavour-diagonal contributions to the structure functions through Eq. (8.17). In the high- Q^2 limit, the off-diagonal contributions should vanish, as the independent partons are unable to exchange momentum. In general we would need to introduce vector couplings to multiple flavour simultaneously to calculate the off-diagonal terms. We choose $(L/2\pi)\mathbf{q} = (3, 5, 0)$, with all momentum projections chosen such that $p_3 = 0$. Since we have coupled to the third spatial component of the vector current, we isolate the first unpolarised structure function,

$$\left. \frac{\partial^2 E_p(\mathbf{p})}{\partial \lambda_f^2} \right|_{\lambda=0}^{\Gamma_{\text{unpol}}} = -\frac{1}{2E_p(\mathbf{p})} \mathcal{F}_{1,p}^{ff}(\omega, Q^2). \quad (8.21)$$

ω	$\frac{L}{2\pi}\mathbf{p}$	$\left(\frac{L}{2\pi}\right)^2\mathbf{p}^2$
$0/17$	(+0, +0, +0)	0
$1/17$	(+2, -1, +0)	5
$2/17$	(-1, +1, +0)	2
$3/17$	(+1, +0, +0)	1
$4/17$	(-2, +2, +0)	8
$5/17$	(+0, +1, +0)	1
$6/17$	(+2, +0, +0)	4
$7/17$	(-1, +2, +0)	5
$8/17$	(+1, +1, +0)	2
$9/17$	(+3, +0, +0)	9
$10/17$	(+0, +2, +0)	4
$11/17$	(+2, +1, +0)	5
$12/17$	(-1, +3, +0)	10
$13/17$	(+1, +2, +0)	5
$14/17$	(+3, +1, +0)	10
$15/17$	(+0, +3, +0)	9
$16/17$	(+2, +2, +0)	8

Table 8.1: Choices of momentum projection \mathbf{p} which minimise the magnitude of the source/sink boost for all accessible values of ω , with $(L/2\pi)\mathbf{q} = (3, 5, 0)$.

Momentum projections to access various values of ω with our chosen values of \mathbf{q} are given in Table 8.1. We only show results for momentum projections with $(L/2\pi)^2\mathbf{p}^2 \leq 5$, as signal-to-noise ratios are too poor above this. In future, we intend to make use of the momentum-smearing of [230] to improve this situation.

8.1.2 Analysis

The analysis of the nucleon correlation function proceeds similarly to Section 7.2.2. Since the linear shift is zero by construction, and the quadratic shift is the quantity of interest, we wish to construct a ratio to isolate the even energy shifts, rather than the odd shifts. Antisymmetries of the spatial components of the vector operator cancel at second order, and so the signals for the forwards and backwards-propagating states, spin-flipped states, and momentum-flipped states (equivalent to flipping the sign of ω) are the same. We average correlators with opposite-sign values of ω ,

$$G(\lambda, \pm\omega, t) \equiv \frac{1}{2}[G(\lambda, +\omega, t) + G(\lambda, -\omega, t)] \quad (8.22)$$

and form the ratio

$$R(\lambda, \pm\omega, t) \equiv \left| \frac{G^+(\lambda, \omega, t) G^-(\lambda, \omega, -t)}{G^+(0, \omega, t) G^-(0, \omega, -t)} \right|^{\frac{1}{2}}. \quad (8.23)$$

Unlike the ratios constructed in previous chapters, this ratio isolates energy shifts at even order in λ at large times, and hence contamination comes in only at quartic order in λ ,

$$R(\lambda, \pm\omega, t) \xrightarrow{\text{large } t} B(\lambda) e^{-\Delta E_{\text{even}}(\lambda)t} + \mathcal{O}(\lambda^4). \quad (8.24)$$

$[\lambda_u]^2$	$[\lambda_u]^4$
-2.866(89)	
-2.794(101)	-23(21)

Table 8.2: Fit parameters for two polynomial fits to the data of Fig. 8.5 for $\omega = 5/17$. Calculated on an $N = 1006$ subset of Ensemble 1, with $m_\pi = 470$ MeV.

Here the even-order energy shifts are defined as

$$E_{\text{even}}(\lambda) \equiv \frac{1}{2}[E(\lambda) + E(-\lambda)]. \quad (8.25)$$

We define the effective Compton structure function,

$$\mathcal{F}_{1,\text{eff}}^{ff}(\lambda_f, t) = \frac{\Delta E_{\text{eff}}(\lambda_f, t)}{\lambda_f^2} \xrightarrow{\text{large } t} \mathcal{F}_1^{ff} + \mathcal{O}(\lambda_f^2), \quad (8.26)$$

which should plateau to \mathcal{F}_1 at large times, provided we are in the quadratic regime.

To renormalise results for the Compton structure functions, we use the scale-independent vector renormalisation determined through enforcing charge conservation in Chapter 7.

8.1.3 Results

Fig. 8.4 shows the effective structure function extracted for a vector coupling to the u quark, extracted for a variety of choices of \mathbf{p} (and hence ω). The plateaux are consistent between different values of λ , which indicates we are in the quadratic regime. Higher-order contamination would manifest as a systematic shift between the plateaux Fig. 8.5 shows the extracted energy shifts as functions of λ , with a polynomial fit including quadratic and quartic terms in λ . The fit parameters for a variety of fits to the $\omega = 5/17$ data of Fig. 8.5 are shown in Table 8.2, where we note no significant shift in the quadratic term from the inclusion of a quartic term.

Fig. 8.6 shows \mathcal{F}_1^{uu} and \mathcal{F}_1^{dd} determined in this calculation through the quadratic energy shifts, where the magnitude of the hadron boost \mathbf{p} is differentiated by different colours and markers. The magnitude of the boost, and hence the quality of the signal, does not correlate with the magnitude of ω . At this stage, one could proceed to reconstruct the corresponding moments of the structure function of the hadron tensor numerically through Eq. (8.14). However, results obtained from the lattice are not yet sufficiently precise for this to be performed with confidence, but with additional statistics this should be remedied.

8.2 Conclusions and Outlook

In this chapter we showed how an extension of the FH method to second order can be used to calculate structure functions of the Compton amplitude in lattice QCD, and how, with a sufficiently high-statistics calculation, one could access the structure functions of the hadron tensors, with none of the twist restrictions of traditional techniques.

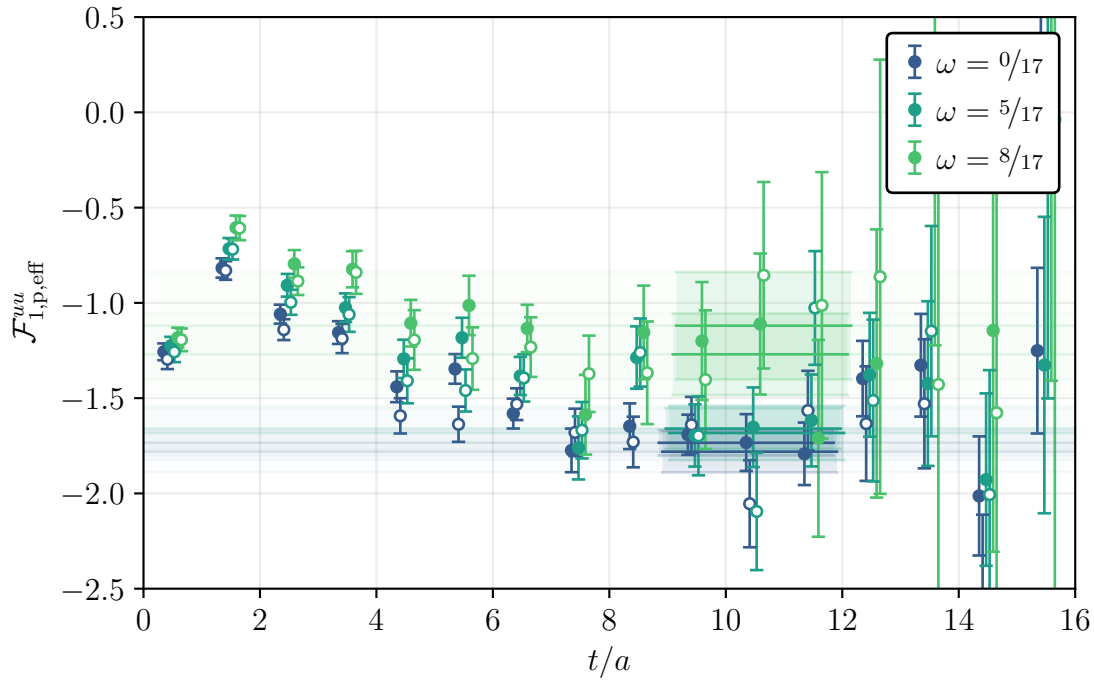


Figure 8.4: uu contribution to the first effective unpolarised structure function of the proton, for different values of ω and $\lambda_u = 0.0375, -0.075$ (filled and unfilled markers). Calculated on an $N = 1006$ subset of Ensemble 1, with $m_\pi = 470$ MeV.

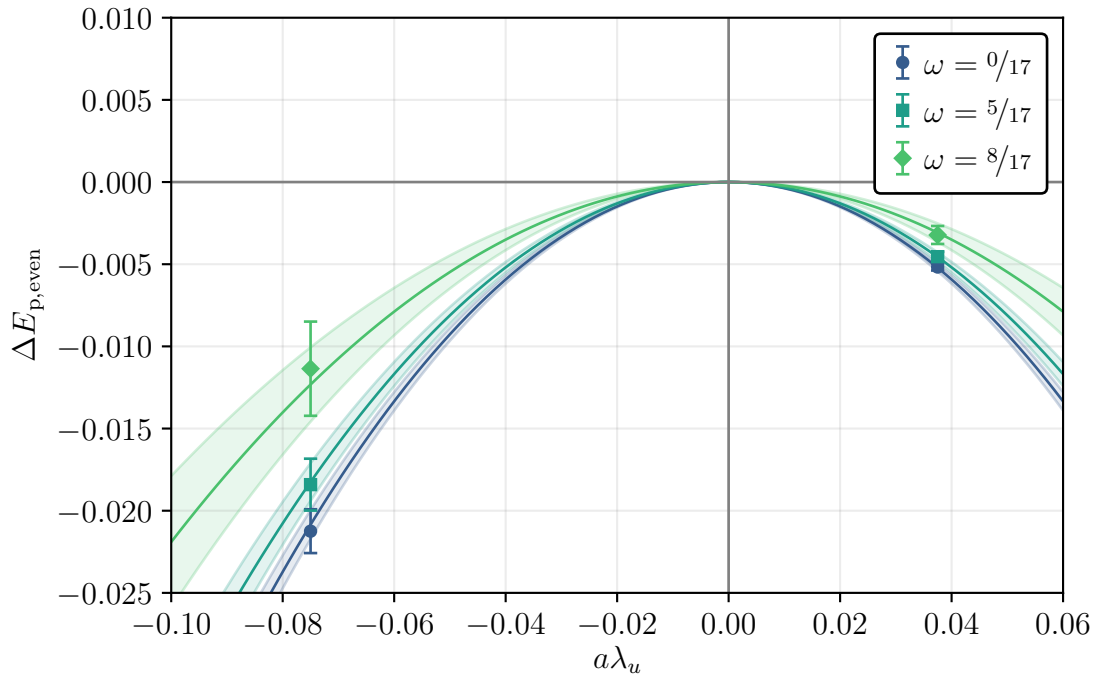


Figure 8.5: Even-order energy shifts resulting from a vector coupling to the u quark, for a variety of different ω . Calculated on an $N = 1006$ subset of Ensemble 1, with $m_\pi = 470$ MeV.

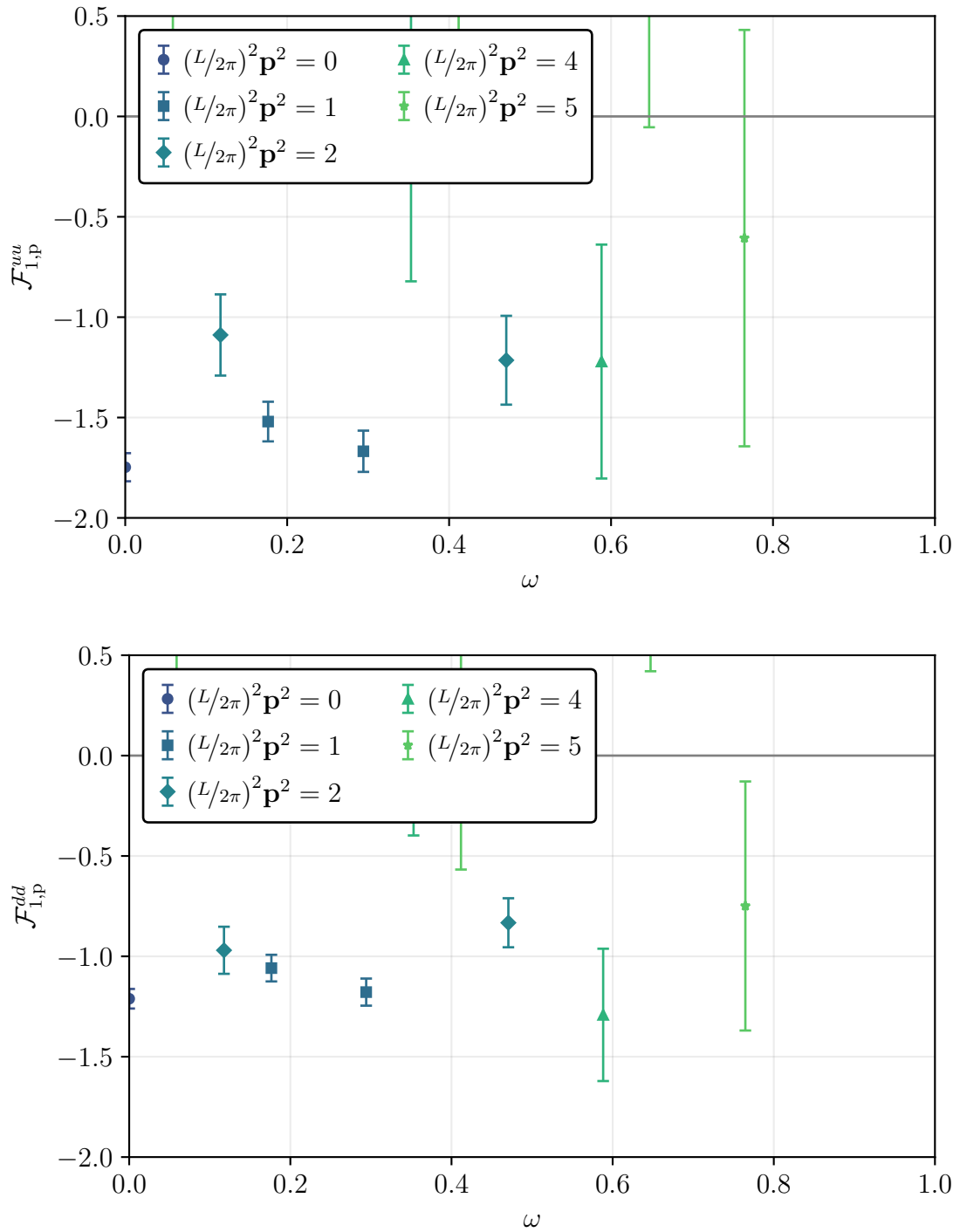


Figure 8.6: uu and dd contributions to the first unpolarised Compton structure function determined through the FH method. Calculated on an $N = 1006$ subset of Ensemble 1, with $m_\pi = 470$ MeV.

While our initial exploratory calculation is not sufficiently precise to perform this extraction with confidence, we have shown that the calculation is possible. There exists a wide scope for more precise calculations, particularly the implementation of the momentum-smeared operators [230] already discussed. In this case, the benefits of these improved operators should be significant, especially as the initial and final hadron states are projected to the same momentum, and so the problems discussed in Section 7.3 do not apply here.

This calculation indicates a significantly expanded scope for lattice calculations of structure functions beyond the lowest moments of the PDFs, and future calculations will provide important tests of scaling-corrections in QCD.

Chapter 9

Conclusions and Outlook

“The worthwhile problems are the ones you can really solve or help solve, the ones you can really contribute something to. . . . No problem is too small or too trivial if we can really do something about it.”

—Richard Feynman, letter to Koichi Mano (1966)

The field of hadron structure sits at the cutting edge of attempts to understand the key fundamental processes that occur at the heart of all matter in the universe. Lattice QCD has been at the forefront of attempts to unlock the secrets of these processes, providing the ideal tool to complement experimental studies and phenomenological models. However, there remain many challenging aspects of lattice calculations, most notably in the control of excited-state contamination, the calculation of disconnected contributions, and poor signal-to-noise ratios at large boosts. In this thesis we have shown the new toolset provided by the FH theorem allows many of these problems to be addressed.

The spin-decomposition of hadrons has long challenged theoretical studies, and lattice has traditionally struggled with excited-state contamination and calculations of the relevant disconnected contributions. Since hadron energies are extracted from two-point functions, control of excited state contamination in the FH approach is much more robust than in three-point analyses. In our comparison with the variational extraction of $g_{A,p}^{u-d}$ in [97], we are able to achieve similar suppression of excited-state contamination. Another strength of the FH approach is the simplicity with which disconnected contributions to observables can be calculated. Modifications to the generation of gauge fields are easily implemented, and although gauge field generation is generally the most costly aspect of a lattice simulation, we have demonstrated that this approach is at least competitive, with our results for Δs_p comparing extremely well with other modern extractions.

Lattice calculations of electromagnetic form factors have become extremely precise at low Q^2 , however simulations at large Q^2 relevant for short-distance information have long been stymied by low signal-to-noise ratios. The FH method also allows access to matrix elements involving much larger momentum transfers than have previously been possible, through taking advantage of Breit frame kinematics, and lower noise in two-point functions. We have calculated the electromagnetic form factors of the pion, proton and neutron up to $Q^2 \approx 6.5 \text{ GeV}^2$. In the case of the

pion, results are not yet precise enough to discriminate between various expectations of phenomenological models. In the nucleon case, while the calculation has been performed at a relatively large pion mass, the linear trend observed in the ratio $G_{E,p}/G_{M,p}$ is surprisingly close to that observed in experiment. This is the first lattice calculation to produce this drop-off.

The calculation of structure functions in lattice has historically been restricted to the lowest moments of the PDFs, which do not allow the structure functions to be reconstructed with higher-twist effects included. The FH method applied to second-order derivatives of the energy allow the Compton structure functions to be calculated including all twists in lattice, from which the structure functions of the hadron tensor can be obtained. While these calculations are still in their infancy, we expect significant progress in the near future.

The potential of the FH method is extremely exciting. The techniques demonstrated are very complimentary to other methods in use and developing in lattice QCD. There is some interest in using variational analyses of two-point functions to isolate matrix elements of particle excitations, and efforts are already under way to use momentum-smearing operators to improve further the results for form factors and structure functions at large boosts. The plethora of potential research projects that beckon is dizzying, and we have great optimism for the future impact of FH results on experimental efforts around the world.

Appendix A

Notational Conventions

The following table summarises indexing conventions throughout this thesis.

Index	Alphabet	Example
Dirac	Greek alphabet starting from α	$\alpha, \beta, \gamma, \delta$
Lorentz	Other Greek letters	$\mu, \nu, \kappa, \lambda$
Spatial	Latin alphabet starting from i	i, j, k
Colour	Latin alphabet starting from a	a, b, c, d
Colour (adjoint)	Latin alphabet starting from u	u, v, w

Unless otherwise stated, the Einstein summation is assumed in all expressions. Where possible, indices are placed consistently up or down, with the exception of Lorentz indices, where up and down correspond to Lorentz contravariance and covariance. In Euclidean space this distinction is not made. All quantities prior to Eq. (3.3) are in Minkowski space, and all subsequent quantities are assumed to be in Euclidean space unless otherwise stated or adorned with a subscript M.

All lattice quantities are stated in lattice units unless specified, and observables include only connected contributions and are unrenormalised unless otherwise noted.

Appendix B

Minkowski and Euclidean Metrics

The metric in Minkowski space is chosen with the $(+1, -1, -1, -1)$ convention, so the metric tensor

$$g_{\mu\nu} = g^{\mu\nu} \equiv \begin{bmatrix} 1 & 0 & 0 & 0 \\ 0 & -1 & 0 & 0 \\ 0 & 0 & -1 & 0 \\ 0 & 0 & 0 & -1 \end{bmatrix}. \quad (\text{B.1})$$

In Euclidean space, the metric is the standard

$$\delta_{\mu\nu} \equiv \begin{bmatrix} 1 & 0 & 0 & 0 \\ 0 & 1 & 0 & 0 \\ 0 & 0 & 1 & 0 \\ 0 & 0 & 0 & 1 \end{bmatrix}. \quad (\text{B.2})$$

In this thesis, the convention for the Wick rotation is chosen as

$$x_M^\mu \equiv (x_M^0, \mathbf{x}_M) \xrightarrow{\text{Wick}} x_\mu \equiv (\mathbf{x}, x_4) = (\mathbf{x}, ix_M^0). \quad (\text{B.3})$$

We can therefore determine the transformation of derivatives,

$$\partial_{\mu,M} \equiv (\partial_{0,M}, \partial_{i,M}) \xrightarrow{\text{Wick}} \partial_\mu \equiv (\partial_i, \partial_4) = (\partial_{i,M}, -i\partial_{0,M}), \quad (\text{B.4})$$

and the transformation of scalar products,

$$(x \cdot y)_M \equiv x_M^\mu g_{\mu\nu} y_M^\nu \xrightarrow{\text{Wick}} x \cdot y \equiv x_\mu \delta_{\mu\nu} x_\nu = -(x \cdot y)_M. \quad (\text{B.5})$$

The change of the γ matrices under the Wick rotation is described in Appendix C.

Appendix C

Clifford Algebra and the Dirac Matrices

Minkowski Spacetime

In Minkowski spacetime, the γ matrices generate a matrix representation of the Clifford algebra $C\ell_{1,3}(\mathbb{R})$,

$$\{\gamma^\mu, \gamma^\nu\} \equiv 2g^{\mu\nu}\mathbb{I}, \quad (\text{C.1})$$

The fifth Dirac matrix is defined as

$$\gamma^5 \equiv i\gamma^0\gamma^1\gamma^2\gamma^3, \quad (\text{C.2})$$

and the antisymmetric matrices

$$\sigma^{\mu\nu} \equiv \frac{i}{2}[\gamma^\mu, \gamma^\nu]. \quad (\text{C.3})$$

The set $\{\mathbb{I}, \gamma_\mu, \gamma_5, \gamma_\mu\gamma_5, \sigma_{\mu\nu}\}$ over the complex numbers forms a basis for the space of 4×4 complex matrices. Independent of representation, the following identities hold

$$\gamma^{5^2} = \mathbb{I}, \quad (\text{C.4})$$

$$\{\gamma^5, \gamma^\mu\} = 0, \quad (\text{C.5})$$

$$\text{Tr}(\Gamma_i\Gamma_j) = 0 \quad \forall i \neq j, \quad (\text{C.6})$$

$$\text{Tr}(\gamma^{\mu_1} \dots \gamma^{\mu_n}) = 0 \quad \forall n \text{ odd}, \quad (\text{C.7})$$

$$\text{Tr}(\gamma^5\gamma^{\mu_1} \dots \gamma^{\mu_n}) = 0 \quad \forall n \text{ odd}, \quad (\text{C.8})$$

$$\text{Tr}(\gamma^\mu\gamma^\nu) = 4g^{\mu\nu}, \quad (\text{C.9})$$

$$\text{Tr}(\gamma^5\gamma^\mu\gamma^\nu) = 0, \quad (\text{C.10})$$

$$\text{Tr}(\gamma^\mu\gamma^\nu\gamma^\kappa\gamma^\lambda) = 4(g^{\mu\nu}g^{\kappa\lambda} - g^{\mu\kappa}g^{\nu\lambda} + g^{\mu\lambda}g^{\nu\kappa}), \quad (\text{C.11})$$

$$\text{Tr}(\gamma^5\gamma^\mu\gamma^\nu\gamma^\kappa\gamma^\lambda) = -4i\epsilon^{\mu\nu\kappa\lambda}. \quad (\text{C.12})$$

We make use of the standard Dirac basis unless otherwise stated,

$$\gamma_4 = \begin{bmatrix} \mathbb{I} & 0 \\ 0 & -\mathbb{I} \end{bmatrix}, \quad \gamma_i = \begin{bmatrix} 0 & \sigma_i \\ -\sigma_i & 0 \end{bmatrix}, \quad \gamma_5 = \begin{bmatrix} 0 & \mathbb{I} \\ \mathbb{I} & 0 \end{bmatrix}, \quad (\text{C.13})$$

where σ_i are the Pauli matrices, described in Appendix E.

Euclidean Spacetime

In the Wick rotation to Euclidean space, we choose the transformation

$$\gamma_M^\mu \equiv (\gamma_M^0, \gamma_M^i) \xrightarrow{\text{Wick}} \gamma_\mu \equiv (\gamma_i, \gamma_4) = (-i\gamma_M^i, \gamma_M^0), \quad (\text{C.14})$$

such that we obtain the correct relationship for Dirac matrices in Euclidean space,

$$\{\gamma_\mu, \gamma_\nu\} = 2\delta_{\mu\nu}\mathbb{I}. \quad (\text{C.15})$$

With this convention, slashed quantities transform with a relative factor of i ,

$$\not{x}_M \equiv \gamma_M^\mu g_{\mu\nu} x_M^\nu \xrightarrow{\text{Wick}} \not{x} \equiv \gamma_\mu \delta_{\mu\nu} x_\nu = i\not{x}_M, \quad (\text{C.16})$$

and slashed derivatives transform as

$$\not{\partial}_M \equiv \gamma_{\mu,M} g^{\mu\nu} \partial_{\nu,M} \xrightarrow{\text{Wick}} \not{\partial} \equiv \gamma_\mu \delta_{\mu\nu} \partial_\nu = -i\not{\partial}_M. \quad (\text{C.17})$$

We choose the fifth Dirac matrix

$$\gamma_5 \equiv \gamma_1 \gamma_2 \gamma_3 \gamma_4 = -\gamma_M^5, \quad (\text{C.18})$$

and the antisymmetric tensor is defined as

$$\sigma_{\mu\nu} \equiv \frac{i}{2} [\gamma_\mu, \gamma_\nu], \quad (\text{C.19})$$

and hence,

$$\sigma_{4i} = -i\sigma_M^{0i}, \quad (\text{C.20})$$

$$\sigma_{ij} = -\sigma_M^{ij}. \quad (\text{C.21})$$

Contractions between Lorentz vectors and the antisymmetric tensor in Minkowski and Euclidean spacetime are related by

$$\sigma_{4\mu} \delta_{\mu\nu} q_\nu = i\sigma_M^{0\mu} g_{\mu\nu} x_M^\nu, \quad (\text{C.22})$$

$$\sigma_{i\mu} \delta_{\mu\nu} q_\nu = \sigma_M^{i\mu} g_{\mu\nu} x_M^\nu. \quad (\text{C.23})$$

The following identities hold independent of representation,

$$\gamma_5^2 = \mathbb{I}, \quad (\text{C.24})$$

$$\{\gamma_5, \gamma_\mu\} = 0, \quad (\text{C.25})$$

$$\text{Tr}(\Gamma_i \Gamma_j) = 0 \forall i \neq j, \quad (\text{C.26})$$

$$\text{Tr}(\gamma_{\mu_1} \dots \gamma_{\mu_n}) = 0 \quad \forall n \text{ odd}, \quad (\text{C.27})$$

$$\text{Tr}(\gamma_5 \gamma_{\mu_1} \dots \gamma_{\mu_n}) = 0 \quad \forall n \text{ odd}, \quad (\text{C.28})$$

$$\text{Tr}(\gamma_\mu \gamma_\nu) = 4\delta_{\mu\nu}, \quad (\text{C.29})$$

$$\text{Tr}(\gamma_5 \gamma_\mu \gamma_\nu) = 0, \quad (\text{C.30})$$

$$\text{Tr}(\gamma_\mu \gamma_\nu \gamma_\kappa \gamma_\lambda) = 4(\delta_{\mu\nu} \delta_{\kappa\lambda} - \delta_{\mu\kappa} \delta_{\nu\lambda} + \delta_{\mu\lambda} \delta_{\nu\kappa}), \quad (\text{C.31})$$

$$\text{Tr}(\gamma_5 \gamma_\mu \gamma_\nu \gamma_\gamma \gamma_\lambda) = 4\epsilon_{\mu\nu\kappa\lambda}. \quad (\text{C.32})$$

In this thesis we use the transformed Dirac basis,

$$\gamma_4 = \begin{bmatrix} \mathbb{I} & 0 \\ 0 & -\mathbb{I} \end{bmatrix}, \quad \gamma_i = \begin{bmatrix} 0 & -i\sigma_i \\ i\sigma_i & 0 \end{bmatrix}, \quad \gamma_5 = \begin{bmatrix} 0 & -\mathbb{I} \\ -\mathbb{I} & 0 \end{bmatrix}, \quad (\text{C.33})$$

where σ_i are the Pauli matrices, and all the matrices are Hermitian.

Appendix D

Levi-Civita Symbol

The Levi-Civita symbol in n dimensions is defined by total antisymmetry in its indices, and the convention that

$$\epsilon^{12\dots n} = +1. \quad (\text{D.1})$$

These properties define the tensor for all other combinations of indices, with

$$\epsilon^{i_1 i_2 \dots i_n} = \begin{cases} 0 & \text{any of } i_1, i_2, \dots, i_n \text{ are equal,} \\ +1 & \text{even permutation of } 1, 2, \dots, n, \\ -1 & \text{odd permutation of } 1, 2, \dots, n. \end{cases} \quad (\text{D.2})$$

Euclidean Space

In three Euclidean dimensions, we define the Levi-Civita tensor with

$$\epsilon_{123} = +1, \quad (\text{D.3})$$

and hence the following identities hold,

$$\epsilon_{ijk}\epsilon_{ijk} = 6, \quad (\text{D.4})$$

$$\epsilon_{imn}\epsilon_{jmn} = 2\delta_{ij}, \quad (\text{D.5})$$

$$\epsilon_{ijk}\epsilon_{imn} = \delta_{jm}\delta_{kn} - \delta_{jn}\delta_{km}, \quad (\text{D.6})$$

$$\epsilon_{ijk}\epsilon_{lmn} = \delta_{il}(\delta_{jm}\delta_{kn} - \delta_{jn}\delta_{km}) - \delta_{im}(\delta_{jl}\delta_{kn} - \delta_{jn}\delta_{kl}) + \delta_{in}(\delta_{jl}\delta_{km} - \delta_{jm}\delta_{kl}). \quad (\text{D.7})$$

Minkowski Spacetime

In Minkowski spacetime, we define the Levi-Civita tensor with

$$\epsilon^{0123} = +1, \quad (\text{D.8})$$

and the following identities hold,

$$\epsilon^{\mu\nu\kappa\lambda}\epsilon_{\mu\nu\kappa\lambda} = -24, \quad (\text{D.9})$$

$$\epsilon^{\mu\nu\kappa\lambda}\epsilon_{\mu\nu\kappa\xi} = -6\delta_\xi^\lambda, \quad (\text{D.10})$$

$$\epsilon^{\mu\nu\kappa\lambda}\epsilon_{\mu\nu\xi o} = -2(\delta_\xi^\kappa\delta_o^\lambda - \delta_o^\kappa\delta_\xi^\lambda), \quad (\text{D.11})$$

$$\epsilon^{0ijk} = \epsilon_{ijk}, \quad (\text{D.12})$$

where the last identity refers to the three-dimensional Euclidean tensor.

Euclidean Spacetime

In Euclidean spacetime we choose the transformation

$$\epsilon_M^{\mu\nu\kappa\lambda} \xrightarrow{\text{Wick}} -\epsilon_{\mu\nu\kappa\lambda}, \quad (\text{D.13})$$

so we have for the Levi-Civita tensor,

$$\epsilon_{1234} = +1, \quad (\text{D.14})$$

and hence the following identities hold,

$$\epsilon_{\mu\nu\kappa\lambda}\epsilon_{\mu\nu\kappa\lambda} = 24, \quad (\text{D.15})$$

$$\epsilon_{\mu\nu\kappa\lambda}\epsilon_{\mu\nu\kappa\xi} = 6\delta_{\lambda\xi}, \quad (\text{D.16})$$

$$\epsilon_{\mu\nu\kappa\lambda}\epsilon_{\mu\nu\xi\sigma} = 2(\delta_{\kappa\xi}\delta_{\lambda\sigma} - \delta_{\kappa\sigma}\delta_{\lambda\xi}), \quad (\text{D.17})$$

$$\epsilon^{ijk4} = \epsilon_{ijk}, \quad (\text{D.18})$$

where the last identity refers to the three-dimensional Euclidean tensor.

Appendix E

Special Unitary Groups

The special unitary group of degree n , denoted $SU(n)$, is the non-Abelian Lie group of $n \times n$ unitary matrices with determinant 1 under multiplication. In the fundamental (or defining) representation, elements of $SU(n)$ are generated by $n^2 - 1$ complex, traceless and Hermitian $n \times n$ matrices t^u , i.e. for each element Ω of $SU(n)$,

$$\Omega = e^{i\omega^u t^u}, \quad (\text{E.1})$$

for some real parameters ω^u . The generators t^u satisfy the commutation relation

$$[t^u, t^v] = i f^{uvw} t^w, \quad (\text{E.2})$$

where f^{uvw} are the fully-antisymmetric structure constants of $SU(n)$. The adjoint representation of $SU(n)$ consists of $(n^2 - 1) \times (n^2 - 1)$ complex matrices, generated by matrices whose elements are given by the structure constants,

$$(T^u)^{vw} = -i f^{uvw}. \quad (\text{E.3})$$

$SU(2)$ and the Pauli Matrices

In the fundamental representation, the three generators of $SU(2)$ are

$$t^u = -\frac{i}{2} \sigma^u, \quad (\text{E.4})$$

where σ^u are the Pauli matrices,

$$\sigma^1 = \begin{bmatrix} 0 & 1 \\ 1 & 0 \end{bmatrix}, \quad \sigma^2 = \begin{bmatrix} 0 & -i \\ i & 0 \end{bmatrix}, \quad \sigma^3 = \begin{bmatrix} 1 & 0 \\ 0 & -1 \end{bmatrix}. \quad (\text{E.5})$$

The structure constants of $SU(2)$ are given by

$$f^{uvw} = \epsilon^{uvw}, \quad (\text{E.6})$$

where ϵ^{uvw} is the antisymmetric Levi-Civita tensor defined in Appendix D.

SU(3) and the Gell-Mann Matrices

In the fundamental representation, the eight generators of SU(3) are

$$t^u = \frac{1}{2}\lambda^u, \quad (\text{E.7})$$

where λ^u are the Gell-Mann matrices,

$$\begin{aligned} \lambda^1 &= \begin{bmatrix} 0 & 1 & 0 \\ 1 & 0 & 0 \\ 0 & 0 & 0 \end{bmatrix}, & \lambda^2 &= \begin{bmatrix} 0 & -i & 0 \\ i & 0 & 0 \\ 0 & 0 & 0 \end{bmatrix}, & \lambda^3 &= \begin{bmatrix} 1 & 0 & 0 \\ 0 & -1 & 0 \\ 0 & 0 & 0 \end{bmatrix}, \\ \lambda^4 &= \begin{bmatrix} 0 & 0 & 1 \\ 0 & 0 & 0 \\ 1 & 0 & 0 \end{bmatrix}, & \lambda^5 &= \begin{bmatrix} 0 & 0 & -i \\ 0 & 0 & 0 \\ i & 0 & 0 \end{bmatrix}, & & (\text{E.8}) \\ \lambda^6 &= \begin{bmatrix} 0 & 0 & 0 \\ 0 & 0 & 1 \\ 0 & 1 & 0 \end{bmatrix}, & \lambda^7 &= \begin{bmatrix} 0 & 0 & 0 \\ 0 & 0 & -i \\ 0 & i & 0 \end{bmatrix}, & \lambda^8 &= \frac{1}{\sqrt{3}} \begin{bmatrix} 1 & 0 & 0 \\ 0 & 1 & 0 \\ 0 & 0 & -2 \end{bmatrix}. \end{aligned}$$

The structure constants of SU(3) are

$$\begin{aligned} f^{123} &= 1, \\ f^{147} &= -f^{156} = f^{246} = f^{257} = f^{345} = -f^{367} = \frac{1}{2}, \\ f^{458} &= f^{678} = \frac{\sqrt{3}}{2}, \end{aligned} \quad (\text{E.9})$$

with all other constants not related to these by permutations being zero.

Appendix F

Spin-Half Particles and the Dirac Equation

Minkowski Spacetime

In Minkowski spacetime, the four-spin vector is defined by the relations

$$p^\mu s_\mu = 0, \quad (\text{F.1})$$

$$s^\mu s_\mu = -1. \quad (\text{F.2})$$

The explicit form is given by

$$s^\mu(p, \sigma) = \left(\frac{\mathbf{p} \cdot \mathbf{s}}{E}, \mathbf{s} \right) = \left(\sigma \frac{\mathbf{p} \cdot \hat{\mathbf{e}}}{m}, \mathbf{s} \right), \quad (\text{F.3})$$

where the relativistic three-spin is given by

$$\mathbf{s}(p, \sigma) = \sigma \left[\hat{\mathbf{e}} + \frac{\mathbf{p} \cdot \hat{\mathbf{e}}}{m(E + m)} \mathbf{p} \right]. \quad (\text{F.4})$$

Here $\hat{\mathbf{e}}$ is the chosen spin-polarisation axis, and $\sigma = \pm 1$ is the spin quantum number. The Dirac equation for a free spin-half particle is given by

$$\left(i[\gamma^\mu]_{\alpha\beta} \partial_\mu - m \delta_{\alpha\beta} \right) [\psi(x)]_\alpha = 0, \quad (\text{F.5})$$

where ψ is a four-component spinor. Assuming matrix-vector notation for the Dirac indices, and Feynman slash notation for the contraction with the γ matrix, this may be written in the more compact form

$$(i\not{\partial} - m)\psi = 0. \quad (\text{F.6})$$

Positive and negative-energy solutions to the free Dirac equation are of the form

$$\psi = u(p, \sigma) e^{-ip \cdot x}, \quad (\text{F.7})$$

$$\psi = v(p, \sigma) e^{+ip \cdot x}, \quad (\text{F.8})$$

where the normalisation of the spinors is chosen to be

$$u(p, \sigma') \bar{u}(p, \sigma) = (\not{p} + m) \frac{1}{2} (\mathbb{I} + \gamma^5 \not{\epsilon}) \delta_{\sigma'\sigma}, \quad (\text{F.9})$$

$$v(p, \sigma') \bar{v}(p, \sigma) = (\not{p} - m) \frac{1}{2} (\mathbb{I} + \gamma^5 \not{\epsilon}) \delta_{\sigma'\sigma}, \quad (\text{F.10})$$

and the adjoint spinor is defined as

$$\bar{\psi} = \psi^\dagger \gamma^0. \quad (\text{F.11})$$

From the normalisation, we can derive the relations

$$\bar{u}(p, \sigma') u(p, \sigma) = 2m \delta_{\sigma'\sigma}, \quad (\text{F.12})$$

$$\bar{u}(p, \sigma') \gamma^5 u(p, \sigma) = 0, \quad (\text{F.13})$$

$$\bar{u}(p, \sigma') \gamma^\mu u(p, \sigma) = 2p^\mu \delta_{\sigma'\sigma}, \quad (\text{F.14})$$

$$\bar{u}(p, \sigma') \gamma^\mu \gamma^5 u(p, \sigma) = 2m s^\mu \delta_{\sigma'\sigma}, \quad (\text{F.15})$$

$$\bar{u}(p, \sigma') \sigma^{\mu\nu} u(p, \sigma) = 2\epsilon^{\mu\nu\kappa\lambda} s_\kappa p_\lambda \delta_{\sigma'\sigma}. \quad (\text{F.16})$$

Euclidean Spacetime

After the Wick rotation to Euclidean spacetime, the four-spin vector is defined by the relations

$$p \cdot s = 0, \quad (\text{F.17})$$

$$s^2 = 1. \quad (\text{F.18})$$

The explicit form is given by

$$s_\mu(p, \sigma) = \left(\mathbf{s}, i \frac{\mathbf{p} \cdot \mathbf{s}}{E} \right) = \left(\mathbf{s}, i \sigma \frac{\mathbf{p} \cdot \hat{\mathbf{e}}}{m} \right), \quad (\text{F.19})$$

where the relativistic three-spin

$$\mathbf{s}(p, \sigma) = \sigma \left[\hat{\mathbf{e}} + \frac{\mathbf{p} \cdot \hat{\mathbf{e}}}{m(E + m)} \mathbf{p} \right]. \quad (\text{F.20})$$

The Dirac equation for a free spin-half particle in Euclidean spacetime is given by

$$([\gamma^\mu]_{\alpha\beta} \partial_\mu + m \delta_{\alpha\beta}) [\psi(x)]_\alpha = 0, \quad (\text{F.21})$$

which may be written in the compact form

$$(\not{\partial} + m) \psi = 0. \quad (\text{F.22})$$

Positive and negative-energy solutions to the free Dirac equation are of the form

$$\psi = u(p, \sigma) e^{+ip \cdot x}, \quad (\text{F.23})$$

$$\psi = v(p, \sigma) e^{-ip \cdot x}, \quad (\text{F.24})$$

where the normalisation of the spinors is chosen to be

$$u(p, \sigma') \bar{u}(p, \sigma) = (-i\not{p} + m) \frac{1}{2} (\mathbb{I} + i\gamma_5 \not{\beta}) \delta_{\sigma'\sigma}, \quad (\text{F.25})$$

$$v(p, \sigma') \bar{v}(p, \sigma) = (-i\not{p} - m) \frac{1}{2} (\mathbb{I} + i\gamma_5 \not{\beta}) \delta_{\sigma'\sigma}, \quad (\text{F.26})$$

and the adjoint spinor is defined as

$$\bar{\psi} = \psi^\dagger \gamma_4. \quad (\text{F.27})$$

From the normalisation condition we can derive the identities

$$\bar{u}(p, \sigma')u(p, \sigma) = 2m\delta_{\sigma'\sigma}, \quad (\text{F.28})$$

$$\bar{u}(p, \sigma')\gamma_5 u(p, \sigma) = 0, \quad (\text{F.29})$$

$$\bar{u}(p, \sigma')\gamma_\mu u(p, \sigma) = -2ip_\mu\delta_{\sigma'\sigma}, \quad (\text{F.30})$$

$$\bar{u}(p, \sigma')\gamma_\mu\gamma_5 u(p, \sigma) = 2ims_\mu\delta_{\sigma'\sigma}, \quad (\text{F.31})$$

$$\bar{u}(p, \sigma')\sigma_{\mu\nu}u(p, \sigma) = 2i\epsilon_{\mu\nu\kappa\lambda}s_\kappa p_\lambda\delta_{\sigma'\sigma}. \quad (\text{F.32})$$

Appendix G

Dirac Projectors, Traces and Vertex Functions

Projectors

Parity and spin projectors for spin-half baryon spectroscopy are defined as

$$\Gamma_{P_{\pm}} = \frac{1}{2}(\mathbb{I} \pm \gamma_4), \quad (\text{G.1})$$

$$\Gamma_{S_{\pm}} = \frac{1}{2}(\mathbb{I} \mp i\hat{\mathbf{e}} \cdot \boldsymbol{\gamma}\gamma_5), \quad (\text{G.2})$$

where $\hat{\mathbf{e}}$ is the chosen spin-polarisation axis. Commonly used combinations of these projectors for nucleon analyses are

$$\Gamma_{\text{unpol}} \equiv \Gamma_{P_+} (\Gamma_{S_+} + \Gamma_{S_-}) = \frac{1}{2}(\mathbb{I} + \gamma_4), \quad (\text{G.3})$$

$$\Gamma_{\text{pol}} \equiv \Gamma_{P_+} (\Gamma_{S_+} - \Gamma_{S_-}) = -\frac{i}{2}(\mathbb{I} + \gamma_4)\hat{\mathbf{e}} \cdot \boldsymbol{\gamma}\gamma_5, \quad (\text{G.4})$$

$$\Gamma_{\text{pol}\pm} \equiv \Gamma_{P_+} \Gamma_{S_{\pm}} = \frac{1}{2}(\mathbb{I} + \gamma_4) \frac{1}{2}(\mathbb{I} \mp i\hat{\mathbf{e}} \cdot \boldsymbol{\gamma}\gamma_5) = \frac{1}{2}(\Gamma_{\text{unpol}} \pm \Gamma_{\text{pol}}). \quad (\text{G.5})$$

Traces

The function F_2 is defined by

$$F_2(\Gamma_{\text{proj}}; \mathbf{p}, m) \equiv \frac{1}{4} \sum_{\sigma} [\Gamma_{\text{proj}}]_{\alpha\beta} u_{\alpha}(p, \sigma) \bar{u}_{\beta}(p, \sigma) = \frac{1}{4} \text{Tr} \Gamma(-i\not{p} + m), \quad (\text{G.6})$$

and is linear in Γ_{proj} . For the basis of Dirac matrices, with kinematic inputs \mathbf{p} and m assumed, it is given by

$$F_2(\mathbb{I}) = m, \quad (\text{G.7})$$

$$F_2(\gamma_{\mu}) = -ip_{\mu}, \quad (\text{G.8})$$

$$F_2(\gamma_5) = F_2(\gamma_{\mu}\gamma_5) = F_2(\sigma_{\mu\nu}) = 0. \quad (\text{G.9})$$

For the common Dirac projectors previously defined,

$$F_2(\Gamma_{\text{unpol}}) = \frac{1}{2}(E_X + m_X), \quad (\text{G.10})$$

$$F_2(\Gamma_{\text{pol}}) = 0, \quad (\text{G.11})$$

$$F_2(\Gamma_{\text{pol}\pm}) = \frac{1}{4}(E_X + m_X). \quad (\text{G.12})$$

The function F_3 is defined as

$$\begin{aligned} F_3(\Gamma_{\text{proj}}, \Gamma_{\mathcal{O}, X}; \mathbf{p}', \mathbf{p}, m_X) &\equiv \frac{1}{4} \sum_{\sigma'\sigma} [\Gamma_{\text{proj}}]_{\alpha\beta} u_\alpha(p', \sigma') \bar{u}(p', \sigma') \Gamma_{\mathcal{O}, X} u(p, \sigma) \bar{u}_\beta(p, \sigma) \\ &= \frac{1}{4} \text{Tr} \Gamma_{\text{proj}} (-i\not{p}' + m) \Gamma_{\mathcal{O}, X} (-i\not{p} + m). \end{aligned} \quad (\text{G.13})$$

In the basis of Dirac matrices,

$$F_3(\mathbb{I}, \mathbb{I}) = -\frac{1}{2}(p' + p)^2 = m^2 - p' \cdot p, \quad (\text{G.14})$$

$$F_3(\mathbb{I}, \gamma_\mu) = -im(p' + p)_\mu, \quad (\text{G.15})$$

$$F_3(\mathbb{I}, \gamma_5) = 0, \quad (\text{G.16})$$

$$F_3(\mathbb{I}, \gamma_\mu \gamma_5) = 0, \quad (\text{G.17})$$

$$F_3(\mathbb{I}, \sigma_{\mu\nu}) = -i(p'_\mu p_\nu - p_\mu p'_\nu), \quad (\text{G.18})$$

$$F_3(\gamma_\mu, \gamma_\nu) = -\left[p'_\mu p_\nu + p_\mu p'_\nu + \frac{1}{2} \delta_{\mu\nu} (p' - p)^2 \right], \quad (\text{G.19})$$

$$F_3(\gamma_\mu, \gamma_5) = 0, \quad (\text{G.20})$$

$$F_3(\gamma_\mu, \gamma_\nu \gamma_5) = -\epsilon_{\mu\nu\kappa\lambda} p'_\kappa p_\lambda, \quad (\text{G.21})$$

$$F_3(\gamma_\mu, \sigma_{\kappa\lambda}) = -m[\delta_{\mu\kappa}(p' - p)_\lambda - \delta_{\mu\lambda}(p' - p)_\kappa], \quad (\text{G.22})$$

$$F_3(\gamma_5, \gamma_5) = -\frac{1}{2}(p' - p)^2, \quad (\text{G.23})$$

$$F_3(\gamma_5, \gamma_\mu \gamma_5) = -im(p' - p)_\mu, \quad (\text{G.24})$$

$$F_3(\gamma_5, \sigma_{\mu\nu}) = -i\epsilon_{\mu\nu\kappa\lambda} p'_\kappa p_\lambda, \quad (\text{G.25})$$

$$F_3(\gamma_\mu \gamma_5, \gamma_\nu \gamma_5) = -\left[p'_\mu p_\nu + p_\mu p'_\nu - \frac{1}{2} \delta_{\mu\nu} (p' + p)^2 \right], \quad (\text{G.26})$$

$$F_3(\gamma_\mu \gamma_5, \sigma_{\kappa\lambda}) = -m\epsilon_{\mu\kappa\lambda\xi} (p' + p)_\xi. \quad (\text{G.27})$$

For the unpolarised projector, we have

$$F_3(\Gamma_{\text{unpol}}, \mathbb{I}) = \frac{1}{2}[(E(\mathbf{p}) + m)(E(\mathbf{p}') + m) - \mathbf{p} \cdot \mathbf{p}'], \quad (\text{G.28})$$

$$F_3(\Gamma_{\text{unpol}}, \gamma_4) = \frac{1}{2}[(E(\mathbf{p}) + m)(E(\mathbf{p}') + m) + \mathbf{p} \cdot \mathbf{p}'], \quad (\text{G.29})$$

$$F_3(\Gamma_{\text{unpol}}, \gamma_i) = -\frac{i}{2}[(E(\mathbf{p}') + m)\mathbf{p} + (E(\mathbf{p}) + m)\mathbf{p}']_i, \quad (\text{G.30})$$

$$F_3(\Gamma_{\text{unpol}}, \gamma_5) = 0, \quad (\text{G.31})$$

$$F_3(\Gamma_{\text{unpol}}, \gamma_4\gamma_5) = 0, \quad (\text{G.32})$$

$$F_3(\Gamma_{\text{unpol}}, \gamma_i\gamma_5) = \frac{1}{2}[\mathbf{p}' \times \mathbf{p}]_i, \quad (\text{G.33})$$

$$F_3(\Gamma_{\text{unpol}}, \sigma_{4i}) = \frac{1}{2}[(E(\mathbf{p}') + m)\mathbf{p} - (E(\mathbf{p}) + m)\mathbf{p}']_i, \quad (\text{G.34})$$

$$F_3(\Gamma_{\text{unpol}}, \sigma_{ij}) = \frac{i}{2}\epsilon_{ijk}[\mathbf{p} \times \mathbf{p}']_k, \quad (\text{G.35})$$

and for the polarised projector,

$$F_3(\Gamma_{\text{pol}}, \mathbb{I}) = \frac{i}{2}\hat{\mathbf{e}} \cdot \mathbf{p} \times \mathbf{p}', \quad (\text{G.36})$$

$$F_3(\Gamma_{\text{pol}}, \gamma_4) = -\frac{i}{2}\hat{\mathbf{e}} \cdot \mathbf{p} \times \mathbf{p}', \quad (\text{G.37})$$

$$F_3(\Gamma_{\text{pol}}, \gamma_i) = -\frac{1}{2}[(E(\mathbf{p}) + m)\mathbf{p}' \times \hat{\mathbf{e}} - (E(\mathbf{p}') + m)\mathbf{p} \times \hat{\mathbf{e}}]_i, \quad (\text{G.38})$$

$$F_3(\Gamma_{\text{pol}}, \gamma_5) = \frac{1}{2}[(E(\mathbf{p}) + m)\mathbf{p}' \cdot \hat{\mathbf{e}} - (E(\mathbf{p}') + m)\mathbf{p} \cdot \hat{\mathbf{e}}], \quad (\text{G.39})$$

$$F_3(\Gamma_{\text{pol}}, \gamma_4\gamma_5) = -\frac{1}{2}[(E(\mathbf{p}) + m)\mathbf{p}' \cdot \hat{\mathbf{e}} + (E(\mathbf{p}') + m)\mathbf{p} \cdot \hat{\mathbf{e}}], \quad (\text{G.40})$$

$$F_3(\Gamma_{\text{pol}}, \gamma_i\gamma_5) = \quad (\text{G.41})$$

$$\frac{i}{2}[(E(\mathbf{p}) + m)(E(\mathbf{p}') + m)\hat{\mathbf{e}} + (\mathbf{p} \cdot \hat{\mathbf{e}})\mathbf{p}' + (\mathbf{p}' \cdot \hat{\mathbf{e}})\mathbf{p} - (\mathbf{p}' \cdot \mathbf{p})\hat{\mathbf{e}}]_i, \quad (\text{G.42})$$

$$F_3(\Gamma_{\text{pol}}, \sigma_{4i}) = -\frac{i}{2}[(E(\mathbf{p}) + m)\hat{\mathbf{e}} \times \mathbf{p}' + (E(\mathbf{p}') + m)\hat{\mathbf{e}} \times \mathbf{p}], \quad (\text{G.43})$$

$$F_3(\Gamma_{\text{pol}}, \sigma_{ij}) = \quad (\text{G.44})$$

$$-\frac{1}{2}\epsilon_{ijk}[(E(\mathbf{p}) + m)(E(\mathbf{p}') + m)\hat{\mathbf{e}} - (\mathbf{p} \cdot \hat{\mathbf{e}})\mathbf{p}' - (\mathbf{p}' \cdot \hat{\mathbf{e}})\mathbf{p} + (\mathbf{p}' \cdot \mathbf{p})\hat{\mathbf{e}}]_k. \quad (\text{G.45})$$

In the Breit frame where $E(\mathbf{p}') = E(\mathbf{p}) = E$, it is convenient to work in terms of the kinematic variables

$$\bar{P} \equiv \frac{1}{2}(p' + p), \quad (\text{G.46})$$

$$\bar{q} \equiv \frac{1}{2}(p' - p) = \frac{1}{2}q. \quad (\text{G.47})$$

For the unpolarised projector and Breit frame kinematics, we have

$$F_3^{\text{Breit}}(\Gamma_{\text{unpol}}, \mathbb{I}) = m(E + m) + \bar{\mathbf{q}}^2, \quad (\text{G.48})$$

$$F_3^{\text{Breit}}(\Gamma_{\text{unpol}}, \gamma_4) = m(E + m) + \bar{\mathbf{P}}^2, \quad (\text{G.49})$$

$$F_3^{\text{Breit}}(\Gamma_{\text{unpol}}, \gamma_i) = -i(E + m)\bar{P}_i, \quad (\text{G.50})$$

$$F_3^{\text{Breit}}(\Gamma_{\text{unpol}}, \gamma_5) = 0, \quad (\text{G.51})$$

$$F_3^{\text{Breit}}(\Gamma_{\text{unpol}}, \gamma_4\gamma_5) = 0, \quad (\text{G.52})$$

$$F_3^{\text{Breit}}(\Gamma_{\text{unpol}}, \gamma_i\gamma_5) = [\bar{\mathbf{q}} \times \bar{\mathbf{P}}]_i, \quad (\text{G.53})$$

$$F_3^{\text{Breit}}(\Gamma_{\text{unpol}}, \sigma_{4i}) = -(E + m)\bar{q}_i, \quad (\text{G.54})$$

$$F_3^{\text{Breit}}(\Gamma_{\text{unpol}}, \sigma_{ij}) = i\epsilon_{ijk}[\bar{\mathbf{P}} \times \bar{\mathbf{q}}]_k, \quad (\text{G.55})$$

and for the polarised projector, we have

$$F_3^{\text{Breit}}(\Gamma_{\text{pol}}, \mathbb{I}) = i\hat{\mathbf{e}} \cdot \bar{\mathbf{P}} \times \bar{\mathbf{q}}, \quad (\text{G.56})$$

$$F_3^{\text{Breit}}(\Gamma_{\text{pol}}, \gamma_4) = -i\hat{\mathbf{e}} \cdot \bar{\mathbf{P}} \times \bar{\mathbf{q}}, \quad (\text{G.57})$$

$$F_3^{\text{Breit}}(\Gamma_{\text{pol}}, \gamma_i) = (E + m)[\hat{\mathbf{e}} \times \bar{\mathbf{q}}]_i, \quad (\text{G.58})$$

$$F_3^{\text{Breit}}(\Gamma_{\text{pol}}, \gamma_5) = (E + m)\hat{\mathbf{e}} \cdot \bar{\mathbf{q}}, \quad (\text{G.59})$$

$$F_3^{\text{Breit}}(\Gamma_{\text{pol}}, \gamma_4\gamma_5) = -(E + m)\hat{\mathbf{e}} \cdot \bar{\mathbf{P}}, \quad (\text{G.60})$$

$$F_3^{\text{Breit}}(\Gamma_{\text{pol}}, \gamma_i\gamma_5) = im(E + m) \left[\hat{\mathbf{e}} + \frac{(\bar{\mathbf{P}} \cdot \hat{\mathbf{e}})\bar{\mathbf{P}}}{m(E + m)} + \frac{\bar{\mathbf{q}} \times (\hat{\mathbf{e}} \times \bar{\mathbf{q}})}{m(E + m)} \right]_i, \quad (\text{G.61})$$

$$F_3^{\text{Breit}}(\Gamma_{\text{pol}}, \sigma_{4i}) = -(E + m)[\hat{\mathbf{e}} \times \bar{\mathbf{P}}]_i, \quad (\text{G.62})$$

$$F_3^{\text{Breit}}(\Gamma_{\text{pol}}, \sigma_{ij}) = -\epsilon_{ijk}m(E + m) \left[\hat{\mathbf{e}} + \frac{(\bar{\mathbf{q}} \cdot \hat{\mathbf{e}})\bar{\mathbf{q}}}{m(E + m)} + \frac{\bar{\mathbf{P}} \times (\hat{\mathbf{e}} \times \bar{\mathbf{P}})}{m(E + m)} \right]_k. \quad (\text{G.63})$$

Vertex Functions

The matrix elements of local, flavour-diagonal quark-bilinear operators are given in terms of vertex functions

$$\langle X(\mathbf{p}', \sigma') | \mathcal{O}(0) | X(\mathbf{p}, \sigma) \rangle = \bar{u}(p', \sigma') \Gamma_{\mathcal{O}, X} u(p, \sigma). \quad (\text{G.64})$$

For the quark bilinear currents

$$\mathcal{S}^f(x) \equiv \bar{\psi}_f(x) \psi_f(x), \quad (\text{G.65})$$

$$\mathcal{P}^f(x) \equiv \bar{\psi}_f(x) \gamma_5 \psi_f(x), \quad (\text{G.66})$$

$$\mathcal{V}_\mu^f(x) \equiv \bar{\psi}_f(x) \gamma_\mu \psi_f(x), \quad (\text{G.67})$$

$$\mathcal{A}_\mu^f(x) \equiv \bar{\psi}_f(x) \gamma_\mu \gamma_5 \psi_f(x), \quad (\text{G.68})$$

$$\mathcal{T}_{\mu\nu}^f(x) \equiv \bar{\psi}_f(x) \sigma_{\mu\nu} \psi_f(x), \quad (\text{G.69})$$

the vertex functions are given explicitly by

$$\Gamma_{S^f, X} = g_{S, X}^f(Q^2), \quad (\text{G.70})$$

$$\Gamma_{P^f, X} = \gamma_5 g_{P, X}^f(Q^2), \quad (\text{G.71})$$

$$\Gamma_{V_\mu^f, X} = \gamma_\mu F_{1, X}^f(Q^2) + \sigma_{\mu\nu} \frac{q_\nu}{2m_X} F_{2, X}^f(Q^2), \quad (\text{G.72})$$

$$\Gamma_{A_\mu^f, X} = \gamma_\mu \gamma_5 g_{A, X}^f(Q^2) - i \gamma_5 \frac{q_\mu}{2m_X} g_{AP, X}^f(Q^2), \quad (\text{G.73})$$

$$\Gamma_{T_{\mu\nu}^f, X} = \sigma_{\mu\nu} A_{T, X}^f(Q^2) - i \frac{\bar{P}_\mu q_\nu - \bar{P}_\nu q_\mu}{m_X^2} \tilde{A}_{T, X}^f(Q^2) - i \frac{\gamma_\mu q_\nu - \gamma_\nu q_\mu}{2m_X} B_{T, X}^f(Q^2). \quad (\text{G.74})$$

Appendix H

Feynman-Hellmann Energy Shifts

Traces

The function $F_{2,\text{FH}}$ is defined as

$$F_{2,\text{FH}}(\Gamma_{\text{proj}}; \mathbf{p}, m_X) = \frac{1}{4} \sum_{\sigma} [\Gamma_{\text{proj}}]_{\alpha\beta} u_{\alpha}(p, \sigma) \bar{u}_{\beta}(p, \sigma) \frac{dE_X(\mathbf{p}, \sigma)}{d\lambda}. \quad (\text{H.1})$$

For the basis of Dirac matrices,

$$F_{2,\text{FH}}(\mathbb{I}) = \frac{m_X}{2} \left[\frac{dE_X(\mathbf{p}, +)}{d\lambda} + \frac{dE_X(\mathbf{p}, -)}{d\lambda} \right], \quad (\text{H.2})$$

$$F_{2,\text{FH}}(\gamma_{\mu}) = -\frac{i}{2} p_{\mu} \left[\frac{dE_X(\mathbf{p}, +)}{d\lambda} + \frac{dE_X(\mathbf{p}, -)}{d\lambda} \right], \quad (\text{H.3})$$

$$F_{2,\text{FH}}(\gamma_5) = 0, \quad (\text{H.4})$$

$$F_{2,\text{FH}}(\gamma_{\mu}\gamma_5) = \frac{i}{2} m s_{\mu} \left[\frac{dE_X(\mathbf{p}, +)}{d\lambda} - \frac{dE_X(\mathbf{p}, -)}{d\lambda} \right], \quad (\text{H.5})$$

$$F_{2,\text{FH}}(\sigma_{\mu\nu}) = -\frac{i}{2} \epsilon_{\mu\nu\kappa\lambda} p_{\kappa} s_{\lambda} \left[\frac{dE_X(\mathbf{p}, +)}{d\lambda} - \frac{dE_X(\mathbf{p}, -)}{d\lambda} \right]. \quad (\text{H.6})$$

For the common projectors defined in Appendix G,

$$F_{2,\text{FH}}(\Gamma_{\text{unpol}}) = \frac{1}{4} [E_X(\mathbf{p}) + m_X] \left[\frac{dE_X(\mathbf{p}, +)}{d\lambda} + \frac{dE_X(\mathbf{p}, -)}{d\lambda} \right], \quad (\text{H.7})$$

$$F_{2,\text{FH}}(\Gamma_{\text{pol}}) = \frac{1}{4} [E_X(\mathbf{p}) + m_X] \left[\frac{dE_X(\mathbf{p}, +)}{d\lambda} - \frac{dE_X(\mathbf{p}, -)}{d\lambda} \right], \quad (\text{H.8})$$

$$F_{2,\text{FH}}(\Gamma_{\text{pol}\pm}) = \frac{1}{4} [E_X(\mathbf{p}) + m_X] \frac{dE_X(\mathbf{p}, \pm)}{d\lambda} \quad (\text{H.9})$$

Energy Shifts

Here we summarise the energy shifts of spin-half particles resulting from the inclusion of quark-bilinear operators in the QCD Lagrangian of the form

$$\mathcal{L}(x) \longrightarrow \mathcal{L}'(x) = \mathcal{L} + 2\lambda_f \cos[\mathbf{q} \cdot (\mathbf{x}' - \mathbf{x})] \bar{\psi}_f(x) \Gamma \psi_f(x). \quad (\text{H.10})$$

Energy shifts are extracted from two-point functions projected to momentum \mathbf{p}' at the sink, relative to \mathbf{x} , with the constraint that the resulting kinematics satisfy the Breit frame condition

$$|\mathbf{p}' \pm \mathbf{q}| = |\mathbf{p}'|, \quad (\text{H.11})$$

and for a positive-parity, definite-spin state, energy shifts are given by

$$\frac{dE_X(\mathbf{p}', \pm)}{d\lambda} = \frac{2F_3(\Gamma_{\text{pol}\pm}, \Gamma_{\mathcal{O}, X}; \mathbf{p}', \mathbf{p}, m_X)}{E_X(\mathbf{p}') [E_X(\mathbf{p}') + m_X]} \equiv \text{FH}(\Gamma_{\mathcal{O}, X}). \quad (\text{H.12})$$

For the basis of γ matrices,

$$\text{FH}(\mathbb{I}) = \frac{m}{E} \left[1 + \bar{\mathbf{q}} \cdot \frac{\bar{\mathbf{q}} \pm i\hat{\mathbf{e}} \times \bar{\mathbf{P}}}{m(E+m)} \right], \quad (\text{H.13})$$

$$\text{FH}(\gamma_4) = \frac{m}{E} \left[1 + \bar{\mathbf{P}} \cdot \frac{\bar{\mathbf{P}} \pm i\hat{\mathbf{e}} \times \bar{\mathbf{q}}}{m(E+m)} \right], \quad (\text{H.14})$$

$$\text{FH}(\gamma_i) = -\frac{i}{E} \left[\bar{\mathbf{P}} \pm i\hat{\mathbf{e}} \times \bar{\mathbf{q}} \right]_i, \quad (\text{H.15})$$

$$\text{FH}(\gamma_5) = \pm \frac{\hat{\mathbf{e}} \cdot \bar{\mathbf{q}}}{E}, \quad (\text{H.16})$$

$$\text{FH}(\gamma_4\gamma_5) = \mp \frac{\hat{\mathbf{e}} \cdot \bar{\mathbf{P}}}{E}, \quad (\text{H.17})$$

$$\text{FH}(\gamma_i\gamma_5) = \frac{m}{E} \left[\bar{\mathbf{q}} \times \frac{\bar{\mathbf{P}} \pm i\hat{\mathbf{e}} \times \bar{\mathbf{q}}}{m(E+m)} \pm i \left(\hat{\mathbf{e}} + \frac{(\bar{\mathbf{P}} \cdot \hat{\mathbf{e}})\bar{\mathbf{P}}}{m(E+m)} \right) \right]_i, \quad (\text{H.18})$$

$$\text{FH}(\sigma_{4i}) = -\frac{1}{E} \left[\bar{\mathbf{q}} \pm i\hat{\mathbf{e}} \times \bar{\mathbf{P}} \right]_i, \quad (\text{H.19})$$

$$\text{FH}(\sigma_{ij}) = i\epsilon_{ijk} \frac{m}{E} \left[\bar{\mathbf{P}} \times \frac{\bar{\mathbf{q}} \pm i\hat{\mathbf{e}} \times \bar{\mathbf{P}}}{m(E+m)} \pm i \left(\hat{\mathbf{e}} + \frac{(\bar{\mathbf{q}} \cdot \hat{\mathbf{e}})\bar{\mathbf{q}}}{m(E+m)} \right) \right]_k. \quad (\text{H.20})$$

For the various quark-bilinear currents, we have

$$\text{FH}(\Gamma_S) = \frac{m}{E} \left[1 + \bar{\mathbf{q}} \cdot \frac{\bar{\mathbf{q}} \pm i\hat{\mathbf{e}} \times \bar{\mathbf{P}}}{m(E+m)} \right] g_S, \quad (\text{H.21})$$

$$\text{FH}(\Gamma_P) = \pm \frac{\hat{\mathbf{e}} \cdot \bar{\mathbf{q}}}{E} g_P, \quad (\text{H.22})$$

$$\text{FH}(\Gamma_{V_4}) = \frac{m}{E} \left\{ \left[1 + \bar{\mathbf{P}} \cdot \frac{\bar{\mathbf{P}} \pm i\hat{\mathbf{e}} \times \bar{\mathbf{q}}}{m(E+m)} \right] F_1 - \bar{\mathbf{q}} \cdot \frac{\bar{\mathbf{q}} \pm i\hat{\mathbf{e}} \times \bar{\mathbf{P}}}{m^2} F_2 \right\}, \quad (\text{H.23})$$

$$\text{FH}(\Gamma_{V_i}) = -\frac{i}{E} \left\{ \left[\bar{\mathbf{P}} \pm i\hat{\mathbf{e}} \times \bar{\mathbf{q}} \right] F_1 + \left[\bar{\mathbf{P}} \times \frac{\bar{\mathbf{q}} \pm i\hat{\mathbf{e}} \times \bar{\mathbf{P}}}{m(E+m)} \pm i\hat{\mathbf{e}} \right] \times \bar{\mathbf{q}} F_2 \right\}_i, \quad (\text{H.24})$$

$$\text{FH}(\Gamma_{A_4}) = \mp \frac{\hat{\mathbf{e}} \cdot \bar{\mathbf{P}}}{2E} g_A, \quad (\text{H.25})$$

$$\begin{aligned} \text{FH}(\Gamma_{A_i}) = & \frac{m}{E} \left\{ \left[\bar{\mathbf{q}} \times \frac{\bar{\mathbf{P}} \pm i\hat{\mathbf{e}} \times \bar{\mathbf{q}}}{m(E+m)} \pm i \left(\hat{\mathbf{e}} + \frac{(\bar{\mathbf{P}} \cdot \hat{\mathbf{e}})\bar{\mathbf{P}}}{m(E+m)} \right) \right] g_A \right. \\ & \left. \mp i \frac{(\hat{\mathbf{e}} \cdot \bar{\mathbf{q}})\bar{\mathbf{q}}}{m^2} g_{AP} \right\}_i, \end{aligned} \quad (\text{H.26})$$

$$\begin{aligned} \text{FH}(\Gamma_{T_{4i}}) = & -\frac{1}{E} \left\{ \left[\bar{\mathbf{q}} \pm i\hat{\mathbf{e}} \times \bar{\mathbf{P}} \right] A_T + 4\frac{E}{m} \left[1 + \bar{\mathbf{q}} \cdot \frac{\bar{\mathbf{q}} \pm i\hat{\mathbf{e}} \times \bar{\mathbf{P}}}{m(E+m)} \right] \bar{\mathbf{q}} \tilde{A}_T \right. \\ & \left. + i \left[1 + \bar{\mathbf{P}} \cdot \frac{\bar{\mathbf{P}} \pm i\hat{\mathbf{e}} \times \bar{\mathbf{q}}}{m(E+m)} \right] \bar{\mathbf{q}} B_T \right\}_i, \end{aligned} \quad (\text{H.27})$$

$$\begin{aligned} \text{FH}(\Gamma_{T_{ij}}) = & \frac{m}{E} \left\{ i\epsilon_{ijk} \left[\bar{\mathbf{P}} \times \frac{\bar{\mathbf{q}} \pm i\hat{\mathbf{e}} \times \bar{\mathbf{P}}}{m(E+m)} \pm i \left(\hat{\mathbf{e}} + \frac{(\hat{\mathbf{e}} \cdot \bar{\mathbf{q}})\bar{\mathbf{q}}}{m(E+m)} \right) \right]_k A_T \right. \\ & - 2\frac{i}{m^2} \left[1 + \bar{\mathbf{q}} \cdot \frac{\bar{\mathbf{q}} \pm i\hat{\mathbf{e}} \times \bar{\mathbf{P}}}{m(E+m)} \right] (\bar{P}_i \bar{q}_j - \bar{P}_j \bar{q}_i) \tilde{A}_T \\ & \left. - \frac{1}{m^2} \left[(\bar{\mathbf{P}} \pm i\hat{\mathbf{e}} \times \bar{\mathbf{q}})_i \bar{q}_j - (\bar{\mathbf{P}} \pm i\hat{\mathbf{e}} \times \bar{\mathbf{q}})_j \bar{q}_i \right] B_T \right\}. \end{aligned} \quad (\text{H.28})$$

Appendix I

Ensembles

In this appendix we summarise the QCDSF/UKQCD ensembles used throughout this thesis, as well as ensembles generated for the disconnected calculations of Chapter 6. See [61] for more details of these ensembles, including the masses of low-lying hadron states.

The number of flavours, inverse coupling β , lattice size and clover parameter c_{SW} as defined in Chapter 3 are the same for all ensembles,

$$N_f = 2 + 1, \tag{I.1}$$

$$\beta = 5.50, \tag{I.2}$$

$$N_L^3 \times N_T = 32^3 \times 64, \tag{I.3}$$

$$c_{\text{SW}} = 2.65. \tag{I.4}$$

The lattice spacing is determined through the scale-setting procedure discussed in Chapter 3, and is the same for all ensembles,

$$a = 0.074(2) \text{ fm}. \tag{I.5}$$

The following table shows the three ensembles used, distinguished by the hopping parameters used, and the resulting pion mass.

Ensemble	(κ_l, κ_s)	m_π [MeV]
1	(0.120900, 0.120900)	466(13)
2	(0.121040, 0.120620)	360(10)
3	(0.121095, 0.120512)	310(09)

Ensembles generated for the calculation of Chapter 6 have a term included in the Lagrangian,

$$\mathcal{L}(x) = \mathcal{L}_0(x) + \lambda_l [\bar{u}(x)\gamma_3\gamma_5 u(x) + \bar{d}(x)\gamma_3\gamma_5 d(x)] + \lambda_s \bar{s}(x)\gamma_3\gamma_5 s(x), \tag{I.6}$$

where \mathcal{L}_0 is the standard QCD Lagrangian. The following table gives the hopping parameters and Feynman-Hellmann parameters for the newly-generated ensembles.

Ensemble	(κ_l, κ_s)	$(a\lambda_l, a\lambda_s)$
A1	(0.120900, 0.120900)	(0.00625, 0.00625)
A2	(0.120900, 0.120900)	(0.01250, 0.01250)
A3	(0.120900, 0.120900)	(-0.03000, -0.03000)
A4	(0.121095, 0.120512)	(0.02500, 0.02500)
A5	(0.121095, 0.120512)	(-0.05000, -0.05000)

Appendix J

Publications by the Author

- A. J. Chambers et al. “Feynman-Hellmann approach to the spin structure of hadrons”. *Phys. Rev.* D90.1 (2014), 014510. DOI: 10.1103/PhysRevD.90.014510. arXiv: 1405.3019 [hep-lat]
- A. J. Chambers, R. Horsley, Y. Nakamura, H. Perlt, P. E. L. Rakow, G. Schierholz, A. Schiller, and J. M. Zanotti. “A novel approach to nonperturbative renormalization of singlet and nonsinglet lattice operators”. *Phys. Lett.* B740 (2015), 30–35. DOI: 10.1016/j.physletb.2014.11.033. arXiv: 1410.3078 [hep-lat]
- A. J. Chambers et al. “Disconnected contributions to the spin of the nucleon”. *Phys. Rev.* D92.11 (2015), 114517. DOI: 10.1103/PhysRevD.92.114517. arXiv: 1508.06856 [hep-lat]
- A. J. Chambers, R. Horsley, Y. Nakamura, H. Perlt, P. E. L. Rakow, G. Schierholz, A. Schiller, K. Somfleth, R. D. Young, and J. M. Zanotti. “Nucleon Structure Functions from Operator Product Expansion on the Lattice”. *Phys. Rev. Lett.* 118.24 (2017), 242001. DOI: 10.1103/PhysRevLett.118.242001. arXiv: 1703.01153 [hep-lat]
- A. J. Chambers et al. “Electromagnetic form factors at large momenta from lattice QCD”. *Phys. Rev.* D96.11 (2017), 114509. DOI: 10.1103/PhysRevD.96.114509. arXiv: 1702.01513 [hep-lat]

References

- [1] Y. Nakamura and H. Stüben. “BQCD - Berlin quantum chromodynamics program”. *PoS LATTICE2010* (2010), 040. arXiv: 1011.0199 [hep-lat].
- [2] P. A. Boyle. “The BAGEL assembler generation library”. *Comput. Phys. Commun.* 180 (2009), 2739–2748. DOI: 10.1016/j.cpc.2009.08.010.
- [3] R. G. Edwards and B. Joo. “The Chroma software system for lattice QCD”. *Nucl. Phys. Proc. Suppl.* 140 (2005), 832. DOI: 10.1016/j.nuclphysbps.2004.11.254. arXiv: hep-lat/0409003 [hep-lat].
- [4] M. Gell-Mann. “A Schematic Model of Baryons and Mesons”. *Phys. Lett.* 8.3 (1964), 214–215. DOI: 10.1016/S0031-9163(64)92001-3.
- [5] G. Zweig. “An SU(3) model for strong interaction symmetry and its breaking. Version 2”. *DEVELOPMENTS IN THE QUARK THEORY OF HADRONS. VOL. 1. 1964 - 1978*. Ed. by D. Lichtenberg and S. P. Rosen. 1964, pp. 22–101. URL: <http://inspirehep.net/record/4674/files/cern-th-412.pdf>.
- [6] E. D. Bloom et al. “High-Energy Inelastic $e - p$ Scattering at 6° and 10° ”. *Phys. Rev. Lett.* 23 (1969), 930–934. DOI: 10.1103/PhysRevLett.23.930.
- [7] M. Breidenbach, J. I. Friedman, H. W. Kendall, E. D. Bloom, D. H. Coward, H. C. DeStaebler, J. Drees, L. W. Mo, and R. E. Taylor. “Observed Behavior of Highly Inelastic electron-Proton Scattering”. *Phys. Rev. Lett.* 23 (1969), 935–939. DOI: 10.1103/PhysRevLett.23.935.
- [8] S. Chatrchyan et al. “Observation of a new boson at a mass of 125 GeV with the CMS experiment at the LHC”. *Phys. Lett.* B716 (2012), 30–61. DOI: 10.1016/j.physletb.2012.08.021. arXiv: 1207.7235 [hep-ex].
- [9] G. Aad et al. “Observation of a new particle in the search for the Standard Model Higgs boson with the ATLAS detector at the LHC”. *Phys. Lett.* B716 (2012), 1–29. DOI: 10.1016/j.physletb.2012.08.020. arXiv: 1207.7214 [hep-ex].
- [10] Y. Fukuda et al. “Evidence for oscillation of atmospheric neutrinos”. *Phys. Rev. Lett.* 81 (1998), 1562–1567. DOI: 10.1103/PhysRevLett.81.1562. arXiv: hep-ex/9807003 [hep-ex].
- [11] Nobelprize.org. *The Nobel Prize in Physics 2015*. 2017. URL: https://www.nobelprize.org/nobel_prizes/physics/laureates/2015/index.html (visited on 12/28/2017).
- [12] S. F. King. “Neutrino mass models”. *Rept. Prog. Phys.* 67 (2004), 107–158. DOI: 10.1088/0034-4885/67/2/R01. arXiv: hep-ph/0310204 [hep-ph].

- [13] W. T. F. Encyclopedia. *Standard Model*. 2017. URL: https://en.wikipedia.org/wiki/Standard_Model (visited on 12/27/2017).
- [14] C.-N. Yang and R. L. Mills. “Conservation of Isotopic Spin and Isotopic Gauge Invariance”. *Phys. Rev.* 96 (1954), 191–195. DOI: 10.1103/PhysRev.96.191.
- [15] R. D. Peccei. “The Strong CP problem and axions”. *Lect. Notes Phys.* 741 (2008), 3–17. DOI: 10.1007/978-3-540-73518-2_1. arXiv: hep-ph/0607268 [hep-ph].
- [16] M. Dine, W. Fischler, and M. Srednicki. “A Simple Solution to the Strong CP Problem with a Harmless Axion”. *Phys. Lett.* 104B (1981), 199–202. DOI: 10.1016/0370-2693(81)90590-6.
- [17] D. J. Gross and F. Wilczek. “Ultraviolet Behavior of Nonabelian Gauge Theories”. *Phys. Rev. Lett.* 30 (1973), 1343–1346. DOI: 10.1103/PhysRevLett.30.1343.
- [18] H. D. Politzer. “Reliable Perturbative Results for Strong Interactions?” *Phys. Rev. Lett.* 30 (1973), 1346–1349. DOI: 10.1103/PhysRevLett.30.1346.
- [19] Nobelprize.org. *The Nobel Prize in Physics 2004*. 2017. URL: https://www.nobelprize.org/nobel_prizes/physics/laureates/2004/index.html (visited on 12/28/2017).
- [20] C. M. Institute. *Yang-Mills and Mass Gap*. 2017. URL: <http://www.claymath.org/millennium-problems/yang%5C%E2%5C%80%5C%93mills-and-mass-gap> (visited on 12/27/2017).
- [21] D. Hanneke, S. Fogwell, and G. Gabrielse. “New Measurement of the Electron Magnetic Moment and the Fine Structure Constant”. *Phys. Rev. Lett.* 100 (2008), 120801. DOI: 10.1103/PhysRevLett.100.120801. arXiv: 0801.1134 [physics.atom-ph].
- [22] K. A. Olive et al. “Review of Particle Physics”. *Chin. Phys.* C38 (2014), 090001. DOI: 10.1088/1674-1137/38/9/090001.
- [23] K. G. Wilson. “Confinement of Quarks”. *Phys. Rev.* D10 (1974), 2445–2459. DOI: 10.1103/PhysRevD.10.2445.
- [24] H.-W. Lin. “Review of Baryon Spectroscopy in Lattice QCD”. *Chin. J. Phys.* 49 (2011), 827. arXiv: 1106.1608 [hep-lat].
- [25] Z. Fodor and C. Hoelbling. “Light Hadron Masses from Lattice QCD”. *Rev. Mod. Phys.* 84 (2012), 449. DOI: 10.1103/RevModPhys.84.449. arXiv: 1203.4789 [hep-lat].
- [26] H.-T. Ding, F. Karsch, and S. Mukherjee. “Thermodynamics of strong-interaction matter from Lattice QCD”. *Int. J. Mod. Phys.* E24.10 (2015), 1530007. DOI: 10.1142/S0218301315300076. arXiv: 1504.05274 [hep-lat].
- [27] D. Trewartha, W. Kamleh, D. Leinweber, and D. S. Roberts. “Quark Propagation in the Instantons of Lattice QCD”. *Phys. Rev.* D88 (2013), 034501. DOI: 10.1103/PhysRevD.88.034501. arXiv: 1306.3283 [hep-lat].
- [28] D. Trewartha, W. Kamleh, and D. Leinweber. “Evidence that centre vortices underpin dynamical chiral symmetry breaking in SU(3) gauge theory”. *Phys. Lett.* B747 (2015), 373–377. DOI: 10.1016/j.physletb.2015.06.025. arXiv: 1502.06753 [hep-lat].

- [29] D. Trewartha, W. Kamleh, and D. Leinweber. “Connection between center vortices and instantons through gauge-field smoothing”. *Phys. Rev. D* 92.7 (2015), 074507. DOI: 10.1103/PhysRevD.92.074507. arXiv: 1509.05518 [hep-lat].
- [30] D. Trewartha, W. Kamleh, and D. Leinweber. “Centre vortex removal restores chiral symmetry”. *J. Phys. G* 44.12 (2017), 125002. DOI: 10.1088/1361-6471/aa9443. arXiv: 1708.06789 [hep-lat].
- [31] S. Syritsyn. “Review of Hadron Structure Calculations on a Lattice”. *PoS LATTICE2013* (2014), 009. arXiv: 1403.4686 [hep-lat].
- [32] M. Constantinou. “Hadron Structure”. *PoS LATTICE2014* (2015), 001. arXiv: 1411.0078 [hep-lat].
- [33] C. Alexandrou. “Hadron Structure in Lattice QCD”. *Prog. Part. Nucl. Phys.* 67 (2012), 101–116. DOI: 10.1016/j.pnpnp.2011.12.003. arXiv: 1111.5960 [hep-lat].
- [34] R. P. Feynman. “Space-time approach to nonrelativistic quantum mechanics”. *Rev. Mod. Phys.* 20 (1948), 367–387. DOI: 10.1103/RevModPhys.20.367.
- [35] W. Celmaster. “Gauge Theories on the Body-Centered Hypercubic Lattice”. *Phys. Rev. D* 26 (1982), 2955. DOI: 10.1103/PhysRevD.26.2955.
- [36] N. H. Christ, R. Friedberg, and T. D. Lee. “Random Lattice Field Theory: General Formulation”. *Nucl. Phys. B* 202 (1982), 89. DOI: 10.1016/0550-3213(82)90222-X.
- [37] R. Morrin, A. O. Cais, M. Peardon, S. M. Ryan, and J.-I. Skullerud. “Dynamical QCD simulations on anisotropic lattices”. *Phys. Rev. D* 74 (2006), 014505. DOI: 10.1103/PhysRevD.74.014505. arXiv: hep-lat/0604021 [hep-lat].
- [38] R. G. Edwards, B. Joo, and H.-W. Lin. “Tuning for Three-flavors of Anisotropic Clover Fermions with Stout-link Smearing”. *Phys. Rev. D* 78 (2008), 054501. DOI: 10.1103/PhysRevD.78.054501. arXiv: 0803.3960 [hep-lat].
- [39] O. Philipsen. “Lattice QCD at finite temperature and density”. *Eur. Phys. J. ST* 152 (2007), 29–60. DOI: 10.1140/epjst/e2007-00376-3. arXiv: 0708.1293 [hep-lat].
- [40] K. Symanzik. “Continuum Limit and Improved Action in Lattice Theories. 1. Principles and ϕ^4 Theory”. *Nucl. Phys. B* 226 (1983), 187–204. DOI: 10.1016/0550-3213(83)90468-6.
- [41] B. Sheikholeslami and R. Wohlert. “Improved Continuum Limit Lattice Action for QCD with Wilson Fermions”. *Nucl. Phys. B* 259 (1985), 572. DOI: 10.1016/0550-3213(85)90002-1.
- [42] C. Morningstar and M. J. Peardon. “Analytic smearing of SU(3) link variables in lattice QCD”. *Phys. Rev. D* 69 (2004), 054501. DOI: 10.1103/PhysRevD.69.054501. arXiv: hep-lat/0311018 [hep-lat].
- [43] S. Duane, A. D. Kennedy, B. J. Pendleton, and D. Roweth. “Hybrid Monte Carlo”. *Phys. Lett. B* 195 (1987), 216–222. DOI: 10.1016/0370-2693(87)91197-X.

- [44] J. Brannick, R. C. Brower, M. A. Clark, J. C. Osborn, and C. Rebbi. “Adaptive Multigrid Algorithm for Lattice QCD”. *Phys. Rev. Lett.* 100 (2008), 041601. DOI: 10.1103/PhysRevLett.100.041601. arXiv: 0707.4018 [hep-lat].
- [45] M. Luscher. “Deflation acceleration of lattice QCD simulations”. *JHEP* 12 (2007), 011. DOI: 10.1088/1126-6708/2007/12/011. arXiv: 0710.5417 [hep-lat].
- [46] J. Brannick, A. Frommer, K. Kahl, B. Leder, M. Rottmann, and A. Strebel. “Multigrid Preconditioning for the Overlap Operator in Lattice QCD”. *Numer. Math.* (2015). DOI: 10.1007/s00211-015-0725-6. arXiv: 1410.7170 [hep-lat].
- [47] M. F. L. Golterman. “How good is the quenched approximation of QCD?” *Pramana* 45 (1995), S141–S154. DOI: 10.1007/BF02907971. arXiv: hep-lat/9405002 [hep-lat].
- [48] M. Hasenbusch. “Speeding up the hybrid Monte Carlo algorithm for dynamical fermions”. *Phys. Lett. B* 519 (2001), 177–182. DOI: 10.1016/S0370-2693(01)01102-9. arXiv: hep-lat/0107019 [hep-lat].
- [49] M. Luscher. “Solution of the Dirac equation in lattice QCD using a domain decomposition method”. *Comput. Phys. Commun.* 156 (2004), 209–220. DOI: 10.1016/S0010-4655(03)00486-7. arXiv: hep-lat/0310048 [hep-lat].
- [50] M. A. Clark and A. D. Kennedy. “Accelerating dynamical fermion computations using the rational hybrid Monte Carlo (RHMC) algorithm with multiple pseudofermion fields”. *Phys. Rev. Lett.* 98 (2007), 051601. DOI: 10.1103/PhysRevLett.98.051601. arXiv: hep-lat/0608015 [hep-lat].
- [51] W. Kamleh and M. Peardon. “Polynomial Filtered HMC: An Algorithm for lattice QCD with dynamical quarks”. *Comput. Phys. Commun.* 183 (2012), 1993–2000. DOI: 10.1016/j.cpc.2012.05.002. arXiv: 1106.5625 [hep-lat].
- [52] T. Haar, W. Kamleh, J. Zanotti, and Y. Nakamura. “Applying polynomial filtering to mass preconditioned Hybrid Monte Carlo”. *Comput. Phys. Commun.* 215 (2017), 113–127. DOI: 10.1016/j.cpc.2017.02.020. arXiv: 1609.02652 [hep-lat].
- [53] S. Aoki et al. “Physical Point Simulation in 2+1 Flavor Lattice QCD”. *Phys. Rev. D* 81 (2010), 074503. DOI: 10.1103/PhysRevD.81.074503. arXiv: 0911.2561 [hep-lat].
- [54] S. Durr, Z. Fodor, C. Hoelbling, S. D. Katz, S. Krieg, T. Kurth, L. Lellouch, T. Lippert, K. K. Szabo, and G. Vulvert. “Lattice QCD at the physical point: Simulation and analysis details”. *JHEP* 08 (2011), 148. DOI: 10.1007/JHEP08(2011)148. arXiv: 1011.2711 [hep-lat].
- [55] S. Aoki et al. “2+1 Flavor Lattice QCD toward the Physical Point”. *Phys. Rev. D* 79 (2009), 034503. DOI: 10.1103/PhysRevD.79.034503. arXiv: 0807.1661 [hep-lat].
- [56] S. Durr, Z. Fodor, C. Hoelbling, S. D. Katz, S. Krieg, T. Kurth, L. Lellouch, T. Lippert, K. K. Szabo, and G. Vulvert. “Lattice QCD at the physical point: light quark masses”. *Phys. Lett. B* 701 (2011), 265–268. DOI: 10.1016/j.physletb.2011.05.053. arXiv: 1011.2403 [hep-lat].

- [57] C. Alexandrou et al. “The pion vector form factor from Lattice QCD at the physical point” (2017). arXiv: 1710.10401 [hep-lat].
- [58] K. Sasaki et al. “Baryon interactions from lattice QCD with physical masses – $S = -2$ sector –”. *PoS LATTICE2016* (2017), 116. arXiv: 1702.06241 [hep-lat].
- [59] N. Tsukamoto, K.-I. Ishikawa, Y. Kuramashi, S. Sasaki, and T. Yamazaki. “Nucleon structure from 2+1 flavor lattice QCD near the physical point”. *35th International Symposium on Lattice Field Theory (Lattice 2017) Granada, Spain, June 18-24, 2017*. 2017. arXiv: 1710.10782 [hep-lat]. URL: <https://inspirehep.net/record/1633437/files/arXiv:1710.10782.pdf>.
- [60] M. Golterman. “Applications of chiral perturbation theory to lattice QCD”. *Modern perspectives in lattice QCD: Quantum field theory and high performance computing. Proceedings, International School, 93rd Session, Les Houches, France, August 3-28, 2009*. 2009, pp. 423–515. arXiv: 0912.4042 [hep-lat]. URL: <https://inspirehep.net/record/840837/files/arXiv:0912.4042.pdf>.
- [61] W. Bietenholz et al. “Flavour blindness and patterns of flavour symmetry breaking in lattice simulations of up, down and strange quarks”. *Phys. Rev. D* 84 (2011), 054509. DOI: 10.1103/PhysRevD.84.054509. arXiv: 1102.5300 [hep-lat].
- [62] R. Sommer. “Scale setting in lattice QCD”. *PoS LATTICE2013* (2014), 015. arXiv: 1401.3270 [hep-lat].
- [63] R. Horsley, J. Najjar, Y. Nakamura, H. Perlt, D. Pleiter, P. E. L. Rakow, G. Schierholz, A. Schiller, H. Stüben, and J. M. Zanotti. “SU(3) flavour symmetry breaking and charmed states”. *PoS LATTICE2013* (2013), 249. arXiv: 1311.5010 [hep-lat].
- [64] V. G. Bornyakov et al. “Wilson flow and scale setting from lattice QCD” (2015). arXiv: 1508.05916 [hep-lat].
- [65] W. Bietenholz et al. “Tuning the strange quark mass in lattice simulations”. *Phys. Lett. B* 690 (2010), 436–441. DOI: 10.1016/j.physletb.2010.05.067. arXiv: 1003.1114 [hep-lat].
- [66] M. Luscher. “Volume Dependence of the Energy Spectrum in Massive Quantum Field Theories. 1. Stable Particle States”. *Commun. Math. Phys.* 104 (1986), 177. DOI: 10.1007/BF01211589.
- [67] M. Luscher. “Volume Dependence of the Energy Spectrum in Massive Quantum Field Theories. 2. Scattering States”. *Commun. Math. Phys.* 105 (1986), 153–188. DOI: 10.1007/BF01211097.
- [68] A. W. Thomas, J. D. Ashley, D. B. Leinweber, and R. D. Young. “Finite volume dependence of hadron properties and lattice QCD”. *J. Phys. Conf. Ser.* 9 (2005), 321. DOI: 10.1088/1742-6596/9/1/061. arXiv: hep-lat/0502002 [hep-lat].
- [69] G. Martinelli, C. Pittori, C. T. Sachrajda, M. Testa, and A. Vladikas. “A General method for nonperturbative renormalization of lattice operators”. *Nucl. Phys. B* 445 (1995), 81–108. DOI: 10.1016/0550-3213(95)00126-D. arXiv: hep-lat/9411010 [hep-lat].

- [70] M. Göckeler, R. Horsley, H. Oelrich, H. Perlt, D. Petters, P. E. L. Rakow, A. Schäfer, G. Schierholz, and A. Schiller. “Nonperturbative renormalization of composite operators in lattice QCD”. *Nucl. Phys.* B544 (1999), 699–733. DOI: 10.1016/S0550-3213(99)00036-X. arXiv: hep-lat/9807044 [hep-lat].
- [71] D. Weingarten. “Monte Carlo Evaluation of Hadron Masses in Lattice Gauge Theories with Fermions”. *Phys. Lett.* 109B (1982), 57. DOI: 10.1016/0370-2693(82)90463-4.
- [72] M. Creutz. “Monte Carlo Study of Quantized SU(2) Gauge Theory”. *Phys. Rev.* D21 (1980), 2308–2315. DOI: 10.1103/PhysRevD.21.2308.
- [73] H. Hamber and G. Parisi. “Numerical Estimates of Hadronic Masses in a Pure SU(3) Gauge Theory”. *Phys. Rev. Lett.* 47 (1981), 1792. DOI: 10.1103/PhysRevLett.47.1792.
- [74] L. Liu, G. Moir, M. Peardon, S. M. Ryan, C. E. Thomas, P. Vilaseca, J. J. Dudek, R. G. Edwards, B. Joo, and D. G. Richards. “Excited and exotic charmonium spectroscopy from lattice QCD”. *JHEP* 07 (2012), 126. DOI: 10.1007/JHEP07(2012)126. arXiv: 1204.5425 [hep-ph].
- [75] J. J. Dudek, R. G. Edwards, and C. E. Thomas. “Energy dependence of the ρ resonance in $\pi\pi$ elastic scattering from lattice QCD”. *Phys. Rev.* D87.3 (2013), 034505. DOI: 10.1103/PhysRevD.87.034505, 10.1103/PhysRevD.90.099902. arXiv: 1212.0830 [hep-ph].
- [76] R. Horsley et al. “Isospin splittings of meson and baryon masses from three-flavor lattice QCD + QED”. *J. Phys.* G43.10 (2016), 10LT02. DOI: 10.1088/0954-3889/43/10/10LT02. arXiv: 1508.06401 [hep-lat].
- [77] A. L. Kiratidis, W. Kamleh, D. B. Leinweber, and B. J. Owen. “Lattice baryon spectroscopy with multi-particle interpolators”. *Phys. Rev.* D91 (2015), 094509. DOI: 10.1103/PhysRevD.91.094509. arXiv: 1501.07667 [hep-lat].
- [78] R. Horsley, Y. Nakamura, A. Nobile, P. E. L. Rakow, G. Schierholz, and J. M. Zanotti. “Nucleon axial charge and pion decay constant from two-flavor lattice QCD”. *Phys. Lett.* B732 (2014), 41–48. DOI: 10.1016/j.physletb.2014.03.002. arXiv: 1302.2233 [hep-lat].
- [79] C. Alexandrou, G. Koutsou, H. Neff, J. W. Negele, W. Schroers, and A. Tsapalis. “Nucleon to delta electromagnetic transition form factors in lattice QCD”. *Phys. Rev.* D77 (2008), 085012. DOI: 10.1103/PhysRevD.77.085012. arXiv: 0710.4621 [hep-lat].
- [80] W. Detmold, C.-J. D. Lin, S. Meinel, and M. Wingate. “ $\Lambda b \rightarrow \Lambda \ell^+ \ell^-$ form factors and differential branching fraction from lattice QCD”. *Phys. Rev.* D87.7 (2013), 074502. DOI: 10.1103/PhysRevD.87.074502. arXiv: 1212.4827 [hep-lat].
- [81] J. Green, S. Meinel, M. Engelhardt, S. Krieg, J. Laeuchli, J. Negele, K. Orginos, A. Pochinsky, and S. Syritsyn. “High-precision calculation of the strange nucleon electromagnetic form factors”. *Phys. Rev.* D92.3 (2015), 031501. DOI: 10.1103/PhysRevD.92.031501. arXiv: 1505.01803 [hep-lat].
- [82] R. A. Briceno, J. J. Dudek, and R. D. Young. “Scattering processes and resonances from lattice QCD” (2017). arXiv: 1706.06223 [hep-lat].

- [83] C. Alexandrou, T. Leontiou, C. N. Papanicolas, and E. Stiliaris. “Novel analysis method for excited states in lattice QCD: The nucleon case”. *Phys. Rev. D* 91.1 (2015), 014506. DOI: 10.1103/PhysRevD.91.014506. arXiv: 1411.6765 [hep-lat].
- [84] G. P. Engel, C. B. Lang, M. Limmer, D. Mohler, and A. Schäfer. “Meson and baryon spectrum for QCD with two light dynamical quarks”. *Phys. Rev. D* 82 (2010), 034505. DOI: 10.1103/PhysRevD.82.034505. arXiv: 1005.1748 [hep-lat].
- [85] R. G. Edwards, J. J. Dudek, D. G. Richards, and S. J. Wallace. “Excited state baryon spectroscopy from lattice QCD”. *Phys. Rev. D* 84 (2011), 074508. DOI: 10.1103/PhysRevD.84.074508. arXiv: 1104.5152 [hep-ph].
- [86] M. S. Mahbub, W. Kamleh, D. B. Leinweber, P. J. Moran, and A. G. Williams. “Roper Resonance in 2+1 Flavor QCD”. *Phys. Lett. B* 707 (2012), 389–393. DOI: 10.1016/j.physletb.2011.12.048. arXiv: 1011.5724 [hep-lat].
- [87] M. S. Mahbub, W. Kamleh, D. B. Leinweber, P. J. Moran, and A. G. Williams. “Structure and Flow of the Nucleon Eigenstates in Lattice QCD”. *Phys. Rev. D* 87.9 (2013), 094506. DOI: 10.1103/PhysRevD.87.094506. arXiv: 1302.2987 [hep-lat].
- [88] B. J. Menadue, W. Kamleh, D. B. Leinweber, and M. S. Mahbub. “Isolating the $\Lambda(1405)$ in Lattice QCD”. *Phys. Rev. Lett.* 108 (2012), 112001. DOI: 10.1103/PhysRevLett.108.112001. arXiv: 1109.6716 [hep-lat].
- [89] B. Blossier, M. Della Morte, G. von Hippel, T. Mendes, and R. Sommer. “On the generalized eigenvalue method for energies and matrix elements in lattice field theory”. *JHEP* 04 (2009), 094. DOI: 10.1088/1126-6708/2009/04/094. arXiv: 0902.1265 [hep-lat].
- [90] M. S. Mahbub, A. O. Cais, W. Kamleh, B. G. Lasscock, D. B. Leinweber, and A. G. Williams. “Isolating the Roper Resonance in Lattice QCD”. *Phys. Lett. B* 679 (2009), 418–422. DOI: 10.1016/j.physletb.2009.07.063. arXiv: 0906.5433 [hep-lat].
- [91] C. R. Allton et al. “Gauge invariant smearing and matrix correlators using Wilson fermions at $\beta = 6.2$ ”. *Phys. Rev. D* 47 (1993), 5128–5137. DOI: 10.1103/PhysRevD.47.5128. arXiv: hep-lat/9303009 [hep-lat].
- [92] F. M. Stokes, W. Kamleh, D. B. Leinweber, M. S. Mahbub, B. J. Menadue, and B. J. Owen. “Parity-expanded variational analysis for nonzero momentum”. *Phys. Rev. D* 92.11 (2015), 114506. DOI: 10.1103/PhysRevD.92.114506. arXiv: 1302.4152 [hep-lat].
- [93] J. Dragos, R. Horsley, W. Kamleh, D. B. Leinweber, Y. Nakamura, P. E. L. Rakow, G. Schierholz, R. D. Young, and J. M. Zanotti. “Nucleon matrix elements using the variational method in lattice QCD”. *Phys. Rev. D* 94.7 (2016), 074505. DOI: 10.1103/PhysRevD.94.074505. arXiv: 1606.03195 [hep-lat].
- [94] B. J. Owen, W. Kamleh, D. B. Leinweber, M. S. Mahbub, and B. J. Menadue. “Transition of $\rho \rightarrow \pi\gamma$ in lattice QCD”. *Phys. Rev. D* 92.3 (2015), 034513. DOI: 10.1103/PhysRevD.92.034513. arXiv: 1505.02876 [hep-lat].

- [95] J. M. M. Hall, W. Kamleh, D. B. Leinweber, B. J. Menadue, B. J. Owen, A. W. Thomas, and R. D. Young. “Lattice QCD Evidence that the $\Lambda(1405)$ Resonance is an Antikaon-Nucleon Molecule”. *Phys. Rev. Lett.* 114.13 (2015), 132002. DOI: 10.1103/PhysRevLett.114.132002. arXiv: 1411.3402 [hep-lat].
- [96] B. Owen, W. Kamleh, D. Leinweber, B. Menadue, and S. Mahbub. “Light Meson Form Factors at near Physical Masses”. *Phys. Rev.* D91.7 (2015), 074503. DOI: 10.1103/PhysRevD.91.074503. arXiv: 1501.02561 [hep-lat].
- [97] B. J. Owen, J. Dragos, W. Kamleh, D. B. Leinweber, M. S. Mahbub, B. J. Menadue, and J. M. Zanotti. “Variational Approach to the Calculation of g_A ”. *Phys. Lett.* B723 (2013), 217–223. DOI: 10.1016/j.physletb.2013.04.063. arXiv: 1212.4668 [hep-lat].
- [98] J. Bulava, M. Donnellan, and R. Sommer. “On the computation of hadron-to-hadron transition matrix elements in lattice QCD”. *JHEP* 01 (2012), 140. DOI: 10.1007/JHEP01(2012)140. arXiv: 1108.3774 [hep-lat].
- [99] H.-W. Lin, S. D. Cohen, R. G. Edwards, and D. G. Richards. “First Lattice Study of the $N - P_{11}$ Transition Form Factors”. *Phys. Rev.* D78 (2008), 114508. DOI: 10.1103/PhysRevD.78.114508. arXiv: 0803.3020 [hep-lat].
- [100] H.-W. Lin, S. D. Cohen, R. G. Edwards, K. Orginos, and D. G. Richards. “Lattice Calculations of Nucleon Electromagnetic Form Factors at Large Momentum Transfer” (2010). arXiv: 1005.0799 [hep-lat].
- [101] B. Yoon et al. “Controlling Excited-State Contamination in Nucleon Matrix Elements”. *Phys. Rev.* D93.11 (2016), 114506. DOI: 10.1103/PhysRevD.93.114506. arXiv: 1602.07737 [hep-lat].
- [102] P. A. Boyle, A. Juttner, C. Kelly, and R. D. Kenway. “Use of stochastic sources for the lattice determination of light quark physics”. *JHEP* 08 (2008), 086. DOI: 10.1088/1126-6708/2008/08/086. arXiv: 0804.1501 [hep-lat].
- [103] J. Foley, K. Jimmy Juge, A. O’Cais, M. Peardon, S. M. Ryan, and J.-I. Skullerud. “Practical all-to-all propagators for lattice QCD”. *Comput. Phys. Commun.* 172 (2005), 145–162. DOI: 10.1016/j.cpc.2005.06.008. arXiv: hep-lat/0505023 [hep-lat].
- [104] G. S. Bali, S. Collins, and A. Schäfer. “Effective noise reduction techniques for disconnected loops in Lattice QCD”. *Comput. Phys. Commun.* 181 (2010), 1570–1583. DOI: 10.1016/j.cpc.2010.05.008. arXiv: 0910.3970 [hep-lat].
- [105] G. S. Bali et al. “Strangeness Contribution to the Proton Spin from Lattice QCD”. *Phys. Rev. Lett.* 108 (2012), 222001. DOI: 10.1103/PhysRevLett.108.222001. arXiv: 1112.3354 [hep-lat].
- [106] R. P. Feynman. “Forces in Molecules”. *Phys. Rev.* 56 (1939), 340–343. DOI: 10.1103/PhysRev.56.340.
- [107] P. Güttinger. “Das Verhalten von Atomen im magnetischen Drehfeld”. *Zeitschrift für Physik* 73 (1932), 3–4.
- [108] W. Pauli. “Principles of Wave Mechanics”. *Handbuch der Physik* 24 (1933), 162.

- [109] H. Hellmann. “Einführung in die Quantenchemie”. *Leipzig: Franz Deuticke* (1937), 285.
- [110] M. Di Ventura and S. T. Pantelides. “Hellmann-Feynman theorem and the definition of forces in quantum time-dependent and transport problems”. *Phys. Rev. B* 61 (23 June 2000), 16207–16212. DOI: 10.1103/PhysRevB.61.16207. URL: <https://link.aps.org/doi/10.1103/PhysRevB.61.16207>.
- [111] R. Car and M. Parrinello. “Unified Approach for Molecular Dynamics and Density-Functional Theory”. *Phys. Rev. Lett.* 55 (22 Nov. 1985), 2471–2474. DOI: 10.1103/PhysRevLett.55.2471. URL: <https://link.aps.org/doi/10.1103/PhysRevLett.55.2471>.
- [112] M. C. Payne, M. P. Teter, D. C. Allan, T. A. Arias, and J. D. Joannopoulos. “Iterative minimization techniques for ab initio total-energy calculations: molecular dynamics and conjugate gradients”. *Rev. Mod. Phys.* 64 (4 Oct. 1992), 1045–1097. DOI: 10.1103/RevModPhys.64.1045. URL: <https://link.aps.org/doi/10.1103/RevModPhys.64.1045>.
- [113] M. Scheffler, J. P. Vigneron, and G. B. Bachelet. “Total-energy gradients and lattice distortions at point defects in semiconductors”. *Phys. Rev. B* 31 (10 May 1985), 6541–6551. DOI: 10.1103/PhysRevB.31.6541. URL: <https://link.aps.org/doi/10.1103/PhysRevB.31.6541>.
- [114] J. Gasser and A. Zepeda. “Approaching the Chiral Limit in QCD”. *Nucl. Phys. B* 174 (1980), 445. DOI: 10.1016/0550-3213(80)90294-1.
- [115] S. Dinter, V. Drach, R. Frezzotti, G. Herdoiza, K. Jansen, and G. Rossi. “Sigma terms and strangeness content of the nucleon with $N_f = 2 + 1 + 1$ twisted mass fermions”. *JHEP* 08 (2012), 037. DOI: 10.1007/JHEP08(2012)037. arXiv: 1202.1480 [hep-lat].
- [116] R. Horsley, Y. Nakamura, H. Perlt, D. Pleiter, P. E. L. Rakow, G. Schierholz, A. Schiller, H. Stüben, F. Winter, and J. M. Zanotti. “Hyperon sigma terms for 2+1 quark flavours”. *Phys. Rev. D* 85 (2012), 034506. DOI: 10.1103/PhysRevD.85.034506. arXiv: 1110.4971 [hep-lat].
- [117] S. Durr et al. “Sigma term and strangeness content of octet baryons”. *Phys. Rev. D* 85 (2012), 014509. DOI: 10.1103/PhysRevD.85.014509, 10.1103/PhysRevD.93.039905. arXiv: 1109.4265 [hep-lat].
- [118] P. E. Shanahan, A. W. Thomas, and R. D. Young. “Sigma terms from an SU(3) chiral extrapolation”. *Phys. Rev. D* 87 (2013), 074503. DOI: 10.1103/PhysRevD.87.074503. arXiv: 1205.5365 [nucl-th].
- [119] M. Engelhardt. “Neutron electric polarizability from unquenched lattice QCD using the background field approach”. *Phys. Rev. D* 76 (2007), 114502. DOI: 10.1103/PhysRevD.76.114502. arXiv: 0706.3919 [hep-lat].
- [120] W. Detmold, B. C. Tiburzi, and A. Walker-Loud. “Extracting Electric Polarizabilities from Lattice QCD”. *Phys. Rev. D* 79 (2009), 094505. DOI: 10.1103/PhysRevD.79.094505. arXiv: 0904.1586 [hep-lat].
- [121] W. Detmold, B. C. Tiburzi, and A. Walker-Loud. “Extracting Nucleon Magnetic Moments and Electric Polarizabilities from Lattice QCD in Background Electric Fields”. *Phys. Rev. D* 81 (2010), 054502. DOI: 10.1103/PhysRevD.81.054502. arXiv: 1001.1131 [hep-lat].

- [122] T. Primer, W. Kamleh, D. Leinweber, and M. Burkardt. “Magnetic properties of the nucleon in a uniform background field”. *Phys. Rev.* D89.3 (2014), 034508. DOI: 10.1103/PhysRevD.89.034508. arXiv: 1307.1509 [hep-lat].
- [123] W. Freeman, A. Alexandru, M. Lujan, and F. X. Lee. “Sea quark contributions to the electric polarizability of hadrons”. *Phys. Rev.* D90.5 (2014), 054507. DOI: 10.1103/PhysRevD.90.054507. arXiv: 1407.2687 [hep-lat].
- [124] W. Detmold. “Flavor singlet physics in lattice QCD with background fields”. *Phys. Rev.* D71 (2005), 054506. DOI: 10.1103/PhysRevD.71.054506. arXiv: hep-lat/0410011 [hep-lat].
- [125] M. J. Savage, P. E. Shanahan, B. C. Tiburzi, M. L. Wagman, F. Winter, S. R. Beane, E. Chang, Z. Davoudi, W. Detmold, and K. Orginos. “Proton-Proton Fusion and Tritium β Decay from Lattice Quantum Chromodynamics”. *Phys. Rev. Lett.* 119.6 (2017), 062002. DOI: 10.1103/PhysRevLett.119.062002. arXiv: 1610.04545 [hep-lat].
- [126] C. Bouchard, C. C. Chang, T. Kurth, K. Orginos, and A. Walker-Loud. “On the Feynman-Hellmann Theorem in Quantum Field Theory and the Calculation of Matrix Elements”. *Phys. Rev.* D96.1 (2017), 014504. DOI: 10.1103/PhysRevD.96.014504. arXiv: 1612.06963 [hep-lat].
- [127] K. Somfleth et al. 2018.
- [128] J. Ashman et al. “A Measurement of the Spin Asymmetry and Determination of the Structure Function g_1 in Deep Inelastic Muon-Proton Scattering”. *Phys. Lett.* B206 (1988), 364. DOI: 10.1016/0370-2693(88)91523-7.
- [129] X.-D. Ji. “Gauge-Invariant Decomposition of Nucleon Spin”. *Phys. Rev. Lett.* 78 (1997), 610–613. DOI: 10.1103/PhysRevLett.78.610. arXiv: hep-ph/9603249 [hep-ph].
- [130] R. L. Jaffe and A. Manohar. “The g_1 problem: Deep inelastic electron scattering and the spin of the proton”. *Nucl. Phys.* B337 (1990), 509–546. DOI: 10.1016/0550-3213(90)90506-9.
- [131] M. Burkardt. “The nucleon spin sum rule”. *AIP Conf. Proc.* 1560.1 (2013), 495–499. DOI: 10.1063/1.4826826.
- [132] F. Myhrer and A. W. Thomas. “Understanding the proton’s spin structure”. *J. Phys.* G37 (2010), 023101. DOI: 10.1088/0954-3899/37/2/023101. arXiv: 0911.1974 [hep-ph].
- [133] M. Anselmino, A. Efremov, and E. Leader. “The Theory and phenomenology of polarized deep inelastic scattering”. *Phys. Rept.* 261 (1995), 1–124. DOI: 10.1016/0370-1573(95)00011-5. arXiv: hep-ph/9501369 [hep-ph].
- [134] B. W. Filippone and X.-D. Ji. “The Spin structure of the nucleon”. *Adv. Nucl. Phys.* 26 (2001), 1. DOI: 10.1007/0-306-47915-X_1. arXiv: hep-ph/0101224 [hep-ph].
- [135] S. D. Bass. “The Spin structure of the proton”. *Rev. Mod. Phys.* 77 (2005), 1257–1302. DOI: 10.1103/RevModPhys.77.1257. arXiv: hep-ph/0411005 [hep-ph].
- [136] C. A. Aidala, S. D. Bass, D. Hasch, and G. K. Mallot. “The Spin Structure of the Nucleon”. *Rev. Mod. Phys.* 85 (2013), 655–691. DOI: 10.1103/RevModPhys.85.655. arXiv: 1209.2803 [hep-ph].

- [137] E. S. Ageev et al. “Measurement of the spin structure of the deuteron in the DIS region”. *Phys. Lett. B*612 (2005), 154–164. DOI: 10.1016/j.physletb.2005.03.025. arXiv: hep-ex/0501073 [hep-ex].
- [138] V. Yu. Alexakhin et al. “The deuteron spin-dependent structure function g_1^d and its first moment”. *Phys. Lett. B*647 (2007), 8–17. DOI: 10.1016/j.physletb.2006.12.076. arXiv: hep-ex/0609038 [hep-ex].
- [139] A. Airapetian et al. “Precise determination of the spin structure function g_1 of the proton, deuteron and neutron”. *Phys. Rev. D*75 (2007), 012007. DOI: 10.1103/PhysRevD.75.012007. arXiv: hep-ex/0609039 [hep-ex].
- [140] B. Adeva et al. “Spin asymmetries A_1 and structure functions g_1 of the proton and the deuteron from polarized high energy muon scattering”. *Phys. Rev. D*58 (1998), 112001. DOI: 10.1103/PhysRevD.58.112001.
- [141] K. Abe et al. “Measurements of the proton and deuteron spin structure functions g_1 and g_2 ”. *Phys. Rev. D*58 (1998), 112003. DOI: 10.1103/PhysRevD.58.112003. arXiv: hep-ph/9802357 [hep-ph].
- [142] M. G. Alekseev et al. “Quark helicity distributions from longitudinal spin asymmetries in muon-proton and muon-deuteron scattering”. *Phys. Lett. B*693 (2010), 227–235. DOI: 10.1016/j.physletb.2010.08.034. arXiv: 1007.4061 [hep-ex].
- [143] A. Adare et al. “Inclusive double-helicity asymmetries in neutral-pion and eta-meson production in p + p collisions at $\sqrt{s} = 200$ GeV”. *Phys. Rev. D*90.1 (2014), 012007. DOI: 10.1103/PhysRevD.90.012007. arXiv: 1402.6296 [hep-ex].
- [144] L. Adamczyk et al. “Precision Measurement of the Longitudinal Double-spin Asymmetry for Inclusive Jet Production in Polarized Proton Collisions at $\sqrt{s} = 200$ GeV”. *Phys. Rev. Lett.* 115.9 (2015), 092002. DOI: 10.1103/PhysRevLett.115.092002. arXiv: 1405.5134 [hep-ex].
- [145] F. Myhrer and A. W. Thomas. “A possible resolution of the proton spin problem”. *Phys. Lett. B*663 (2008), 302–305. DOI: 10.1016/j.physletb.2008.04.034. arXiv: 0709.4067 [hep-ph].
- [146] S. E. Kuhn, J.-P. Chen, and E. Leader. “Spin Structure of the Nucleon - Status and Recent Results”. *Prog. Part. Nucl. Phys.* 63 (2009), 1–50. DOI: 10.1016/j.ppnp.2009.02.001. arXiv: 0812.3535 [hep-ph].
- [147] M. Burkardt, C. A. Miller, and W. D. Nowak. “Spin-polarized high-energy scattering of charged leptons on nucleons”. *Rept. Prog. Phys.* 73 (2010), 016201. DOI: 10.1088/0034-4885/73/1/016201. arXiv: 0812.2208 [hep-ph].
- [148] H.-Y. Cheng. “Status of the proton spin problem”. *Int. J. Mod. Phys. A*11 (1996), 5109–5182. DOI: 10.1142/S0217751X96002364. arXiv: hep-ph/9607254 [hep-ph].
- [149] S. Sasaki, K. Orginos, S. Ohta, and T. Blum. “Nucleon axial charge from quenched lattice QCD with domain wall fermions”. *Phys. Rev. D*68 (2003), 054509. DOI: 10.1103/PhysRevD.68.054509. arXiv: hep-lat/0306007 [hep-lat].

- [150] T. D. Cohen. “The Extraction of g_A from finite volume systems: The Long and short of it”. *Phys. Lett.* B529 (2002), 50–56. DOI: 10.1016/S0370-2693(02)01241-8. arXiv: hep-lat/0112014 [hep-lat].
- [151] R. L. Jaffe. “Delocalization of the axial charge in the chiral limit”. *Phys. Lett.* B529 (2002), 105–110. DOI: 10.1016/S0370-2693(02)01242-X. arXiv: hep-ph/0108015 [hep-ph].
- [152] J. D. Bratt et al. “Nucleon structure from mixed action calculations using 2+1 flavors of asqtad sea and domain wall valence fermions”. *Phys. Rev.* D82 (2010), 094502. DOI: 10.1103/PhysRevD.82.094502. arXiv: 1001.3620 [hep-lat].
- [153] S. N. Syritsyn, J. R. Green, J. W. Negele, A. V. Pochinsky, M. Engelhardt, P. Hagler, B. Musch, and W. Schroers. “Quark Contributions to Nucleon Momentum and Spin from Domain Wall fermion calculations”. *PoS LATTICE2011* (2011), 178. arXiv: 1111.0718 [hep-lat].
- [154] A. Sternbeck et al. “First moments of the nucleon generalized parton distributions from lattice QCD”. *PoS LATTICE2011* (2011), 177. arXiv: 1203.6579 [hep-lat].
- [155] C. Alexandrou, M. Constantinou, S. Dinter, V. Drach, K. Jansen, C. Kallidonis, and G. Koutsou. “Nucleon form factors and moments of generalized parton distributions using $N_f = 2 + 1 + 1$ twisted mass fermions”. *Phys. Rev.* D88.1 (2013), 014509. DOI: 10.1103/PhysRevD.88.014509. arXiv: 1303.5979 [hep-lat].
- [156] P. Hagler. “Hadron structure from lattice quantum chromodynamics”. *Phys. Rept.* 490 (2010), 49–175. DOI: 10.1016/j.physrep.2009.12.008. arXiv: 0912.5483 [hep-lat].
- [157] M. Deka et al. “Lattice study of quark and glue momenta and angular momenta in the nucleon”. *Phys. Rev.* D91.1 (2015), 014505. DOI: 10.1103/PhysRevD.91.014505. arXiv: 1312.4816 [hep-lat].
- [158] S. Dinter, C. Alexandrou, M. Constantinou, V. Drach, K. Jansen, and D. B. Renner. “Precision Study of Excited State Effects in Nucleon Matrix Elements”. *Phys. Lett.* B704 (2011), 89–93. DOI: 10.1016/j.physletb.2011.09.002. arXiv: 1108.1076 [hep-lat].
- [159] S. Capitani, M. Della Morte, G. von Hippel, B. Jäger, A. Juttner, B. Knippschild, H. B. Meyer, and H. Wittig. “The nucleon axial charge from lattice QCD with controlled errors”. *Phys. Rev.* D86 (2012), 074502. DOI: 10.1103/PhysRevD.86.074502. arXiv: 1205.0180 [hep-lat].
- [160] T. Bhattacharya, S. D. Cohen, R. Gupta, A. Joseph, H.-W. Lin, and B. Yoon. “Nucleon Charges and Electromagnetic Form Factors from 2+1+1-Flavor Lattice QCD”. *Phys. Rev.* D89.9 (2014), 094502. DOI: 10.1103/PhysRevD.89.094502. arXiv: 1306.5435 [hep-lat].
- [161] B. Jäger, T. D. Rae, S. Capitani, M. Della Morte, D. Djukanovic, G. von Hippel, B. Knippschild, H. B. Meyer, and H. Wittig. “A high-statistics study of the nucleon EM form factors, axial charge and quark momentum fraction”. *PoS LATTICE2013* (2013), 272. arXiv: 1311.5804 [hep-lat].

- [162] G. S. Bali, S. Collins, B. Gläbke, M. Göckeler, J. Najjar, R. Rödl, A. Schäfer, R. Schiel, A. Sternbeck, and W. Söldner. “Moments of structure functions for $N_f = 2$ near the physical point”. *PoS LATTICE2013* (2014), 290. arXiv: 1311.7041 [hep-lat].
- [163] A. J. Chambers et al. “Feynman-Hellmann approach to the spin structure of hadrons”. *Phys. Rev. D* 90.1 (2014), 014510. DOI: 10.1103/PhysRevD.90.014510. arXiv: 1405.3019 [hep-lat].
- [164] A. J. Chambers et al. “Disconnected contributions to the spin of the nucleon”. *Phys. Rev. D* 92.11 (2015), 114517. DOI: 10.1103/PhysRevD.92.114517. arXiv: 1508.06856 [hep-lat].
- [165] A. J. Chambers, R. Horsley, Y. Nakamura, H. Perlt, P. E. L. Rakow, G. Schierholz, A. Schiller, and J. M. Zanotti. “A novel approach to nonperturbative renormalization of singlet and nonsinglet lattice operators”. *Phys. Lett. B* 740 (2015), 30–35. DOI: 10.1016/j.physletb.2014.11.033. arXiv: 1410.3078 [hep-lat].
- [166] A. W. Thomas, S. Theberge, and G. A. Miller. “The Cloudy Bag Model of the Nucleon”. *Phys. Rev. D* 24 (1981), 216. DOI: 10.1103/PhysRevD.24.216.
- [167] A. W. Thomas. “Chiral Symmetry and the Bag Model: A New Starting Point for Nuclear Physics”. *Adv. Nucl. Phys.* 13 (1984), 1–137. DOI: 10.1007/978-1-4613-9892-9_1.
- [168] G. A. Miller. “Building the Nucleus From Quarks: the Cloudy bag Model and the Quark Description of the Nucleon-nucleon Wave Functions”. *Int. Rev. Nucl. Phys.* 1 (1984), 189–323. DOI: 10.1142/9789814415132_0003.
- [169] P. E. Shanahan, A. W. Thomas, K. Tsushima, R. D. Young, and F. Myhrer. “Octet Spin Fractions and the Proton Spin Problem”. *Phys. Rev. Lett.* 110.20 (2013), 202001. DOI: 10.1103/PhysRevLett.110.202001. arXiv: 1302.6300 [nucl-th].
- [170] A. M. Ferrenberg and R. H. Swendsen. “Optimized Monte Carlo analysis”. *Phys. Rev. Lett.* 63 (1989), 1195–1198. DOI: 10.1103/PhysRevLett.63.1195.
- [171] A. M. Ferrenberg and R. H. Swendsen. “New Monte Carlo Technique for Studying Phase Transitions”. *Phys. Rev. Lett.* 61 (1988), 2635–2638. DOI: 10.1103/PhysRevLett.61.2635.
- [172] B. Joo, B. Pendleton, S. M. Pickles, Z. Sroczynski, A. C. Irving, and J. C. Sexton. “Parallel tempering in lattice QCD with $\mathcal{O}(a)$ -improved Wilson fermions”. *Phys. Rev. D* 59 (1999), 114501. DOI: 10.1103/PhysRevD.59.114501. arXiv: hep-lat/9810032 [hep-lat].
- [173] G. Boyd. “Tempered fermions in the hybrid Monte Carlo algorithm”. *Nucl. Phys. Proc. Suppl.* 60A (1998), 341–344. DOI: 10.1016/S0920-5632(97)00495-7. arXiv: hep-lat/9712012 [hep-lat].
- [174] M. Engelhardt. “Strange quark contributions to nucleon mass and spin from lattice QCD”. *Phys. Rev. D* 86 (2012), 114510. DOI: 10.1103/PhysRevD.86.114510. arXiv: 1210.0025 [hep-lat].

- [175] A. Abdel-Rehim, C. Alexandrou, M. Constantinou, V. Drach, K. Hadjiyianakou, K. Jansen, G. Koutsou, and A. Vaquero. “Disconnected quark loop contributions to nucleon observables in lattice QCD”. *Phys. Rev.* D89.3 (2014), 034501. DOI: 10.1103/PhysRevD.89.034501. arXiv: 1310.6339 [hep-lat].
- [176] R. W. McAllister and R. Hofstadter. “Elastic Scattering of 188 MeV Electrons From the Proton and the α Particle”. *Phys. Rev.* 102 (1956), 851–856. DOI: 10.1103/PhysRev.102.851.
- [177] R. Hofstadter, H. R. Fechter, and J. A. McIntyre. “High-Energy Electron Scattering and Nuclear Structure Determinations”. *Phys. Rev.* 92.4 (1953), 978. DOI: 10.1103/PhysRev.92.978.
- [178] R. Hofstadter and R. W. McAllister. “Electron Scattering From the Proton”. *Phys. Rev.* 98 (1955), 217–218. DOI: 10.1103/PhysRev.98.217.
- [179] G. A. Miller. “Transverse Charge Densities”. *Ann. Rev. Nucl. Part. Sci.* 60 (2010), 1–25. DOI: 10.1146/annurev.nucl.012809.104508. arXiv: 1002.0355 [nucl-th].
- [180] G. A. Miller. “Charge Densities of the Neutron and Proton”. *Phys. Rev. Lett.* 99 (2007), 112001. DOI: 10.1103/PhysRevLett.99.112001. arXiv: 0705.2409 [nucl-th].
- [181] G. A. Miller. “Singular Charge Density at the Center of the Pion?” *Phys. Rev.* C79 (2009), 055204. DOI: 10.1103/PhysRevC.79.055204. arXiv: 0901.1117 [nucl-th].
- [182] G. A. Miller, M. Strikman, and C. Weiss. “Pion transverse charge density from timelike form factor data”. *Phys. Rev.* D83 (2011), 013006. DOI: 10.1103/PhysRevD.83.013006. arXiv: 1011.1472 [hep-ph].
- [183] C. E. Carlson and M. Vanderhaeghen. “Empirical transverse charge densities in the nucleon and the nucleon-to-Delta transition”. *Phys. Rev. Lett.* 100 (2008), 032004. DOI: 10.1103/PhysRevLett.100.032004. arXiv: 0710.0835 [hep-ph].
- [184] G. Adylov et al. “The Pion Radius”. *Phys. Lett.* 51B (1974), 402. DOI: 10.1016/0370-2693(74)90239-1.
- [185] G. T. Adylov et al. “A Measurement of the Electromagnetic Size of the Pion from Direct Elastic Pion Scattering Data at 50-GeV/c”. *Nucl. Phys.* B128 (1977), 461–505. DOI: 10.1016/0550-3213(77)90056-6.
- [186] E. B. Dally et al. “Elastic Scattering Measurement of the Negative Pion Radius”. *Phys. Rev. Lett.* 48 (1982), 375–378. DOI: 10.1103/PhysRevLett.48.375.
- [187] E. B. Dally et al. “Direct Measurement of the π^- Form-Factor.” *Phys. Rev. Lett.* 39 (1977), 1176–1179. DOI: 10.1103/PhysRevLett.39.1176.
- [188] E. B. Dally et al. “Measurement of the π^- Form-factor”. *Phys. Rev.* D24 (1981), 1718–1735. DOI: 10.1103/PhysRevD.24.1718.
- [189] S. R. Amendolia et al. “A Measurement of the Space - Like Pion Electromagnetic Form-Factor”. *Nucl. Phys.* B277 (1986), 168. DOI: 10.1016/0550-3213(86)90437-2.

- [190] S. R. Amendolia et al. “Measurement of the Pion Form-factor in the Timelike Region for q^2 Values Between 0.1 GeV/ c^2 and 0.18 GeV/ c^2 ”. *Phys. Lett.* 138B (1984), 454–458. DOI: 10.1016/0370-2693(84)91938-5.
- [191] H. Ackermann, T. Azemoon, W. Gabriel, H. D. Mertiens, H. D. Reich, G. Specht, F. Janata, and D. Schmidt. “Determination of the Longitudinal and the Transverse Part in π^+ Electroproduction”. *Nucl. Phys.* B137 (1978), 294–300. DOI: 10.1016/0550-3213(78)90523-0.
- [192] P. Brauel, T. Canzler, D. Cords, R. Felst, G. Grindhammer, M. Helm, W.-D. Kollmann, H. Krehbiel, and M. Schadlich. “Separation of σ_L and σ_U in π^+ Electroproduction Above the Resonance Region”. *Phys. Lett.* 69B (1977), 253–256. DOI: 10.1016/0370-2693(77)90656-6.
- [193] P. Brauel, T. Canzler, D. Cords, R. Felst, G. Grindhammer, M. Helm, W. D. Kollmann, H. Krehbiel, and M. Schadlich. “Electroproduction of π^+n , π^-p and $K^+\Lambda$, $K^+\Sigma^0$ Final States Above the Resonance Region”. *Z. Phys.* C3 (1979), 101. DOI: 10.1007/BF01443698.
- [194] P. Brauel, T. Canzler, D. Cords, R. Felst, G. Grindhammer, M. Helm, W. D. Kollmann, H. Krehbiel, and M. Schadlich. “ π^- Electroproduction Off Deuterium Above the Resonance Region”. *Phys. Lett.* 65B (1976), 184–186. DOI: 10.1016/0370-2693(76)90028-9.
- [195] J. Volmer et al. “Measurement of the Charged Pion Electromagnetic Form-Factor”. *Phys. Rev. Lett.* 86 (2001), 1713–1716. DOI: 10.1103/PhysRevLett.86.1713. arXiv: nucl-ex/0010009 [nucl-ex].
- [196] T. Horn et al. “Determination of the Charged Pion Form Factor at $Q^2 = 1.60$ and 2.45 GeV/ c^2 ”. *Phys. Rev. Lett.* 97 (2006), 192001. DOI: 10.1103/PhysRevLett.97.192001. arXiv: nucl-ex/0607005 [nucl-ex].
- [197] V. Tadevosyan et al. “Determination of the pion charge form-factor for $Q^2 = 0.60$ GeV 2 - 1.60 GeV 2 ”. *Phys. Rev.* C75 (2007), 055205. DOI: 10.1103/PhysRevC.75.055205. arXiv: nucl-ex/0607007 [nucl-ex].
- [198] H. P. Blok et al. “Charged pion form factor between $Q^2 = 0.60$ and 2.45 GeV 2 . I. Measurements of the cross section for the $^1\text{H}(e^-, e'^-\pi^+)n$ reaction”. *Phys. Rev.* C78 (2008), 045202. DOI: 10.1103/PhysRevC.78.045202. arXiv: 0809.3161 [nucl-ex].
- [199] G. M. Huber et al. “Charged pion form-factor between $Q^2 = 0.60$ GeV 2 and 2.45 GeV 2 . II. Determination of, and results for, the pion form-factor”. *Phys. Rev.* C78 (2008), 045203. DOI: 10.1103/PhysRevC.78.045203. arXiv: 0809.3052 [nucl-ex].
- [200] S. R. Amendolia et al. “A Measurement of the Pion Charge Radius”. *Phys. Lett.* 146B (1984), 116–120. DOI: 10.1016/0370-2693(84)90655-5.
- [201] J. J. Sakurai. “Theory of strong interactions”. *Annals Phys.* 11 (1960), 1–48. DOI: 10.1016/0003-4916(60)90126-3.
- [202] G. R. Farrar and D. R. Jackson. “The Pion Form-Factor”. *Phys. Rev. Lett.* 43 (1979), 246. DOI: 10.1103/PhysRevLett.43.246.
- [203] A. V. Efremov and A. V. Radyushkin. “Factorization and Asymptotical Behavior of Pion Form-Factor in QCD”. *Phys. Lett.* 94B (1980), 245–250. DOI: 10.1016/0370-2693(80)90869-2.

- [204] G. P. Lepage and S. J. Brodsky. “Exclusive Processes in Perturbative Quantum Chromodynamics”. *Phys. Rev. D* 22 (1980), 2157. DOI: 10.1103/PhysRevD.22.2157.
- [205] L. Chang, I. C. Cloët, C. D. Roberts, S. M. Schmidt, and P. C. Tandy. “Pion electromagnetic form factor at spacelike momenta”. *Phys. Rev. Lett.* 111.14 (2013), 141802. DOI: 10.1103/PhysRevLett.111.141802. arXiv: 1307.0026 [nucl-th].
- [206] T. Horn and C. D. Roberts. “The pion: an enigma within the Standard Model”. *J. Phys. G* 43.7 (2016), 073001. DOI: 10.1088/0954-3899/43/7/073001. arXiv: 1602.04016 [nucl-th].
- [207] M. N. Rosenbluth. “High Energy Elastic Scattering of Electrons on Protons”. *Phys. Rev.* 79 (1950), 615–619. DOI: 10.1103/PhysRev.79.615.
- [208] I. A. Qattan et al. “Precision Rosenbluth measurement of the proton elastic form-factors”. *Phys. Rev. Lett.* 94 (2005), 142301. DOI: 10.1103/PhysRevLett.94.142301. arXiv: nucl-ex/0410010 [nucl-ex].
- [209] L. Andivahis et al. “Measurements of the electric and magnetic form-factors of the proton from $Q^2 = 1.75 \text{ GeV}/c^2$ to $8.83 \text{ GeV}/c^2$ ”. *Phys. Rev. D* 50 (1994), 5491–5517. DOI: 10.1103/PhysRevD.50.5491.
- [210] M. E. Christy et al. “Measurements of electron proton elastic cross-sections for $0.4 < Q^2 < 5.5 \text{ GeV}/c^2$ ”. *Phys. Rev. C* 70 (2004), 015206. DOI: 10.1103/PhysRevC.70.015206. arXiv: nucl-ex/0401030 [nucl-ex].
- [211] M. K. Jones et al. “ $G_{E,p}/G_{M,p}$ ratio by polarization transfer in polarized $e^- p \rightarrow e^- \vec{p}$ ”. *Phys. Rev. Lett.* 84 (2000), 1398–1402. DOI: 10.1103/PhysRevLett.84.1398. arXiv: nucl-ex/9910005 [nucl-ex].
- [212] O. Gayou et al. “Measurement of $G_{E,p}/G_{M,p}$ in polarized $e^- p \rightarrow e^- \vec{p}$ to $Q^2 = 5.6 \text{ GeV}^2$ ”. *Phys. Rev. Lett.* 88 (2002), 092301. DOI: 10.1103/PhysRevLett.88.092301. arXiv: nucl-ex/0111010 [nucl-ex].
- [213] V. Punjabi et al. “Proton elastic form-factor ratios to $Q^2 = 3.5 \text{ GeV}^2$ by polarization transfer”. *Phys. Rev. C* 71 (2005), 055202. DOI: 10.1103/PhysRevC.71.055202, 10.1103/PhysRevC.71.069902. arXiv: nucl-ex/0501018 [nucl-ex].
- [214] A. J. R. Puckett et al. “Recoil Polarization Measurements of the Proton Electromagnetic Form Factor Ratio to $Q^2 = 8.5 \text{ GeV}^2$ ”. *Phys. Rev. Lett.* 104 (2010), 242301. DOI: 10.1103/PhysRevLett.104.242301. arXiv: 1005.3419 [nucl-ex].
- [215] A. J. R. Puckett et al. “Final Analysis of Proton Form Factor Ratio Data at $Q^2 = 4.0, 4.8$ and 5.6 GeV^2 ”. *Phys. Rev. C* 85 (2012), 045203. DOI: 10.1103/PhysRevC.85.045203. arXiv: 1102.5737 [nucl-ex].
- [216] P. A. M. Guichon and M. Vanderhaeghen. “How to reconcile the Rosenbluth and the polarization transfer method in the measurement of the proton form-factors”. *Phys. Rev. Lett.* 91 (2003), 142303. DOI: 10.1103/PhysRevLett.91.142303. arXiv: hep-ph/0306007 [hep-ph].
- [217] P. G. Blunden, W. Melnitchouk, and J. A. Tjon. “Two-photon exchange in elastic electron-nucleon scattering”. *Phys. Rev. C* 72 (2005), 034612. DOI: 10.1103/PhysRevC.72.034612. arXiv: nucl-th/0506039 [nucl-th].

- [218] M. Diehl and P. Kroll. “Nucleon form factors, generalized parton distributions and quark angular momentum”. *Eur. Phys. J. C* 73.4 (2013), 2397. DOI: 10.1140/epjc/s10052-013-2397-7. arXiv: 1302.4604 [hep-ph].
- [219] I. C. Cloët, G. Eichmann, B. El-Bennich, T. Klahn, and C. D. Roberts. “Survey of nucleon electromagnetic form factors”. *Few Body Syst.* 46 (2009), 1–36. DOI: 10.1007/s00601-009-0015-x. arXiv: 0812.0416 [nucl-th].
- [220] R. S. Sufian, G. F. de Téra mond, S. J. Brodsky, A. Deur, and H. G. Dosch. “Analysis of nucleon electromagnetic form factors from light-front holographic QCD : The spacelike region”. *Phys. Rev. D* 95.1 (2017), 014011. DOI: 10.1103/PhysRevD.95.014011. arXiv: 1609.06688 [hep-ph].
- [221] M. Meziane et al. “Search for effects beyond the Born approximation in polarization transfer observables in $e^- - p$ elastic scattering”. *Phys. Rev. Lett.* 106 (2011), 132501. DOI: 10.1103/PhysRevLett.106.132501. arXiv: 1012.0339 [nucl-ex].
- [222] V. Punjabi, C. F. Perdrisat, M. K. Jones, E. J. Brash, and C. E. Carlson. “The Structure of the Nucleon: Elastic Electromagnetic Form Factors”. *Eur. Phys. J. A* 51 (2015), 79. DOI: 10.1140/epja/i2015-15079-x. arXiv: 1503.01452 [nucl-ex].
- [223] S. Collins et al. “Dirac and Pauli form factors from lattice QCD”. *Phys. Rev. D* 84 (2011), 074507. DOI: 10.1103/PhysRevD.84.074507. arXiv: 1106.3580 [hep-lat].
- [224] C. Alexandrou, M. Brinet, J. Carbonell, M. Constantinou, P. A. Harraud, P. Guichon, K. Jansen, T. Korzec, and M. Papinutto. “Nucleon electromagnetic form factors in twisted mass lattice QCD”. *Phys. Rev. D* 83 (2011), 094502. DOI: 10.1103/PhysRevD.83.094502. arXiv: 1102.2208 [hep-lat].
- [225] P. E. Shanahan, A. W. Thomas, R. D. Young, J. M. Zanotti, R. Horsley, Y. Nakamura, D. Pleiter, P. E. L. Rakow, G. Schierholz, and H. Stüben. “Magnetic form factors of the octet baryons from lattice QCD and chiral extrapolation”. *Phys. Rev. D* 89 (2014), 074511. DOI: 10.1103/PhysRevD.89.074511. arXiv: 1401.5862 [hep-lat].
- [226] P. E. Shanahan, A. W. Thomas, R. D. Young, J. M. Zanotti, R. Horsley, Y. Nakamura, D. Pleiter, P. E. L. Rakow, G. Schierholz, and H. Stüben. “Electric form factors of the octet baryons from lattice QCD and chiral extrapolation”. *Phys. Rev. D* 90 (2014), 034502. DOI: 10.1103/PhysRevD.90.034502. arXiv: 1403.1965 [hep-lat].
- [227] J. R. Green, J. W. Negele, A. V. Pochinsky, S. N. Syritsyn, M. Engelhardt, and S. Krieg. “Nucleon electromagnetic form factors from lattice QCD using a nearly physical pion mass”. *Phys. Rev. D* 90 (2014), 074507. DOI: 10.1103/PhysRevD.90.074507. arXiv: 1404.4029 [hep-lat].
- [228] S. Capitani, M. Della Morte, D. Djukanovic, G. von Hippel, J. Hua, B. Jäger, B. Knippschild, H. B. Meyer, T. D. Rae, and H. Wittig. “Nucleon electromagnetic form factors in two-flavor QCD”. *Phys. Rev. D* 92.5 (2015), 054511. DOI: 10.1103/PhysRevD.92.054511. arXiv: 1504.04628 [hep-lat].

- [229] J. Koponen, A. C. Zimmermann-Santos, C. T. H. Davies, G. P. Lepage, and A. T. Lytle. “Pseudoscalar meson electromagnetic form factor at high Q^2 from full lattice QCD”. *Phys. Rev. D* 96.5 (2017), 054501. DOI: 10.1103/PhysRevD.96.054501. arXiv: 1701.04250 [hep-lat].
- [230] G. S. Bali, B. Lang, B. U. Musch, and A. Schäfer. “Novel quark smearing for hadrons with high momenta in lattice QCD”. *Phys. Rev. D* 93.9 (2016), 094515. DOI: 10.1103/PhysRevD.93.094515. arXiv: 1602.05525 [hep-lat].
- [231] J.-W. Chen, S. D. Cohen, X. Ji, H.-W. Lin, and J.-H. Zhang. “Nucleon Helicity and Transversity Parton Distributions from Lattice QCD”. *Nucl. Phys. B* 911 (2016), 246–273. DOI: 10.1016/j.nuclphysb.2016.07.033. arXiv: 1603.06664 [hep-ph].
- [232] C. Alexandrou, K. Cichy, M. Constantinou, K. Hadjiyiannakou, K. Jansen, F. Steffens, and C. Wiese. “Updated Lattice Results for Parton Distributions”. *Phys. Rev. D* 96.1 (2017), 014513. DOI: 10.1103/PhysRevD.96.014513. arXiv: 1610.03689 [hep-lat].
- [233] B. Yoon, M. Engelhardt, R. Gupta, T. Bhattacharya, J. R. Green, B. U. Musch, J. W. Negele, A. V. Pochinsky, A. Schäfer, and S. N. Syritsyn. “Nucleon Transverse Momentum-dependent Parton Distributions in Lattice QCD: Renormalization Patterns and Discretization Effects”. *Phys. Rev. D* 96.9 (2017), 094508. DOI: 10.1103/PhysRevD.96.094508. arXiv: 1706.03406 [hep-lat].
- [234] A. J. Chambers et al. “Electromagnetic form factors at large momenta from lattice QCD”. *Phys. Rev. D* 96.11 (2017), 114509. DOI: 10.1103/PhysRevD.96.114509. arXiv: 1702.01513 [hep-lat].
- [235] J. Dragos. “Improved determination of hadron matrix elements using the variational method”. PhD thesis. The University of Adelaide, 2017.
- [236] J. J. Kelly. “Simple parametrization of nucleon form factors”. *Phys. Rev. C* 70 (2004), 068202. DOI: 10.1103/PhysRevC.70.068202.
- [237] J. D. Bjorken and E. A. Paschos. “Inelastic Electron Proton and gamma Proton Scattering, and the Structure of the Nucleon”. *Phys. Rev.* 185 (1969), 1975–1982. DOI: 10.1103/PhysRev.185.1975.
- [238] J. Blumlein. “The Theory of Deeply Inelastic Scattering”. *Prog. Part. Nucl. Phys.* 69 (2013), 28–84. DOI: 10.1016/j.pnpnp.2012.09.006. arXiv: 1208.6087 [hep-ph].
- [239] H. W. Kendall. “Deep inelastic scattering: Experiments on the proton and the observation”. *Rev. Mod. Phys.* 63 (1991), 597–614. DOI: 10.1103/RevModPhys.63.597.
- [240] B. Badelek, M. Krawczyk, K. Charchula, and J. Kwiecinski. “Small x physics in deep inelastic lepton hadron scattering”. *Rev. Mod. Phys.* 64 (1992), 927–960. DOI: 10.1103/RevModPhys.64.927.
- [241] R. Placakyte. “Parton Distribution Functions”. *Proceedings, 31st International Conference on Physics in collisions (PIC 2011): Vancouver, Canada, August 28-September 1, 2011*. 2011. arXiv: 1111.5452 [hep-ph]. URL: <https://inspirehep.net/record/954990/files/arXiv:1111.5452.pdf>.
- [242] M. Dittmar et al. “Parton Distributions” (2009). arXiv: 0901.2504 [hep-ph].

- [243] S. Boffi and B. Pasquini. “Generalized parton distributions and the structure of the nucleon”. *Riv. Nuovo Cim.* 30 (2007), 387. DOI: 10.1393/ncr/i2007-10025-7. arXiv: 0711.2625 [hep-ph].
- [244] A. V. Radyushkin. “Generalized parton distributions” (2000). DOI: 10.1142/9789812810458_0027. arXiv: hep-ph/0101225 [hep-ph].
- [245] M. Diehl. “Generalized parton distributions”. *Phys. Rept.* 388 (2003), 41–277. DOI: 10.1016/j.physrep.2003.08.002, 10.3204/DESY-THESIS-2003-018. arXiv: hep-ph/0307382 [hep-ph].
- [246] A. Metz, D. Pitonyak, A. Schafer, M. Schlegel, W. Vogelsang, and J. Zhou. “Single-spin asymmetries in inclusive deep inelastic scattering and multiparton correlations in the nucleon”. *Phys. Rev. D* 86 (2012), 094039. DOI: 10.1103/PhysRevD.86.094039. arXiv: 1209.3138 [hep-ph].
- [247] C. Kouvaris, J.-W. Qiu, W. Vogelsang, and F. Yuan. “Single transverse-spin asymmetry in high transverse momentum pion production in pp collisions”. *Phys. Rev. D* 74 (2006), 114013. DOI: 10.1103/PhysRevD.74.114013. arXiv: hep-ph/0609238 [hep-ph].
- [248] A. Metz and A. Vossen. “Parton Fragmentation Functions”. *Prog. Part. Nucl. Phys.* 91 (2016), 136–202. DOI: 10.1016/j.pnnp.2016.08.003. arXiv: 1607.02521 [hep-ex].
- [249] J. D. Bjorken. “Asymptotic Sum Rules at Infinite Momentum”. *Phys. Rev.* 179 (1969), 1547–1553. DOI: 10.1103/PhysRev.179.1547.
- [250] R. P. Feynman. “The behavior of hadron collisions at extreme energies”. *Conf. Proc.* C690905 (1969), 237–258.
- [251] R. P. Feynman. “Very high-energy collisions of hadrons”. *Phys. Rev. Lett.* 23 (1969), 1415–1417. DOI: 10.1103/PhysRevLett.23.1415.
- [252] G. Martinelli and C. T. Sachrajda. “A Lattice Study of Nucleon Structure”. *Nucl. Phys.* B316 (1989), 355–372. DOI: 10.1016/0550-3213(89)90035-7.
- [253] M. Göckeler, R. Horsley, E.-M. Ilgenfritz, H. Perlt, P. E. L. Rakow, G. Schierholz, and A. Schiller. “Polarized and unpolarized nucleon structure functions from lattice QCD”. *Phys. Rev. D* 53 (1996), 2317–2325. DOI: 10.1103/PhysRevD.53.2317. arXiv: hep-lat/9508004 [hep-lat].
- [254] M. Constantinou. “Recent progress in hadron structure from Lattice QCD”. *PoS CD15* (2015), 009. arXiv: 1511.00214 [hep-lat].
- [255] H.-W. Lin. “From C to Parton Sea: Bjorken-x Dependence of the PDFs”. *PoS LATTICE2016* (2016), 005. arXiv: 1612.09366 [hep-lat].
- [256] W. Zimmermann. “Normal products and the short distance expansion in the perturbation theory of renormalizable interactions”. *Annals Phys.* 77 (1973), 570–601. DOI: 10.1016/0003-4916(73)90430-2.
- [257] J. C. Collins, D. E. Soper, and G. F. Sterman. “Factorization of Hard Processes in QCD”. *Adv. Ser. Direct. High Energy Phys.* 5 (1989), 1–91. DOI: 10.1142/9789814503266_0001. arXiv: hep-ph/0409313 [hep-ph].
- [258] H.-W. Lin et al. “Parton distributions and lattice QCD calculations: a community white paper” (2017). arXiv: 1711.07916 [hep-ph].

-
- [259] G. Martinelli and C. T. Sachrajda. “On the difficulty of computing higher twist corrections”. *Nucl. Phys.* B478 (1996), 660–686. DOI: 10.1016/0550-3213(96)00415-4. arXiv: hep-ph/9605336 [hep-ph].
- [260] A. J. Chambers, R. Horsley, Y. Nakamura, H. Perlt, P. E. L. Rakow, G. Schierholz, A. Schiller, K. Somfleth, R. D. Young, and J. M. Zanotti. “Nucleon Structure Functions from Operator Product Expansion on the Lattice”. *Phys. Rev. Lett.* 118.24 (2017), 242001. DOI: 10.1103/PhysRevLett.118.242001. arXiv: 1703.01153 [hep-lat].